Degradation of Per- and Poly-fluoroalkyl Substances via Advanced Oxidation Processes

A Major Qualifying Project Report

Submitted to the faculty of
WORCESTER POLYTECHNIC INSTITUTE

In partial fulfillment of the requirements for the degree of
Bachelor of Science
By

Alexis Clark
Katherine Lacroix
Shayla Nguyen

Report submitted to
Professor John A. Bergendahl
Professor Stephen J. Kmiotek

April 25, 2023

This report represents work of WPI undergraduate students submitted to the faculty as evidence of a degree requirement. WPI routinely publishes these reports on its website without editorial or peer review. For more information about the projects program at WPI, see https://www.wpi.edu/Academics/Projects

Abstract

Per- and poly-fluoroalkyl substances (PFAS) are a group of synthetic chemicals containing over 9,000 variations. While found in over 4,000 products, PFAS are highly resistant to degradation and have been linked to adverse health effects in humans. According to the EPA, the most effective treatment options are granular activated carbon, ion exchange resins, and high-pressure membrane systems. Research suggests that advanced oxidation reactions may be a beneficial destructive method due to their complete elimination of pollutants and high efficiency. This study examined the efficacy of the three following advanced oxidation reactions on pure water samples of PFOA and GenX: PMS/Ga_2O_3/UV, PMS/TiO_2/UV, and heat/zeolite/PS. For each reaction studied, degradation was quantified using NMR.

Executive Summary

The Issue

Per- and polyfluoroalkyl substances (PFAS) are a group of man-made synthetic chemicals found in many commercial applications, such as firefighting foams, firefighter suits, water-resistant fabrics, nonstick cookware, and personal care products. However, the same properties that give PFAS their surfactant nature and high thermal and chemical stability make them highly resistant to chemical and biological degradation. Consequently, PFAS have been found to bioaccumulate in waterways, soils, vegetation, animals, and humans, earning them their title as "forever chemicals." While current understanding of PFAS toxicological effects is limited, they have been linked to adverse health effects in plants, animals, and humans. *Figure 1* illustrates the cycle of PFAS transfer from commercial products into our environment.

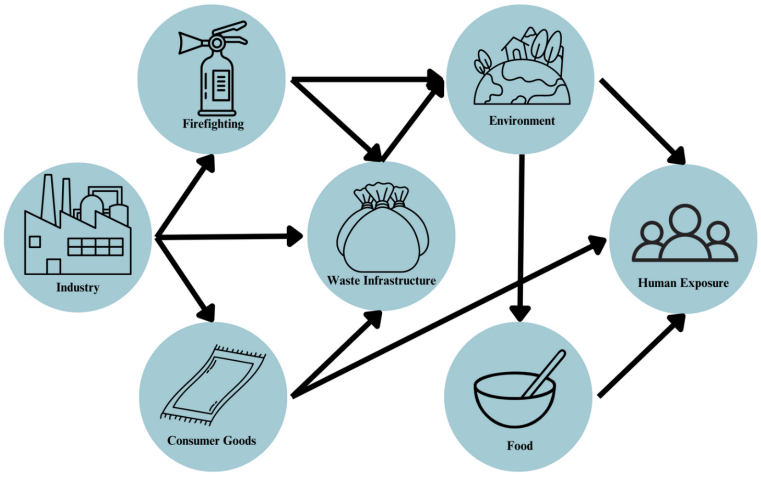

Figure 1. PFAS chain of exposure

While the most commonly used treatment options are granular activated carbon (GAC), ion exchange resins, and high-pressure membrane systems, recent research suggests that advanced oxidation reactions may be a beneficial destructive method for PFAS water treatment. Some benefits of advanced oxidation reactions are their rapid reaction rates, small footprint, and easy automation. This study investigates the viability of advanced oxidation reactions as a water treatment option for long chain PFAS such as perfluorooctanoic acid (PFOA) and shorter chain alternatives such as GenX by examining the three following processes: PMS/Ga_2O_3/UV, PMS/TiO_2/UV, and heat/zeolite/PS.

Objectives

In this project, there were three main objectives that guided us in our research and execution of experiments:

1. Conduct three different advanced oxidation reactions in aqueous solutions of PFOA
2. Utilize NMR to quantify PFAS degradation in each of the three reactions
3. Test the most successful reaction on a 1 mM aqueous solution of GenX

Currently, there's lots of research with conflicting data on the effectiveness of advanced oxidation reactions. With our first objective, the aim was to test three reactions that have reportedly high rates of PFOA degradation and confirm that they really work.

As for the second objective, developing techniques for PFAS detection is very challenging because PFAS are typically found at very low concentrations in natural samples. Currently, the most common detection method is liquid chromatography-mass spectrometry (LC-MS). However, this technique requires extensive sample preparation. In our project, our team expanded on the work of past MQPs in developing a quantitative method to detect PFAS using NMR (Choi et al., 2019). The benefit of NMR is that it allows for the detection of PFAS at relatively low concentrations without extensive sample preparation.

In response to phasing out of long chain PFAS like PFOA and PFOS, many companies began manufacturing shorter chain alternatives like GenX. With the third objective of our lab, we sought to compare the degradation of PFOA to GenX to test if the shorter chain alternative is easier to degrade.

Approach

Tackling the second objective first, the team created standard curves for PFOA and GenX to track the concentration throughout each reaction studied. To create these standard curves, solutions of GenX and PFOA were prepared at the five following concentrations: 4, 2, 1, 0.5, and 0.1mM. Next, the samples were transferred to NMR tubes and prepared in ratios of 90% water to 10% deuterated methanol. In each sample tested, the team found a correlation between the concentration and the area under the peak for the terminal methyl group, $-CF_3$. The standard curve for PFOA is shown in *Figure 2*; the R^2 for a linear fit is approximately 0.999, indicating a high degree of correlation between PFOA concentration and the peak integral area of the $-CF_3$ group.

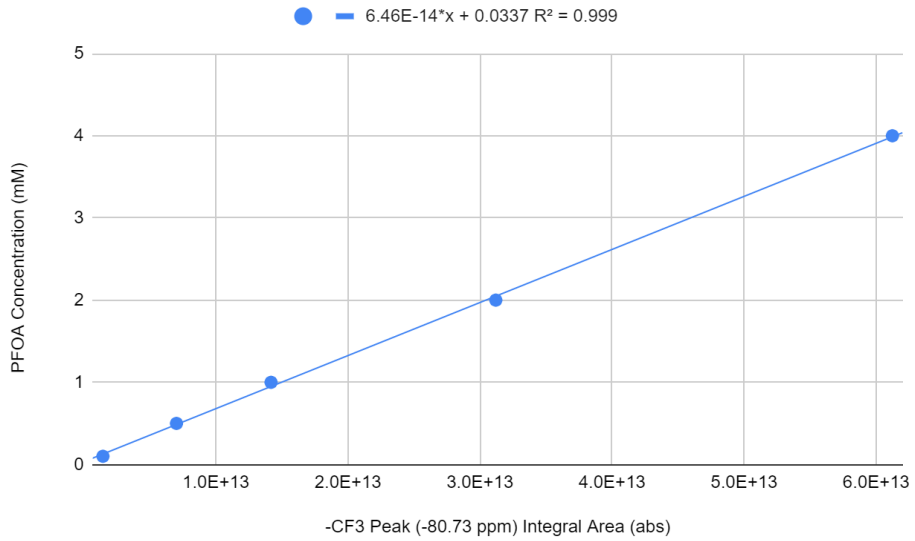

Figure 2. PFOA Standard curve plots concentration versus peak area of terminal -CF_3 group.

Figures 3 and *4* show the standard curves created for GenX. As GenX contains two -CF_3 groups, the team created two standard curves. Similar to PFOA, the concentration of GenX in solution affects the strength of the -CF_3 signal. In both standard curves, the R^2 value for a linear fit was 0.999, indicating a high degree of correlation between GenX concentration and the peak integral areas under the -CF_3 peaks.

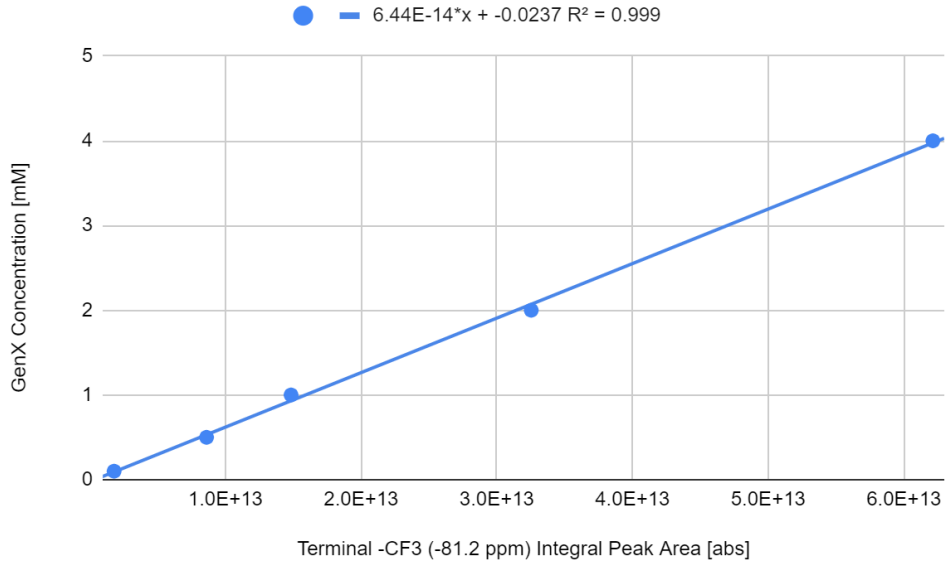

Figure 3. GenX standard curve plots concentration versus peak area of terminal -CF_3 group.

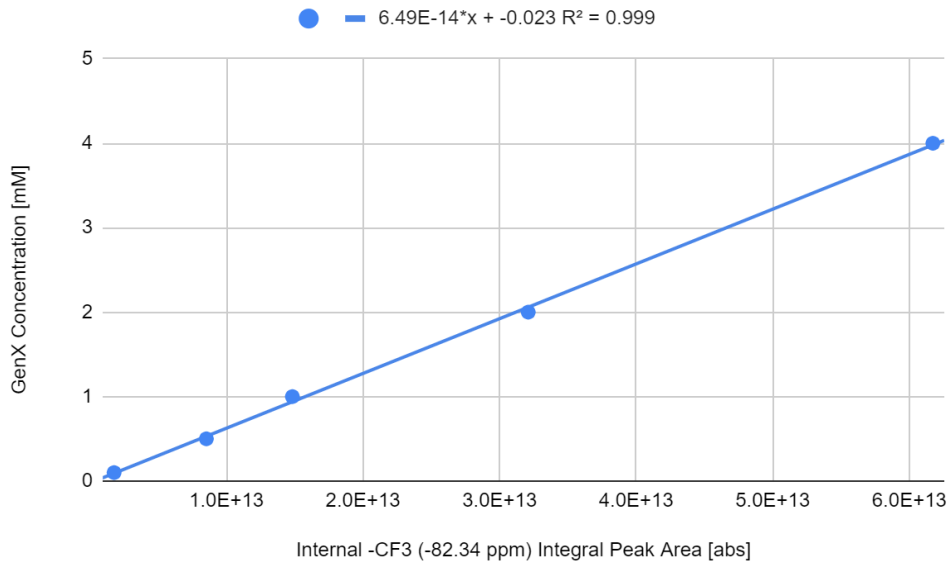

Figure 4. GenX standard curve plots concentration versus peak area of internal -CF_3 group.

Transitioning back to the first objective, the team studied the three following advanced oxidation reactions in 1 mM aqueous solutions of PFOA:

1. PMS/Ga_2O_3/UV: Gallium oxide (Ga_2O_3) assisted with peroxymonosulfate (PMS) under UV light at 254 nm
2. PMS/TiO_2/UV: Titanium dioxide (TiO_2) assisted with PMS under UV light at 254 nm
3. Heat/Zeolite/PS: Heat activated persulfate assisted with BEA Zeolite.

For the reactions with Ga_2O_3 and TiO_2, the team conducted three trials using the following molar ratios of PMS to PFOA: 1:1, 2:1 and 4:1. For each trial studied, two reactions ran simultaneously. For the control reaction, there was no UV light assisting the degradation. For the experimental reaction, the team used a 254 nm UV lamp with water flowing through it. Both reactions were conducted for a total of 100 minutes, with NMR samples, pH, and temperature collected every 20 minutes. *Figure 5* below shows the experimental apparatus used for both PMS/Ga_2O_3/UV and PMS/TiO_2/UV.

Figure 5. Ga_2O_3/PMS/UV and TiO_2/PMS/UV apparatus.

The last method examined heat-activated persulfate assisted with BEA zeolite. For this reaction, the team conducted a control with no zeolite and three trials with the following zeolite dosages: 2.5, 5, and 10g/L. As seen in *Figure 6* below, the solution with zeolite was placed into a laboratory shaker for two hours. After the shaking process, the reaction was conducted in a water bath at 70℃ for 100 minutes. Every 20 minutes, the pH and temperature were recorded. Additionally, samples were collected in 1.5 mL centrifuge tubes. At the end of the reaction, all collected samples were centrifuged for five minutes at 2400 RPM and then transferred to NMR tubes for later analysis.

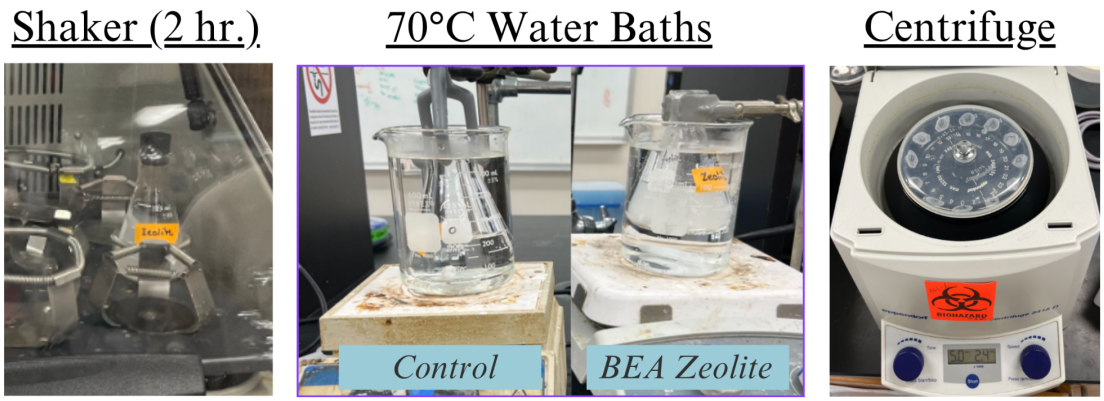

Figure 6. Experimental schematic of the degradation of PFOA and GenX forms of PFAS using heat-activated persulfate in the presence of zeolite.

Findings

As mentioned previously, the standard curves for PFOA and GenX were created by looking at the integral area under the -CF_3 peak for concentrations of 4, 2, 1, 0.5, and 0.1 mM. As seen in *Figure 7*, the NMR spectra obtained for the aqueous solution of PFOA contains seven different peaks. The peaks correspond to each unique fluorine group. As PFOA contains seven carbon atoms bonded directly to fluorine, this result was expected.

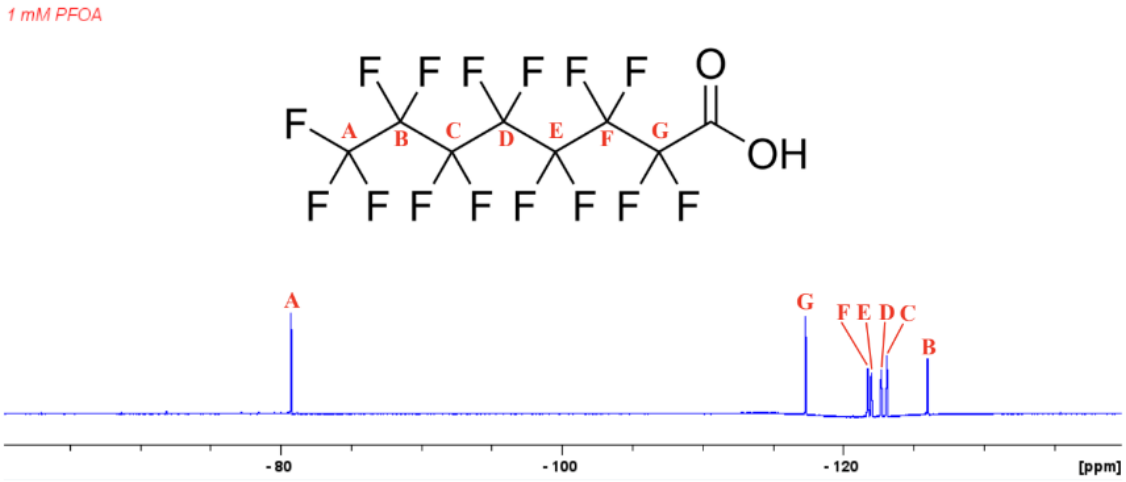

Figure 7. NMR Spectra for a 1mM aqueous PFOA solution.

The terminal methyl group used for quantification is denoted "A" in *Figure 7* above. While difficult to observe in this view, the group exhibits a triplet shape due to the two neighboring fluorine atoms in the carbon chain. This shape is consistent in other PFAS compounds; however, the chemical shift of the peak will vary slightly based on the length of the carbon chain.

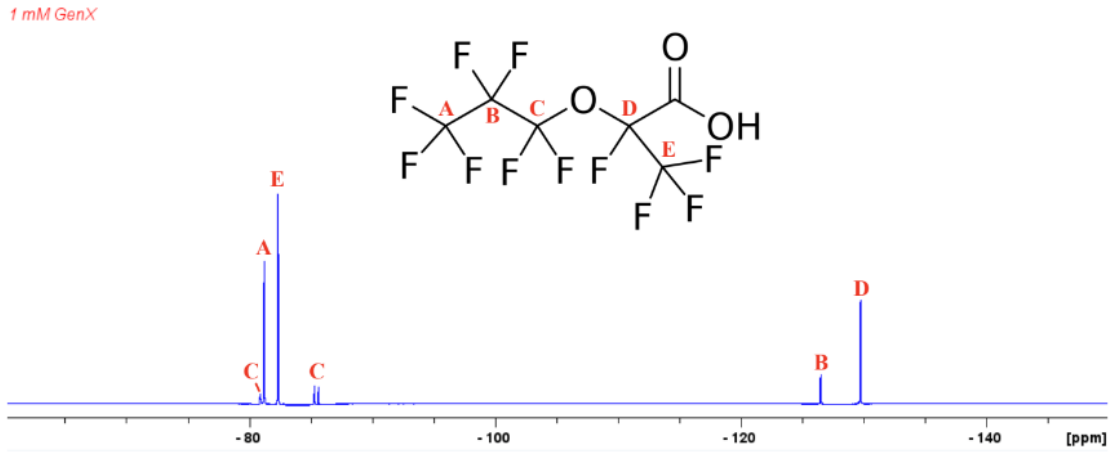

Figure 8. NMR Spectra for a 1mM aqueous GenX solution.

The spectrum for GenX in *Figure 8* above contains fewer peaks than PFOA because there are fewer fluorine groups. Unlike PFOA, the GenX spectrum contains many peaks in the -80 ppm region, corresponding to the terminal -CF_3 group (A), the internal -CF_3 group neighboring the carboxylic acid (E), and the internal -CF_2 group neighboring the ether linkage (C). The internal -CF_2 group is broken into two regions, one located before (C_1) and one after (C_2) the -CF_3 group.

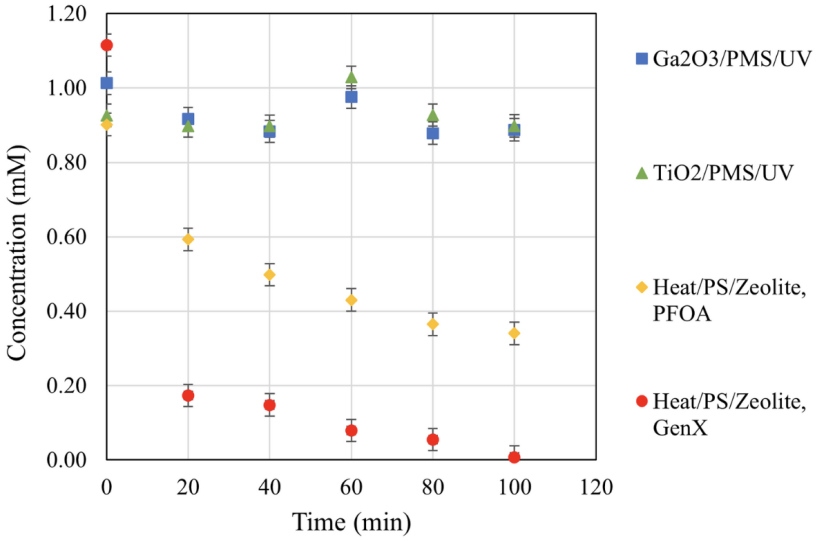

Figure 9. Concentration profiles of each reaction studied over the course of 100 minutes.

Figure 9 above plots the concentration profiles for each of the three reactions studied over 100 minutes. The reactions with Ga_2O_3/PMS/UV and TiO_2/PMS/UV showed minimal degradation of PFOA as the concentration remained fairly the same throughout the course of the experiment. The Heat/PS/Zeolite reaction, on the other hand, showed a visibly more significant level of degradation, with the concentration dropping from 0.90 ± 0.03 mM to 0.34 ± 0.03 mM in 100 minutes.

Figure 10 below shows the NMR spectra of samples taken at (a) 0 minutes and (b) 100 minutes from the heat-activated control. The intensity of the -CF_3 signal decreased over time, signaling a decrease in PFOA concentration. In the sample taken at 100 minutes, there are additional peaks observed in the -75 to -83, -115 to -135, -161 ppm regions. The formation of new peaks indicates the formation of by-products throughout the reaction.

(a)

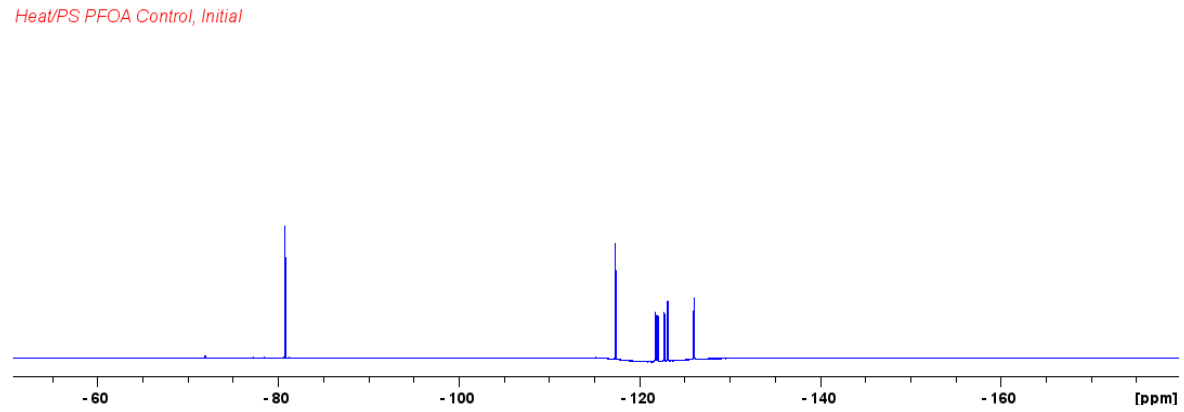

(b)

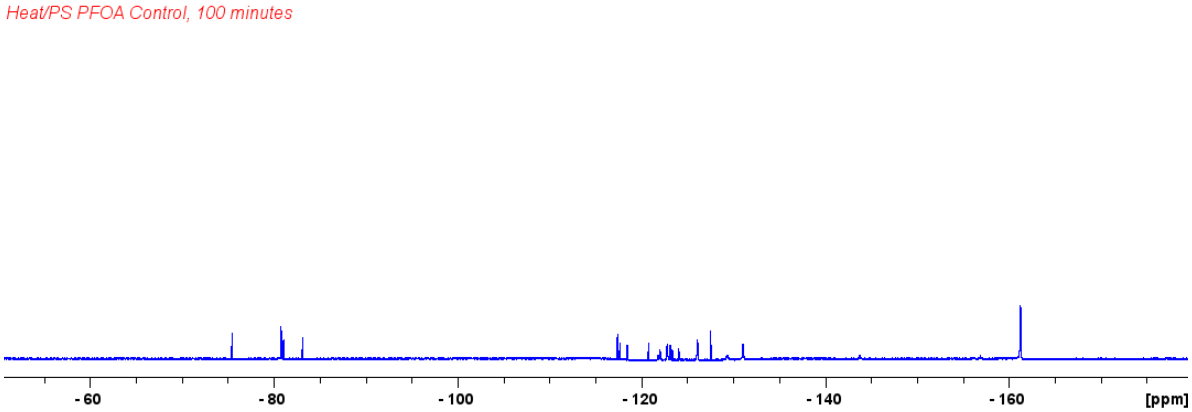

Figure 10. NMR spectra for samples taken at (a) 0 minutes and (b) 100 minutes from the PFOA, heat activated persulfate control.

As discussed previously, the terminal methyl group has a chemical shift in the -80 ppm region and a distinct triplet shape. There were seven triplets observed in the region of -75 to -83 ppm that were identified in *Figure 11*. These seven peaks correspond to the seven following perfluoroalkyl carboxylic acids: PFOA (C8), PFHpA (C7), PFPxA (C6), PFPeA (C5), PFBA (C4), PFPrA (C3), and TFA (C2).

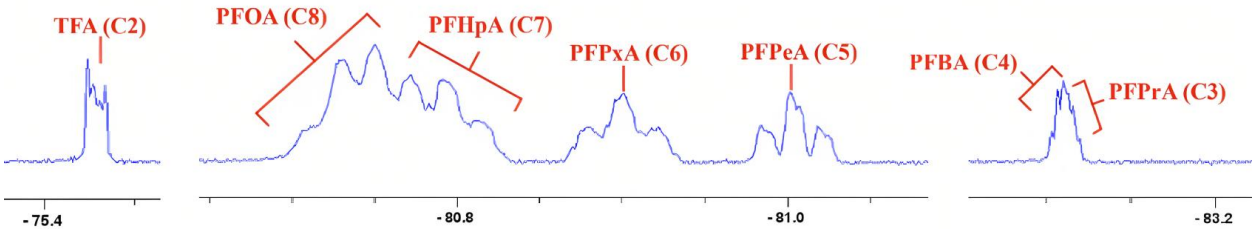

Figure 11. NMR spectrum [-75, -83 ppm] for sample taken at 100 minutes from the PFOA, heat activated persulfate control.

The decline in the intensity of the PFOA signal over the course of the reaction coupled with the formation of shorter chain perfluoroalkyl carboxylic acids indicates that the use of heat activated persulfate was successful at degrading PFOA. *Figure 12* below illustrates the proposed mechanism of shortening of the carbon chain from PFOA to the point of mineralization- with CO_2, H_2O, and F^- ions.

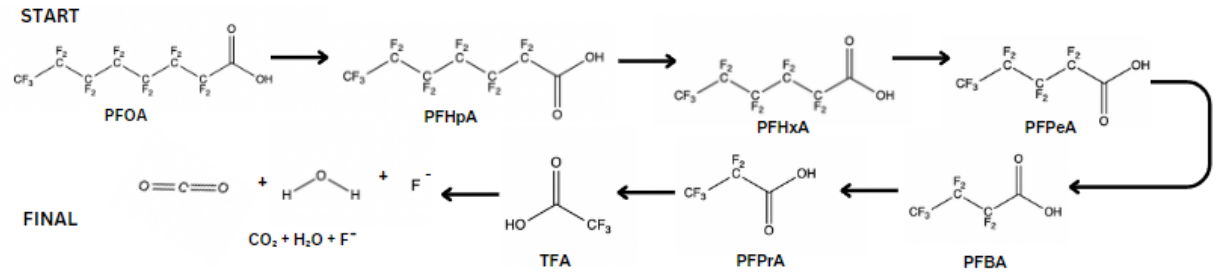

Figure 12. Reaction mechanism for the shortening of the carbon chain in PFOA.

Based on these results, the team decided to investigate the heat-activated persulfate reaction in aqueous solutions of GenX. As shown in *Figure 9*, compared to PFOA, we observed a much more rapid reduction in GenX concentration. Over the course of 100 minutes, while the heat activated persulfate reaction yielded a 62.3 $\pm$ 5.8% decrease in PFOA concentration following second order kinetics, GenX experienced a 99.8 $\pm$ 4.9% decrease in concentration according to first order kinetics.

Recommendations

The team has several recommendations for further study. First, we suggest investigating zeolite dosage beyond 10.0 g/L for the heat-activated persulfate reaction. Our results showed that all zeolite dosages studied were almost 100% effective at degrading GenX, however PFOA did not show as efficient degradation. We believe that increasing the zeolite dosage may increase the percent of PFOA adsorbed after two hours, and this assistance could likely facilitate the

degradation process. Additionally, we recommend investigating different types of zeolites with larger pore sizes as there may be another framework better suited to larger PFAS chains, such as PFOA. For example, other forms of Beta zeolites such as BEA35 have been recorded by other studies to also be successful and would be worth testing (Qian et al., 2022).

Secondly, we suggest examining the effects of competing ions in the solution. All reactions were conducted on pure samples of water. The presence of competing ions has been reported to lower the efficiency of the advanced oxidation reactions because they interact with the radicals in solution and interfere with the redox chemistry. Investigating solutions with competing ions would also provide insight into how these reactions would perform in large-scale water treatment. Traditional water treatment methods must handle a variety of contaminants, and those contaminants could affect the reaction chemistry illustrated in these experiments.

Third, we recommend exploring the applicability of the heat-activated persulfate reaction for PFAS with alternative functional groups, such as PFOS, to see if a similar reaction mechanism is possible. PFAS exists in thousands of commercial products. It would be beneficial to experiment with the most prominent groups to limit human exposure as much as possible. By performing these experiments on other types of PFAS, we could expand the scope of this treatment method and make a more plausible solution.

Finally, it would be beneficial for future MQP teams to perform these advanced oxidation reactions in a continuous flow reactor. Our study looks at the efficacy of these reactions on a much smaller scale than necessary in large-scale treatment plants. Each reaction studied was conducted as a batch process in a beaker. A continuous flow reactor, on the other hand, would allow for continuous operation and may increase the quantity of water treated for industrial applications.

Acknowledgements

This project would not have been possible without the help of several outstanding WPI faculty and staff. We would like to thank Instrumentation Core Technician of the Life Sciences and Bioengineering Center, Daryl Johnson, for his assistance with the credential and training session required to use the Gateway Lab NMR Spectrometer. We would also like to thank the Life Sciences & Bioengineering Center Director, Andrew Butler, for his assistance with project guidance and TopSpin software used to analyze our results. We would also like to thank Professor of Chemistry and Biochemistry, John MacDonald for allowing us into his classroom and providing a fundamental NMR and TopSpin tutorial. Their knowledge of NMR analysis and previous MQP experience was crucial for the outcome of our project.

We would also like to thank Tiffany Royal for helping us acquire all the necessary equipment and lab materials. Our experiments would not have been able to be completed without her help.

Finally, We also want to thank our advisors, Professor of Civil, Environmental, and Architectural Engineering, John Bergendahl, and Professor of Chemical Engineering, Stephen Kmiotek, for their extensive knowledge, support, and positivity. Without their guidance and encouragement, our project would not be where it is today.

Table of Contents

Table of Figures

Table of Tables

1.0 Introduction

Per- and poly-fluoroalkyl substances (PFAS) are a group of synthetic chemicals containing over 9,000 variations and residing within over 4,000 commercial products (The National Institute for Occupational Safety and Health [NIOSH], 2022; About PFASs - OECD Portal on Per and Poly Fluorinated Chemicals, n.d.). While commonly used in commercial applications, these compounds are highly resistant to chemical and biological degradation. Consequently, PFAS have been found to bioaccumulate in waterways, soils, vegetation, animals, and humans, earning them their title as“forever chemicals.” While current understanding of PFAS toxicological effects is limited, they have been linked to adverse health effects in plants, animals, and humans.

According to the EPA, the only known effective treatment options are granular activated carbon (GAC), ion exchange resins, and high-pressure membrane systems. The percentage of PFAS removal is up to 100 percent for all three methods, depending on bed depth, flow rate, and the type of resin. However, recent research suggests that advanced oxidation reactions may be a beneficial destructive method for PFAS water treatment due to their wide applicability, complete elimination of pollutants, and high efficiency. Some benefits of advanced oxidation reactions are their rapid reaction rates, small footprint, and easy automation. Additionally, these processes do not produce “spent carbon”generated in traditional activated carbon adsorptions.

Ultimately, the goal of this research was to investigate the viability of advanced oxidation reactions as an alternative water treatment option for long chain PFAS such as perfluorooctanoic acid (PFOA) and shorter chain alternatives such as GenX. Additionally, our research expands on the work of past MQP teams in demonstrating the effectiveness of Nuclear Magnetic Spectroscopy (NMR) in PFAS detection and quantification.

In this study, the team examined the efficacy of the three following advanced oxidation reactions on a 1 mM aqueous solution of PFOA: PMS/Ga_2O_3/UV, PMS/TiO_2/UV, and heat/zeolite/PS. For each reaction studied, degradation was quantified using standard curves developed from the peak integral area of the terminal -CF_3 group in the NMR spectra. After analyzing the results on PFOA, the team conducted the most successful of the three reactions on a 1mM aqueous solution of GenX to investigate whether this mechanism could degrade shorter chain alternatives.

2.0 Background

2.1 Per- and Polyfluoroalkyl Substances

2.1.1 Classifications

Per- and poly-fluoroalkyl substances (PFAS) are a class of synthetic chemicals containing over 9,000 variations (The National Institute for Occupational Safety and Health [NIOSH], 2022). All varieties of PFAS are composed of a carbon chain bonded to fluorine. As illustrated in *Figure 13*, PFAS are divided into two primary classes based on the length of the carbon backbone: polymers and non-polymers (Interstate Technology Regulatory Council, 2022a).

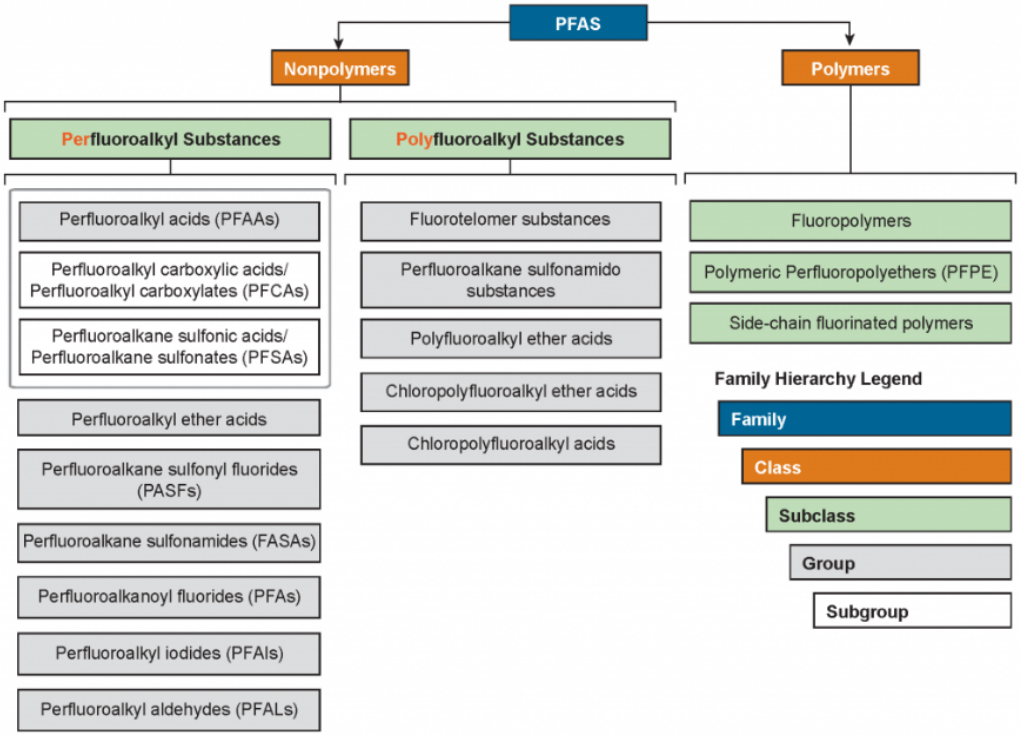

Figure 13. Breakdown of PFAS classifications.

Non-polymer chains contain between 2 and 13 carbon atoms, while polymers are composed of very long carbon chains, with many repeating units (Fidra, n.d.). Compared to polymers, the non-polymers tend to be more mobile and reactive. Therefore, in this review, the non-polymers will be the main area of focus, as they are more easily transferred into the environment and humans.

Figure 13 shows that the non-polymers are further divided into two subgroups: perfluorinated and polyfluorinated. In poly-fluoroalkyl substances, the carbon chain is partially fluorinated,

meaning fluorine atoms partially replace the hydrogen atoms in the C-H bond. Perfluoroalkyl substances, on the other hand, are fully fluorinated, meaning fluorine atoms replace all the hydrogen atoms on a given carbon atom. *Figure 14* below shows the chemical structure of a fully fluorinated PFAS molecule (Benford, 2008).

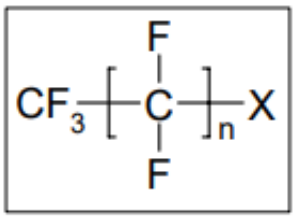

Figure 14. Chemical structure of perfluoroalkyl substances.

The "X" in *Figure 14* above represents the functional group, also referred to as the headgroup. As shown in *Figure 13*, perfluoroalkyl substances are further divided based on the functional group present. Perfluoroalkyl acids (PFAAs), for instance, contain carboxylic acid (R-COOH) or sulfonic acid ($R\text{-}SO_2OH$) headgroups.

In addition to fluorination, non-polymers are also grouped by the length of the carbon chain. For perfluoroalkyl sulfonic acids, "long-chain" molecules typically contain six or more carbon atoms, while "short-chain" chemicals contain less than six carbons (Brendel, 2018). For perfluoroalkyl carboxylic acids, "long-chain" chemicals contain seven or more carbons, while "short-chain" molecules contain less than seven carbons (Brendel, 2018).

2.1.2 Chemical Structure

The properties of PFAS are linked to the unique characteristics of the C-F bond. Due to the small atomic radius and high electronegativity of the fluorine atom, the C-F bond is one of the strongest in all organic chemistry. In fact, its bond enthalpy, 485 kJ/mol, is roughly 1.4 times the bond enthalpy of a traditional C-C bond, 347 kJ/mol, and about 1.2 times the bond enthalpy of a C-H bond, 413 kJ/mol (Soung & Le, 2020). The strength of the C-F bonds, therefore, makes this class of chemicals extremely resistant to chemical, thermal, and biological degradation (Glüge et al., 2020).

In addition to high chemical stability, PFAS have a characteristic amphiphilic structure. The C-F backbone is hydrophobic, while the polar functional group - carboxylic acid, sulfonic acid, etc. - is hydrophilic. *Figure 15* below shows how these compounds orient themselves along the air-water interface, lining up so that the hydrophobic tail faces the air and the hydrophilic head faces the water (Adamson et al., 2020).

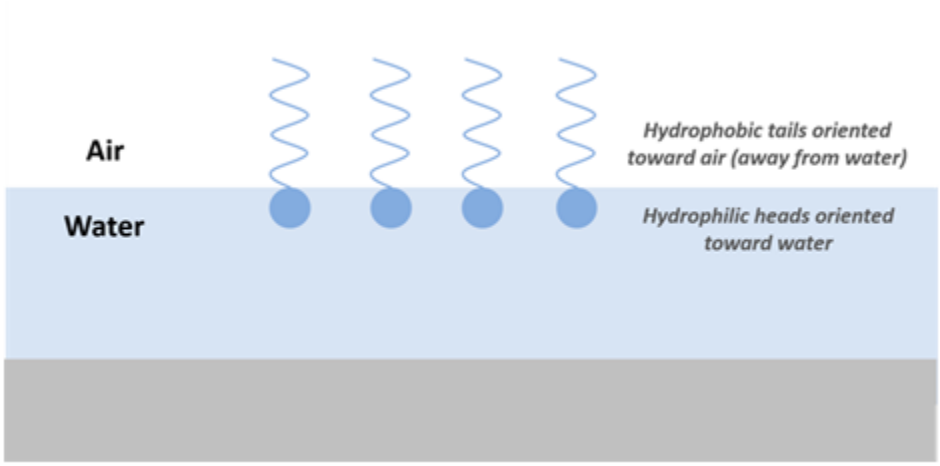

Figure 15. Orientation of PFAS at the air-water interface.

Compared to hydrocarbons, PFAS have a strong affinity for the air-water interface. The low polarizability of the C-F bond leads to weak intermolecular forces and low surface energy (Interstate Technology Regulatory Council, 2022b). This combination of properties makes PFAS strong surfactants, and therefore, resistant to water and grease.

2.1.3 PFOA and GenX

Two of the most widely used and studied PFAS are perfluorooctanoic acid (PFOA) and perfluorooctanesulfonic acid (PFOS) (United States Environmental Protection Agency [EPA], 2022). Please see *Figure 16* below for their chemical structures.

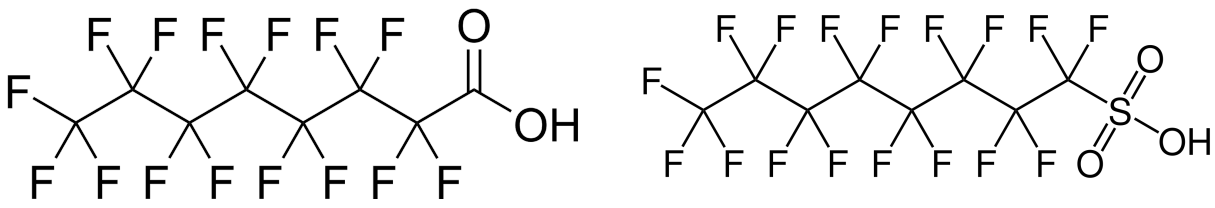

PFOA ($C_8HF_{15}O_2$) **PFOS ($C_8HF_{17}O_3S$)**

Figure 16. Chemical structure of PFOA and PFOS.

Both PFOA and PFOS are long-chain perfluoroalkyl acids with eight carbon atoms. The only difference between PFOA and PFOS is the identity of the headgroup. PFOA contains a carboxylic acid functional group, while PFOS contains a sulfonic acid functional group. In recent years, studies have demonstrated the bioaccumulation of PFOA and PFOA in both human bodies and the environment (Yadava et al., 2022). Therefore, many chemical manufacturers have phased out PFOA and PFOS in favor of short-chain alternatives (Yadava et al., 2022). One such example

is 2,3,3,3- Tetrafluoro-2-(heptafluoropropyl)propanoic acid, more commonly referred to as GenX.

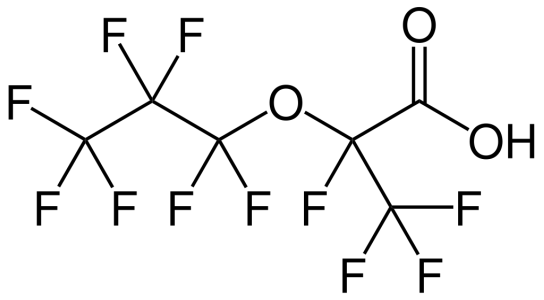

GenX ($C_6HF_{11}O_3$)

Figure 17. Chemical structure of GenX.

As shown in *Figure 17*, GenX consists of a six-carbon chain with two -CF_3 groups, an ether linkage, and a carboxylic acid headgroup. In chemical and product manufacturing, GenX is often used as a replacement for PFOA because the ether group is intended to make the compound more susceptible to degradation. As DuPont introduced GenX back in 2009, there is limited data on its long-term health impacts. According to environmental epidemiologist, Jane Hoppin, GenX is a "regrettable substitute" with potential effects that may be just as bad as PFOA (Ahearn, 2019).

This study looks at treatment techniques for both PFOA and its substitute GenX. The physical and chemical properties of PFOA and GenX are summarized in *Table 1*.

Table 1. Physical and chemical properties of PFOA and GenX.

Property	**PFOA**	**GenX**
Chemical formula	$C_8HF_{15}O_2$	$C_6HF_{11}O_3$
Molecular weight (g/mol)	414.07	347.08
Boiling point (°C)	189	-
Vapor pressure at 25°C (Pa)	69	-
Water Solubility at 20°C (g/L)	3.4	-

2.2 Applications of Per- and Polyfluoroalkyl Substances

Per- and polyfluoroalkyl chemicals were first discovered in the 1930s. Products containing PFAS have been produced and sold in the industrial sphere since the 1950s. These substances were attractive for commercial products because of their chemical properties. PFAS include strong C-F bonds, which cause the substances to be hydrophobic and lipophobic (Buck et al., 2011). They are also very thermally stable.

According to a survey conducted by the Organization for Economic Cooperation and Development, the CAS (Chemical Abstract Service) states that approximately 4,730 PFAS-classified chemicals are in products distributed globally (*About PFASs - OECD Portal on Per and Poly Fluorinated Chemicals*, n.d.). However, many studies conclude that it is challenging to differentiate commercially relevant and commonly used PFAS from other minimally used chemicals that fit within the category. One study examining the OECD list states that only 256, less than 6%, of the listed substances are relevant in global commercial distribution (Buck et al., 2021). Therefore, conducting a proper risk assessment on an entire group of chemicals or pinpointing the specific PFAS typically contained in widely available commercial products is difficult.

However, it has been determined that fluorinated polymers have been found in various products. Coatings or products impervious to heat, oil, grease, water, and staining will likely contain fluorinated substances (*Perfluorooctanoic Acid (PFOA) Factsheet*). Everyday items such as carpeting, furniture, glues, wire insulation, nonstick pans, and many other products contain these substances. PFASs are also identified in textile stain repellant and grease-repelling food contact paper (Banks et al., 2013). Further, these chemicals can lower the surface tension of other chemicals making their properties useful in the aqueous film–forming foams (AFFFs) used to extinguish fires (Banks et al., 2013).

PFOA, the form of PFAS our study focuses on, was commonly used for manufacturing polytetrafluoroethylene (*Perfluorooctanoic Acid (PFOA) Factsheet | National Biomonitoring Program | CDC*, 2021). However, this chemical was phased out of manufacturing practice around 2002 and replaced with the compound GenX. GenX, the second specific PFAS used in our study, was used as a replacement for PFOA in the same products (*Perfluorooctanoic Acid (PFOA) Factsheet | National Biomonitoring Program | CDC*, 2021).

2.3 Contamination of Per- and Polyfluoroalkyl Substances

2.3.1 Environmental Impact

Per- and polyfluoroalkyl substances are pervasive in earth's ecology as they are incredibly resistant to degradation. The persevering chemical qualities that make them effective in commercial products also classify them as "forever chemicals" (Dhore & Murthy, 2021). PFAS are in a wide array of products resulting in various waste cycles. PFOA and other varieties of PFAS are considered widespread organic pollutants (Bonato et al., 2020). Their persistent nature causes them to be prone to bioaccumulation in ecosystems and, therefore, the organisms in those ecosystems.

Per- and polyfluoroalkyl substances enter ecosystems through point and nonpoint sources. Further, they are also found in byproduct gas emissions in the manufacturing of other chemicals and goods (Dhore & Murthy, 2021). Once exposed to the environment, they can permeate soils and waterways. Current research indicates that PFOA and PFOS are absorbed from water and soil through the root system of various plant species (Stahl et al., 2009). The ability of the plant to absorb the substances depends on multiple factors, including but not limited to the chemical's functional group, chain length, concentration, the plant's type, and soil properties (Dhore & Murthy, 2021). The absorption of different types of PFAS into edible plants is highly dependent on the solubility of the chemical. PFAS with shorter chains tend to have higher hydrophilic tendencies and can diffuse in the water much more readily (Dhore & Murthy, 2021). These chemicals can also enter waterways and contaminate drinking water, and PFASs can contaminate wastewater and treated wastewater used to irrigate crops. Leafy plants also can absorb PFAS directly from the air through respiration. However, studies show that the concentration of PFAS in a specific plant is more dependent on PFAS soil concentration (Stahl et al., 2009). This study also indicates that PFAS concentrations are higher in the plant's vegetative parts than in the storage organs (Stahl et al., 2009).

The chains of the per- and polyfluoroalkyl substances are one of the main factors contributing to where the substances occur. Short-chain PFASs are far more prevalent in aquatic environments, whereas long chains are found more frequently in soil (Dhore & Murthy, 2021). Many shorter chained molecules were created later to phase out longer chained molecules in hopes of less bioaccumulation. However, the shorter chained PFASs are more mobile and minimally easier to degrade (Dhore & Murthy, 2021).

The varieties of types and mobilities of various PFASs have led to multiple paths of plant, animal, and human exposure. While there is some understanding of the toxicology regarding PFASs, it is still evident that data is insufficient to understand the hazards of these chemicals to

the environment distinctly (Sinclair et al., 2020). However, they are pervasive in ecological food webs and can enter them at various trophic levels (Dhore & Murthy, 2021).

2.3.2 Health Effects

Concern for these chemicals is growing rapidly as they are being detected in drinking water systems all over the world. They are also being detected in human bodies. One study reported that 27.2% of the US population had detectable amounts of at least one PFAS in their urine (Calafat et al., 2019). Another study conducted on subjects from Catalonia, Spain found that the occurrence of PFAS could be found in all human tissues (Pérez, 2013). These chemicals have gone undetected in our products, drinking water, and environments for enough time that they are now accumulating within our bodies.

The health impacts of this are just in the beginning stages of discovery. According to the Agency for Toxic Substance and Disease Registry (ATSDR), PFAS in the human body may lead to increased cholesterol levels, a decrease in vaccine response in children, changes in liver enzymes, small decreases in infant birth weights, increased risk of high blood pressure for preeclampsia in pregnant women, and increased risk of kidney or testicular cancer (Potential health effects of Pfas Chemicals 2022). Firefighters are exposed to PFAS from fire foam and their suits, and it ultimately gets absorbed into their bloodstream. The CDC published a study by the National Institute for Occupational Safety and Health (NIOSH), the 30,000 studied firefighters showed to have higher rates of certain types of cancer than the general population; bladder and prostate cancer (*Findings from a Study of Cancer among U.S. Fire Fighters*, n.d.).

Another study states exposure to PFAS can negatively affect immune function, metabolic function, and neurodevelopment (Sunderland et al. 2019). These effects are only a few among the predicted but not yet investigated serious conditions. While the health impacts of PFAS are not widely studied for each individual chemical, it is becoming clear that these substances must be removed from human drinking water sources.

2.4 Regulations

PFAS regulations differ by state, ranging from drinking water, food packaging, firefighting foam, textiles, litigation, and cosmetics. As of June 2022, the EPA released some guidelines for PFAS in drinking water; the interim updated Health Advisory for PFOA is 0.004 nanograms per liter (ng/L), or parts per trillion (ppt), and a Final Health Advisory for GenX chemicals is 10 ng/L (Protection, *Per- and polyfluoroalkyl substances (PFAS)*). These regulations have decreased since 2016, from 70 ppt, to aim for 0 ppt. While not every state has integrated strict regulations, there are a few states that have adopted enforceable standards for maximum contaminant levels

(MCLs) for PFAS. These states include Maine, Massachusetts, Michigan, New Hampshire, New Jersey, New York, Pennsylvania, Rhode Island, Vermont, and Wisconsin (*PFAS action*, 2023).

2.4.1 MassDEP

In Massachusetts, the Department of Environmental Protection has addressed the PFAS contamination. MassDEP has partnered with Public Water Suppliers (PWS), and tests all sources of water on a regular basis. Depending on the test results prior, that will depend how frequent a specific source will be tested and what additional monitoring is needed, typically if the system detects any contaminants above the standard MCL. MassDEP has established a grant called the "PFAS6 Treatment Grant", which is awarded to towns who need treatment from any of the 6 specific types of PFAS (MassDEP, n.d.).

2.5 Current Remediation Techniques

According to the EPA, the only known effective treatment options are granular activated carbon (GAC), ion exchange resins, and high-pressure membrane systems (US EPA, 2022). GAC is the most commonly used technique for long chain PFAS removal, due to carbon being an effective adsorbent for natural organic compounds, taste and odor compounds, and synthetic organic chemicals in drinking water treatment systems. With its highly porous surface, the GAC provides a bigger surface area to absorb contaminants. Additionally, GAC is a cheaper alternative, and the percentage of PFAS removal is dependent on bed depth and flow rate.

Ion exchange (IEX) is another common alternative for treating PFAS. The resins are highly porous, and are made from hydrocarbons, — insolubility in water, acid, and bases. Positively charged anion exchange resin specifically, is commonly used for removing PFAS due to PFAS being a negatively charged contaminant. Ultimately, the PFAS would be attracted and held on by the resin. The percentage of PFAS removal is dependent on the type of resin.

High pressure membrane systems, such as nanofiltration and reverse osmosis (RO) show effective treatment for PFAS as well. Reverse osmosis, however, proved to have a higher percentage of removal. Reverse osmosis is a process that uses pressure which forces water through a semipermeable membrane, filtering out PFAS, both long and short chains. RO systems continuously recycle water through the filter membrane that consists of small pores, which are better at removing the smaller molecules. It has proven to remove a higher percentage of PFAS than GAC and IEX, however, it is the most expensive method.

2.6 Advanced Oxidation and Reduction Processes

2.6.1 Advanced Oxidation and Reduction Mechanisms

While physical separation techniques such as granular activated carbon, ion exchange resins, and high-pressure membrane systems are the most common PFAS remediation options, these techniques only transfer PFAS molecules from one medium to another (Leonello et al., 2021). Therefore, they require further downstream treatment and disposal. To eliminate or reduce these down-stream processing steps, destructive methods for PFAS water treatment are critical areas of research.

Advanced oxidation processes (AOPs), advanced reduction processes (ARPs), and combined advanced oxidation/reduction processes (AO/RPs) prove to be promising water treatment options due to their wide applicability, complete elimination of pollutants, and high efficiency (American Water Works Association, 2019).

Fluorine has a reduction potential of approximately $E^o = 3.6$ V, making it one of the strongest inorganic oxidants (Franke, 2019). It is thermodynamically unfavorable to oxidize fluorine in PFAS (-1) to its elemental state F_2 (0) using another one-electron oxidant (Franke, 2019). Advanced oxidation and reduction processes, therefore, seek to overcome this hurdle. Advanced oxidation processes utilize a reactive oxidant species (ROS) to destroy the carbon-fluorine bonds in PFAS, separate the head groups, and scissor the carbon-carbon chain (Alalm, 2022). Commonly used oxidizing species in water treatment include hydroxyl radicals ($\cdot OH$) and sulfate radicals ($\cdot SO_4^-$). Advanced reduction processes (ARPs), on the other hand, produce strongly reducing hydrated electrons (e^-_{aq}) that cleave resistant C-F bonds (Khan et al., 2019). Combined advanced oxidation/reduction processes (AO/RPs) generate both oxidizing and reducing species. Together, these redox processes allow for the continuous defluorination and degradation of the carbon chain, creating shorter and safer molecules. Ultimately, these shorter-chain intermediates mineralize to form CO_2 and fluoride ions (Leonello et al., 2021).

The mechanism of PFAS degradation consists of a series of stepwise elementary reactions by which the pollutant is converted to other products. The level of degradation is based on three steps: the generation of the reactive radicals, the fate of the radicals in water, and the attack of the reactive radicals on the PFAS (Khan et al., 2019). The generation of the reactive radicals depends on the type of reactive species used. Many AO/RPs involve a photochemical process to generate the oxidizing or reductive species. Specifically, photochemical processes utilize UV light to activate inorganic compounds. UV light, for instance, transforms hydrogen peroxide (H_2O_2) into hydroxyl radicals according to Mechanism 1. Under UV light, ozone (O_3) also decomposes to produce hydroxyl radicals (Mechanism 2).

$$H_2O_2 + hv \rightarrow 2 \cdot OH \quad (1)$$

$$O_3 + hv \rightarrow O_2 + O \quad (2)$$
$$O + H_2O + hv \rightarrow 2 \cdot OH$$

However, both molecular ozone, E^o= 2.07 V, and the hydroxyl radical, E^o = 2.8 V, have been shown to be insufficient in degrading PFAS because their redox potentials are too low (Franke, 2019). While hydroxyl radicals have limited success, several studies found that the application of sulfate radicals leads to more efficient degradation of perfluoroalkyl carboxylic acids such as PFOA (Franke, 2019). As shown in Mechanism 3, inorganic salts containing persulfate, PS, ($S_2O_8^{2-}$) can generate sulfate radicals when exposed to UV light. Additionally, peroxymonosulfate, PMS, (HSO_5^-) creates sulfate radicals under UV (Mechanism 4).

$$S_2O_8^{2-} + hv \rightarrow 2SO_4^{\cdot -} \quad (3)$$

$$HSO_5^- + hv \rightarrow SO_4^{\cdot -} + \cdot OH \quad (4)$$

Photocatalysts are often used to facilitate these photochemical reactions. A photocatalyst is a semiconducting material, typically activated by UV light (Khan et al., 2019). There are two primary types of photocatalysts. Heterogeneous photocatalysis involves the use of a catalyst in a different phase from the reactants, while homogeneous photocatalysis uses a photocatalyst in the same phase as the reactants. Titanium oxide (TiO_2) is one of the most commonly used heterogeneous photocatalysts due to its low cost, low toxicity, and high chemical/thermal stability (Khan et al., 2019). The adsorption of organic molecules to the catalyst's active sites leads to more effective degradation by holes generated at the surface of the catalyst. Absorption of PFAS molecules onto the TiO_2 surface is often achieved by carrying out the reaction in acidic conditions (Leonello et al., 2021). Therefore, most research for TiO_2 is performed at pH levels below 4. One of the most commonly used homogeneous photocatalysis processes is the Fenton reaction. The Fenton reaction couples UV or solar light with the Fenton reagent- ferrous iron (Fe^{2+}) and peroxide (H_2O_2)- to produce hydroxyl radicals according to Equation 5.

$$Fe^{2+} + H_2O_2 \rightarrow Fe^{3+} + \cdot OH + OH^- \quad (5)$$
$$Fe^{3+} + H_2O + hv \rightarrow Fe^{2+} + \cdot OH + H^+$$

The radicals generated have strong oxidation and reduction potentials, making them extremely reactive. Because these radicals attack the pollutant very rapidly, the reaction is mostly diffusion controlled. At the beginning of the reaction, the concentration of the reactive species increases until reaching a plateau. From this point on, the concentration of the reactive species declines,

until finally reaching a steady state. The fate of these radical species typically depends on both the concentration of the PFAS and the concentrations of other natural organic matter and inorganic ions in the water sample. As the concentration of PFAS in the sample decreases, the number of molecules degraded decreases very sharply because there is a lower chance of collision. Studies have shown that radical consumers such as CO_3^{2-}, HCO^{3-}, SO_4^{2-}, and Cl^- also decrease the number of PFAS molecules degraded because they reduce the efficiency of AO/RPs (Alalm, 2022).

In this investigation, the team performed the three following advanced oxidation reactions on PFOA and GenX water solutions:

1. PMS/Ga_2O_3/UV
2. PMS/TiO_2/UV
3. Heat/zeolite/PS

Please see the following sections for more information on each reaction studied.

2.6.2 PMS/Ga_2O_3/UV and PMS/TiO_2/UV

The first method investigates the photocatalytic ability of Gallium Oxide (Ga_2O_3) assisted with PMS under UV light. Ga_2O_3 is a promising heterogeneous photocatalyst due to its high chemical and biological stability, easy availability, and low toxicity (Xu et al., 2020). Recent research suggests that Ga_2O_3 may work better than TiO_2 at treating PFOA in solution (Loped de Silva et al., 2017). Xu et al. found that Ga_2O_3 on its own was only able to degrade 58.3% of an aqueous PFOA sample in 180 mins. However, when PMS (0.41 g/L) and Ga_2O_3 (0.25 g/L) were used together, 100% of the PFOA solution was degraded in approximately 120 minutes. The addition of PMS effectively increased the rate constant by a factor of 3.8. Additionally, using a 3:1 molar ratio of PMS to Ga_2O_3, the researchers were able to degrade 100% PFOA within 90 minutes under UV 254 nm and 60 minutes under UV 185 nm.

Five types of active species are produced in the PMS/Ga_2O_3/UV system (Xu et al., 2020). Sulfate radicals are generated according to Mechanism 1. Photoinduced holes (h^+) and electrons (e^-) can be produced following Mechanism 2. Hydroxyl radicals are produced via Mechanisms 1 and 3. Finally, superoxide radical anions ($O_2^{\cdot -}$) are generated according to Mechanism 4.

Active Species	**Mechanism**	
Sulfate and hydroxyl radicals	$HSO_5^- + hv \rightarrow SO_4^{\cdot -} + \cdot OH$	(1)
Photoinduced holes and electrons	$Ga_2O_3 + hv \rightarrow Ga_2O_3(h^+ + e^-)$	(2)

Hydroxyl radicals $$h^+ + H_2O \rightarrow \cdot OH + H^+ \quad (3)$$

Superoxide radical anions $$e^- + O_2 \rightarrow O_2^{\cdot -} \quad (4)$$

Using radical scavengers, the researchers concluded that sulfate radicals produced by PMS, superoxide radical anions, and photogenerated electrons played major roles in degrading PFOA. These radical species, therefore, serve as the main electron sources.

The shortening of the carbon chain takes place in seven distinct steps. As shown below, if the reaction makes it to the seventh and final step, the final products are carbon dioxide and water.

	Reaction Pathway	**Initial PFAS**	**Final PFAS**
(1)	$C_6F_{13} - CF_2 - COOH \rightarrow C_6F_{13} - COOH$	PFOA	PFHpA
(2)	$C_5F_{11} - CF_2 - COOH \rightarrow C_5F_{11} - COOH$	PFHpA	PFHxA
(3)	$C_4F_9 - CF_2 - COOH \rightarrow C_4F_9 - COOH$	PFHxA	PFPeA
(4)	$C_3F_7 - CF_2 - COOH \rightarrow C_3F_7 - COOH$	PFPeA	PFBA
(5)	$C_2F_5 - CF_2 - COOH \rightarrow C_2F_5 - COOH$	PFBA	PFPrA
(6)	$CF_3 - CF_2 - COOH \rightarrow CF_3 - COOH$	PFPrA	TFA
(7)	$CF_3 - COOH \rightarrow CO_2 + H_2O + F^-$	TFA	None

Each step involves two-electron transfers, followed by the cleavage of a -CH_2 group. The electron transfers replace the two fluorine atoms on the terminal -CF_2 group with two hydrogen atoms. Once the fluorine atoms have been replaced, cleavage of the -CH_2 group creates a new chain with one fewer carbon atom. The mechanism for this reaction pathway is as follows:

Mechanism	**Lost**	**Gained**
$C_6F_{13} - CF_2 - COOH \rightarrow C_6F_{13} - CHF - COOH$	$- F^-$	$+ e$
$C_6F_{13} - CHF - COOH \rightarrow C_6F_{13} - CH_2 - COOH$	$- F^-$	$+ e$
$C_6F_{13} - CH_2 - COOH \rightarrow C_6F_{13} - COOH$	$- : CH_2$	

As TiO_2 is a commonly used photocatalyst, the team studied a second reaction using a similar methodology with TiO_2 as opposed to Ga_2O_3.

2.6.3 Heat/zeolite/PS

The final proposed method investigates the effectiveness of heat-activated persulfate (PS) in degrading PFOA and GenX adsorbed to zeolites. PS can be thermally activated using elevated temperature above 50^0C, as shown by Equation 1:

$$S_2O_8^{2-} + \Delta \rightarrow 2SO_4^{\cdot -} \quad (1)$$

When using active persulfate in a reaction, the resulting sulfate radicals are the reactive species (Qian et al., 2022). The low reaction rate of the single-electron step strongly limits PS-based processes.

The selectivity for PFOA in a reaction can be increased by adsorbing PFOA onto the surface of a synthetic, commercial BEA framework type zeolite, BEA35 (Qian et al., 2022). Zeolites essentially work as a net to hold PFOA in place allowing for an increased chance of molecular interactions and increasing the overall reactivity.

Zeolites can hold PFASs and other substances because of their unique structure. Zeolites are microporous crystalline structures composed of corner-sharing tetrahedra arrangements of TO4, where the "Ts" are typically aluminum or silicon atoms (Pérez-Botella et al., 2022). Due to the tetrahedral framework, negative charges form and are compensated for by an extra framework. These cations become the center of the pores, allowing the zeolite to become a cation exchanger within the internal working of their sieve-like framework (Pérez-Botella et al., 2022). Like those used in current PFASs experimentation, BEA zeolites exhibit a three-dimensional pore system formed by 12-membered ring channels with a diameter of 0.76 x 0.64 and 0.55 x 0.55 nm (O. Bok et al., 2020). In our experiment, we used a beta zeolite like the one described in the experiment performed by Quian et al., 2022.

A current study conducted the degradation experiment in an aqueous PFOA and zeolite mixture. The mixture was shaken until approximately 99.9% of the PFOA was absorbed into the zeolite (Qian et al., 2022). The mixtures were then heated to 70^oC to activate the introduced persulfate (Qian et al., 2022). The samples were added to methanol to dislodge the produced PFOA intermediates and then centrifuged to separate the zeolite. The collected samples were then analyzed utilizing LC-MS (Qian et al., 2022).

The study reported evidence of a stepwise degradation of the PFOA chain (Qian et al., 2022). Previous studies state that a singular electron transfer mechanism is used for a sulfate radical to attack the carboxylic group of PFASs and produce a carboxylic radical (equation X) (Qian et al., 2022). This is followed by a decarboxylation reaction to yield perfluorinated alkyl radicals and carbon dioxide (eq X) (Qian et al., 2022). The perfluorinated alkyl radicals then react preferentially with dissolved oxygen in the water to produce the peroxyl radical (eq X) (Qian et al., 2022). The reaction series continues through several radical reactions and hydrolysis processes. This process continues to create shorter PFCAs chains or until they are entirely mineralized. The equations below show the reaction series (Qian et al., 2022).

$$C_7F_{15}COO^- + SO_4^- \bullet \rightarrow C_7F_{15}COO \bullet + SO_4^{2-} \quad (2)$$

$$C_7F_{15}COO \bullet \rightarrow \bullet C_7F_{15} + CO_2 \quad (3)$$

$$\bullet C_7F_{15} + O_2 \rightarrow C_7F_{15}COO \bullet \quad (4)$$

$$2C_7F_{15}COO \bullet \rightarrow C_7F_{15}OO - OOC_7F_{15} \quad (5)$$

$$C_7F_{15}OO - OOC_7F_{15} \rightarrow 2C_7F_{15}O \bullet + O_2 \quad (6)$$

$$C_7F_{15}O \bullet + HSO_4^- \rightarrow C_7F_{15}OH + SO_4^- \bullet \quad (7)$$

$$C_7F_{15}OH \rightarrow C_7F_{13}OF + HF \quad (8)$$

$$C_7F_{13}OF + H_2O \rightarrow C_6F_{13}COOH + HF \quad (9)$$

The study concluded that heat-activated persulfate is a significantly more effective treatment method when PFOA is absorbed into the surface of a zeolite (Qian et al., 2022). The study also found adequate performance in neutral pH and the zeolite could be re-used without significant degradation in 6 cycles (Qian et al., 2022).

2.7 Detection Techniques

2.7.1 LC-MS & LC-MS/MS,

Liquid chromatography-mass spectrometry (LC-MS) is an analytical technique used to identify and measure the concentration of components in a sample. Liquid chromatography (LC) separates the compounds in a mixture based on their affinities for either the mobile or stationary phase. After separation, the mass spectrometer ionizes the components and uses their

mass-to-charge ratio (m/z) to identify their structures. Similar analytical techniques include liquid chromatography-tandem mass spectrometry (LC-MS/MS) and high-performance liquid chromatography-mass spectrometry (HPLC-MS). LC-MS/MS utilizes LC, however, it combines two mass analyzers in one mass spectrometer. HPLC-MS, on the other hand, uses high-performance liquid chromatography (HPLC), which uses a pump as opposed to gravity to pass pressurized liquid through a column. LC-MS is the most widely used detection method for aqueous PFAS samples. Currently, over 750 types of PFAS have been identified using LC-MS (Camdzic, 2021). While commonly used for PFAS detection, there are several limitations to LC-MS such as the limited number of reference materials, poor ionization efficiency, sensitivity to matrix effects, and extensive sample preparation (Camdzic, 2021). Therefore, there is a critical need to develop alternative detection and quantification techniques for PFAS.

2.7.2 Nuclear Magnetic Resonance

Nuclear magnetic resonance (NMR) spectroscopy is a non-destructive technique commonly used to identify organic compounds. When exposed to a strong, external magnetic field (B_o), the nuclei in a liquid sample will either orient themselves with or against the field. This change in the nuclear spin orientation generates a magnetic moment (Edwards, 2012).

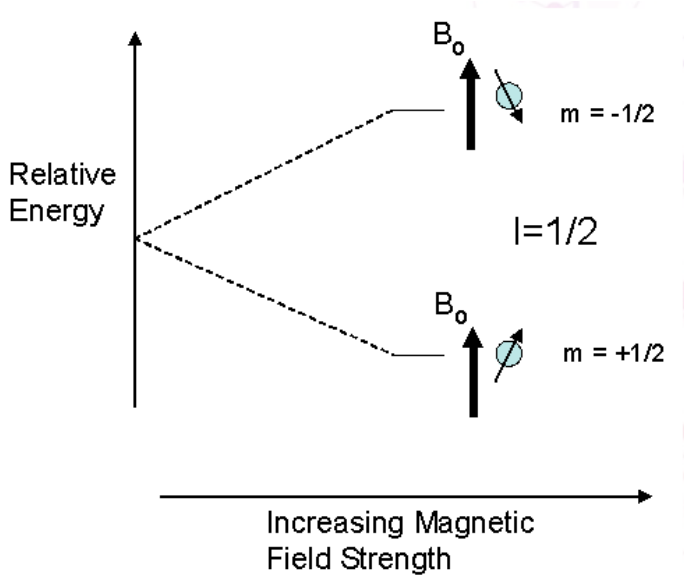

Figure 18. Relative energies of the α-spin and β-spin states

As demonstrated in *Figure 18* above, when nuclear spins align with the field, they adopt the lower energy α-spin state. When nuclear spins align against the field, they adopt the higher energy β-spin state. After adopting either the α-spin or β-spin states, a radio frequency generator pulses the sample to create "spin-flips." A "spin-flip" occurs when nuclei aligned with the field absorb electromagnetic radiation to adopt the higher energy α-spin state, which is in "resonance"

with the field. The resonant frequencies of the nuclei are converted into an NMR spectrum that plots the applied radio frequency versus absorption.

The primary characteristics of peaks on an NMR spectrum are intensity, chemical shift, and shape. The intensity refers to the height of the peak and represents the number of nuclei that resonated at a specific frequency. The chemical shift, on the other hand, is the position on the scale (in units of ppm) where the peak occurs, or where the nuclei absorb energy. To account for spectrometers of various frequencies, the formula below can be used to determine the chemical shift:

$$Chemical\ shift\ =\ \frac{frequency\ of\ signal - frequency\ of\ standard}{spectrometer\ frequency}$$

where the standard frequency refers to the absorption frequency of a reference compound. In NMR, the absorption frequency of nuclei is measured relative to a reference point, or standard. The most common standards are tetramethylsilane (TMS) and deuterochloroform ($CDCl_3$). Finally, the shape of the peak indicates the number of neighboring nuclei. One adjacent atom, for instance, will split the signal to create a duplet. On the other hand, two adjacent nuclei will split the signal twice to create a triplet. This pattern is summarized by the N+1 rule, where the number of times the signal splits can be predicted by the number of neighboring atoms, N, plus one. *Figure 19* below shows examples of the different signals commonly produced by peak splitting (Gevorg, 2021):

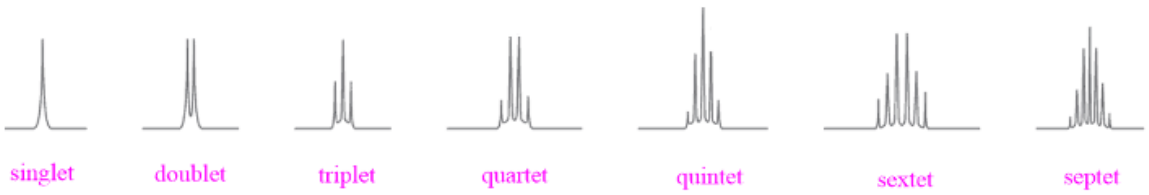

Figure 19. Peak splitting patterns.

Isotopes that contain an odd number of protons generate an intrinsic magnetic field, making them useful in NMR analysis. Common examples of such nuclei are protons (^{1}H), carbon (^{13}C), phosphorous (^{31}P), and fluorine (^{19}F). While liquid chromatography with mass spectrometry (LC-MS) is the most widely used identification technique for PFAS, recent research suggests that ^{19}F-NMR may be a suitable alternative. Some advantages of this technique are that ^{19}F-NMR has high reproducibility, reduces sample preparation, and does not require reference standards for quantification. However, the level of PFAS detection depends on the specific fluorine probe used (Camdzic et al., 2021).

The degree of electron shielding will influence the chemical shift of a particular type or group of nuclei. Groups that are less electronically shielded, for instance, tend to have higher chemical shifts. Whereas, groups that experience more electron shielding have lower chemical shifts. As fluorine is extremely electronegative, compounds containing fluorine typically have chemical shifts between -80 and -130 ppm (Clark, 2014). This feature makes PFAS compounds very easy to distinguish from other organic materials because the chemical shift for hydrogen is between 0-12 ppm. The two most identifiable chemical shifts for PFAS are the terminal trifluoromethyl group ($-CF_3$) and the terminal $-CF_2$ group. A recent study analyzed the spectra for over 30 different types of PFAS (Camdzic et al., 2021). Please see *Table 2* below for the chemical shifts reported for PFOA and GenX.

Table 2. Chemical shifts of the terminal $-CF_2$ and $-CF_3$ groups in PFOA and GenX.

Type of PFAS	**[$-CF_2$] closet to acid end (ppm)**	**Terminal $-CF_3$ (ppm)**
PFOA	-120.2	-82.4
GenX	-132.9	-82.9

Unlike PFOA, GenX has two $-CF_3$ groups; therefore, its spectrum will contain two peaks in the -80 ppm region. Additionally, as shown in *Table 2*, the chemical shift of the terminal $-CF_2$ group is higher in GenX than in PFOA. This difference is likely attributed to the ether group in the middle of the GenX chain. *Figure 20* below shows a sample NMR spectrum for GenX (Camdzic et al., 2021). The ether linkages show characteristic reference signals represented by peaks "c, c^1" and "a."

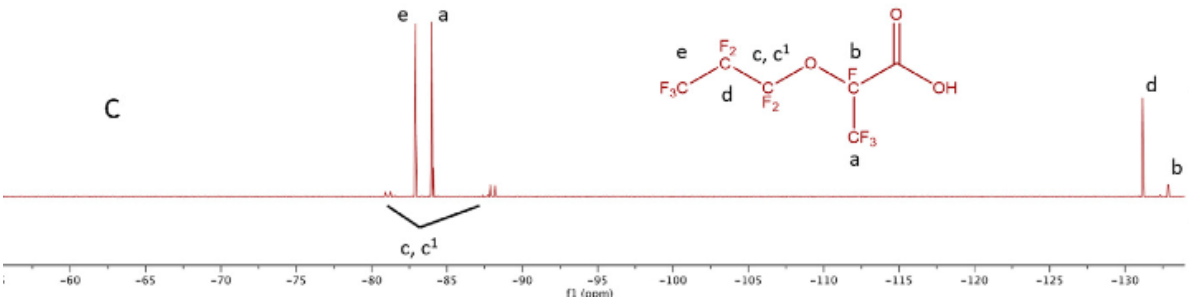

Figure 20. Sample NMR spectrum for GenX.

Between the $-CF_2$ and $-CF_3$ groups, the terminal $-CF_3$ group is typically better for quantification analysis. Regardless of the headgroup, the intensity of the $-CF_3$ signal or the area under the peak can be used to determine the total PFAS content.

3.0 Methodology

The goal of this MQP was to evaluate advanced oxidation reactions as a viable water treatment option for PFAS. To accomplish this goal, the team tested the three following advanced oxidation reactions on a 1 mM aqueous solution of PFOA:

- Ga_2O_3/PMS/UV
- TiO_2/PMS/UV
- Heat/zeolite/PS

Conducting these reactions was the first step in achieving the objectives of this analysis. The three objectives of this MQP are summarized below:

1. Conduct three different advanced oxidation reactions in aqueous solutions of PFOA
2. Utilize NMR to quantify PFAS degradation in each of the three reactions
3. Test the most successful reaction on a 1 mM aqueous solution of GenX

3.1 Materials/Compounds Used:

PFOA, GenX, potassium peroxymonosulfate, and deuterated methanol were purchased from Sigma Aldrich. Sodium persulfate, titanium dioxide, and gallium (III) oxide were obtained from the lab in Kaven Hall. BEA zeolite was purchased from Zeolysty International. Phosphoric acid, acetone, and methanol were purchased from the stockroom in Goddard Hall. Finally, purified water was produced in the Kaven Hall laboratory using a Barnstead Labtower Reverse Osmosis water purifier.

Table 3. Chemical specifications for the materials used.

Chemical Name	Abbreviation	Formula	Purity (wt%)	CAS Number
Perfluorooctanoic acid	PFOA	$C_8HF_{15}O_2$	95%	335-67-1
2,3,3,3-Tetrafluoro-2-(heptafluoropropoxy)propanoic acid	GenX	$C_6H_4F_{11}NO_3$	95%	62037-80-3
Methanol-d_4	-	CD_3OD	99.8%	811-98-3
Potassium peroxymonosulfate	Oxone or PMS	$KHSO_5 \cdot \frac{1}{2}KHSO_4 \cdot \frac{1}{2}K_2SO_4$	-	70693-62-8
Sodium persulfate	PS	$Na_2O_8S_2$	98.0%	7775-27-1
Titanium dioxide	-	TiO_2	99+%	1317-70-0

Gallium (III) oxide	-	Ga_2O_3	99.99%	12024-21-4
Phosphoric acid	-	H_3PO_4	85%	7664-38-2
Acetone	-	C_3H_6O	99.5%	67-64-1
Methanol	-	CH_3OH	99.5%	67-56-1
Beta Zeolite	BEA	150 SiO_2/Al_2O_3 mole ratio	100%	1318-02-1

3.2 Cleaning Glassware Procedure:

The glassware used was provided in WPI's Kaven Hall Laboratory and required cleaning to prevent contamination from prior use. The glassware and plasticware were prepared via the following procedure:

1. Visual inspection of the item for damage (cracks, chips, etc.). Damaged pieces were discarded.
2. Three preliminary rinses with tap water.
3. One rinse with acetone.
4. Three final rinses with purified water.
5. A 15-minute air dry on a paper towel, excess moisture wiped off with a Kimwipe for immediate use or left to air dry overnight for future use.

3.3 Preparing Stock Solutions:

400 and 100 mL PFOA and GenX stock solutions were prepared using purified water. Please see *Table 4* below for the concentrations of each solution and the amount of each component required. The equipment and procedure used for preparing the stocks are also provided below.

Table 4. Amounts of PFOA and GenX required to prepare 400 and 100 mL stock solutions.

Compound	Concentration	Volume of purified water (mL)	Mass of Compound (g)
PFOA	4 mM	400	0.6625
PFOA	4 mM	100	0.1656
GenX	4 mM	100	0.1388
GenX	4 mM	400	0.5553

Equipment:

- 100-mL graduated cylinder (to measure purified water)
- Weighing paper and balance (to record mass used)
- 500-mL glass beakers
- Stir bar and stir plate
- PFOA, GenX

Procedure:

1. Place a 500-mL beaker on a stir plate fitted with a stir bar.
2. Measure 400 mL of purified water using a 100 mL graduated cylinder and add water to the beaker. Turn on the stir plate so that the stir bar begins mixing
3. Using a piece of weighing paper and the mass balance, measure out 0.6625 grams of PFOA. Record the mass used and add half the powder to the beaker on the stir plate.
4. Let the solution mix for 10 minutes, or until all the powder has dissolved.
5. Once half the powder has dissolved, add the second half of the solid powder to the beaker on the stir plate. Let the solution mix for 10 minutes or until there is no solid dispensed in the water
6. Repeat steps 1-5 for GenX using the amounts in *Table 4*.
7. Store the stock solutions in the refrigerator
    a. Sample the PFAS stock solutions at the end of each week to see if new stock solutions need to be prepared

3.4 Creating NMR Standard Curves:

This lab used the Bruker BioSpin 500 MHz Avance AV-III Digital NMR Spectrometer equipped with an F_{19}-NMR cryoprobe located at Gateway Park to measure PFAS concentration. All PFAS compounds have two prominent, identifiable chemical shifts. The terminal -CF_3 group has a chemical shift of approximately -80 ppm, and the internal -CF_2 group has a chemical shift of approximately -120 ppm. The integral areas of the -CF_3 peak were used to determine the PFAS concentration in a given sample. To do this, standard curves were prepared for both GenX and PFOA. These standard curves plot the concentration of the sample on the y-axis (mM) versus the integral area on the x-axis. This methodology is based on the work from a previous MQP group. It is important to note that based on 1024 cycles, this method has a minimum detection concentration of 0.08 mg/L, meaning the machine will not register peaks below this concentration.

Equipment:

- Methanol d-4
- PFOA
- GenX
- Purified Water
- 500 mL glass beaker

- 50 mL glass beakers
- Norrel 502-7 NMR tubes
- Fisherbrand Finnpipette II 20-200 µL automatic pipettes
- Weighing paper and mass balance
- 5-mL graduated pipettes
- Stir bars and stir plate

Table 5. Preparation of PFAS standard solutions from a 4 mM base solution.

Concentration (mM)	**Dilution 1**		**Dilution 2**	
	Stock Volume (mL)	**Water Volume (mL)**	**Dilution 1 Volume (mL)**	**Water Volume (mL)**
4.0	20.0	0	-	-
2.0	10.0	10.0	-	-
1.0	5.0	15.0	-	-
0.5	5.0	15.0	10.0	10.0
0.1	5.0	15.0	2.0	18.0

Procedure:

1. Remove the stock solution from the fridge. Place the beaker on a stir plate and let the stock solution mix for 10 minutes.
    a. Label the beaker “Stock” or “4mM”
2. After approximately 10 minutes of mixing, combine 540 µL of the solution from the beaker with 60 µL of deuterated methanol in a 5 mm NMR test tube using the automatic micropipette for later NMR analysis
    a. 90% water-based to 10% d-4
3. Next, measure out 10 mL of purified water using a 5 mL graduated pipette and transfer it to a 50 mL glass beaker fitted with a stir bar.
4. To this 50-glass beaker, add 10 mL of the 4 mM stock solution using a new 5 mL graduated pipette according to dilution 1 in *Table 5*. Let the solution mix for 3 minutes.
    a. Label beaker “2 mM”
5. Once dissolved, combine 540 µL of the solution from the beaker with 60 µL of deuterated methanol in a 5 mm NMR test tube using a micropipette.
6. Repeat steps 3-5 at 1, 0.5, and 0.1 mM using the dilutions shown in *Table 5.*
7. Repeat steps 1-6 for GenX
8. Dispose of waste and clean glassware (See cleaning procedure).

3.5 PMS/Ga_2O_3/UV:

Three trials of the PMS/Ga_2O_3/UV reaction were conducted under the following PMS to PFOA molar ratios: 1 to 1, 2 to 1, and 4 to 1. For each set of conditions, a constant 3:1 molar ratio of PMS to Ga_2O_3 was maintained. Please see *Table 6* below for the amounts of Ga_2O_3 and PMS used in each trial.

Table 6. Amounts of Ga_2O_3 and PMS used for trials 1-3 of the PMS/Ga2O3/UV reaction.

Trial Number	PMS: PFOA Ratio	PMS Concentration (g/L)	Ga_2O_3 Concentration (g/L)	PMS Mass (g)	Ga_2O_3 Mass (g)
1	1:1	0.307	0.062	0.0615	0.0125
2	2:1	0.615	0.125	0.1230	0.0250
3	4:1	1.23	0.250	0.2460	0.0500

In each trial, a control beaker was used to study the reaction in the absence of UV light. Please see *Figure 5* below for the apparatus setup.

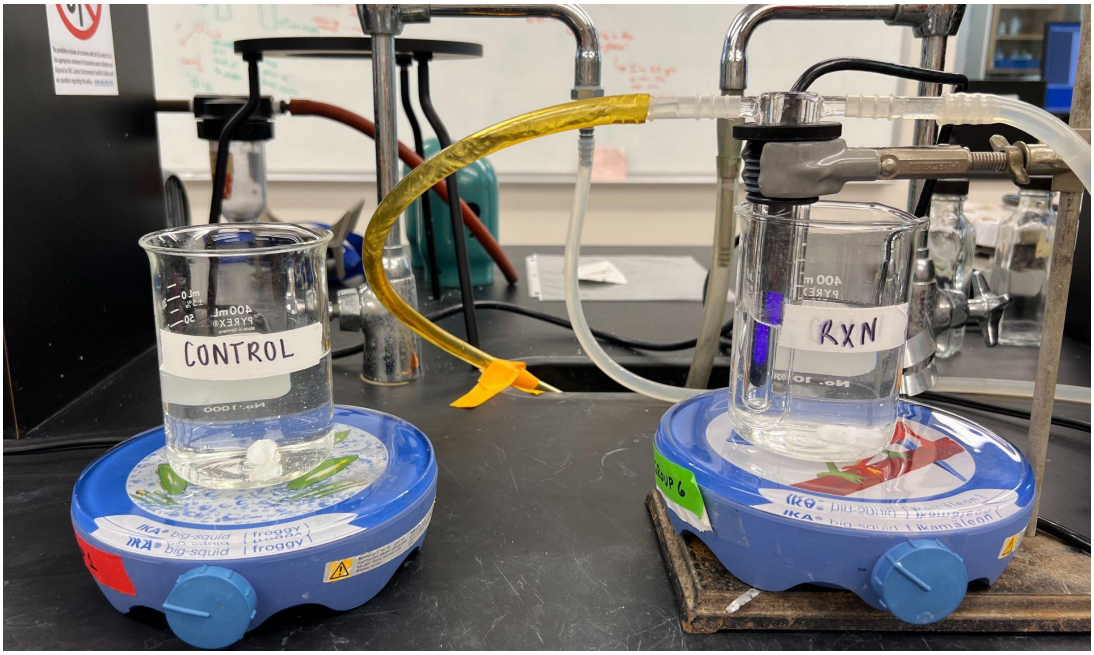

Figure 5. Ga_2O_3/PMS/UV apparatus.

As shown above, water was provided to maintain sufficient cooling to the UV throughout the course of the reaction.

Equipment:

- 254 nm UV light
- 400mL glass beakers
- Stir plates
- Magnetic stir bars
- Ring stands
- Rubber tubing
- pH strips
- Fisherbrand Finnpipette II 20-200 µL automatic pipettes
- Norrel 502-7 NMR tubes
- PFOA stock solution
- GenX stock solution
- Phosphoric Acid
- Deuterated methanol
- Ga_2O_3
- PMS

Procedure:

1. Take the 4 mM stock solution out of the fridge. Place the beaker on a stir plate and let the solution mix for 10 minutes.
    a. Label "stock"
2. Make a 200 mL, 1mM solution of PFOA by combining 50 mL of the stock solution and 150 mL of purified water in a 400 mL beaker.
    a. Label "Rxn Mixture"
3. Add a stir bar to the 400 mL beaker and let mix for 3 minutes.
4. Use an automatic micropipette to combine 540 µL of the PFAS solution and 60 µL of deuterated methanol in a 5 mm NMR tube for later analysis.
5. Repeat steps 2-4 with a new 400 mL glass beaker. Label this beaker "Control."
6. Connect the 254 nm UV lamp onto a ring stand and submerge the lamp in the "Rxn Mixture" beaker as shown in *Figure 5*. Attach two rubber tubes to the sides of the lamp, attaching the end of one to the water faucet and the other to the sink. Turn on the cooling water.
    a. DO NOT TURN ON THE LIGHT YET
7. Measure out 0.0615 g of PMS (See *Table 6*). Add the solid powder to the "Rxn Mixture" beaker and let stir.
8. Repeat step 7 simultaneously for the "Control" beaker.
9. After all the PMS has dissolved, measure out 0.0125 g of Ga_2O_3 (See *Table 6*). Add the solid powder to the "Rxn Mixture" beaker.
10. Repeat step 9 simultaneously for the "Control" beaker.
11. After adding the Ga_2O_3, check the pH of both the "Rxn Mixture" and "Control" beaker using pH strips to record the initial pH. Add drops of phosphoric acid using a plastic pipette until the pH reaches 2.
12. Once the pH reaches 2, turn on the UV light and start the timer.
13. Collect 540 µL samples from both the "Control" and "Rxn mixture" beakers every 20 minutes for NMR analysis. Make sure to dissolve in 60 µL of deuterated methanol in a 5mm NMR tube.

14. Once the reaction has reached 100 minutes and the final samples are taken, turn off the UV light and disassemble the apparatus.
15. Dispose of any waste and clean glassware (See cleaning procedure)

3.6 PMS/TiO_2/UV

Three trials of the PMS/TiO_2/UV reaction were conducted under the following PMS to PFOA molar ratios: 1 to 1, 2 to 1, and 4 to 1. For each set of conditions, a constant 3:1 molar ratio of PMS to TiO_2 was maintained. Please see *Table 7* below for the amounts of TiO_2 and PMS used in each trial.

Table 7. Amounts of Ga_2O_3 and PMS used for trials 1-3 of the PMS/TiO_2/UV reaction.

Trial Number	PMS: PFOA Ratio	PMS Concentration (g/L)	TiO_2 Concentration (g/L)	PMS Mass (g)	TiO_2 Mass (g)
1	1:1	0.307	0.027	0.0615	0.0053
2	2:1	0.615	0.053	0.1230	0.0106
3	4:1	1.23	0.106	0.2460	0.0213

Equipment:

- 254 nm UV light
- 400mL glass beakers
- Stir plates
- Magnetic stir bars
- Ring stands
- Rubber tubing
- pH strips
- Fisherbrand Finnpipette II 20-200 µL automatic pipettes
- Norrel 502-7 NMR tubes
- PFOA stock solution
- GenX stock solution
- Phosphoric Acid
- Deuterated methanol
- TiO_2
- PMS

Procedure:

1. Take the 4 mM stock solution out of the fridge. Place the beaker on a stir plate and let the solution mix for 10 minutes.
    a. Label “stock”
2. Make a 200 mL, 1mM solution of PFOA by combining 50 mL of the stock solution and 150 mL of purified water in a 400 mL beaker.
    a. Label “Rxn Mixture”
3. Add a stir bar to the 400 mL beaker and let mix for 3 minutes.
4. Use an automatic micropipette to combine 540 µL of the PFAS solution and 60 µL of deuterated methanol in a 5 mm NMR tube for later analysis.
5. Repeat steps 2-4 with a new 400 mL glass beaker. Label this beaker “Control.”
6. Connect the 254 nm UV lamp onto a ring stand and submerge the lamp in the “Rxn Mixture” beaker as shown in *Figure 5*. Attach two rubber tubes to the sides of the lamp, attaching the end of one to the water faucet and the other to the sink. Turn on the cooling water.
    a. DO NOT TURN ON THE LIGHT YET
7. Measure out 0.0615 g of PMS (See *Table 7*). Add the solid powder to the “Rxn Mixture” beaker and let stir.
8. Repeat step 7 simultaneously for the “Control” beaker.
9. After all the PMS has dissolved, measure out 0.0053 g of TiO_2 (See *Table 7*). Add the solid powder to the “Rxn Mixture” beaker.
10. Repeat step 9 simultaneously for the “Control” beaker.
11. After adding the TiO_2, check the pH of both the “Rxn Mixture” and “Control” beaker using pH strips to record the initial pH. Add drops of phosphoric acid using a plastic pipette until the pH reaches 2.
12. Once the pH reaches 2, turn on the UV light and start the timer.
13. Collect 540 µL samples from both the “Control” and “Rxn mixture” beakers every 20 minutes for NMR analysis. Make sure to dissolve in 60 µL of deuterated methanol in a 5mm NMR tube.
14. Once the reaction has reached 100 minutes and the final samples are taken, turn off the UV light and disassemble the apparatus.
15. Dispose of any waste and clean glassware (See cleaning procedure)

3.7 Heat/Zeolite/PS:

The trials for the heat/zeolite/PS reaction were conducted at the following BEA zeolite dosages: 5, 50, and 100 g/L. Please see *Table 8* below for the amount of zeolite required for an 80 mL PFAS solution.

Table 8. Zeolite Dosage per trial.

Trial Number	Zeolite Dosage (g/L)	Zeolite Mass in 80 mL PFAS Solution (g)
1	2.5	0.2
2	5	0.4
3	10	0.8

For each trial, a control was conducted in the absence of zeolite. Please see *Figure 6* for a schematic of the apparatus setup.

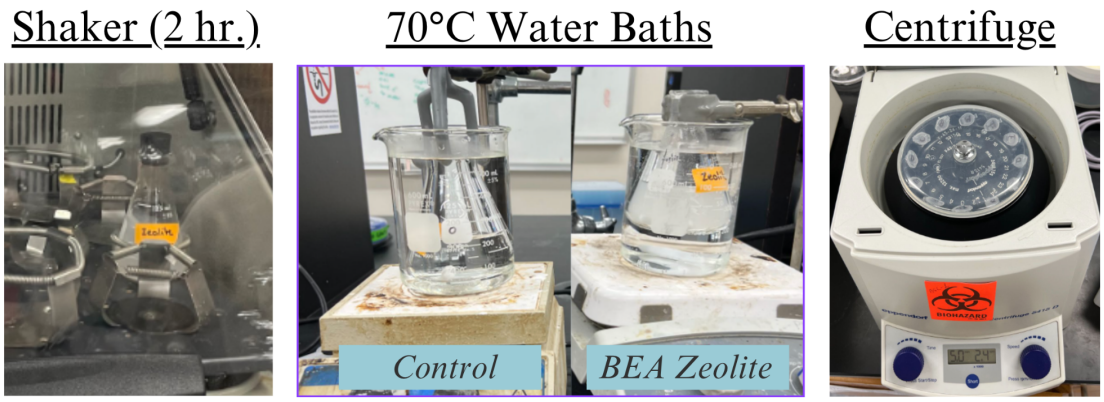

Figure 6. Experimental schematic of the degradation of PFOA and GenX forms of PFAS using heat-activated persulfate in the presence of zeolite.

Equipment:

- BEA Zeolite
- Sodium persulfate
- PFOA Stock Solution
- GenX Stock solution
- Purified water
- Methanol
- 125 mL Erlenmeyer flasks
- Laboratory Shaker

- Centrifuge
- 1.5 mL centrifuge tubes
- 100 mL graduated cylinder
- Thermometers
- Hot plate (x2)
- 500 mL beaker (x2)
- Stir bars
- pH strips
- Fisherbrand Finnpipette II 20-200 µL automatic pipettes
- Norrel 502-7 NMR tubes

Procedure:

1. Acquire all necessary equipment.
2. Take the 4 mM stock solution out of the fridge and transfer it to a stir plate. Let the solution mix for 10 minutes.
3. Once the solution is done mixing, use a micropipette to combine 540 µL of the stock solution and 60 µL of deuterated methanol in a 5mm NMR tube for later analysis.
4. Measure 60 mL of purified water and 20 mL of PFOA stock using a 100 mL graduated cylinder and add it to a 125 mL Erlenmeyer flask fitted with a stir bar. Label the flask "Zeolite" and let it mix on a stir plate for 3 minutes.
5. Use a micropipette to combine 540 µL of the solution and 60 µL of deuterated methanol in a 5mm NMR tube for later analysis.
6. Repeat steps 4-5 with a new 50 mL Erlenmeyer flask. Label this flask "Control."
7. To the "Zeolite" flask, add 0.4 grams of BEA zeolite (See *Table 8*).
8. Shake the "Zeolite" flask for 2 hours in the laboratory shaker.
9. At the end of 2 hours, use a micropipette to combine 540 µL from the "Control Flask" and 60 µL of deuterated methanol in a 5mm NMR tube for later analysis.
10. Using a micropipette add 1000 µL of methanol and 100 µL of Zeolite suspension to a 1.5 mL centrifuge tube.
    a. Make sure to fill a second centrifuge tube with just water. This ensures that the centrifuge is balanced
11. Centrifuge the sample prepared in step 10 at 2500 rpm for 5 minutes.
    a. Make sure to load water opposite of the zeolite tube to keep the centrifuge balanced.
12. After five minutes, use a micropipette to combine 540 µL of the supernatant and 60 µL of deuterated methanol in a 5mm NMR tube for later analysis.
    a. This is to see how much PFAS adsorbed to the zeolite surface
13. Add two 500 mL beakers to two separate hot plates, each fitted with a magnetic stir bar (See *Figure 6*). Using a 100 mL graduated cylinder, add 300-400 mL of water to both beakers, and turn on the heating. Place thermometers inside each water bath to record when the temperature reaches 70℃.
14. Once the temperature reaches 70℃, add a stir bar to each flask and submerge each flask into the water baths.
15. Next, measure two separate samples of 1.9524 grams of sodium persulfate (100 mM or 23.81 g/L) and add them to each flask.
16. Once the sodium persulfate is added, start a timer, record the initial pH in both flasks

using pH strips, and record the temperature.

17. Let the reaction run for 100 minutes. Every 20 minutes, record the pH and temperature and take samples for later NMR analysis.
18. To collect samples from the control beaker follow the steps below:
    a. Using a micropipette, add 1000 μL of the flask solution in a 1.5 mL centrifuge tube.
    b. Centrifuge the sample at 2500 rpm for 5 minutes.
    c. After five minutes, use a micropipette to combine 540 μL of the supernatant and 60 μL of deuterated methanol in a 5mm NMR tube for later analysis.
19. To collect each sample in the "zeolite" beaker follow the steps below:
    a. Using a micropipette, add 1000 μL of methanol and 100 μL of zeolite suspension to a 1.5 mL centrifuge tube.
    b. Centrifuge the sample prepared in step 10 at 2500 rpm for 5 minutes.
    c. After five minutes, use a micropipette to combine 540 μL of the supernatant and 60 μL of deuterated methanol in a 5mm NMR tube for later analysis.
20. After 100 minutes, turn hot plates off and dispose of waste and clean glassware (See cleaning procedure)
21. Repeat steps 1-20 at the two zeolite dosages listed in *Table 8* (2.5 and 10 g/L)

4.0 Results and Discussion

4.1 PFAS Detection and Quantification using NMR

The team utilized NMR to quantify the concentration of PFOA and GenX over the course of each reaction. Please refer to the following sections for more information on the NMR spectra collected from samples of PFOA and GenX prepared at ratios of 90% water to 10% deuterated methanol. Additionally, the standard curves for both compounds were based on concentrations of 4, 2, 1, 0.5, and 0.1 mM.

4.1.1 PFOA Standard Curve

After obtaining NMR spectra with varying PFOA concentration, each spectrum was processed to adjust the peak phases. Additionally, as shown in *Figure 21* below, the F_{19}-NMR cryoprobe produces a distinct, wavy baseline that must be corrected before continuing further analysis.

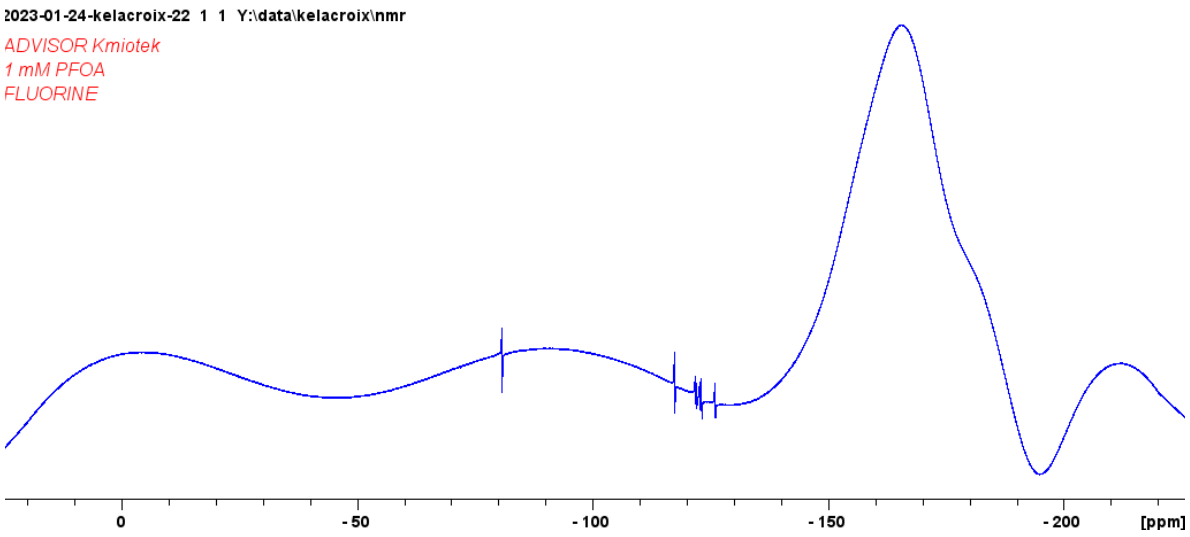

Figure 21. Unprocessed NMR spectrum for an aqueous 1 mM PFOA sample.

NMR spectra include peaks for each unique fluorine group. As PFOA contains seven carbon atoms bonded directly to fluorine, the team expected to observe seven distinct peaks. *Figure 7* below is the NMR spectrum obtained for a 1 mM aqueous solution of PFOA.

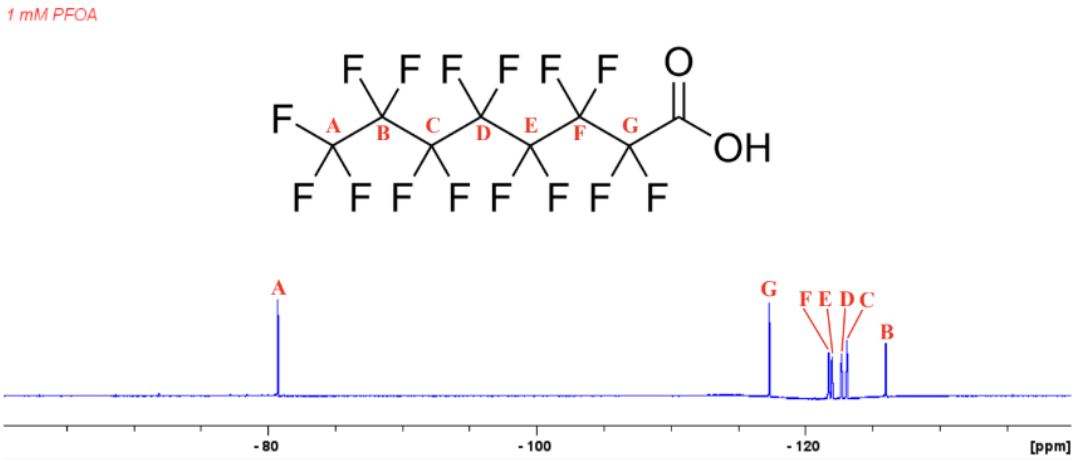

Figure 7. NMR Spectra for a 1mM aqueous PFOA solution.

As predicted, the spectrum did contain seven peaks for each fluorine group. *Table 9* below indicates the average chemical shift for each peak.

Table 9. Chemical shifts of each of the seven peaks indicated by letters "A-G" in Figure X.

Chemical Shifts (ppm)						
A	**B**	**C**	**D**	**E**	**F**	**G**
-80.73	-125.97	-123.07	-122.7	-121.98	-121.71	-117.30

The terminal -CF_3 group, denoted by "A" in *Figure 7*, is the most distinctive of the seven peaks as it is located far away from adjacent groups. These three fluorine atoms also have two adjacent fluorine neighbors. Consequently, the team predicted a signal with a triplet shape. *Figure 22* below is a zoomed in view of the terminal -CF_3 signal.

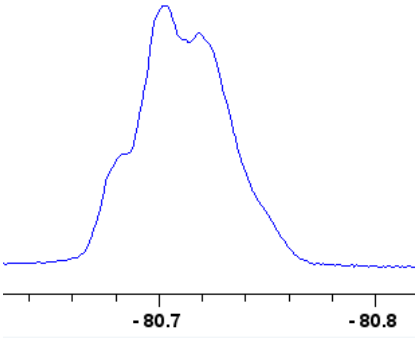

Figure 22. Zoomed in view of the terminal -CF_3 peak, detonated "A" in Figure 7.

While broad in shape, *Figure 22* shows that there are three distinctive points in the -CF_3 peak. This observation is consistent with predicted triplet shape and will be significant for later analysis. *Figure 23* below is the NMR spectra obtained for PFOA solutions at the two following concentrations: 4 and 0.1 mM.

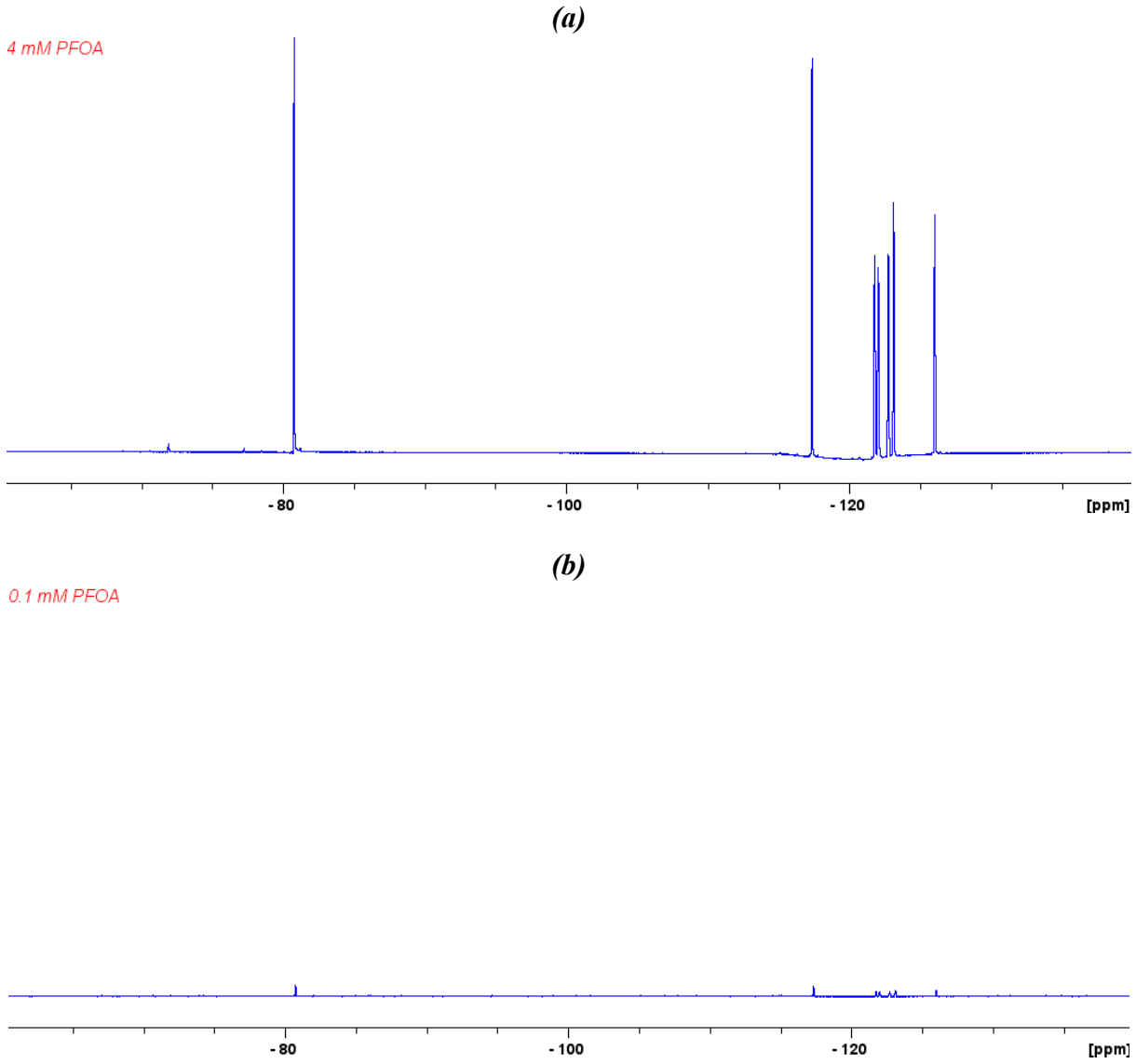

Figure 23. Sample NMR Spectra for (a) 4mM and (b) 0.1mM aqueous PFOA solutions.

As shown above, the concentration of PFOA in solution affects the strength or intensity of terminal -CF_3 signal. The team, therefore, predicted that the area under this peak could accurately quantify PFOA concentration. *Figure 2* below plots PFOA concentration versus the area under the terminal -CF_3 peak.

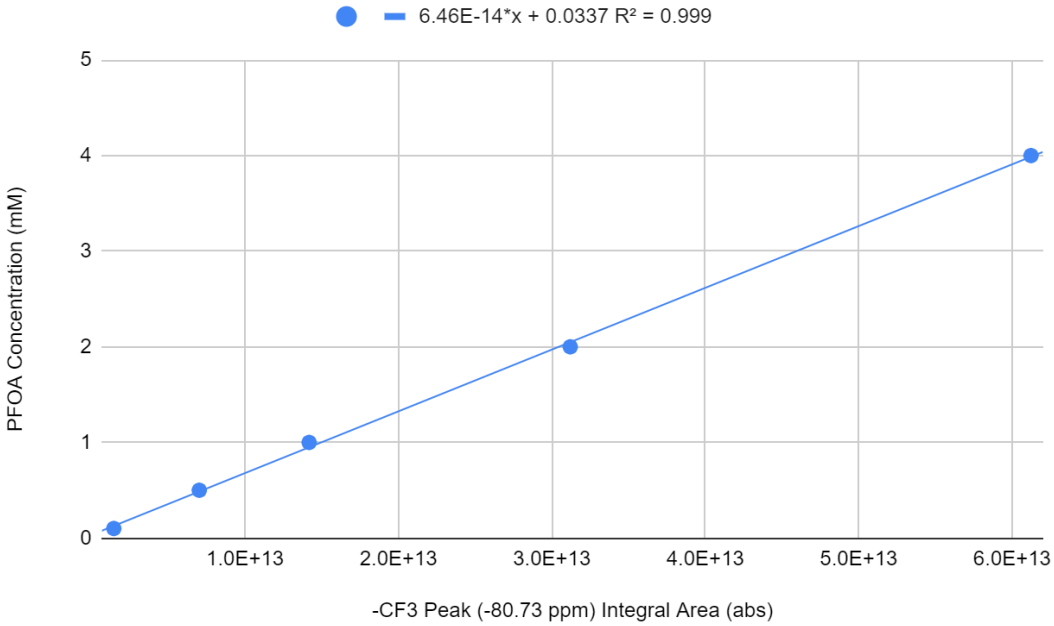

Figure 2. PFOA Standard curve plots concentration versus peak area of terminal -CF_3 group.

In the standard curve above, the R^2 value for a linear fit was 0.999, indicating a very high degree of correlation between PFOA concentration and the peak integral area of the -CF_3 group. Therefore, the team used this standard curve to calculate the concentration of PFOA over the course of the three reactions studied.

4.1.2 GenX Standard Curves

As GenX is a "short chain" alternative for PFOA, the compound has a unique NMR spectrum.

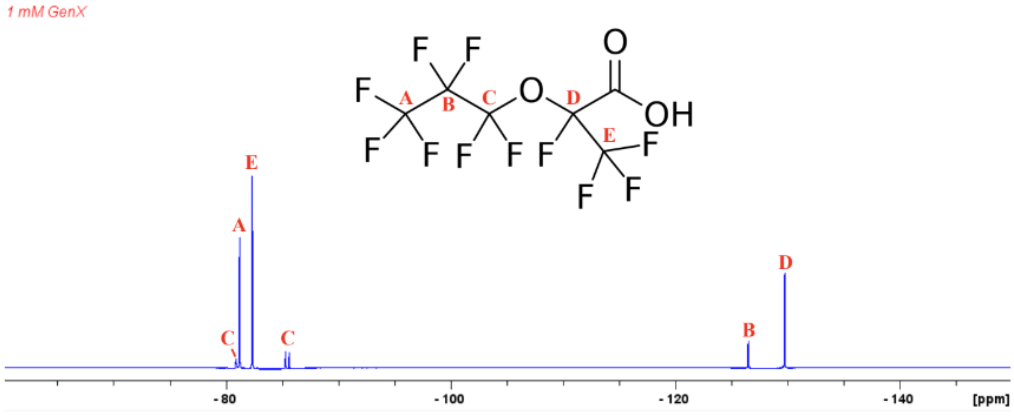

Figure 8. NMR Spectra for a 1mM aqueous GenX solution.

Figure 8 above is the NMR spectrum obtained for a 1 mM aqueous solution of GenX. As predicted, the spectrum for GenX contains fewer peaks than PFOA because there are fewer fluorine groups. Additionally, unlike PFOA, the GenX spectrum contains many peaks in the -80 ppm region. As shown in *Figure 8*, these peaks correspond to the terminal -CF_3 group (A), the internal -CF_3 group neighboring the carboxylic acid (E), and the internal -CF_2 group neighboring the ether linkage (C). Additionally, the internal -CF_2 group is broken into two regions, one located before (C_1) and one after (C_2) the -CF_3 peaks. In total, there are six distinct peak regions in the GenX NMR spectrum. *Table 10* below indicates the average chemical shift for each peak.

Table 10. Chemical shifts of each of the six peak regions indicated by letters "A-E" in Figure 16.

Chemical Shifts (ppm)					
A	**B**	**C_1**	**C_2**	**D**	**E**
-81.20	-126.52	-80.88	-85.46	-129.75	-82.34

Figure 24 below is the NMR spectra obtained for GenX solutions at the two following concentrations: 4 and 0.1 mM.

(a)

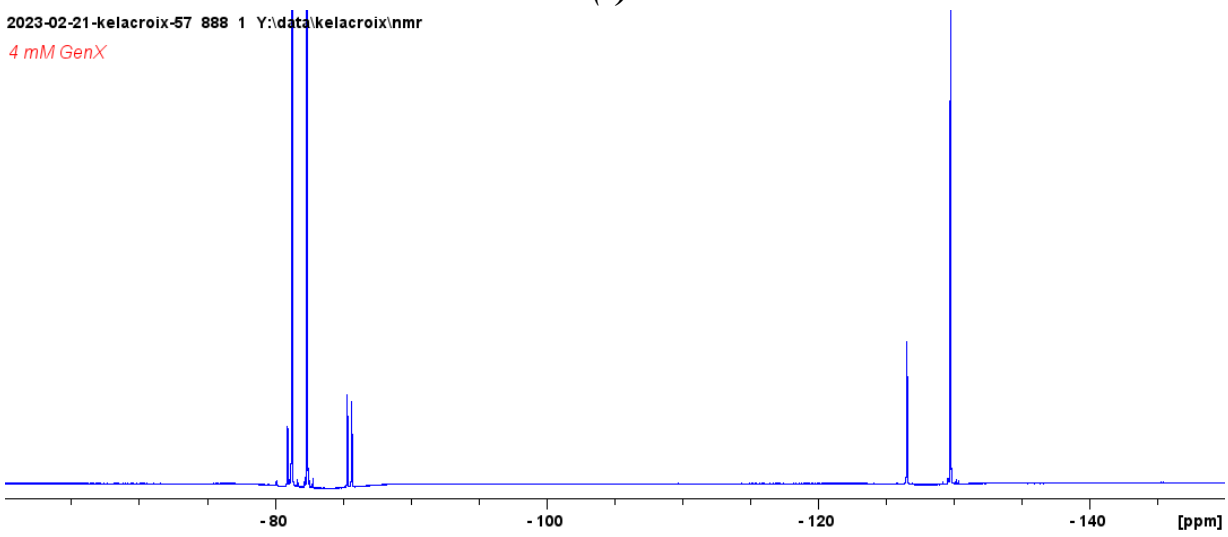

(b)

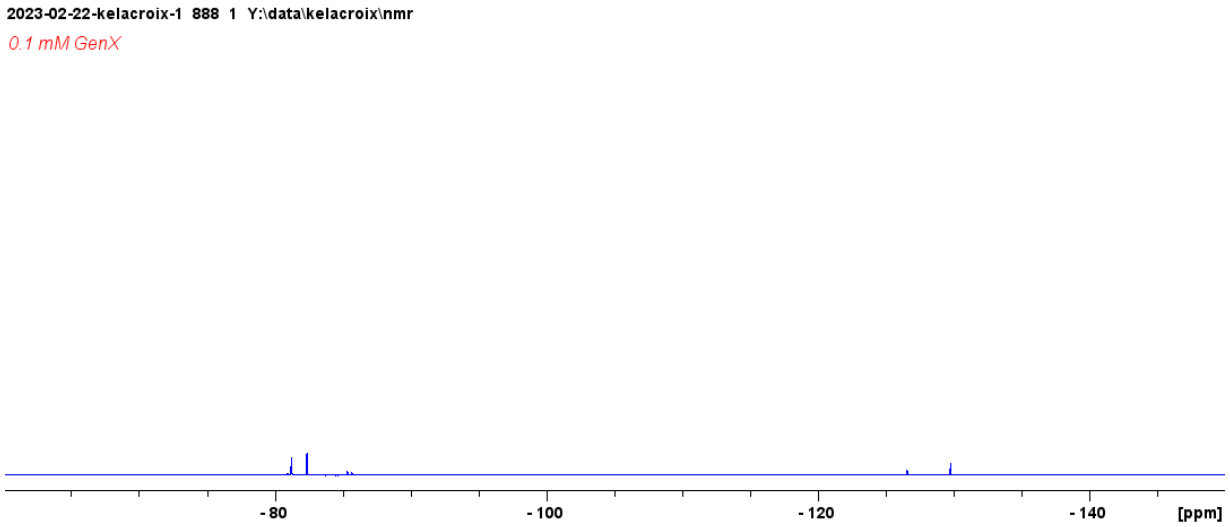

Figure 24. Sample NMR Spectra for (a) 4mM and (b) 0.1mM aqueous GenX solutions.

Similar to PFOA, the concentration of GenX in solution affects the strength of the -CF_3 signal. However, because there are two -CF_3 signals in the GenX spectra, the compound requires two standard curves. *Figures 3 & 4* below plot the GenX concentration versus the area under the terminal and internal -CF_3 peaks, respectively.

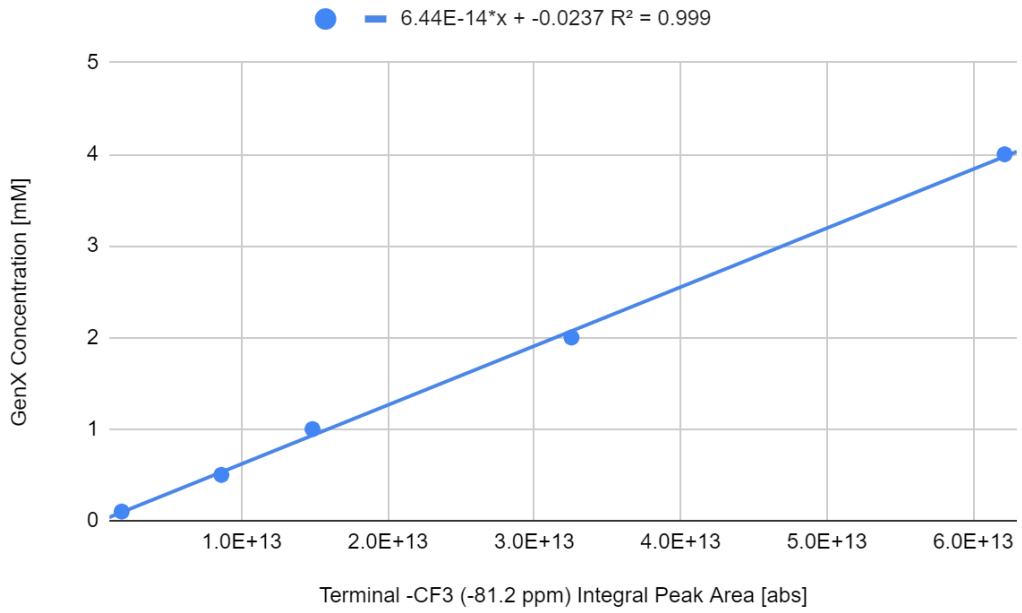

Figure 3. GenX standard curve plots concentration versus peak area of terminal -CF_3 group.

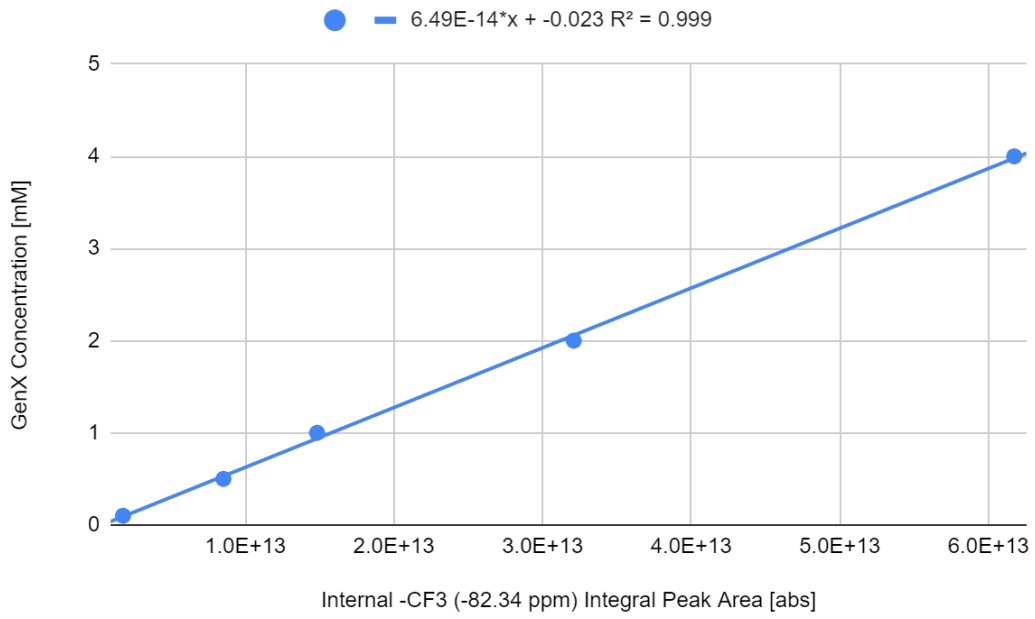

Figure 4. GenX standard curve plots concentration versus peak area of internal -CF_3 group.

In both standard curves, the R^2 value for a linear fit was 0.999, indicating a high degree of correlation between GenX concentration and the peak integral areas under the -CF_3 peaks. Therefore, the team calculated the concentration of GenX samples as the average between both standard curves.

4.1.3 Stock Concentration over Time

As part of the methodology, 4 mM stock solutions were prepared to facilitate the dilution process. The team stored the stock in plastic containers and kept them in the fridge. While convenient, the team had a few concerns with this storage process. Namely that the PFAS would dissolve out of solution when placed in the fridge for long periods of time and that PFAS would potentially stick to the walls of the plastic container. Therefore, the team took samples from the stock solution before each experiment and prepared a new stock solution at the end of each week. *Figure 25* below displays the concentration of the PFOA stock over the course of our lab work.

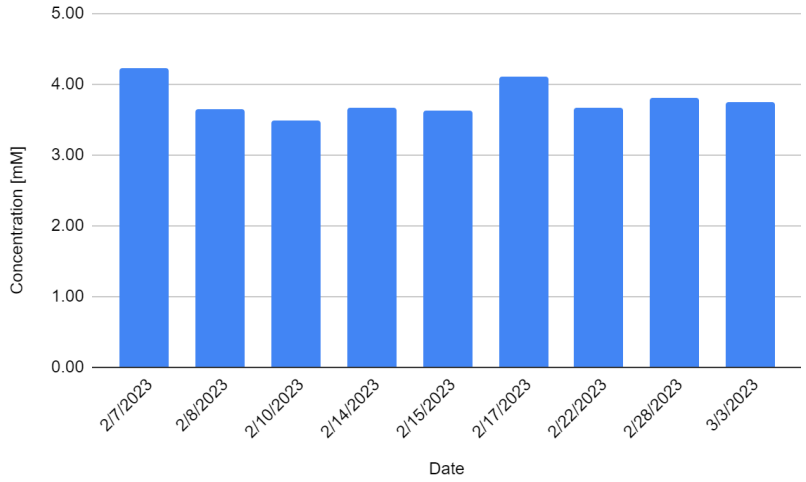

Figure 25. Concentration of 4 mM PFOA stock solution over time.

While the same procedure was followed in preparing each solution, the stock concentration did not precisely match the desired 4mM. On 2/7/23 and 2/17/23, the stock was slightly higher than 4mM. On the rest of the dates, the stock was somewhat less concentrated than 4mM. As mentioned previously, this may be attributed to the storage of the stock solution.

4.2 Ga_2O_3 Photocatalytic Degradation of PFOA Assisted with PMS

The first set of experiments sought to degrade 1 mM aqueous solutions of PFOA using a Ga_2O_3 photocatalyst assisted with PMS. In total, the team conducted three trials using the following molar ratios of PMS to PFOA: 1:1, 2:1 and 4:1. For each trial studied, two reaction beakers ran simultaneously, one containing a 254 nm UV lamp and one without a UV lamp. Additionally, each reaction was monitored for a total of 100 minutes.

As mentioned in section *3.5*, the team collected samples every 20 minutes to track the change in PFOA concentration over time. *Figure 26* below shows the NMR spectra for samples taken at (a) 0 and (b) 100 minutes from the 1:1 PMS to PFOA trial with UV light.

(a)

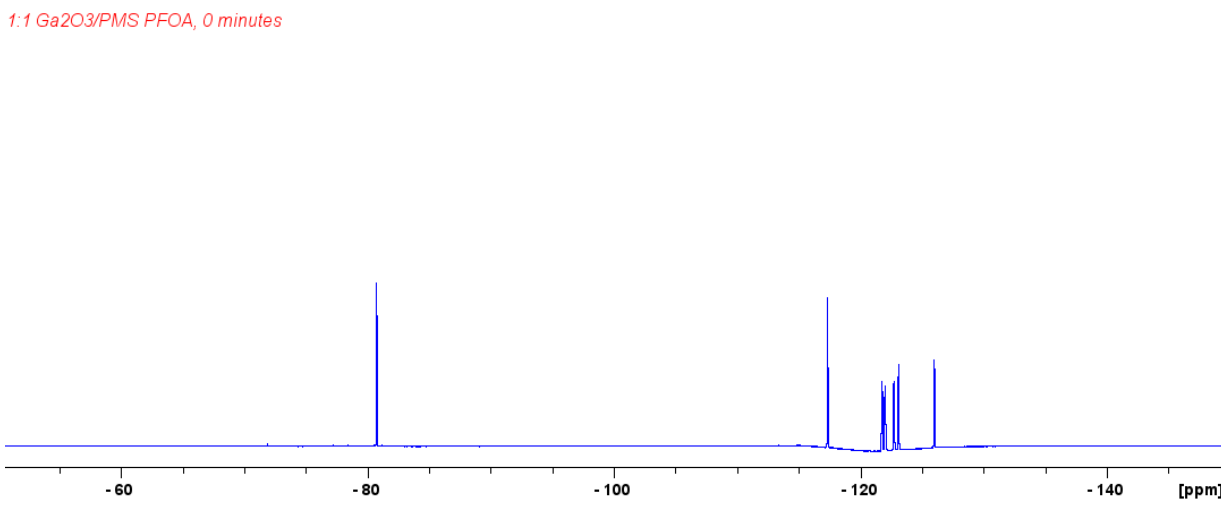

(b)

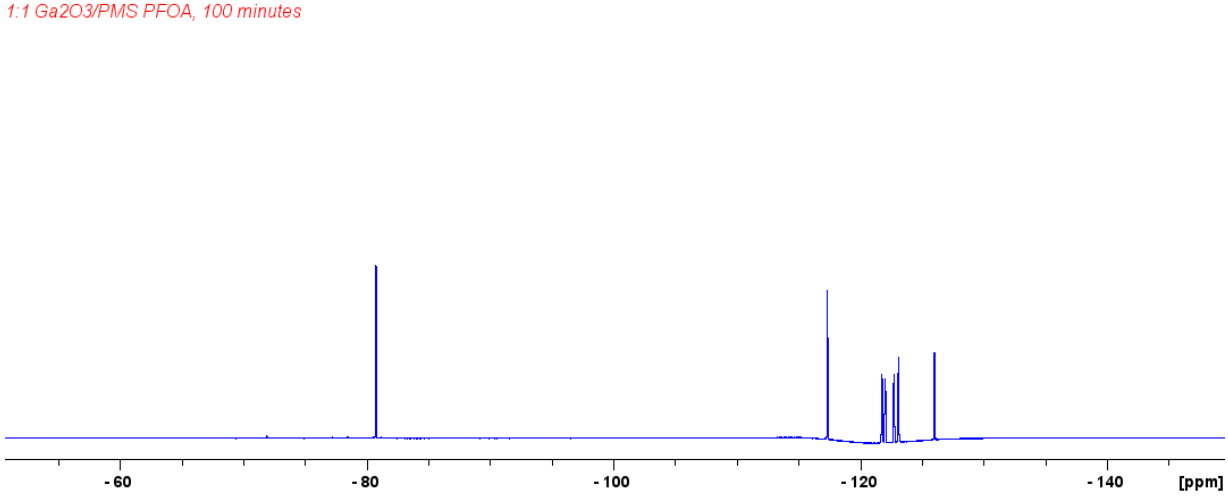

Figure 26. NMR spectra for samples taken at (a) 0 minutes and (b) 100 minutes from the 1:1 Ga_2O_3/PMS/UV PFOA reaction.

As shown in *Figure 26* above, there is no noticeable reduction in peak intensity between the sample collected 0 minutes and the sample collected at 100 minutes. This finding seems to suggest little to no reduction in PFOA concentration over the course of the 100 minutes. Additionally, no additional peaks appear in the spectrum at 100 minutes. NMR is incredibly sensitive to fluorine atoms in distinct chemical environments. Therefore, the absence of new peaks likely indicates the absence of byproducts. Together, these two findings indicate that this oxidation mechanism was not successful at significantly reducing the PFOA concentration or degrading the molecule in the 100 minute time span studied.

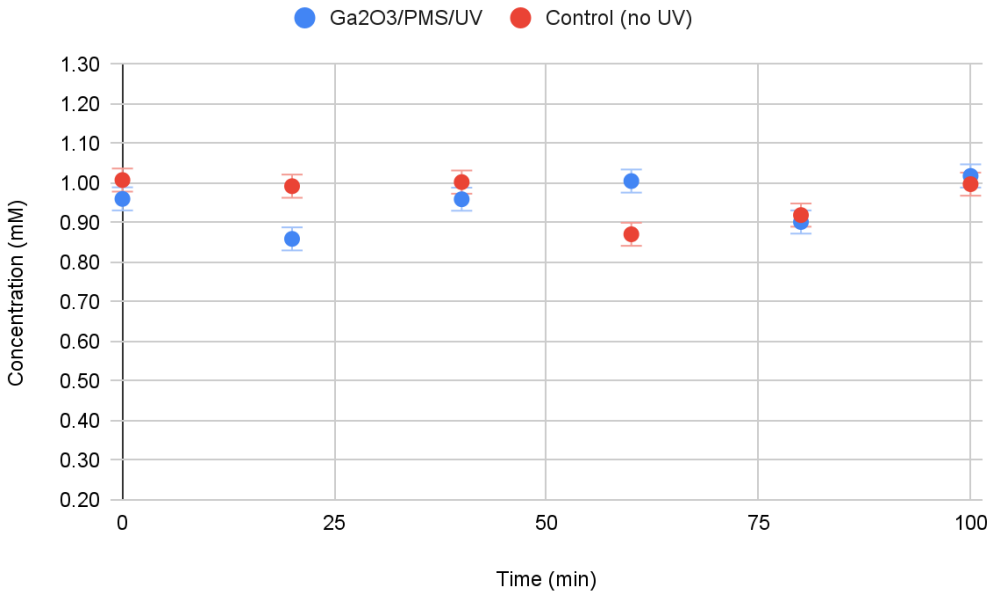

Figure 27. Plot of PFOA concentration versus time for 100 minutes Ga_2O_3 and UV-Activated PMS oxidative reaction conducted at a 1:1 PMS to PFOA dosage.

Figure 27 above plots the PFOA concentration versus time for the first trial (1:1 molar ratio of PMS to PFOA). The team expected the PFOA concentration to decrease over time. However, the concentration in the UV reactor, represented by the blue data points, and the control beaker, represented by the red data points, oscillate within a narrow range, approximately 0.8 to 1.1 mM. This rise and fall in the concentration profiles seems to illustrate PFOA's high chemical stability and incredible resistance to degradation. Over 100 minutes, the reaction mixture exposed to UV light experienced a 15.8 $\pm$5.1% increase in concentration, while the control experienced a 1.0 $\pm$ 0.3% reduction in concentration.

These results were unexpected. Firstly, it is very unlikely that the PFOA concentration in the beaker exposed to UV increased over the course of 100 minutes. This would suggest that broken down PFOA radicals recombined in solution. However, the chain length of PFOA reduces the probability of this type of collision from being statistically likely. The oscillating shape of the concentration profile indicates that the concentration of PFOA remained relatively unchanged throughout the reaction. Therefore, an increase in the PFOA concentration is likely explained by errors in the collection technique, such as using a larger volume of the reaction mixture and a smaller volume of deuterated methanol than originally intended in the 90% to 10% ratio. As the total volume is on the micro-liter scale, these small fluctuations in volume have the potential to dilute or alter the final concentration recorded. The second unexpected result was the comparison between the control and the UV beakers. UV light activates the species that drive the oxidation process: sulfate radicals and Ga_2O_3. Therefore, the team expected a lower degradation rate in the

control beaker as the conditions do not facilitate the creation of radical species. In this trial, the use of UV light did not facilitate or enhance the degradation process as originally expected, likely because the concentration of Ga_2O_3 and PMS were too low.

Table 11: Table of the percent of PFOA degraded in 100 minutes in the Ga_2O_3/PMS reaction with and without UV light at the three following PMS:PFOA molar ratios: 1:1, 2:1, 4:1.

PMS:PFOA Molar Ratio	Percent of PFOA Degradation in Control	Percent of PFOA Degradation with UV
1:1	1.0 ±0.3%	- 15.8 ± 5.1%
2:1	4.9 ±2.1%	12.0 ± 4.2%
4:1	1.0 ±0.3%	1.5 ±0.3%

Table 11 above shows the percent of PFOA degraded in 100 minutes using 2:1 and 4:1 ratios of PMS to PFOA. Like the spectra in trial one, over the course of 100 minutes, there was no significant reduction in the peak intensity and no additional peaks formed. These observations, again, indicate that at the oxidant concentrations studied, the mechanism was relatively unsuccessful at degrading PFOA.

As shown in *Table 11* above, increasing the oxidant concentration had little effect on the percent of PFOA degraded after 100 minutes. This was unexpected because increasing the concentration of PMS should increase the number of sulfate radicals in solution and the probability of collision. However, these results indicate that the oxidant concentrations studied are likely too low; therefore, the effect of increasing oxidant concentration doesn't significantly increase the collisions between the radicals and the PFOA molecules. Between trials, the addition of UV light also seems to have little effect on the percent of PFOA degraded. While unexpected, this finding indicates that the limiting factor is likely the concentration of oxidants used. Therefore, it may be beneficial for future studies to examine molar ratios above 4:1.

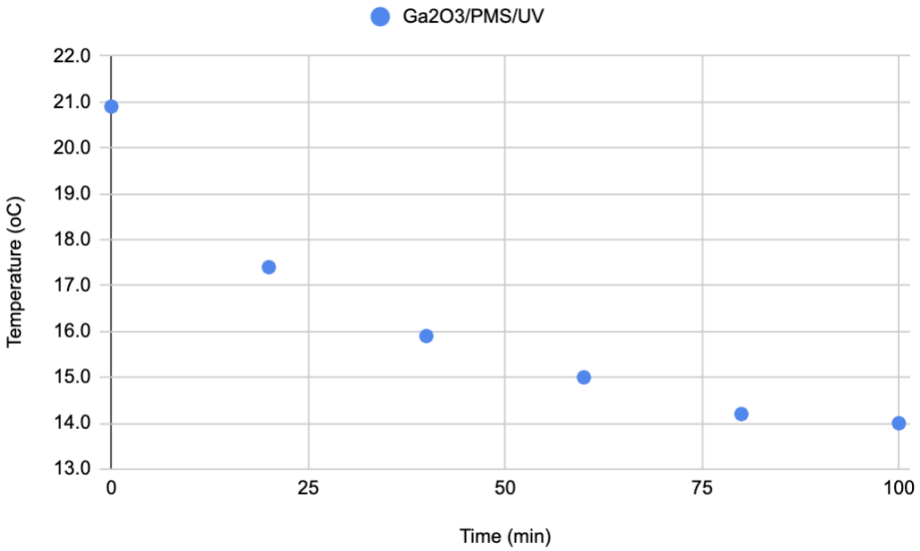

Figure 28. Plot of temperature versus time for 100 minute TiO_2 and UV-Activated PMS oxidative reaction conducted at a 4:1 PMS to PFOA dosage.

Figure 28 above plots the temperature of the 4:1 Ga_2O_3/PMS/UV reaction mixture versus time. In this trial, the temperature profile exhibits a decreasing exponential trend, plateauing between 80 and 100 minutes.The UV lamp requires cooling water to prevent a build up of heat. Initially, the team suspected that the cooling water could explain the decreasing temperature trend. However, the temperature of the cooling water used was approximately 22.0 ± 0.1^oC, while reaction flask reached a minimum temperature of 14.0 ± 0.1^oC at 100 minutes. As the reaction mixture reaches lower temperatures, the water cooling water can not be responsible for heat transfer observed. Based on these observations, the team concluded that the reaction is likely endothermic. Therefore, in addition to low oxidant concentration, the mechanism may require additional heat sources to drive the reaction. However, as the team did not record the temperature profiles in the two previous trials, this observation has a low level of reproducibility.

4.3 TiO_2 Photocatalytic Degradation of PFOA Assisted with PMS

The second advanced oxidation reaction studied the use of titanium dioxide (TiO_2) and UV-activated peroxymonosulfate (PMS) on a 1mM aqueous solution of PFOA. Three trials were conducted using molar ratios of 1:1, 2:1, and 4:1 of PMS to PFOA. Each trial set consisted of an experimental reaction exposed to a 254 nm UV lamp and a simultaneous control reaction without UV exposure. The reaction solutions were sampled every 20 minutes from 0 to 100 minutes and quantified with NMR.

As mentioned previously, the first experiment used a 1:1 molar ratio of PMS to PFOA. The NMR spectra for samples taken at 0 and 100 minutes are shown in *Figure 29* below. Similarly to spectra with Ga_2O_3, there is no clear reduction in peak intensity or formation of new peaks over the course of 100 minutes. This observation also holds true for the spectra in trials 2 and 3 with higher oxidant concentration (See *Appendix C*).

(a)

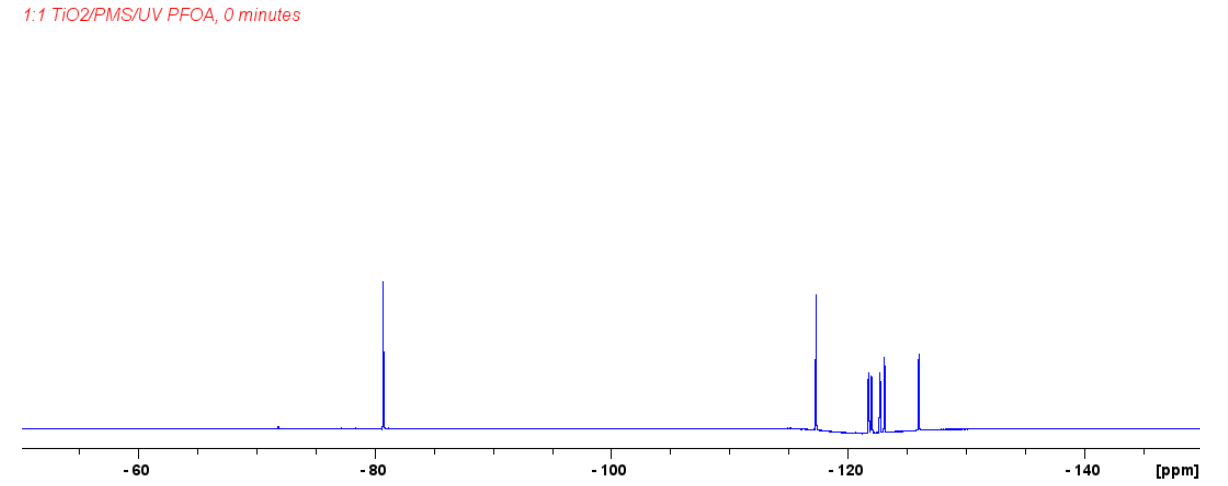

(b)

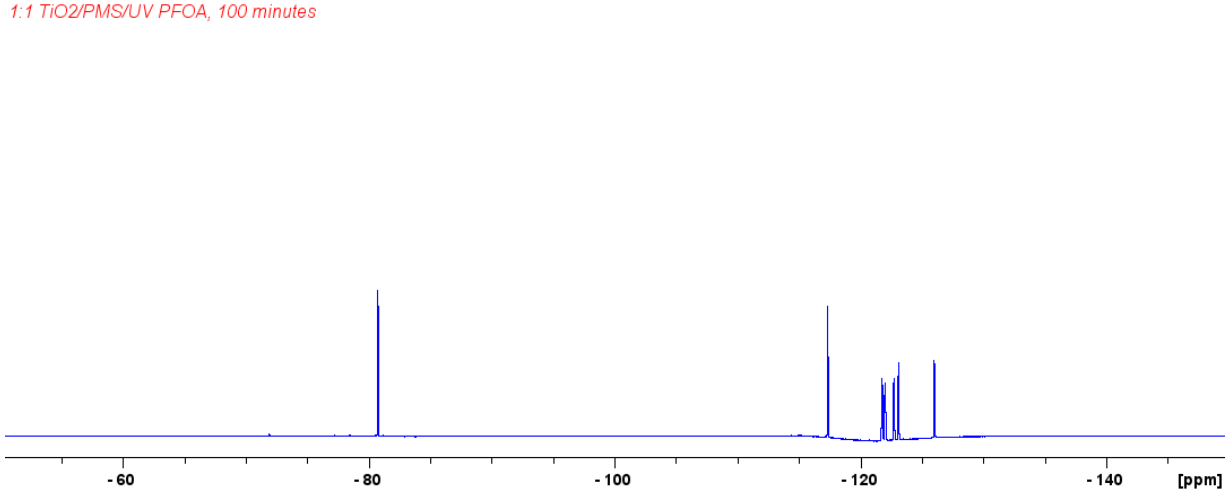

Figure 29. NMR spectra for samples taken at (a) 0 minutes and (b) 100 minutes from the 1:1 TiO_2/PMS/UV PFOA reaction.

The NMR results are quantified in *Figure 30* below. Over the course of the 100 minutes, the concentration profile of the control and the UV reactor show no explicit trend or correlation. Additionally, the experimental group with UV-light exposure saw a 3.1% PFOA degradation in 100 minutes, while the control experienced a 1.4% increase in PFOA concentration in 100 minutes.

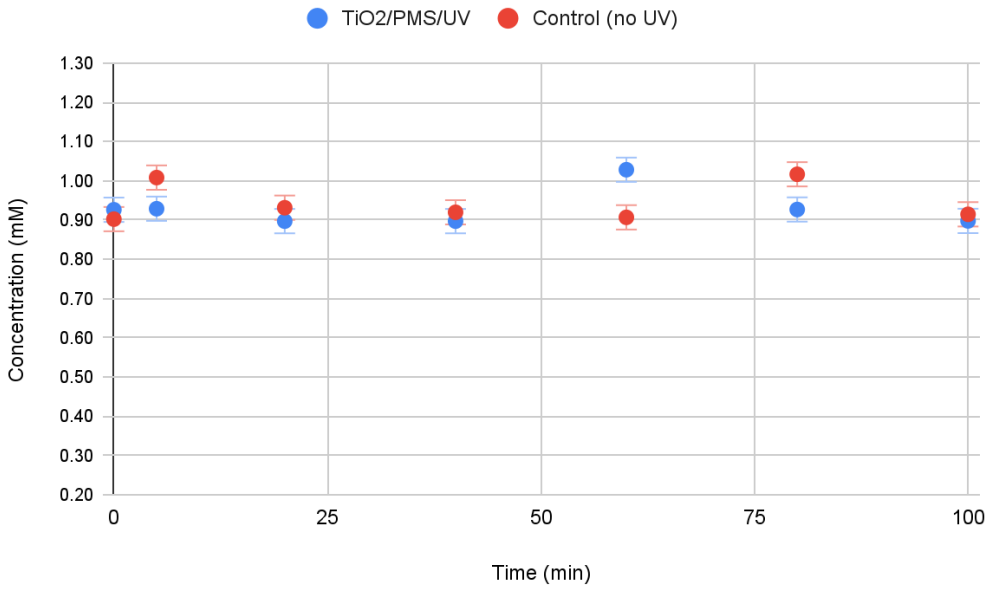

Figure 30. Plot of PFOA concentration versus time for 100 minutes TiO_2 and UV-Activated PMS oxidative reaction conducted at a 1:1 PMS to PFOA dosage.

Similar amounts of degradation occurred in the 2:1 ratio and the 4:1 ratio of PMS to PFOA. The degradation data is shown below in *Table 12*. These degradation amounts lie within our presumed error and therefore have no definitive significance. Further, it is unlikely that our control test produced more PFOA and was likely a result of measurement error. The advanced oxidation reaction likely did not occur or only occurred below the detectable limit.

Table 12: The percentage of PFOA degradation over a 100 minutes TiO_2 and UV-Activated PMS oxidative reaction conducted at 1:1, 2:1, and 4:1 PMS to PFOA dosage.

PMS to PFOA Dosage Ratio	TiO2/PMS/UV PFOA Degradation	Control PFOA Degradation
1:1	3.1%	-1.4%
2:1	1.5%	-7.4%
4:1	0.6%	-7.6%

Throughout the lab the temperature of both the experimental group and control group were recorded every 20 minutes. The temperature data displayed below in *Figure 31* displays that the experimental group saw a temperature decrease displaying a 6.7 C° decrease over the course of the reaction while the control remained relatively constant. This is in part contributed to by the flow of water through the outer shell of the UV lamp meant to keep it cool. However, the

temperature dropped below the temperature of the cooling water indicating the possibility that the reaction could be endothermic.

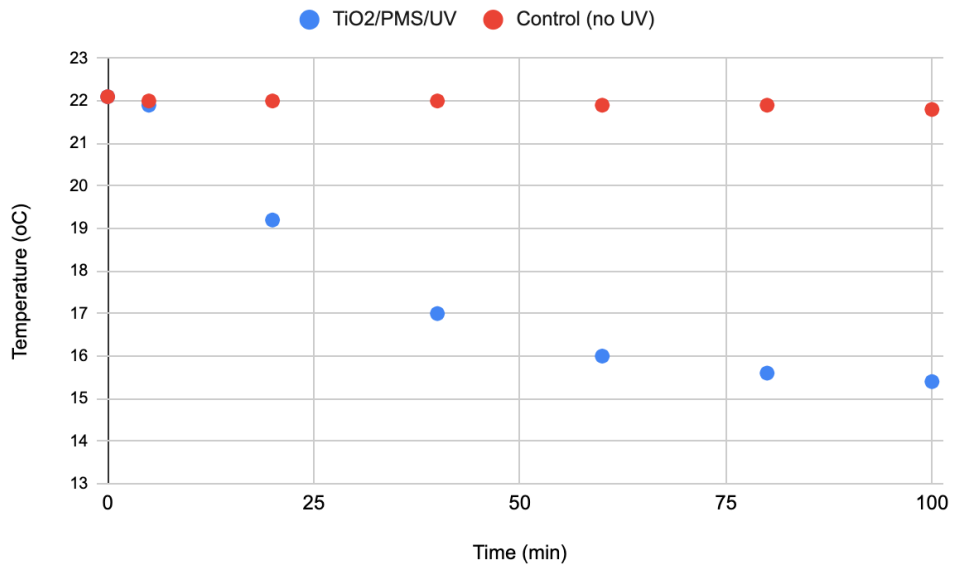

Figure 31: Temperature change over a 100 minutes TiO_2 and UV-Activated PMS oxidative reaction conducted at 1:1 PMS to PFOA dosage.

Similar phenomenon was seen in all trials of our experiment. *Table 13* displays the total temperature decreases over the 100 minutes for all dosages. The experimental group consistently saw a 6-7 degree temperature decrease whereas the control group remained at a relatively constant temperature. This reinforces our belief that the reaction could possibly be endothermic.

Table 13: The temperature difference over a 100 minutes TiO_2 and UV-Activated PMS oxidative reaction conducted at 1:1, 2:1, and 4:1 PMS to PFOA dosage.

PMS to PFOA Dosage Ratio	**TiO2/PMS/UV PFOA Temperature Change**	**Control PFOA Temperature Change**
1:1	-6.7C°	-0.3C°
2:1	-6.8C°	-0.1C°
4:1	-7.3C°	-0.2C°

4.4 Degradation of PFOA using Heat Activated Persulfate Assisted with Zeolite

The final advanced oxidation reaction studied was the use of heat activated persulfate (PS). In this set of experiments, four trials were performed over the course of 100 minutes. The control utilized heat activated persulfate in the absence of zeolite. The remaining trials used BEA-framework zeolites at the three following dosages: 2.5, 5, and 10 g/L.

4.4.1 Heat Activated Persulfate Control

Figure 10 below shows the NMR spectrum for samples taken from the 1 mM PFOA control flask at 0 and 100 minutes.

(a)

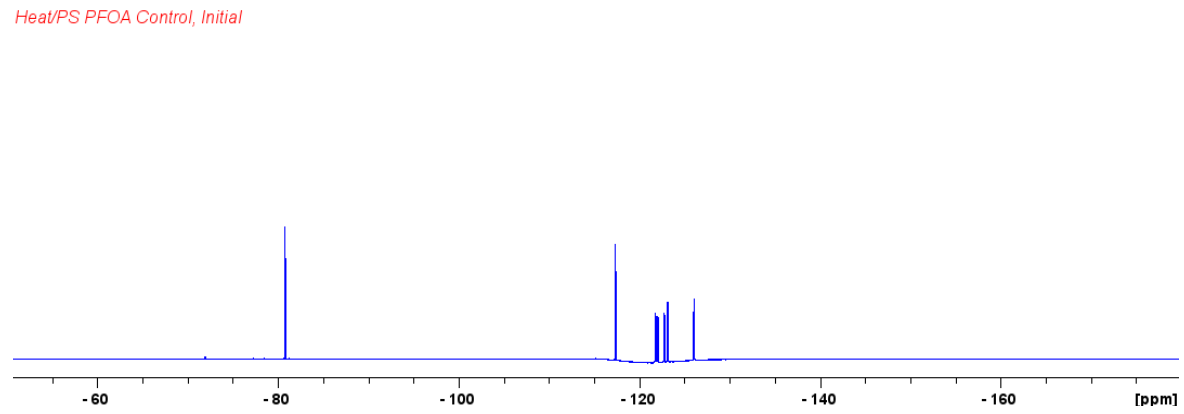

(b)

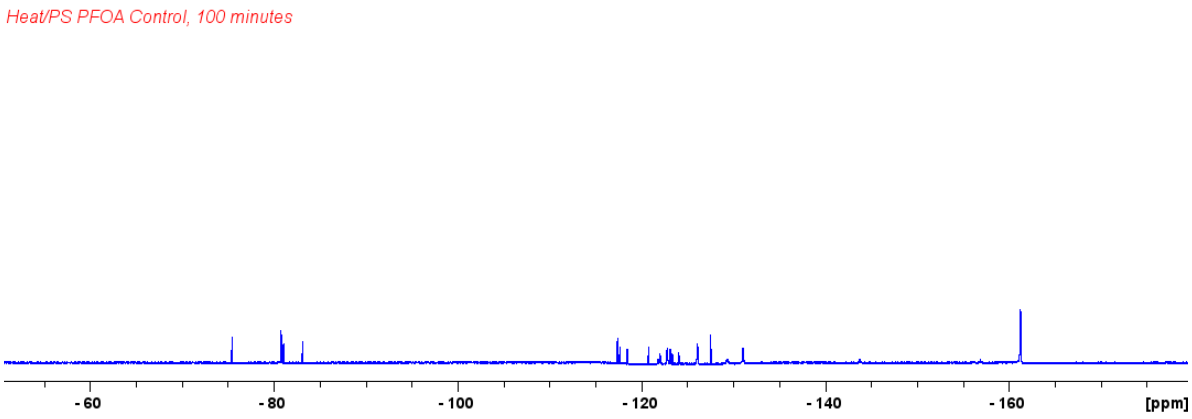

Figure 10. NMR spectra for samples taken at (a) 0 minutes and (b) 100 minutes from the PFOA, heat activated persulfate control.

There are two distinct changes in the NMR spectrum over the course of the reaction. Firstly, the intensity of the -CF_3 signal decreased over time. This observation suggests that the concentration of PFOA in solution decreased as the reaction progressed. The second change is the formation of new peaks. As shown in *Figure 27*, by the end of the reaction, there are many additional peaks observed in the -115 to -135 ppm region. Additionally, there are three clear peaks located at approximately -75, -83, and -161 ppm. The formation of new peaks suggests the formation of by-products. *Figure 32* below shows the change in the NMR spectrum between 20 and 40 minutes.

(a)

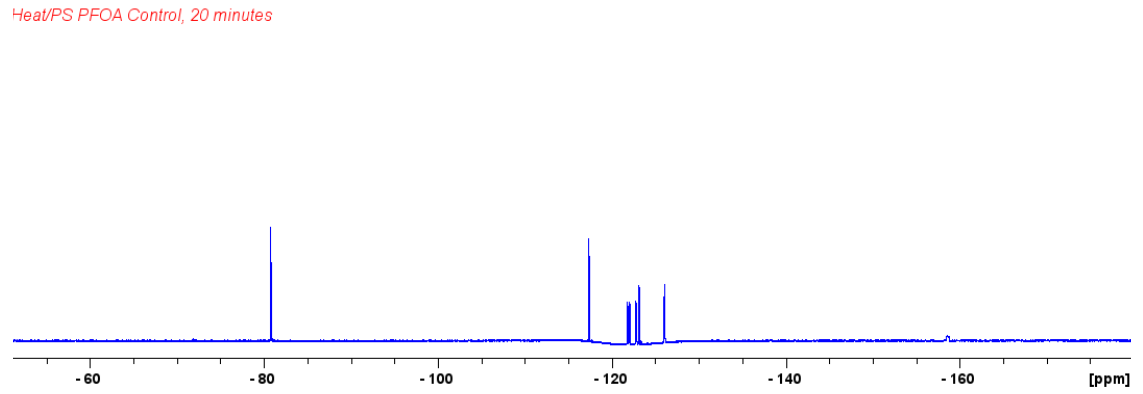

(b)

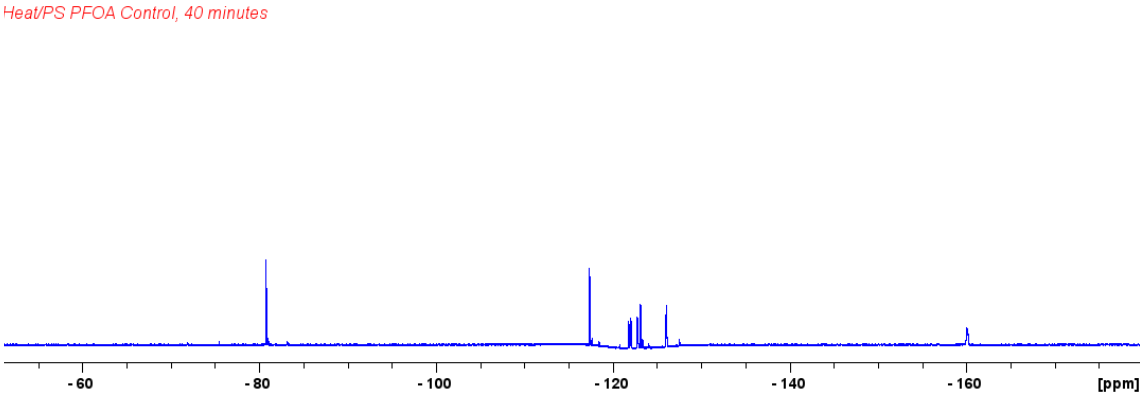

Figure 32. NMR spectra for samples taken at (a) 20 and (b) 40 minutes from the PFOA, heat activated persulfate control.

As shown above, the peak located around -161 ppm first appears in the sample taken at 20 minutes. This signal likely indicates the replacement of fluorine atoms in the carbon chain.

According to the Organic Chemistry database, trifluoromethane (CHF_3) has a chemical shift of approximately -78.6 ppm (Reich, 2020). Difluoromethane (CF_2H_2), however, has a reported chemical shift of approximately -143.6 ppm (Reich, 2020). In this case, partially replacing fluorine with hydrogen seems to deshield the remaining fluorine atoms, resulting in a higher chemical shift. As discussed in *2.6.2*, it is suspected that in the oxidation process, hydrogen atoms replace the fluorine atoms on the carbon atom closest to the headgroup, resulting in the generation of fluorine ions. Therefore, this signal around -161 ppm likely represents the formation of fluorine ions over the course of the oxidation process.

As shown in *Figure 32*, additional peaks in the -115 to -135 ppm region first appear at 40 minutes. In a pure sample of PFOA, the signals in this region represent the $-CF_2$ groups in the carbon chain. Therefore, the creation of additional peaks in this region suggests the formation of new PFAS molecules with varying chain lengths. Finally, the peaks located at around -75 and -83 ppm also become visible on the spectrum at 40 minutes. While these peaks are the most visible, additional peaks can also be observed by zooming in on the spectra. *Figure 33* below is a zoomed in view of the terminal $-CF_3$ peak over the course of the reaction.

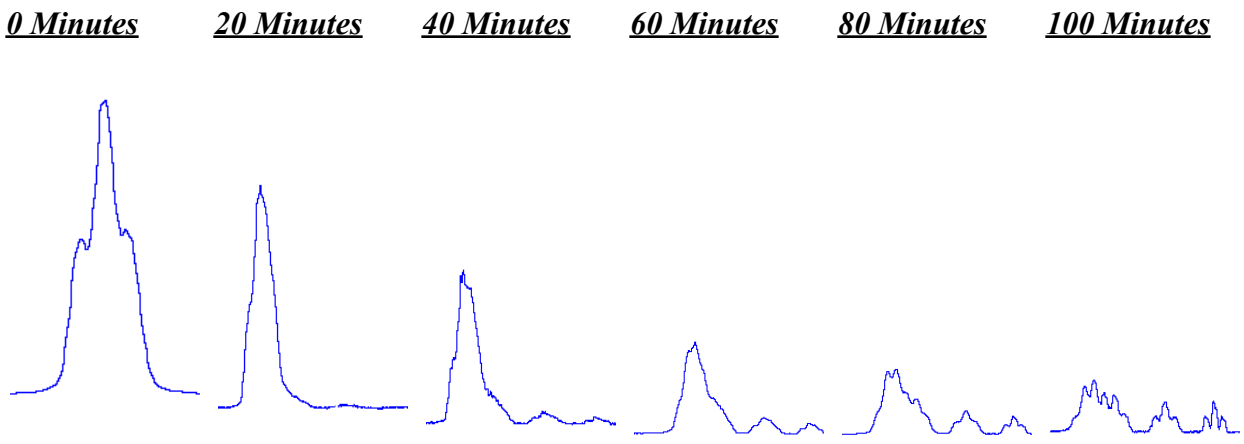

Figure 33. Change in PFOA $-CF_3$ peak shape over 100 minute-heat activated persulfate reaction.

As shown in *Figure 33* above, two new peaks emerge at roughly 40 minutes. Around this same time, the $-CF_3$ signal also begins to broaden in shape. From 40 to 100 minutes, there's continued deformation of the $-CF_3$ signal, and the intensity of the new peaks continue to increase. These observations seem to confirm the continued degradation of PFOA over the course of the reaction.

As discussed previously, the terminal $-CF_3$ group appears as a triplet in the NMR spectrum. In addition to PFOA, many other PFAS contain this terminal group. Therefore, one would expect to

observe this same triplet signal in the NMR spectra for other PFAS compounds. However, the chemical shift of the -CF_3 peak depends on the chain length of the molecule. By the end of 100 minutes, the new peaks also exhibit this triplet shape. Even the initial -CF_3 signal from PFOA appears to contain two triplets merged together. These observations of multiple triplets with varying chemical shifts confirms the formation of new PFAS molecules with varying chain lengths. *Table 14* below compares the reported chemical shifts of -CF_3 peaks in PFAS with carboxylic functional groups to the chemical shifts observed in our NMR spectrum at 100 minutes (Camdzic et al., 2021).

Table 14. Comparison of the reported -CF_3 chemical shifts in perfluoroalkyl acids with the observed chemical shifts at 100 minutes (Camdzic et al., 2021).

Chain Length	**PFAS Compound**	**Abbreviation**	**Reported -CF_3 Chemical shift (ppm)**	**Observed -CF_3 Chemical shift (ppm)**
8	Perfluorooctanoic acid	PFOA	-82.4	-80.74
7	Perfluoroheptanoic acid	PFHpA	-82.4	-80.79
6	Perfluorohexanoic acid	PFHxA	-82.5	-80.90
5	Perfluoropentanoic acid	PFPeA	-82.6	-81.00
4	Perfluorobutanoic acid	PFBA	-	-83.11
3	Pentafluoropropionic acid	PFPra	-84.9	-83.12
2	Trifluoroacetic acid	TFA	-	-75.43

As shown in *Table 14* above, as the chain length of the perfluoroalkyl acid decreases, the magnitude of the chemical shift increases, with the exception of TFA. While the study from Camdzic et al. does not provide a chemical shift for TFA, the SpectraBase indicates a chemical shift at roughly -77 ppm (Smyth et al., 1998). *Figure 11* below is a zoomed in view of the NMR spectrum in the -75 to -83 ppm region at 100 minutes.

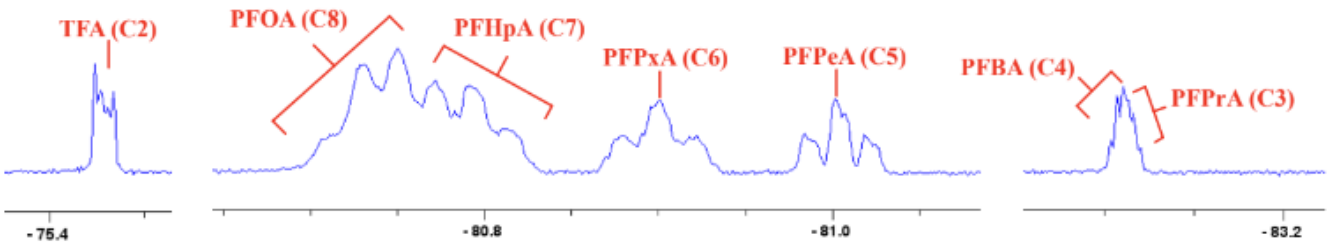

Figure 11. NMR spectrum [-75, -83 ppm] for sample taken at 100 minutes from the PFOA, heat activated persulfate control.

As shown above, our team identified seven distinct triplets in the region of -75 to -83 ppm. While the numerical values of these chemical shifts differ slightly from the reported values in *Table 14*, they follow the same trend. Therefore, the seven peaks observed in the -75 to -83 ppm region likely indicate the presence of PFOA (C8), PFHpA (C7), PFPxA (C6), PFPeA (C5), PFBA (C4), PFPrA (C3), and TFA (C2).

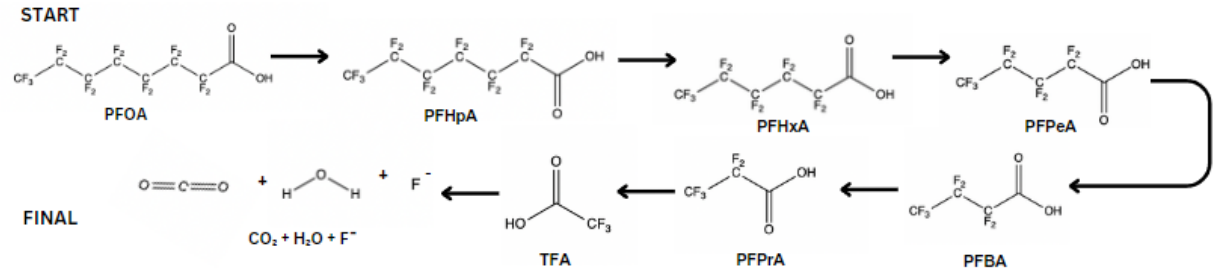

Figure 12. Reaction mechanism for the shortening of the carbon chain in PFOA.

The decline in the intensity of the PFOA signal over the course of the reaction, coupled with the existence of shorter chain perfluoroalkyl acids in solution indicates that this reaction was successful at degrading PFOA. Please see *Figure 12* above for the proposed mechanism of shortening of the carbon chain from PFOA to the point of mineralization- with CO_2, H_2O, and F^- ions. Additionally, *Figure 34* below plots the concentration of PFOA versus time.

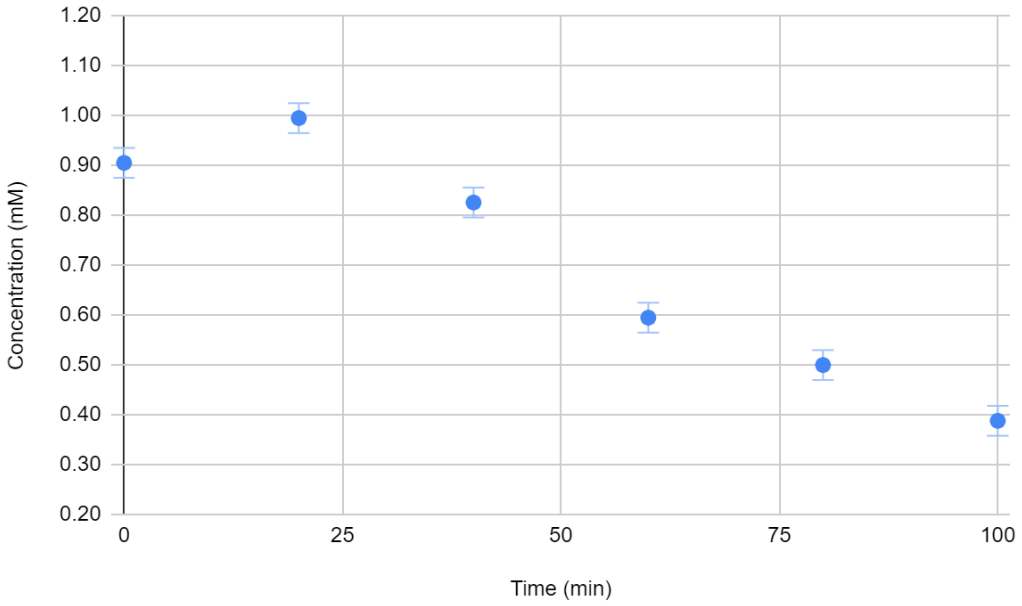

Figure 34. Plot of PFOA concentration versus time for heat activated persulfate control.

As shown above, in the first 20 minutes, the concentration of PFOA in solution slightly increased. From 20 minutes on, the concentration then steadily decreased, reaching a minimum value of 0.39 $\pm$ 0.03 mM in 100 minutes. Over the course of 100 minutes, the use of heat activated persulfate successfully reduced the concentration of PFOA by 7.2 $\pm$ 4.8%.

4.4.2 Zeolite Dosages

Figure 35 below shows the NMR spectra for a 1mM aqueous solution of PFOA with 2.5 g/L of BEA zeolites before and after 2 hours in the laboratory shaker.

(a)

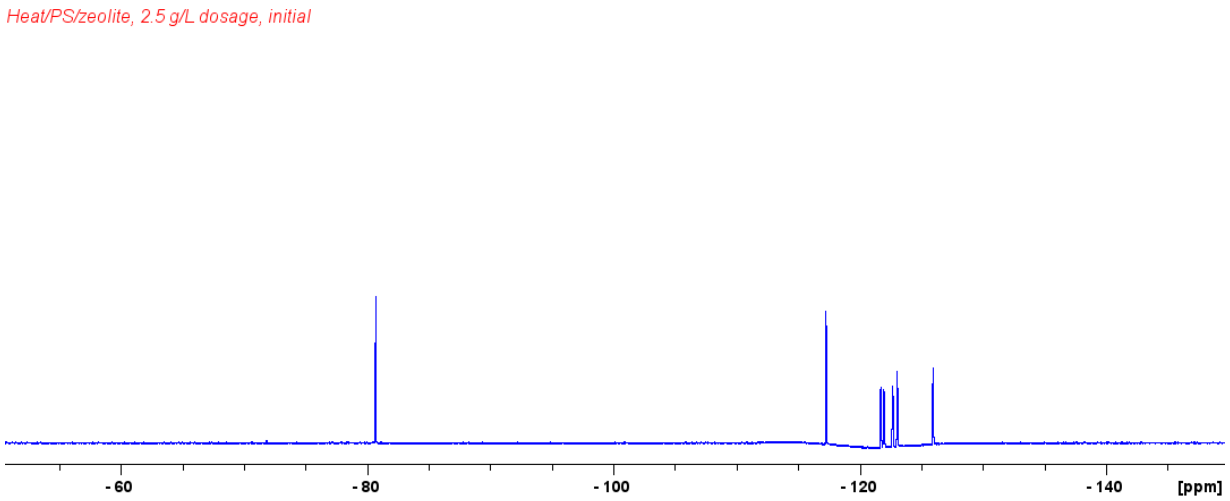

(b)

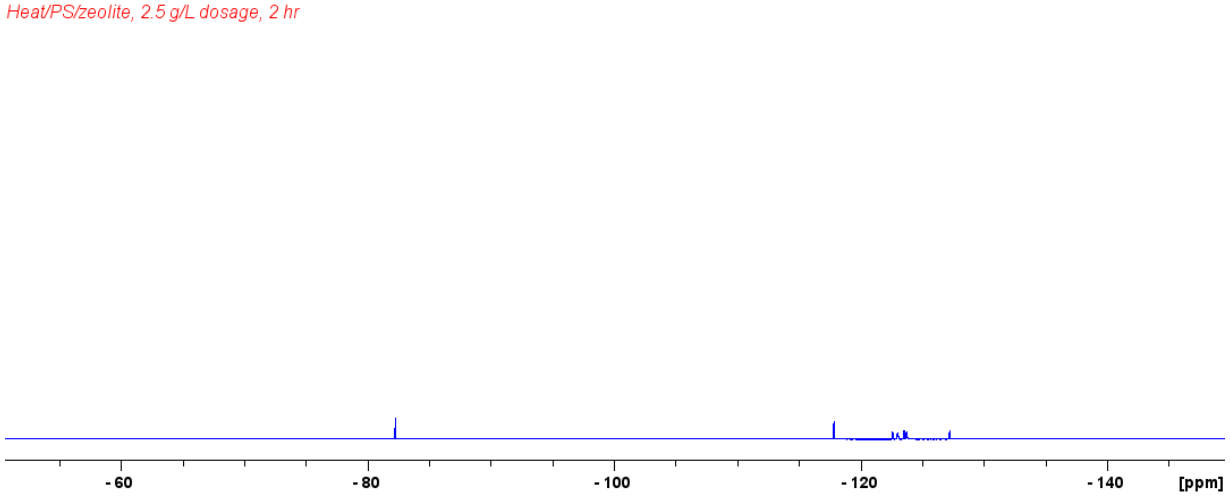

Figure 35. NMR spectrum for a 1 mM aqueous solution of PFOA with 2.5 g/L of BEA zeolites (a) before and (b) after 2 hours in the laboratory shaker.

As shown above, after 2 hours, the intensity of the signals drastically declined. This finding indicates that the concentration of PFOA in solution likely decreased due to the adsorption of PFOA onto the surface of the zeolites. *Table 15* below shows the percent of PFOA adsorbed after 2 hours at the three following zeolite dosages: 2.5, 5, and 10 g/L.

Table 15. Percent of PFOA adsorbed after 2 hours of shaking.

BEA Zeolite Dosage (g/L)	Percent of PFOA Adsorbed after 2 Hours
2.5	84.2 ± 15.5%
5	85.8 ± 19.8%
10	89.9 ± 29.0%

As the zeolite dosage increased, there was a slight increase in the percentage of PFOA adsorbed. This finding suggests that increasing the zeolite dosage effectively increases the number of zeolite particles available to adsorb PFOA molecules. *Figure 36* below plots the concentration of PFOA versus time for the control (no zeolite) and the 2.5 g/L zeolite dosage. One important thing to note is that there are no data points included at 80 and 100 minutes. The lack of data points at these times is due to automation failures with the NMR machine.

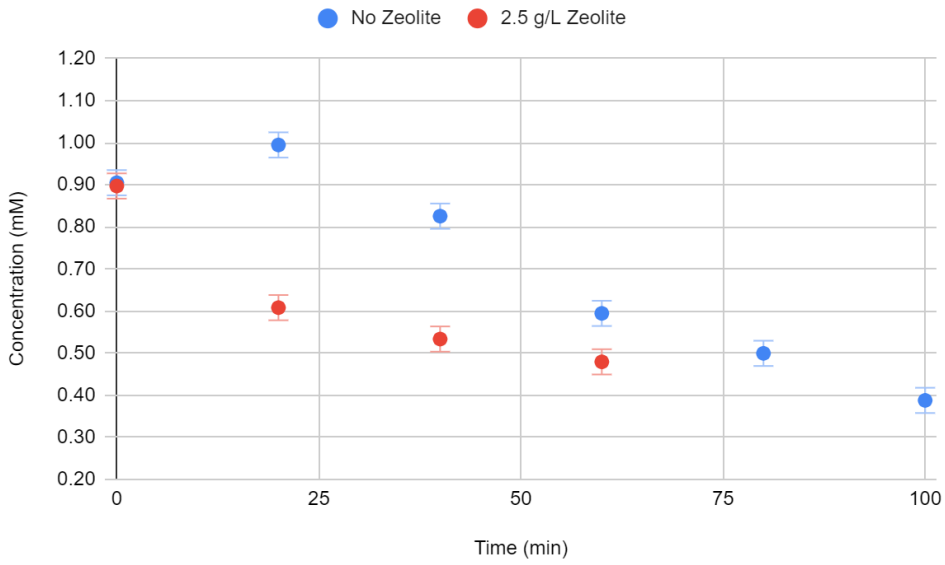

Figure 36. Plot of PFOA concentration versus time for 100 minute heat activated persulfate reaction with a 2.5 g/L zeolite dosage.

Unlike the control, the PFOA concentration does not increase from 0 to 20 minutes, but instead steadily declines over the entire 60 minutes. While we do not have data points for the concentration at 100 minutes, there was a 46.6 ± 3.3% reduction in the concentration of PFOA in 60 minutes. *Figure 37* below plots the temperature of the control and the 2.5 g/L zeolite flasks versus time.

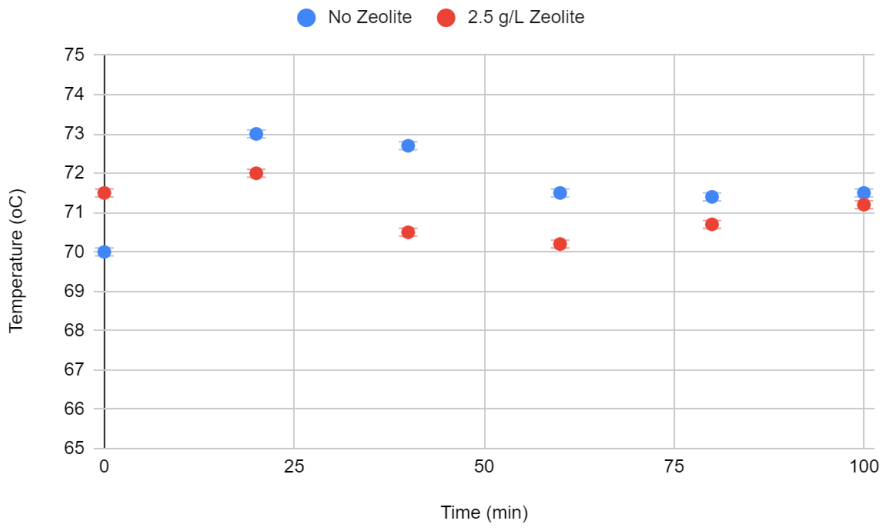

Figure 37. Plot of temperature versus time for 100 minute heat activated persulfate reaction with 1mM aqueous PFOA and a 2.5 g/L zeolite dosage.

As shown above, the temperature of the control flask was generally higher than the temperature in the 2.5 g/L zeolite flask. However, from 40 to 100 minutes, the control and 2.5 g/L zeolite flask slowly approach the same temperature.

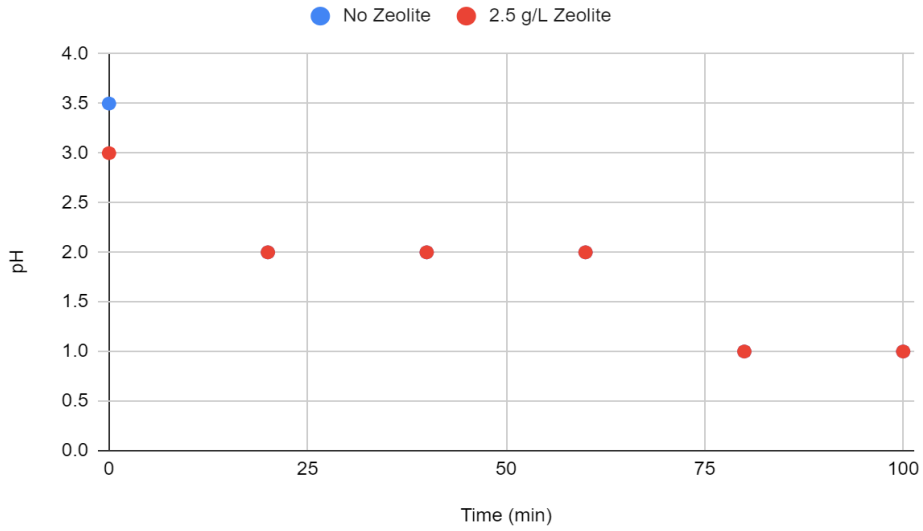

Figure 38. Plot of pH versus time for 100 minute heat activated persulfate reaction with 1mM aqueous PFOA and a 2.5 g/L zeolite dosage.

Figure 38 above plots the pH as a function of time for the control and 2.5 g/L zeolite flasks. While the starting pH of the solutions slightly vary, both the control and 2.5 g/L zeolite flasks exhibit the same change in pH over the course of the reaction. This reduction in pH from 3 or 3.5

to 1 signals a changing, more acidic environment over the course of the reaction. This evidence of a changing chemical environment supports the degradation of PFOA observed in the NMR spectrum and the reduction in concentration observed in the concentration profiles. *Figure 39* below plots the concentration profile of the control and 5 g/L zeolite flasks over the course of the 100 minute reaction.

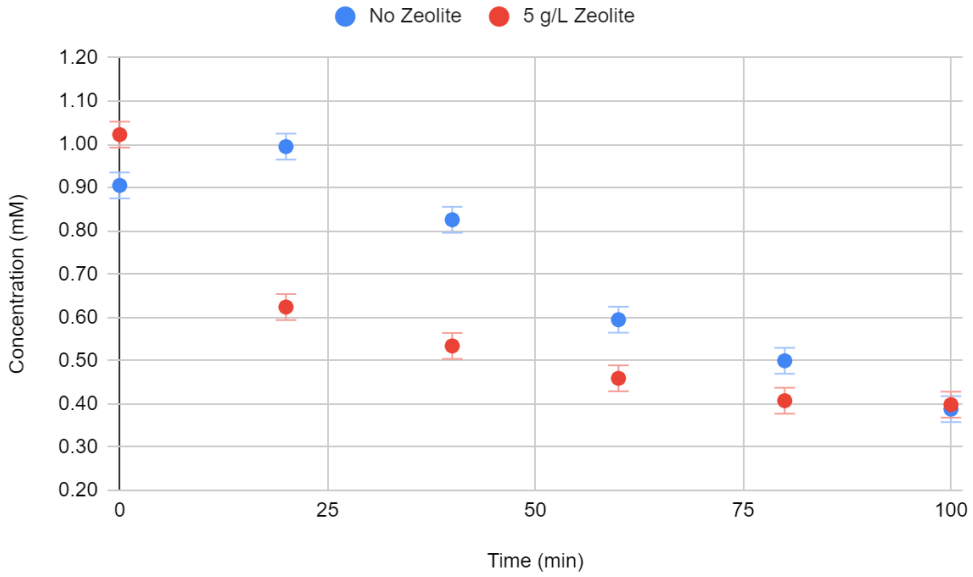

Figure 39. Plot of PFOA concentration versus time for 100 minute heat activated persulfate reaction with a 5 g/L zeolite dosage.

The 5 g/L zeolite dosage exhibits the same decreasing concentration profile observed in the 2.5 g/L trial. While the control continues to steadily decline over the course of 100 minutes, the concentration profile for the 5 g/L trial begins to plateau around 40 to 60 minutes. By the end of 100 minutes, the concentration in the control and 5 g/L flasks is roughly the same. However, as the zeolite flask has a higher initial concentration, 61.1 $\pm$ 4.9% of the PFOA was degraded by the end of the 100 minutes as opposed to the 57.2 $\pm$ 4.8% degraded in the control flask. *Figure 40* below plots the temperature profiles for the control and the 5 g/L zeolite flasks over time.

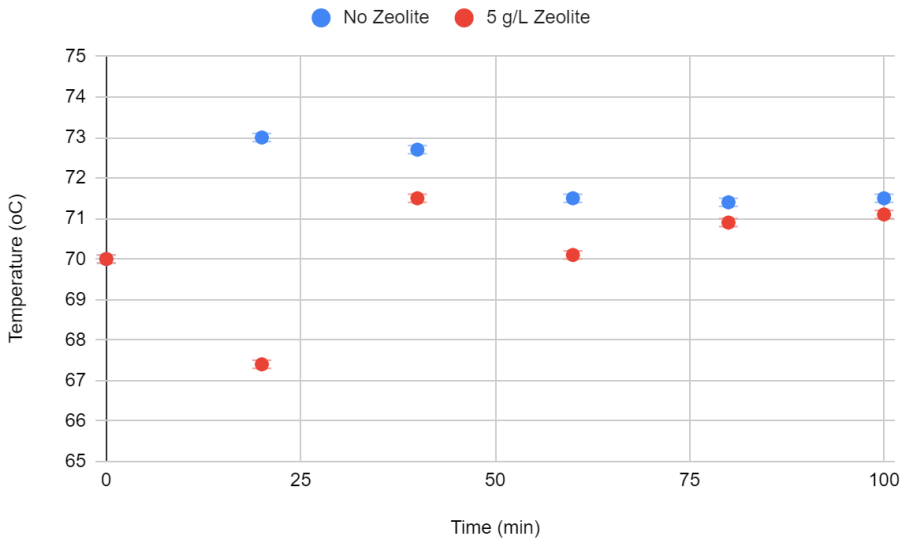

Figure 40. Plot of temperature versus time for 100 minute heat activated persulfate reaction with 1mM aqueous PFOA and a 5 g/L zeolite dosage.

Similar to the 2.5 g/L zeolite dosage, the temperature profile in the control flask is higher than in the zeolite flask. Again, as the reaction progresses, the temperatures in both flasks slowly approach the same value. As shown below, the 5 g/L zeolite dosage exhibits the same change in pH observed in the control and the 2.5 g/L zeolite trial (*Figure 41*). Again, this change in pH supports the success of PFOA degradation over time.

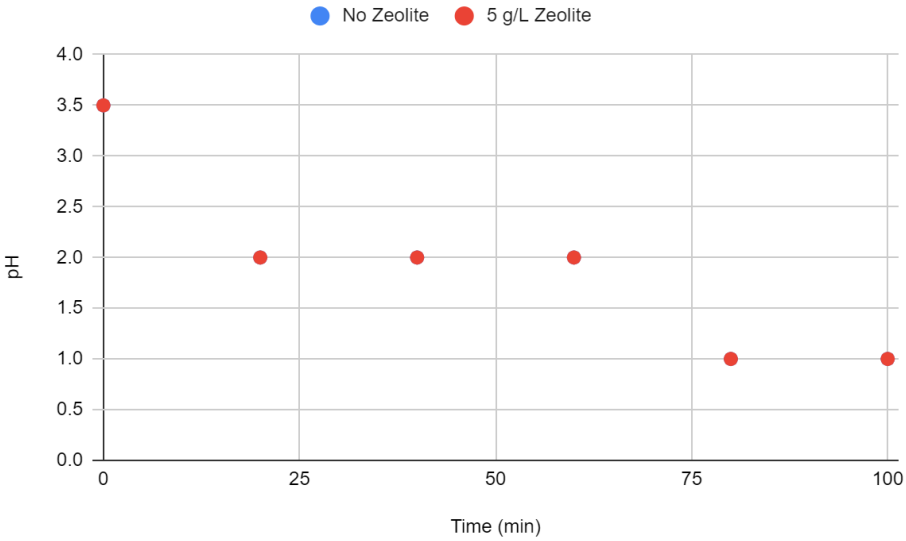

Figure 41. Plot of pH versus time for 100 minute heat activated persulfate reaction with 1mM aqueous PFOA and a 5 g/L zeolite dosage.

Finally, *Figures 42-44* plot the concentration, temperature, and pH profiles for the 10 g/L zeolite trial against the control.

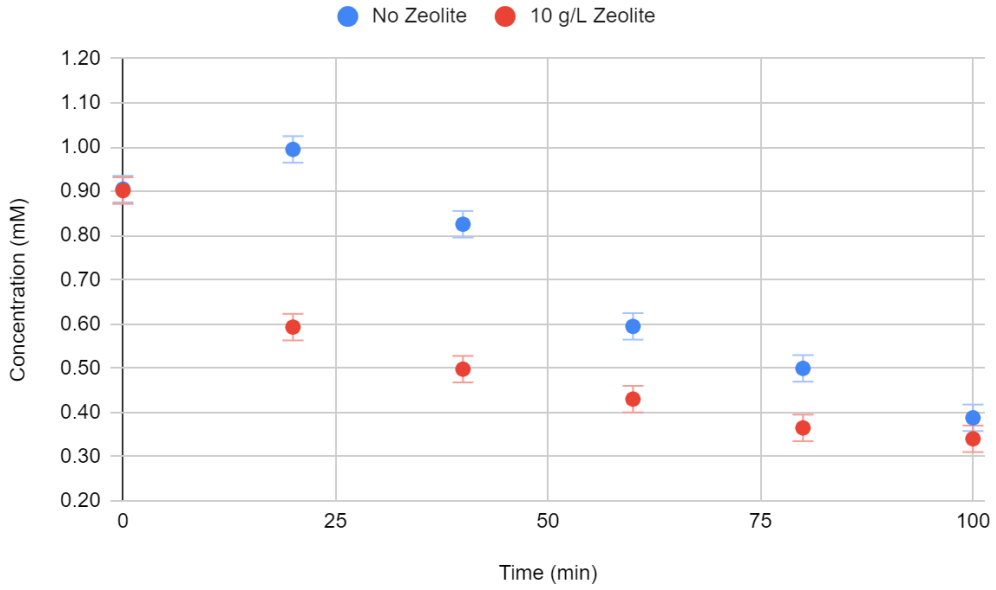

Figure 42. Plot of PFOA concentration versus time for 100 minute heat activated persulfate reaction with a 10 g/L zeolite dosage.

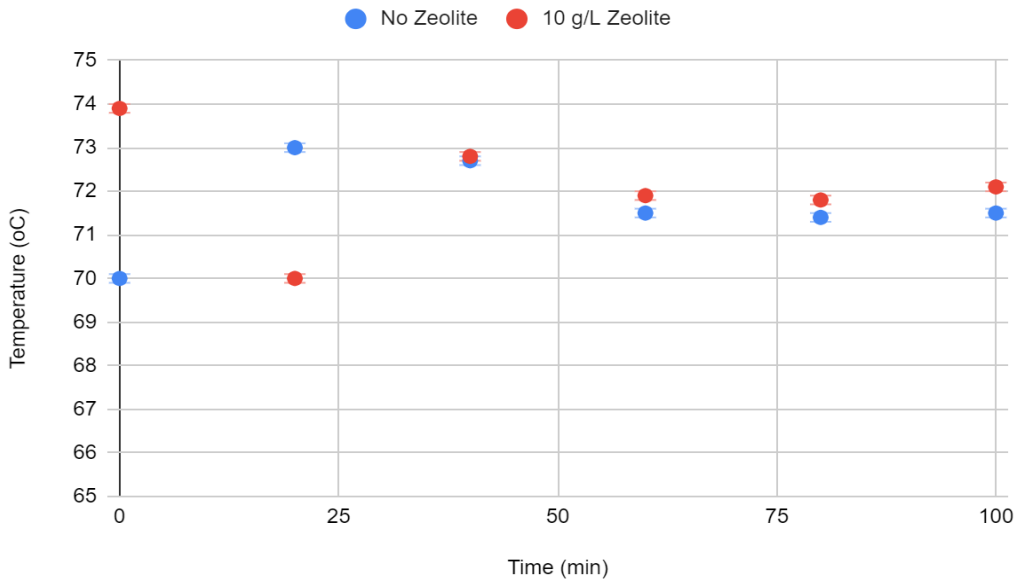

Figure 43. Plot of temperature versus time for 100 minute heat activated persulfate reaction with 1mM aqueous PFOA and a 10 g/L zeolite dosage.

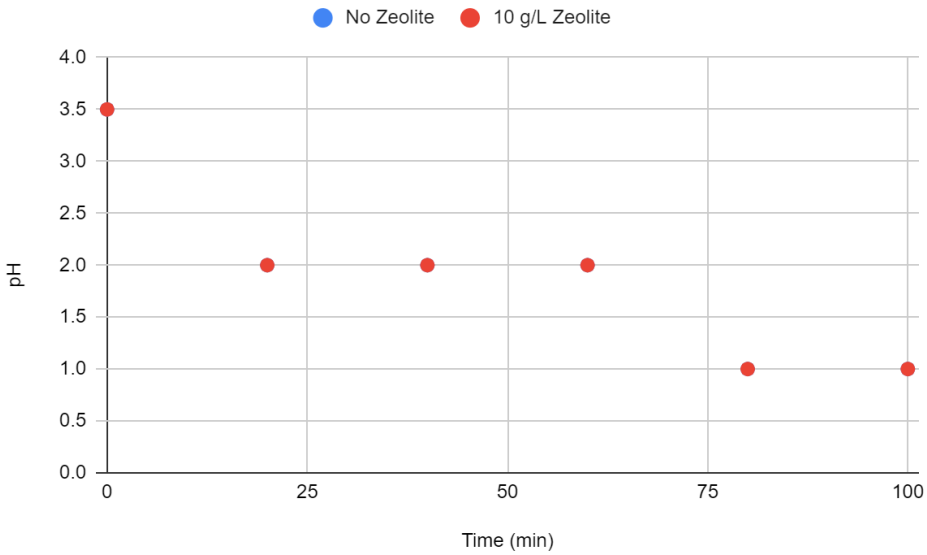

Figure 44. Plot of pH versus time for 100 minute heat activated persulfate reaction with 1mM aqueous PFOA and a 10 g/L zeolite dosage.

The 10 g/L zeolite trial exhibited the same pH change observed in the other three trials, which gives this observation a relatively high degree of reproducibility. On the other hand, the temperature profile in the 10 g/L zeolite trial differs from the temperature profiles observed in the 2.5 and 5 g/L trials. Unlike the lower dosages, the temperature in the 10 g/L flask exceeds the control flask as the reaction progresses. As for the concentration profile, like the 5 g/L zeolite trial, the concentration of PFOA steadily decreased over time, plateauing between 40 to 60 minutes. However, unlike the 5 g/L trial, the concentration of PFOA at the end of 100 minutes was lower than the concentration of PFOA in the control flask. In this trial, the team observed a c at the end of 100 minutes, the highest observed between the four trials studied.

4.4.3 PFOA Reaction Kinetics

After conducting the heat activated persulfate reactions, the kinetics were approximated using zero, first, and second order models. Each model plots a variation of PFOA concentration versus time. As shown by equation 1 below, zero order kinetics produces a linear trendline by plotting PFOA concentration versus time. As shown by equation 2, with first order kinetics, there's a linear relationship between the natural log of concentration and time. Finally, the second order plots a linear relationship between the inverse of concentration and time.

$$Zeroth\ Order\colon\ [A] = [A]_0 - kt \qquad (1)$$

$$First\ Order:\ ln[A] = ln[A]_0 - kt \quad (2)$$

$$Second\ Order:\ \frac{1}{[A]} = \frac{1}{[A]_0} + kt \quad (3)$$

Figure 45 below plots the inverse of the PFOA concentration versus time for the control and the two following zeolite dosages: 5 and 10 g/L. The 2.5 g/L zeolite dosage was excluded from this analysis due to the lack of available data points at 80 and 100 minutes. Of the three models studied, the second order approximation provided the best linear fit. Additionally, between the three trials, the lowest R^2 value observed was 0.936 (5 g/L Zeolite). Based on these observations, the heat activated persulfate reaction seems to adhere to second order kinetics.

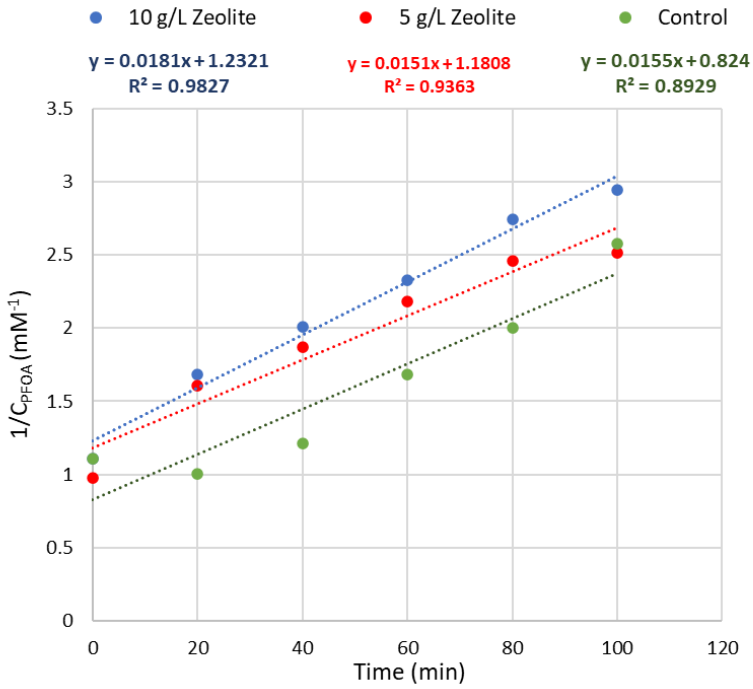

Figure 45. Plot of the inverse of the PFOA concentration versus time for heat activated persulfate reaction control, 5 g/L zeolite dosage, and 10 g/L zeolite dosage.

After identifying the reaction order, the rate constants, k, were approximated using the slopes of the linear trend lines displayed in *Figure 43*. The rate constants for the control, 5 g/L zeolite dosage, and 10 g/L zeolite dosage are shown in *Table 16* below.

Table 16. Second order rate constants for the heat activated persulfate reaction on PFOA at the tree following conditions: no zeolite (control), 5 g/L zeolite, and 10 g/L zeolite.

Trial Conditions	k ($mM^{-1}min^{-1}$)	Rate Law
Control	0.0155	$Rate = k[PFOA]^2$
5 g/L Zeolite	0.0151	$Rate = k[PFOA]^2$
10 g/L Zeolite	0.0181	$Rate = k[PFOA]^2$

As the team observed an increase in the percentage of PFOA degraded using zeolites, it was expected that the rate constant would also increase. However, as shown in *Table 16*, the rate constant for the control and the 5 and 10 g/L zeolite dosages were approximately equal. These findings suggest that the addition of zeolites within the dosages studied had limited success in enhancing the kinetics of the heat activated persulfate reaction.

While initially unexpected, these findings make sense because the concentration profiles for the 5 and 10 g/L zeolite trials plateaued around 40 to 60 minutes. The concentration profile for the control, on the other hand, continued to steadily decline over time. In each of the three zeolite dosages studied, the percentage of PFOA adsorbed after 2 hours did not exceed 90%. Based on these findings, two potential suggestions can be made. Firstly, the concentration of PFOA studied may require a higher zeolite dosage to effectively adsorb the PFOA in solution. Alternatively, the samples may also require additional time in the shaker. Because the percentage of PFOA degradation increased when the zeolite dosage was increased from 5 to 10 g/L, it may be beneficial to study dosages above 10 g/L to test whether higher concentrations might enhance the reaction kinetics.

4.5 Comparison of PFOA Reactions

The third objective of the lab was to replicate the most successful of the three reactions in aqueous solutions of GenX in order to investigate if the mechanism could successfully degrade shorter chain alternatives. For the Ga_2O_3/PMS/UV reaction, the most successful oxidant concentration studied was a 1:1 molar ratio of PMS to PFOA. The most successful trial for the TiO_2/PMS/UV reaction was the 2:1 molar ratio of PMS to PFOA. Finally, for the heat activated persulfate reaction, the best outcome was observed using 10 g/L of BEA zeolite. *Figure 46* below, plots the concentration of PFOA versus time for the most successful trials of Ga_2O_3/PMS/UV, TiO_2/PMS/UV, and Heat/PS/Zeolite.

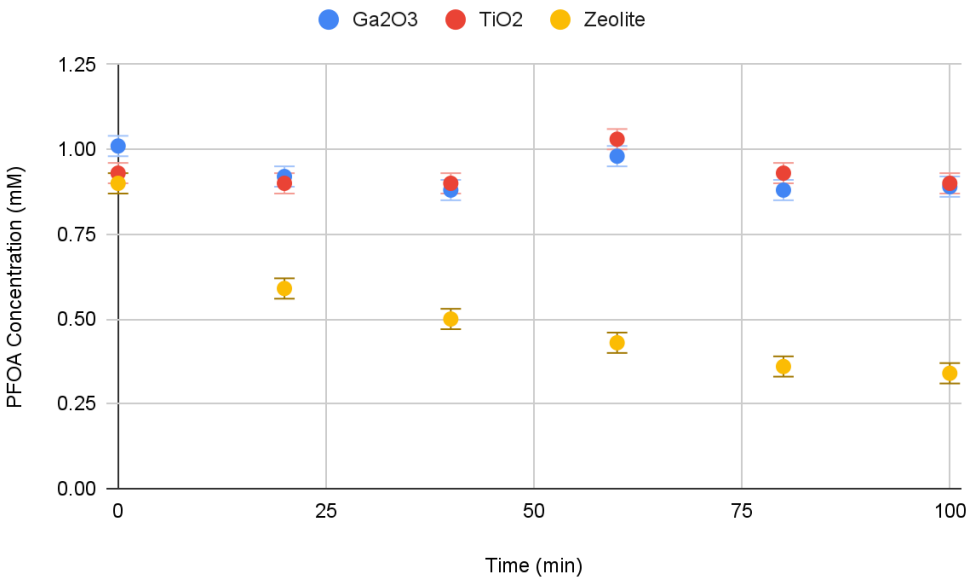

Figure 46. Plot of 2:1 reaction of the Ga_2O_3/PMS/UV, 1:1 reaction of the TiO_2/PMS/UV, and 10g/L dosage of zeolite.

As shown above, the Ga_2O_3/PMS/UV and TiO_2/PMS/UV reactions yielded almost identical concentration profiles. In both cases, little to no PFOA degradation was observed over the course of 100 minutes. The Heat/PS/Zeolite reaction, on the other hand, yielded much better results. Compared to the UV reactions, a significant reduction in the PFOA concentration was observed over 100 minutes. Therefore, based on these results, the team decided to investigate heat activated persulfate reactions with GenX at dosages of 5 and 10 g/L of BEA zeolite.

4.6 Degradation of GenX using Heat Activated Persulfate Assisted with Zeolite

The most effective degradation mechanism studied for PFOA was the use of heat activated persulfate assisted with zeolite. Therefore, the team chose to test this method on GenX, a short-chain PFAS, specifically designed to replace PFOA. We conducted three experiments with 1 mM aqueous solutions under the following conditions: 0 (control), 5, and 10 g/L BEA zeolite.

4.6.1 GenX Control

The control trial for GenX was conducted without the presence of zeolite. This was done to compare the effect of zeolite on the overall reaction. This experiment was conducted over a period of 100 minutes and samples were collected every 20 minutes from 0-100 minutes. Temperature and pH were also recorded every 20 minutes.

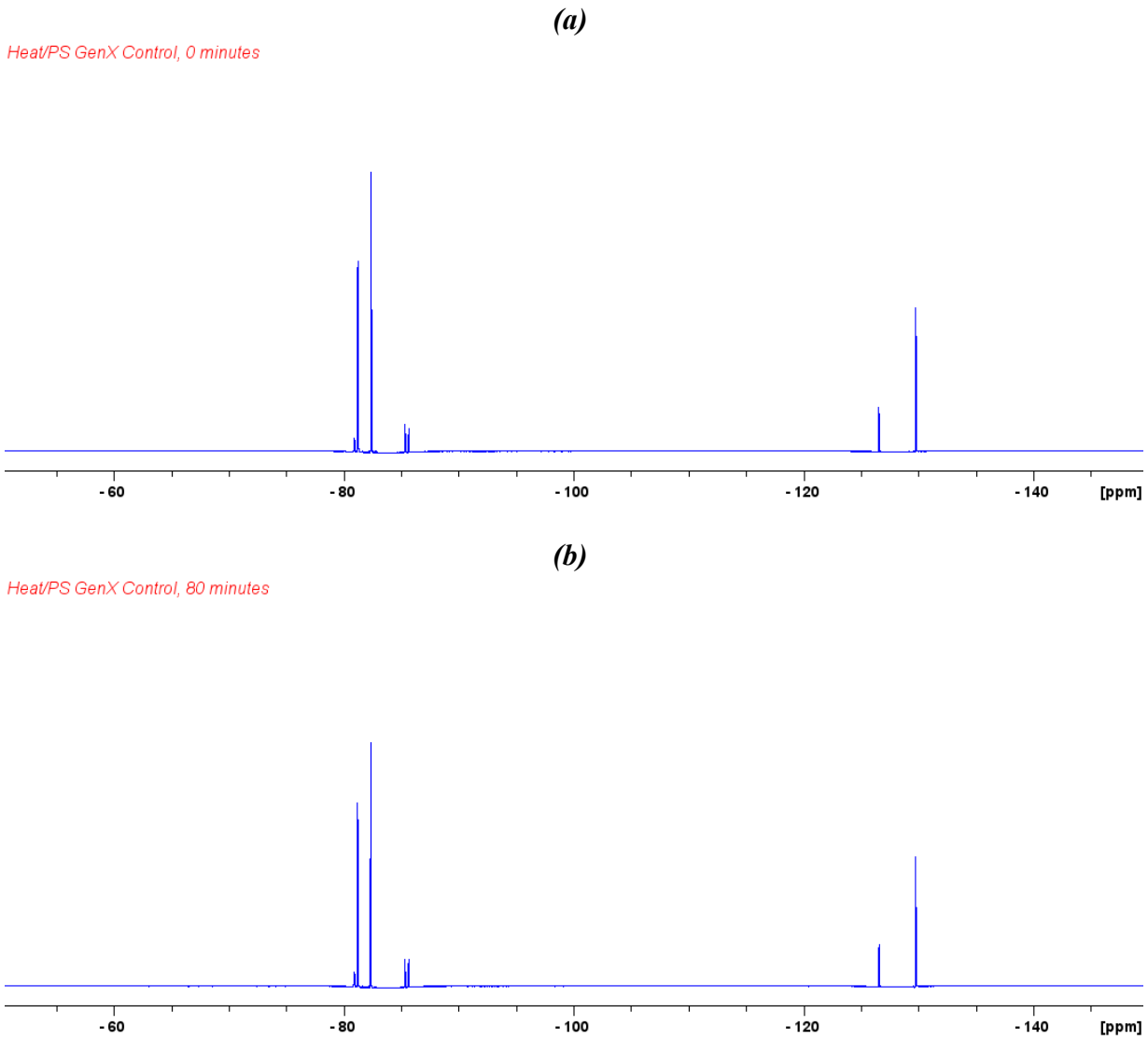

Figure 47. NMR spectra for samples taken at (a) 0 minutes and (b) 80 minutes from the GenX, heat activated persulfate control.

Figure 47 above shows the NMR spectra obtained from samples collected at (a) 0 and (b) 80 minutes from the control flask. One thing to note is that data from the final sample collected at 100 minutes was improperly processed by the NMR and concentration data was unable to be collected. Between the samples collected at 0 minutes and 80 minutes, the amplitude of the peaks did not significantly decrease, signifying that the PFOA concentration was relatively unchanged. Additionally, there is no creation of peaks, indicating that new compounds were likely not perceived by NMR. This illustrates that the reaction mechanism did not proceed effectively enough for the reaction products to be measured by NMR.

The peak integral area from the -CF_3 group was used to track the concentration of the sample from 0-80 minutes, which is modeled in *Figure 48* below. The percent of GenX degraded over 80 minutes was calculated as 102.2 $\pm$ 12.1%, indicating that GenX was produced. From 20 to 80 minutes, there's a slight reduction in the GenX concentration; however, the trendline remains relatively constant, signifying the reaction does not proceed at a significant rate.

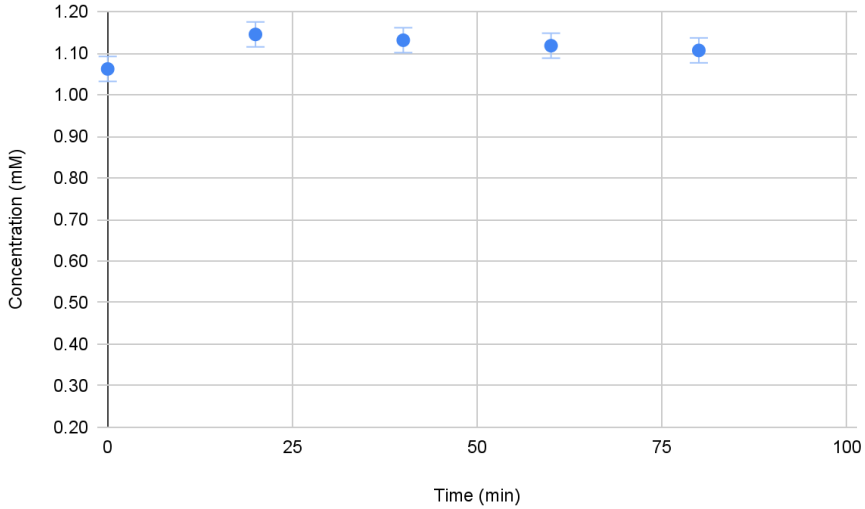

Figure 48. Plot of GenX concentration versus time for 100 minute heat activated persulfate reaction without zeolite dosage control trial

Over the course of the experiment, the temperature remained relatively constant with the exemption of the temperature at 20 minutes (*Figure 49)*. This is likely due to user error in which the hot plate was heated past optimal conditions and was later remedied.

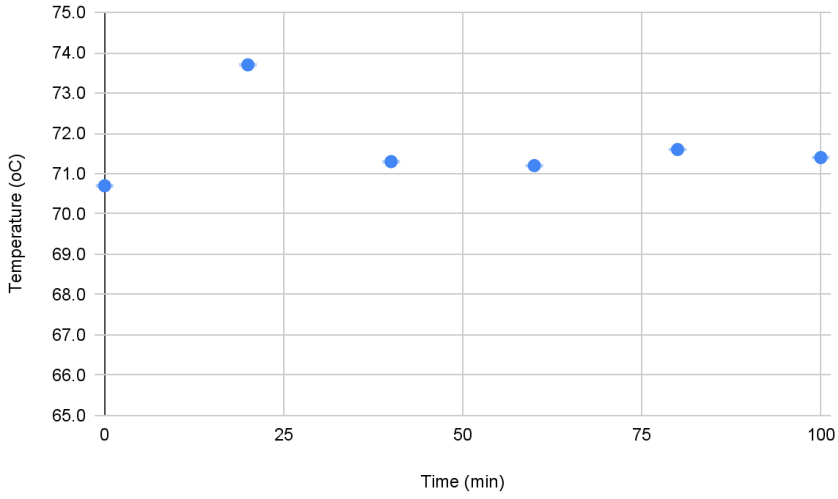

Figure 49 Plot of GenX temperature versus time for 100 minute heat activated persulfate reaction without zeolite dosage control trial

Finally, over the course of the 100-minute control experiment the pH of the solution gradually decreased. The pH was initially 2 and decreased to a pH of 1 by 40 minutes (*Figure 50*). This illustrates an increase in hydroniums in the reaction solution. This is because oxidation reactions produce hydronium atoms from the water in the aqueous environment. While the reaction did proceed enough to produce a notable change in concentration of GenX, the pH change indicates that the reaction did proceed in meager amounts. This indicates that the reaction may have proceeded more if it was conducted for a longer period. Further, it indicates the necessity of the presence of the zeolite for the reaction to proceed in a manageable time frame.

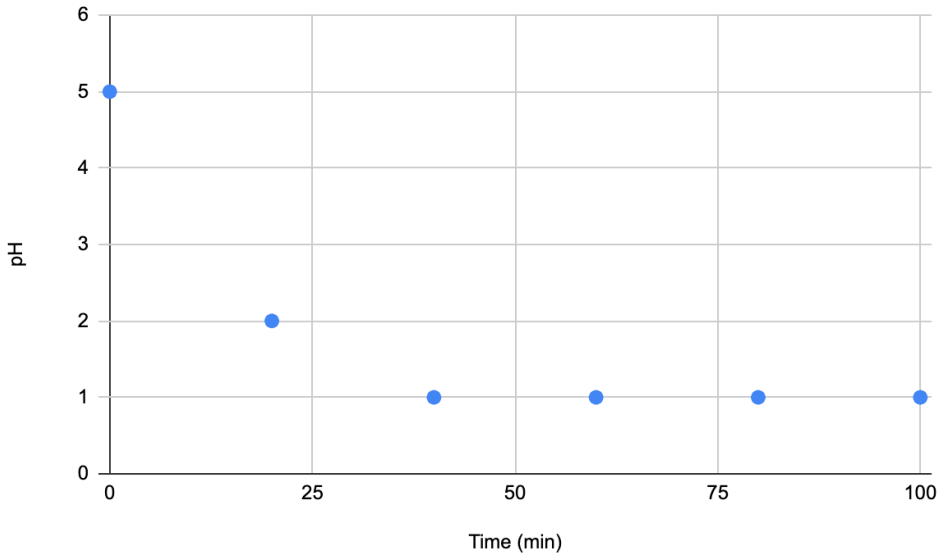

Figure 50. Plot of GenX pH versus time for 100 minute heat activated persulfate reaction without zeolite dosage control trial

4.6.2 GenX Zeolite Dosages

For GenX, the two following zeolite dosages were tested with the heat activated persulfate reaction: 5 and 10 g/L. As shown in *Table 17* below, the percent of GenX adsorbed after two hours in the laboratory shaker was approximately 81% for both dosages tested.

Table 17. Percent of GenX adsorbed after 2 hours of shaking.

BEA Zeolite Dosage (g/L)	Percent of PFOA Adsorbed after 2 Hours
5	81.0 ± 14.0%
10	81.1 ± 14.0%

(a)

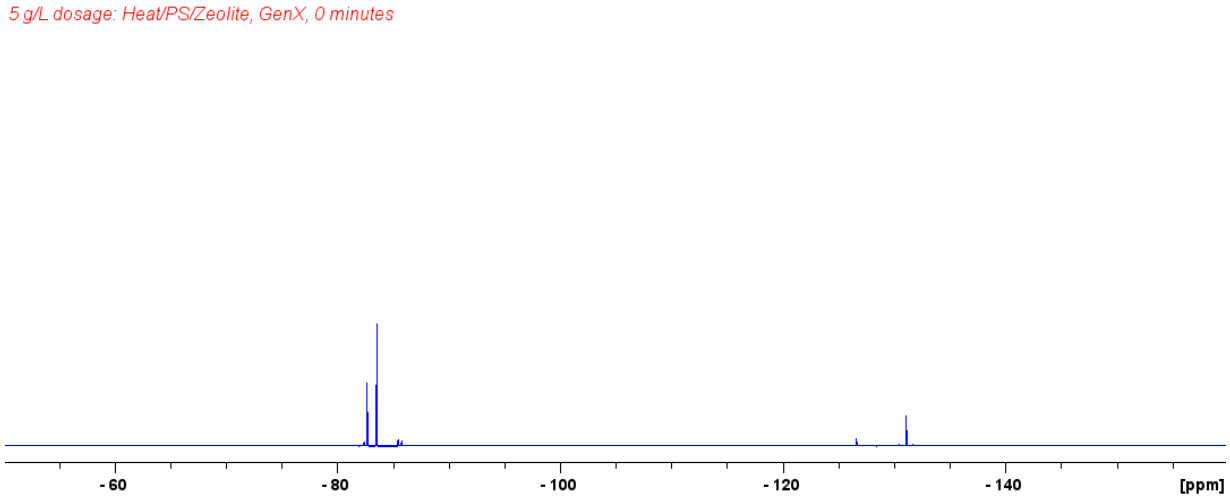

(b)

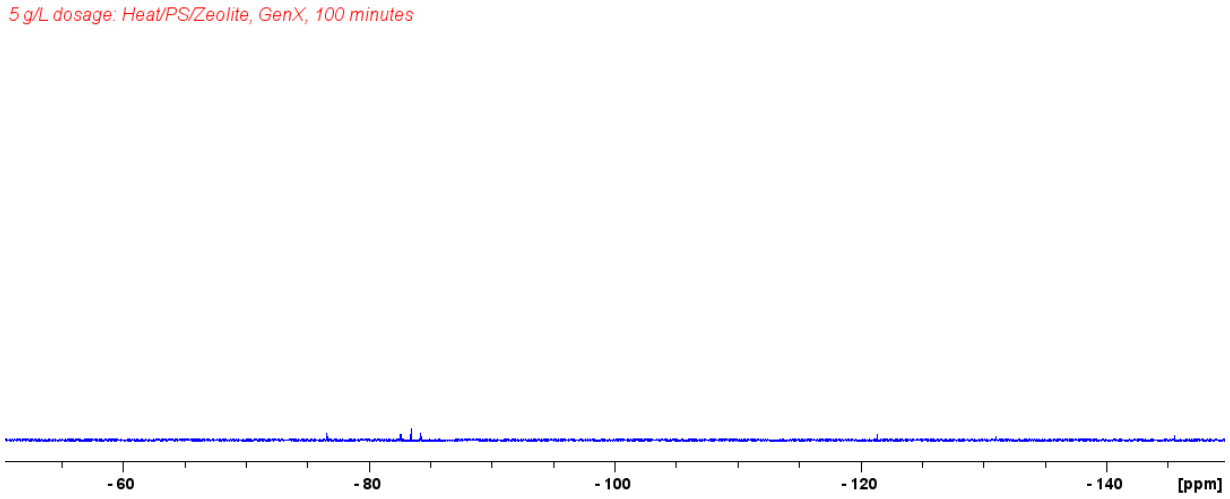

Figure 51. NMR spectra for samples taken at (a) 0 minutes and (b) 100 minutes from the GenX, heat activated persulfate reaction with a 5 g/L zeolite dosage.

Figure 51 above shows the NMR spectra for the 5 g/L zeolite dosage at 0 and 100 minutes.From 0 to 100 minutes, there's a reduction in peak intensity, signaling a decrease in the GenX concentration over the course of the reaction. Additionally, a new signal appears in the 100 minute sample at approximately -75 ppm. The creation of peaks signals the presence of by-products in the reaction mixture. The reduction in GenX concentration coupled with the formation of by-products suggest that the addition of zeolites facilitated the heat activated persulfate reaction. Together, these observations indicate that the reaction mechanism was successful at degrading GenX. *Figure 52* below tracks the terminal -CF_3 signal over the course of the 100 minute reaction.

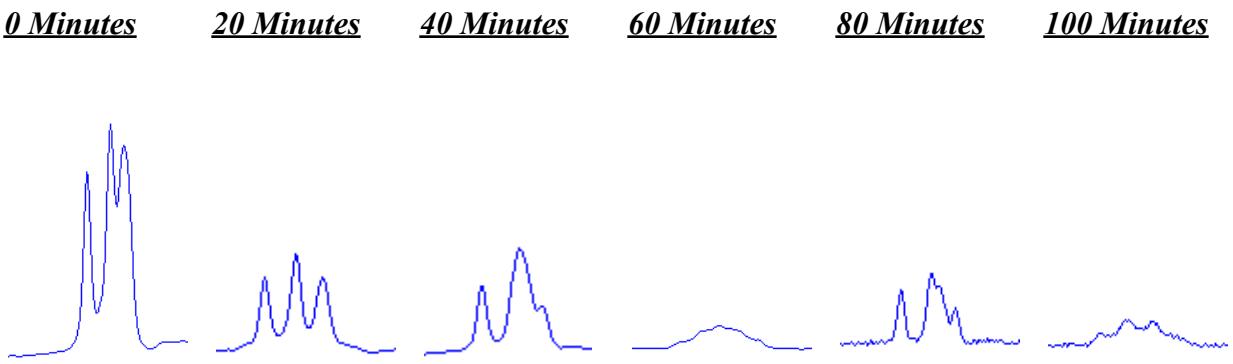

Figure 52. Change in the GenX terminal -CF_3 peaks over 100 minutes using 5 g/L of zeolite.

As expected, the intensity of the signal decreased over the course of the reaction. However, the largest reduction in signal intensity was observed between 0 and 20 minutes. This observation indicates a rapid reduction in GenX concentration over the first twenty minutes and a more gradual decline in concentration over the remaining 80 minutes. The shape of the peak also varies over the course of the reaction. In the sample taken at 0 minutes, the signal exhibits the expected triplet shape of the -CF_3 group. In the samples taken between 20 and 100 minutes, there's broadening and flattening of the peaks. This finding of varied peak shape over the course of the reaction suggests varying chemical environments, which is consistent with the formation of by-products.

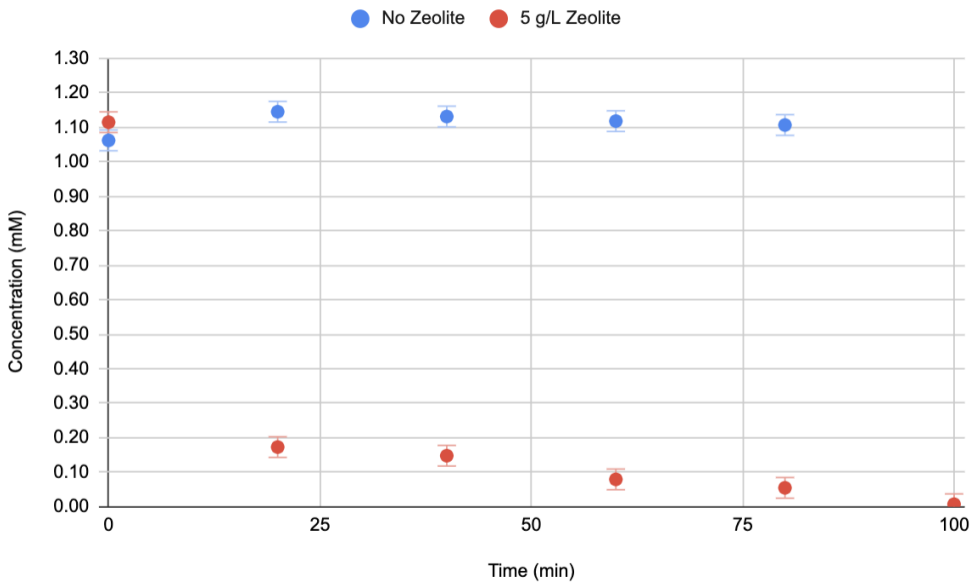

Figure 53. Plot of GenX concentration versus time for 100 minute heat activated persulfate reaction with a 5 g/L zeolite dosage.

Figure 53 above plots the concentration profile of the control and the 5.0 g/L zeolite dosage over 100 minutes. Without the use of zeolites, there's no observed reduction in GenX concentration over the course of the reaction. However, the addition of 5 g/L of BEA zeolite yields a distinct, improved decrease in concentration of GenX over time. In the first twenty minutes, there's a steep reduction in GenX concentration that levels out over the remaining 80 minutes, reaching a minimum value of 0.01 $\pm$ 0.03 mM in 100 minutes. While the concentration in the control remained relatively constant over time, adding 5.0g/L of zeolite resulted in a degradation percentage of 99.3 $\pm$ 4.9% of the GenX in 100 minutes.

Throughout the reaction, the temperature in the 5.0g/L zeolite flask remained higher than the temperature in the control flask (*Figure 54*). *Figure 55* below plots the pH of the control and 5.0 g/L zeolite flasks over time. There is a notable reduction in pH of 5 to 2 in the first twenty minutes. The zeolite flask remained at a constant pH of 2 from 40 to 100 minutes. While the pH of the control flask was slightly lower, the change in reaction pH coupled with the declining concentration profile confirm the success of the heat activated persulfate reaction assisted with zeolite.

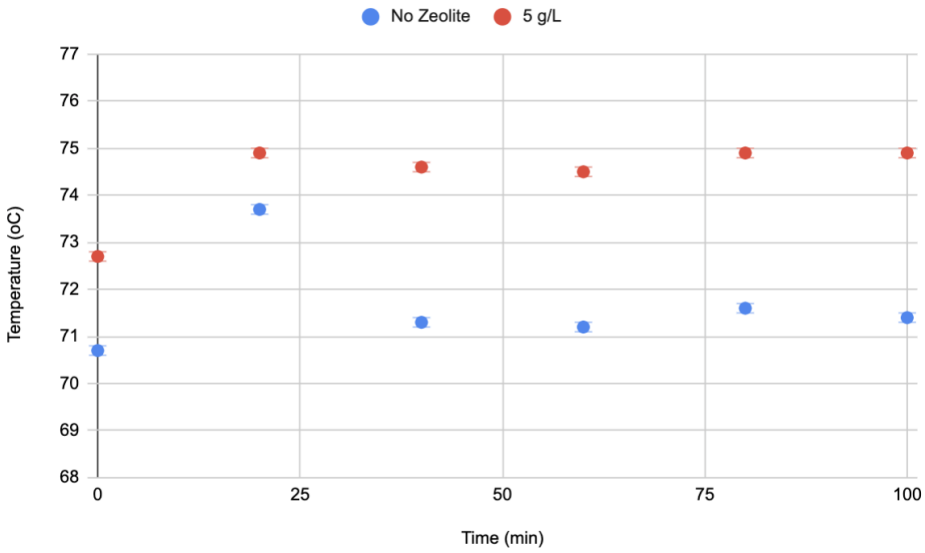

Figure 54. Plot of temperature versus time for 100 minute heat activated persulfate reaction with 1mM aqueous GenX and a 5 g/L zeolite dosage.

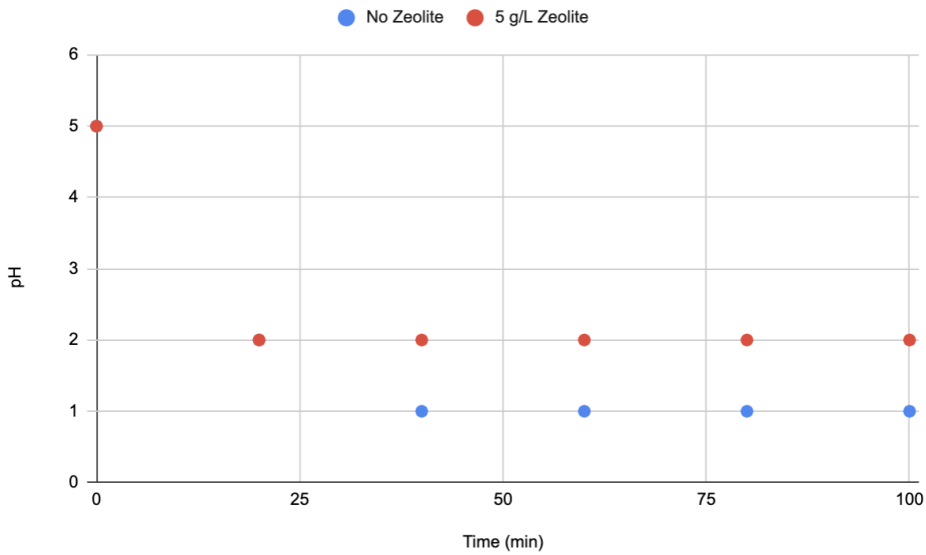

Figure 55. Plot of pH versus time for 100 minute heat activated persulfate reaction with 1mM aqueous GenX and a 5 g/L zeolite dosage.

Figure 56 below shows the NMR spectra for the 10 g/L zeolite dosage at 0 and 100 minutes.

(a)

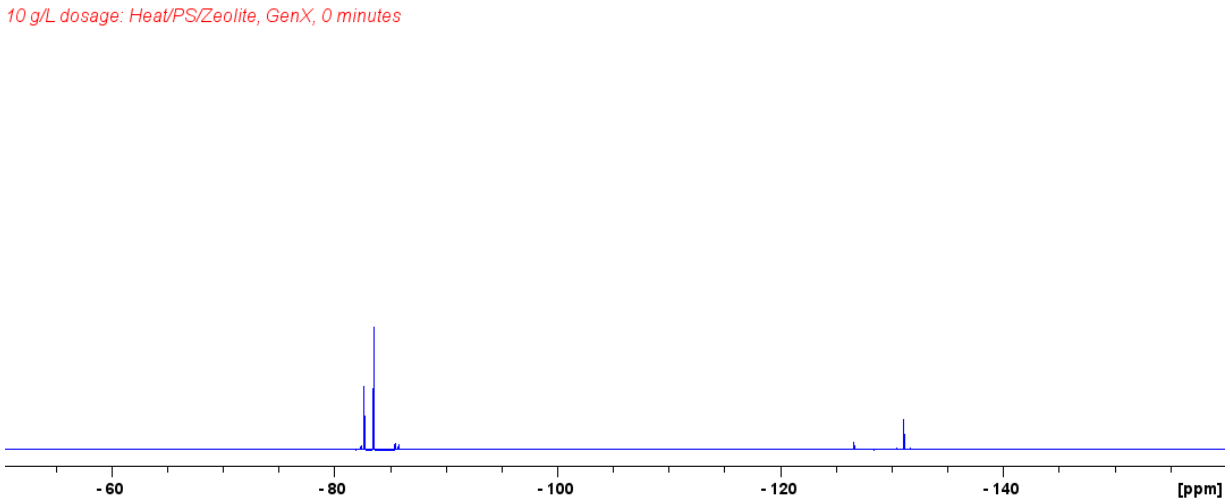

(b)

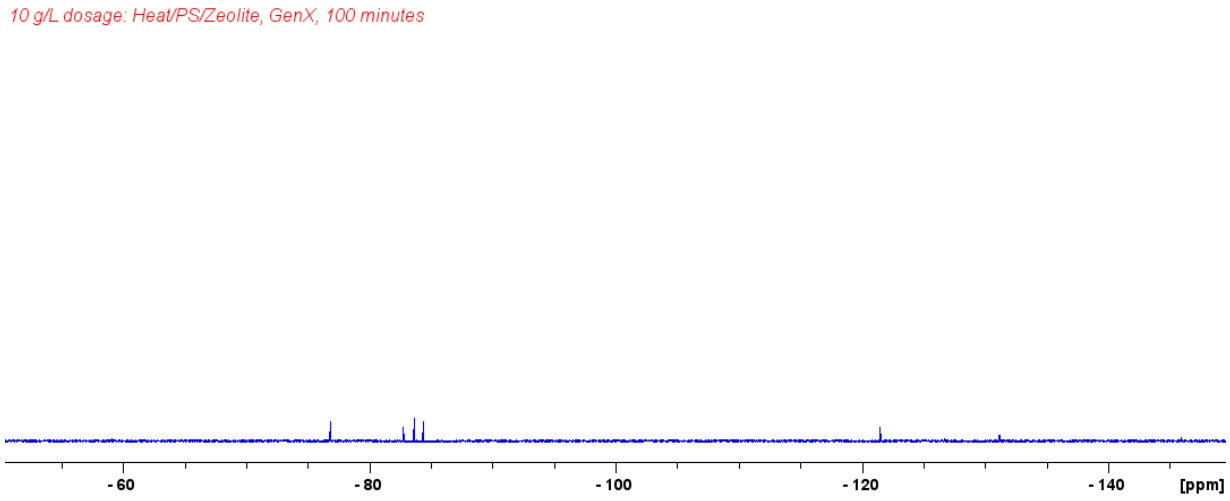

Figure 56. NMR spectra for samples taken at (a) 0 minutes and (b) 100 minutes from the GenX, heat activated persulfate reaction with a 10 g/L zeolite dosage.

Similar to the 5 g/L dosage, there's a reduction in peak intensity between 0 and 100 minutes. This reduction in peak intensity signals a reduction in GenX concentration over the course of the

reaction. Additionally, in the 100 minute sample, a new signal appears at approximately -75 ppm, indicating the presence of by-products in the reaction mixture. The reduction in GenX concentration coupled with the formation of by-products suggest that the addition of zeolites facilitated the heat activated persulfate reaction. Together, these observations indicate that the reaction mechanism was successful at degrading GenX. *Figure 57* below tracks the terminal $-CF_3$ signal over the course of the 100 minute reaction.

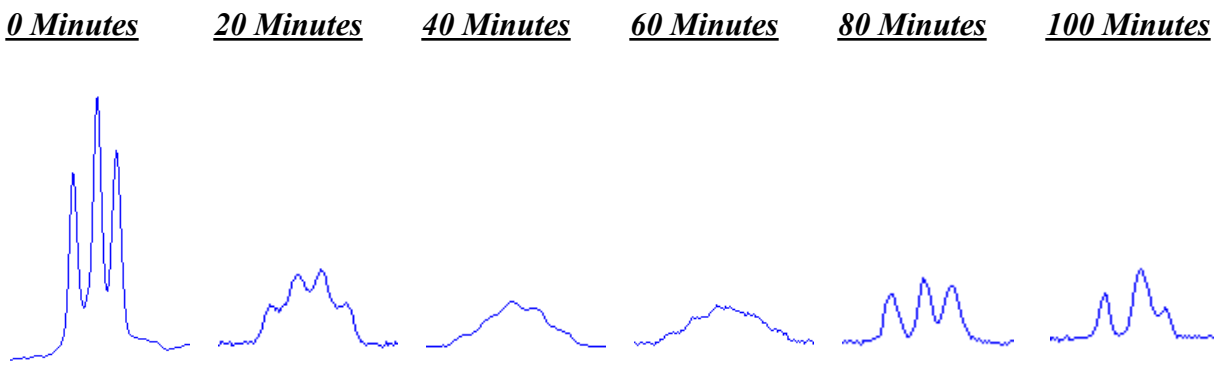

Figure 57. Change in the GenX terminal $-CF_3$ peak over 100 minutes using 10 g/L of zeolite.

As expected, the intensity of the signal decreased over the course of the reaction. However, the largest reduction in signal intensity was observed between 0 and 20 minutes. This observation indicates a rapid reduction in GenX concentration over the first twenty minutes and a more gradual decline in concentration over the remaining 80 minutes. The shape of the peak also varies over the course of the reaction. In the sample taken at 0 minutes, the signal exhibits the expected triplet shape of the $-CF_3$ group. In the samples taken between 20 and 60 minutes, there's broadening and flattening of the peaks. Finally, in the samples taken at 80 and 100 minutes, the triplet shape returns, but the peaks in the triplet are more isolated. This finding of varied peak shape over the course of the reaction suggests varying chemical environments, which is consistent with the formation of by-products.

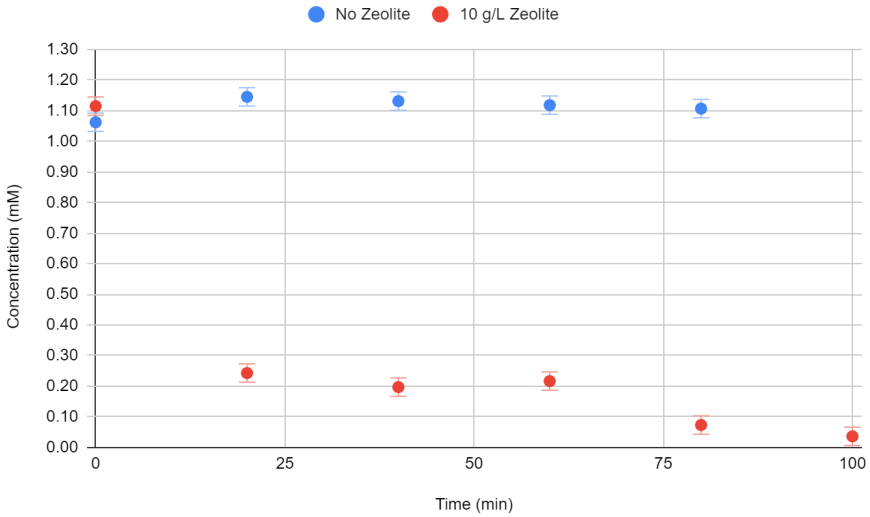

Figure 58. Plot of GenX concentration versus time for 100 minute heat activated persulfate reaction with a 10 g/L zeolite dosage.

Figure 58 above plots the concentration profile of the control and the 10 g/L zeolite dosage over 100 minutes. The concentration profile for the 10 g/L dosage followed the same trend observed in the 5 g/L trial. In the first twenty minutes, there's a steep reduction in GenX concentration that levels out over the remaining 80 minutes, reaching a minimum value of 0.036 ± 0.03 mM. While the concentration in the control remained relatively constant over the course of the reaction, the addition of 10 g/L zeolite degraded $96.8 \pm 4.7\%$ of the GenX in 100 minutes.

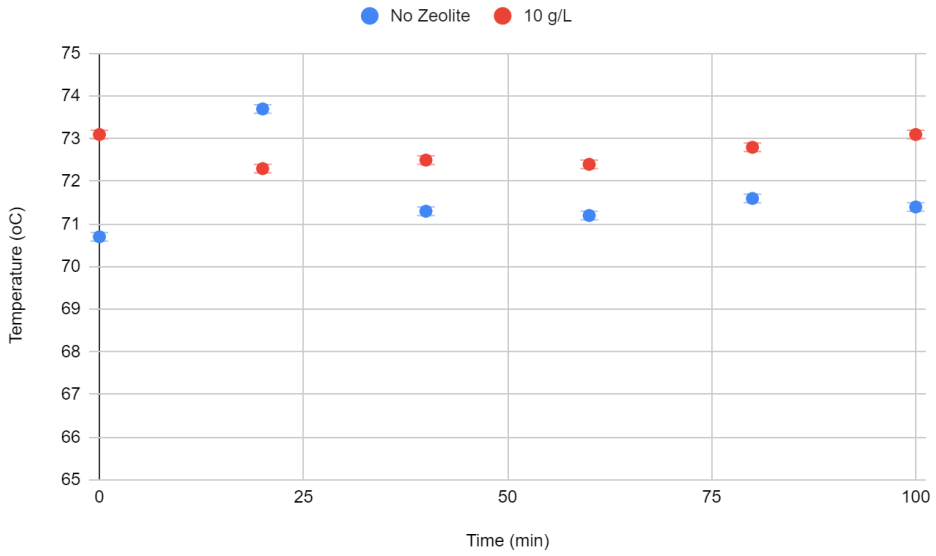

Figure 59. Plot of temperature versus time for 100 minute heat activated persulfate reaction with 1mM aqueous GenX and a 10 g/L zeolite dosage.

Like the 5 g/L dosage, the temperature in the 10 g/L zeolite flask remained higher than the temperature in the control flask throughout the majority of the reaction (*Figure 59*). However, unlike the 5 g/L trial, the difference between the temperature profiles is much more narrow in range. *Figure 60* below plots the pH of the control and 10 g/L zeolite flasks over time. The 10 g/L dosage exhibited the same behaviors as the previous dosage, with the same reduction in pH of 5 to 2 in the first twenty minutes. Again, the zeolite flask remained at a constant pH of 2 from 40 to 100 minutes. While the pH of the control flask was slightly lower, the change in reaction pH coupled with the declining concentration profile confirm the success of the heat activated persulfate reaction assisted with zeolite.

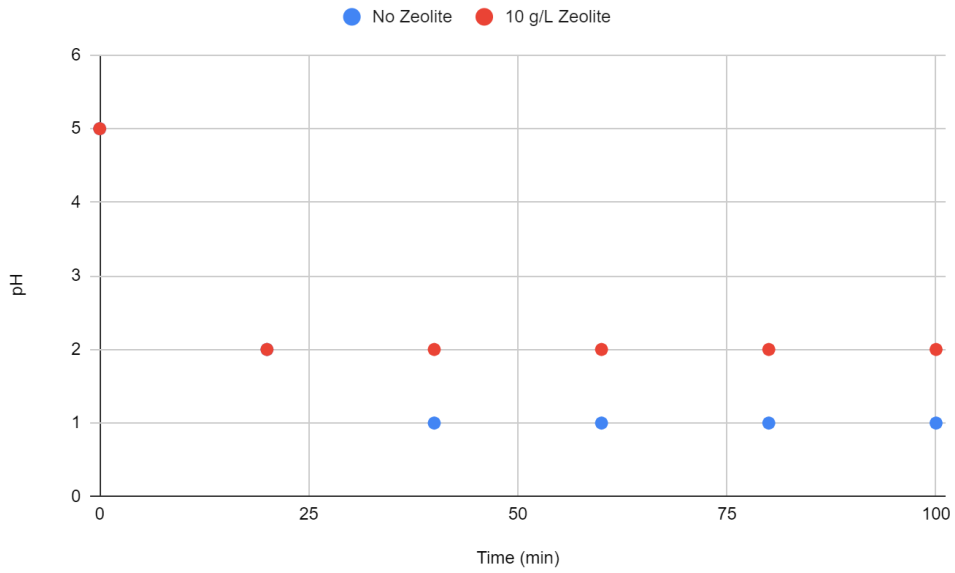

Figure 60. Plot of pH versus time for 100 minute heat activated persulfate reaction with 1mM aqueous GenX and a 10 g/L zeolite dosage.

Between the two trials, a slightly higher percent of GenX was degraded using 5 g/L of zeolite as opposed to 10 g/L. This result was initially unexpected, as increasing the zeolite dosage increased the percent of PFOA degraded. However, given that approximately 81% of the GenX was absorbed in both trials, it makes sense that a similar percentage of GenX was degraded in both trials. As shown in *Table 18* below, nearly 100% percent of the GenX was degraded in 100 minutes using 5 and 10 g/L of BEA zeolite. This finding indicates that a very small percentage of zeolite is needed to facilitate the advanced oxidation process for a shorter chain alternative like GenX.

Table 18. Percent of GenX degraded at the end of the heat activated persulfate reaction at the two following zeolite dosages: 5 and 10 g/L.

Zeolite Dosage (g/L)	Percent of GenX Degraded
5	99.8 ± 4.9%
10	96.8 ± 4.7%

4.6.3 Reaction Kinetics

Using the concentration data from the GenX experiments with heat-treated persulfate and BEA zeolite, we analyzed the kinetics of each reaction. This was done using the integrated rate law of the zeroth, first, and second-order kinetics. The GenX concentration data was altered with the integrations of each rate law and plotted against time. The most linear set of integrated data, the trendline yielding the highest r^2 value, was taken as the kinetic law most closely modeling the reaction mechanism for GenX. *Table 19* below shows the R^2 values for the various integrated rates for the control, 5g/L dosage, and the 10g/L dosage trials.

Table 19. R^2 values for linear approximations of zeroth, first, and second order kinetics on the GenX heat activated persulfate reaction at the following conditions: 0 (control), 5, and 10 g/L zeolite.

Reaction Series	0^{th} Order r^2	1^{st} Order r^2	2^{nd} Order r^2
Control	0.0996	0.9781	0.980
5 g/L	0.5672	0.9105	0.608
10 g/L	0.6145	0.8901	0.7595

The R^2 value for all three zeolite dosages was highest with the first order integration when excluding the first data point (displayed in *Figure* 61). The first data point before the control trial was excluded as it was extraneous and therefore was not a good measurement of the true reaction rate.

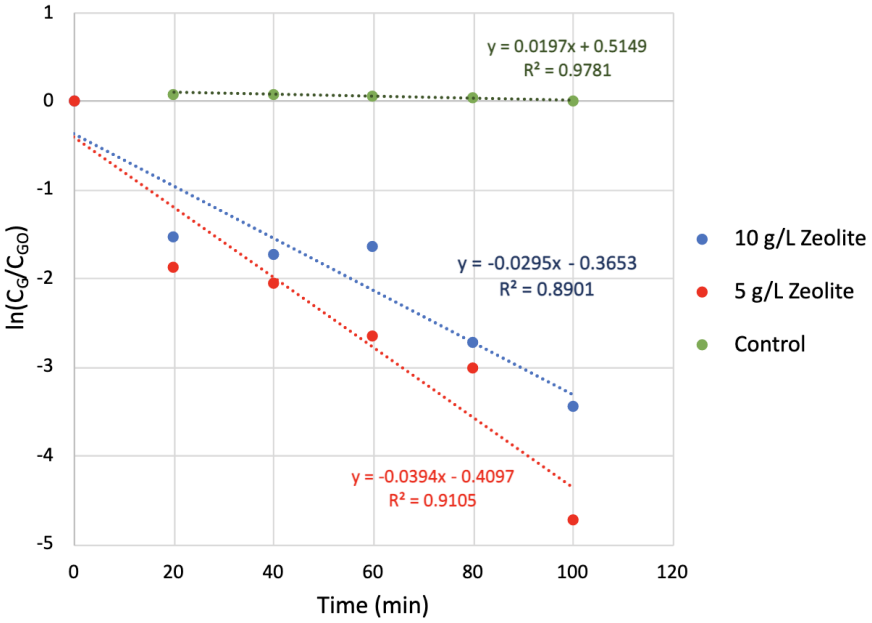

Figure 61: The first order integrated data and trend lines for control, 5g/L dosage, and the 10g/L dosage trials

The overall rate law was then calculated using the first order kinetics. The slope of the line was used as the first order rate constant, shown in the equations below.

Control: $$rate = k[GenX] \rightarrow k = 0.0003\ min^{-1} \quad (1)$$

5 g/L: $$rate = k[GenX] \rightarrow k = 0.0394\ min^{-1} \quad (2)$$

10 g/L: $$rate = k[GenX] \rightarrow k = 0.0295\ min^{-1} \quad (3)$$

Some errors can be attributed to these rate law calculations. The first data point at zero minutes had to be excluded from the control rate law to obtain a more accurate calculation. As shown above, compared to the control, the addition of 5 g/L of zeolite effectively increased the rate constant by nearly 13 times. This increase in the rate constant indicates that the addition of zeolites increased the kinetics of the first order reaction and facilitated the advanced oxidation reaction.

4.7 PFOA to GenX Comparison

The third objective of this study was to test the most effective advanced oxidation reaction on aqueous solutions of GenX. The purpose of this experimentation was to investigate whether short chain alternatives are in fact easier to degrade. As discussed previously, the heat activated persulfate reaction yielded the highest degree of PPAS degradation of the three reactions studied. *Figure 62* below plots the concentration profiles of PFOA and GenX over the course of 100 minutes for the most successful trials, 10 g/L BEA zeolite for PFOA and 5 g/L BEA zeolite for GenX.

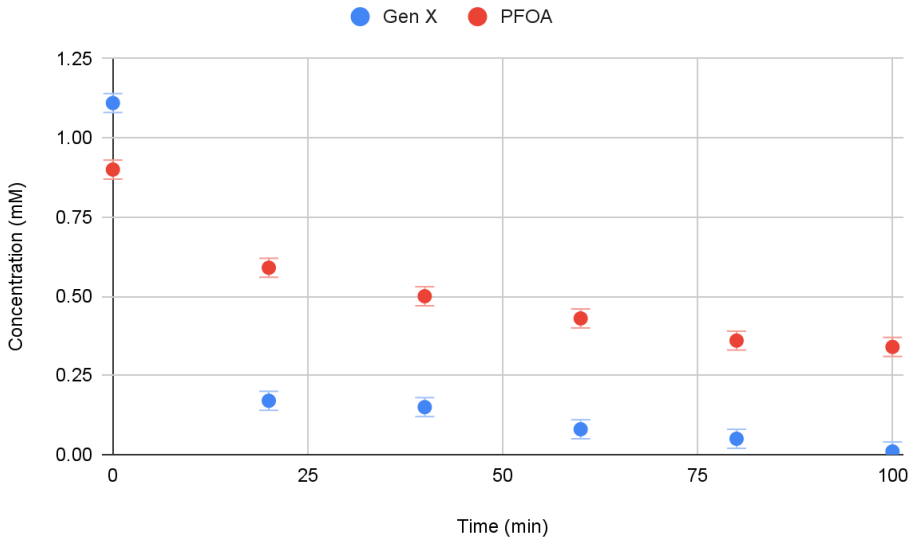

Figure 62. Concentration versus time graph for the heat activated persulfate reaction on 1 mM aqueous solutions of PFOA with 10 g/L of BEA zeolite and GenX with 5 g/L of BEA zeolite.

Over the course of the reaction, the concentrations of PFOA and GenX follow a decreasing trend, with the most pronounced reduction occurring in the first 20 minutes. While exhibiting similar concentration profiles, the reduction in GenX concentration occurs at a much more significant rate. More specifically, the oxidation mechanism for PFOA follows second order kinetics, while the oxidation reaction with GenX follows first order kinetics. In 100 minutes, the team observed a 62.3 $\pm$ 5.8% reduction in PFOA concentration and a 99.8 $\pm$ 4.9% reduction in GenX concentration.

Chemical manufacturers began manufacturing shorter chain alternatives like GenX with the intent of creating compounds that are easier to break down. Compared to PFOA, the backbone in GenX contains two fewer carbon atoms. Therefore, the team expected to observe a faster degradation rate in GenX because there are less carbons to break down. Additionally, BEA zeolite is better suited to smaller molecules, so the GenX likely receives more support from the

added adsorbent. This result of higher GenX degradation seems to support the claim that some shorter chain PFAS are easier to degrade; however, there is still limited data on the long term health effects of compounds like GenX.

One interesting difference between the reactions with GenX and PFOA is the control trials. In solutions of PFOA, the heat-activated persulfate reaction preceded without the use of zeolite. The heat activated persulfate reaction, however, did not produce a significant level of GenX degradation without zeolite. This result was not initially expected; however, the acidity of the compounds may explain this difference. For PFOA, the starting pH for each of the reactions studied was approximately 3. The starting pH for GenX, on the other hand, was approximately 5. These advanced oxidations favor acidic conditions to generate radical species. While PFOA and GenX contain the same functional group, the branching and ether linkage in the carbon chain reduces the acidity of GenX. Therefore, in a less acidic environment, as is the case for GenX, the addition of zeolites is necessary to increase the molecular interactions.

5.0 Conclusion and Recommendations

5.1 Conclusions and Major Findings

When conducting this study, our team had three overarching objectives. They were as follows,

1. Study and perform three advanced oxidation reactions to test their efficacy at degrading PFOA
2. Use NMR technology to analyze and quantify PFAS degradation in our oxidation experimentation
3. Determine the most effective oxidation reaction and perform the reaction on GenX, a short-chain alternative to PFOA

The study has provided a series of significant findings by completing these objectives. The first finding is that NMR is an adequate tool for detecting and quantifying PFAS at the concentration levels relevant to this study, with an approximate detection limit of 0.08 mg/L (0.0002 mM). NMR technology allowed our analysis to detect the presence of specific molecules and quantify the concentration of the molecules at various points throughout the reaction. Further, because NMR uses the frequency emitted by individual nuclei of the various atoms in different molecules, our team was able to differentiate species within each 20-minute increment test. From this, our team could hypothesize about the mechanisms PFAS were being broken down into. The NMR spectra allowed us a glance at the elementary reactions within the overall oxidation reaction and further proved the mechanisms discussed in other literature.

Our second key finding was identifying the most effective degradation method when degrading PFOA. Our data shows that heat-activated persulfate assisted with zeolite was the most effective at degrading PFOA. In the 5g/L and the 10g/L zeolite dosage trials, PFOA was degraded by over 60% of the original amount at the end of 100 minutes. Ga_2O_3 photocatalytic degradation of PFOA assisted with PMS only reaching 40% degradation efficacies at a 4:1 ratio of PMS to PFOA. Degradation efficacies for TiO_2 Photocatalytic Degradation of PFOA Assisted with PMS did not surpass 5% for any trial. Our experiments illustrate that with the resources we acquired and the conditions in which the experiments were conducted, heat-activated persulfate assisted with zeolite was the most effective at degrading PFOA. This success could be attributed to various factors; however, we believe the zeolite assistance likely made the most difference. Zeolite acts as a surface for the reaction to occur, increasing the chance of kinetic action. From our results, the presence of the zeolites seemed to have a more significant effect than any of the other factors in the other reactions.

Our team's third significant finding is that heat-activated persulfate assisted with zeolite was also a successful degradation method for the short-chain variant GenX. Our results indicate that this

method was even more successful at degrading GenX. In all three trials at various zeolite doses, the was degraded by over 95% by the end of 100 minutes. In our higher dose trials of 5g/L and 10g/L of zeolite, GenX was degraded by nearly 100% by the end of the experiment. These findings indicate that shorter-chain PFAS are more easily degraded chemically than longer-chain PFOA. Other chemical and kinetic factors could also influence this conclusion, but it is a positive indication that shorter-chain molecules degrade more easily overall.

Our fourth and final significant finding is the lack of success in our other two degradation methods. The Ga_2O_3 photocatalytic degradation of PFOA assisted with PMS reaction, and the TiO_2 photocatalytic degradation of PFOA assisted with PMS reaction had far inferior results compared to the zeolite reaction. These reactions were executed with the same procedure excluding the type of oxidant. Many reasons may have contributed to the lack of completion in these experiments. Our team believes that the amount of oxidant used in these reactions could have been too low, which could have limited the amount that the reaction could proceed and therefore limited the overall reaction. Further, our temperature data implies that the reaction may be endothermic and require additional heat sources beyond UV light. Adding a heat source could make the reaction more kinetically favorable and allow the forward reaction to occur at a higher rate. Additionally, due to the complexity of chemistry and thermodynamics, additional factors beyond what is conceivable to our team likely played a role in the failure of both reactions.

5.2 Areas for Further Study

Our study displays promising results from the heat-activated persulfate oxidation assisted with zeolite that were promising for PFOA and GenX degradation. However, there are various research areas to study further to optimize, improve efficiency, and implement this reaction on a larger scale.

Firstly, our team believes it would be valuable to investigate zeolite dosage beyond ten g/L. While the tested doses were almost 100% effective for the shorter-chain GenX, we think a higher zeolite dosage could improve degradation efficacy in other forms of PFAS. Additionally, it may be beneficial to perform investigations with different types of zeolites. The pore size in zeolites can vary widely, and there may be another type of framework better suited to larger PFAS chains, such as PFOA. As zeolites seemed to be the most promising factor in our study, we believe investigating them further will provide the most promising research.

Secondly, studying the effects on competing ions in the solutions would provide insight into how these reactions would perform in large-scale water treatment. Traditional water treatment methods must handle a variety of contaminants, and those contaminants could affect the reaction chemistry illustrated in these experiments. Our team believes it is vital to investigate the effects

of other contaminants in wastewater on the degradation efficacy in small or large-scale heat-activated persulfate oxidation assisted with zeolite reactions.

Additionally, exploring the applicability of heat-activated persulfate assisted with zeolite reaction for other long-chain PFAS with alternative functional groups, such as PFOS, could help assess the versatility of the mechanism. Thousands of PFAS species exist in the commercial realm and therefore need to be broken down by our treatment methods. It would be beneficial to experiment with the most prominent groups to limit human exposure as much as possible. By performing these experiments on other types of PFAS, we could expand the scope of this treatment method and make a more truly plausible solution.

Finally, designing a continuous flow reactor for this reaction could completely change the plausibility of this solution to being implemented in the real world. Our study looks at the efficacy of this reaction on a much smaller scale than necessary in large-scale treatment plants. If this model could effectively be scaled up to treat large quantities of PFAS, the capabilities could be monumental in preventing human, animal, and environmental exposure to PFAS contaminants.

In conclusion, the heat-activated persulfate oxidation assisted with zeolite could be enhanced with further study. This mechanism, when expanded upon, could lead to a more efficient and sustainable approach to mitigating the harmful effects of PFAS contamination.

6.0 References

About PFASs—OECD Portal on Per and Poly Fluorinated Chemicals. (n.d.). Retrieved March 14, 2023, from https://www.oecd.org/chemicalsafety/portal-perfluorinated-chemicals/aboutpfass/

Adamson, D.T., Nickerson, A., Kulkarni, P.R., Higgins, C.P., Popovic, J., Field, J., Rodowa, A., Newell, C., DeBlanc, P., & Kornuc, J.J. (2020, December 3). Mass-based, field-scale demonstration of PFAS retention within AFFF-associated source areas. *Environmental Science & Technology, 54*(24), 15768-15777. https://doi.org/10.1021/acs.est.0c04472

Ahearn, A. (2019, March 14). A regrettable substitute: The story of GenX. *Environmental Health Perspectives, 2019*(1), 1-3. https://doi.org/10.1289/EHP5134

Alalm, M.G., & Boffito, C. Mechanisms and pathways of PFAS degradation by advanced oxidation and reduction processes: A critical review. *Chemical Engineering Journal, 450*(4), 1-14. https://doi.org/10.1016/j.cej.2022.138352.

American Water Works Association. (2019, August 12). *Per- and polyfluoroalkyl substances (PFAS) treatment*. AWWA. https://www.awwa.org/Portals/0/AWWA/ETS/Resources/Per-andPolyfluoroalkylSubstances(PFAS)-Treatment.pdf?ver=2019-08-14-090249-580#:~:text=Advanced%20oxidation%20transforms%20PFAS%20using,to%2090%25%20degradation%20of%20PFOA

Banks, R. E., Smart, B. E., & Tatlow, J. C. (2013). *Organofluorine Chemistry: Principles and Commercial Applications*. Springer Science & Business Media.

Benford, D. (2008, February 21). Opinion of the Scientific Panel on Contaminants in the Food Chain on perfluorooctane sulfonate (PFOS), perfluorooctanoic acid (PFOA), and their salts. *The EFSA Journal*, (653), 1-131. https://pure.uva.nl/ws/files/4299097/62823_EFSA_J_2008_653_PFOS_PFOA.pdf

Bonato, M., Corrà, F., Bellio, M., Guidolin, L., Tallandini, L., Irato, P., Santovito, G., & Link to external site, this link will open in a new window. (2020). PFAS Environmental Pollution and Antioxidant Responses: An Overview of the Impact on Human Field. *International Journal of Environmental Research and Public Health*, *17*(21), 8020. https://doi.org/10.3390/ijerph17218020

Brendel, S. (2018, February 27). Short-chain perfluoroalkyl acids: environmental concerns and a regulatory strategy under REACH. *Environmental Science Europe, 30*(9). https://doi.org/10.1186/s12302-018-0134-4

Buck, R. C., Franklin, J., Berger, U., Conder, J. M., Cousins, I. T., de Voogt, P., Jensen, A. A., Kannan, K., Mabury, S. A., & van Leeuwen, S. P. (2011). Perfluoroalkyl and Polyfluoroalkyl Substances in the Environment: Terminology, Classification, and Origins. *Integrated Environmental Assessment and Management*, *7*(4), 513–541. https://doi.org/10.1002/ieam.258

Buck, R. C., Korzeniowski, S. H., Laganis, E., & Adamsky, F. (2021). Identification and

classification of commercially relevant per- and poly-fluoroalkyl substances (PFAS). *Integrated Environmental Assessment and Management*, *17*(5), 1045–1055. https://doi.org/10.1002/ieam.4450

Calafat, A. M., Kato, K., Hubbard, K., Jia, T., Botelho, J. C. & Wong, L.-Y. (2019). Legacy and alternative per- and polyfluoroalkyl substances in the U.S. general population: Paired serum-urine data from the 2013–2014 national health and nutrition examination survey. *Environment International*, *131*, 105048. https://doi.org/10.1016/j.envint.2019.105048.

Camdzic, D., Dickman, R. A., & Aga, D. S. (2021). Total and class-specific analysis of per-and polyfluoroalkyl substances in environmental samples using nuclear magnetic resonance spectroscopy. J*ournal of Hazardous Materials Letters*, *2*, 100023. https://doi.org/10.1016/j.hazl.2021.100023

Centers for Disease Control and Prevention. (2022, November 1). Potential health effects of Pfas Chemicals. Centers for Disease Control and Prevention. Retrieved February 28, 2023, from https://www.atsdr.cdc.gov/pfas/health-effects/index.html

Choi, A., Muise, D., & Weiland, Z. (2019). *Designing a total organic fluorine test: PFAS characterization & quantification utilizing NMR analysis* (Unpublished Undergraduate Major Qualifying Project). Worcester Polytechnic Institute.

Clark, J. (2014). What is nuclear magnetic resonance (NMR)? *Chemguide*. https://www.chemguide.co.uk/analysis/nmr/background.html

Dhore, R., & Murthy, G. S. (2021). Per/polyfluoroalkyl substances production, applications and environmental impacts. *Bioresource Technology*, *341*, 125808. https://doi.org/10.1016/j.biortech.2021.125808

Edwards, J.C. (2012). *Principles of NMR*. Process NMR Associates, LLC. https://process-nmr.com/principles-of-nmr/

Fidra. (n.d.). *The science*. PFAS Free. https://www.pfasfree.org.uk/about-pfas/pfas-science-the-basics

Franke, V., Schäfers, M.D., Lindberg, J.J., & Ahrens, L. (2019). Removal of per- and polyfluoroalkyl substances (PFASs) from tap water using heterogeneously catalyzed ozonation. *Environmental Science Water Research & Technology, 5*, 1887-1896. https://doi.org/10.1039/C9EW00339H

Gevorg, S. (2021). *Splitting and multiplicity (N + 1 rule) in NMR spectroscopy*. Chemistry Steps. https://www.chemistrysteps.com/splitting-multiplicity-n1-rule-nmr/

Glüge, J., Scheringer, M., Cousins, I.T., DeWitt, J.C., Goldenman, G., Herzke, D., Lohmann, R.; Ng, C.A., Trier, X., and Wang, Z. (2020). An overview of the uses of per- and polyfluoroalkyl substances (PFAS). *Environmental Science: Processes & Impacts*, *22* (12), 2345–2373. https://doi.org/10.1039/D0EM00291G.

Interstate Technology Regulatory Council. (2022a, June). *Chemistry, terminology, and*

acronyms. Per- and Polyfluoroalkyl Substances. https://pfas-1.itrcweb.org/2-2-chemistry-terminology-and-acronyms/

Interstate Technology Regulatory Council. (2022b, June). *4 physical and chemical properties*. Per- and Polyfluoroalkyl Substances. https://pfas-1.itrcweb.org/4-physical-and-chemical-properties/

Khan, S., Sayed, M., Sohail, M., Shah, L.A., & Raja, M.A. (2019). Advanced oxidation and reduction processes. *Advances in Water Purification Techniques,* 135-164. https://doi.org/10.1016/B978-0-12-814790-0.00006-5

Leonello, D., Fendrich, M.A., Parrino, F., Patel, N., Orlandi, M., & Antonio, M. (2021, September 12). Light-induced advanced oxidation processes as PFAS remediation methods: A review. *Applied Sciences, 11*(18), 8458. https://doi.org/10.3390/app11188458

Lopes de Silva, F., Laitinen, T., Pirila, M., Keiski, R., & Ojala, S. (2017). Photocatalytic degradation of perfluorooctanoic acid (PFOA) from wastewaters by TiO_2, In_2O_3 and Ga_2O_3 catalysts. *Top Catal, 60*, 1345–1358. https://doi.org/10.1007/s11244-017-0819-8

MassDEP. (n.d.). *Story map series*. mass. Retrieved February 28, 2023, from https://mass-eoeea.maps.arcgis.com/apps/MapSeries/index.html?appid=aaf23d08bb834ffaa0625328f6734eae#

O. Bok, T., P. Andriako, E., E. Knyazeva, E., & I. Ivanova, I. (2020). Engineering of zeolite BEA crystal size and morphology via seed-directed steam assisted conversion. *RSC Advances*, *10*(63), 38505–38514. https://doi.org/10.1039/D0RA07610D

Per- and Polyfluorinated Substances (PFAS) Factsheet | National Biomonitoring Program |CDC. (2022, May 3). https://www.cdc.gov/biomonitoring/PFAS_FactSheet.html

Pérez-Botella, E., Valencia, S., & Rey, F. (2022). Zeolites in Adsorption Processes: State of the Art and Future Prospects. *Chemical Reviews*, *122*(24), 17647–17695. https://doi.org/10.1021/acs.chemrev.2c00140

Pérez, F., Nadal, M., Navarro-Ortega, A., Fàbrega, F., Domingo, J. L., Barceló, D., & Farré, M. (2013). Accumulation of perfluoroalkyl substances in human tissues. *Environment International*, *59*, 354–362. https://doi.org/10.1016/j.envint.2013.06.004.

Perfluorooctanoic Acid (PFOA) Factsheet | National Biomonitoring Program | CDC. (2021, September 2). https://www.cdc.gov/biomonitoring/PFOA_FactSheet.html

Protection, M. D. of E. (n.d.). Per- and polyfluoroalkyl substances (PFAS). Mass.gov. Retrieved February 28, 2023, from https://www.mass.gov/info-details/per-and-polyfluoroalkyl-substances-pfas

Qian, L., Kopinke, F.-D., Scherzer, T., Griebel, J., & Georgi, A. (2022). Enhanced degradation of perfluorooctanoic acid by heat-activated persulfate in the presence of zeolites. *Chemical*

Engineering Journal, *429*, 132500. https://doi.org/10.1016/j.cej.2021.132500

Reich, H.J. (2020, Feb.). *Hans Reich's collection. NMR spectroscopy.* Organic Chemistry Data. https://organicchemistrydata.org/hansreich/resources/nmr/?index=nmr_index%2F19F_shift#f-data02

Safer States. (2023, February 8). *PFAS action: Governments, retailers, and brands are stepping up*. Safer States. Retrieved February 28, 2023, from https://www.saferstates.com/assets/Resources/PFAS-Momentum-Factsheet-2.8.2023.pdf

Sinclair, G. M., Long, S. M., & Jones, O. A. H. (2020). What are the effects of PFAS exposure at environmentally relevant concentrations? *Chemosphere*, *258*, 127340. https://doi.org/10.1016/j.chemosphere.2020.127340

Smyth, T.P & Corby, B.W. (1998). Toward a clean alternative to friedel−crafts acylation: In situ formation, observation, and reaction of an acyl bis(trifluoroacetyl)phosphate and related structures. *J. Org. Chem.*, *63* (24), 8946 - 8951. DOI: 10.1021/jo981264v

Soung, Kim, & Le, Donald. (2020, August 21). *Bond energies*. LibreTexts Chemistry. https://chem.libretexts.org/Bookshelves/Physical_and_Theoretical_Chemistry_Textbook_Maps/Supplemental_Modules_(Physical_and_Theoretical_Chemistry)/Chemical_Bonding/Fundamentals_of_Chemical_Bonding/Bond_Energies

Stahl, T., Heyn, J., Thiele, H., Hüther, J., Failing, K., Georgii, S., & Brunn, H. (2009). Carryover of Perfluorooctanoic Acid (PFOA) and Perfluorooctane Sulfonate (PFOS) from Soil to Plants. *Archives of Environmental Contamination and Toxicology*, *57*(2), 289–298. https://doi.org/10.1007/s00244-008-9272-9

Sunderland, E. M., Hu, X. C., Dassuncao, C., Tokranov, A. K., Wagner, C. C., Allen, J. G. (2019). A review of the pathways of human exposure to poly- and perfluoroalkyl substances (PFASs) and present understanding of health effects. *J Expo Sci Environ Epidemiol*, *29*(2), 131–147. https://doi.org/10.1038/s41370-018-0094-1.

The National Institute for Occupational Safety and Health. (2022, September). *Per- and Polyfluoroalkyl Substances (PFAS).* Centers for Disease Control and Prevention. https://www.cdc.gov/niosh/topics/pfas/default.html

United States Environmental Protection Agency. (2022, March 16). *Our current understanding of the human health and environmental risks of PFAS*. EPA. https://www.epa.gov/pfas/our-current-understanding-human-health-and-environmental-risks-pfas

US EPA. (2022). *PFAS treatment in drinking water and wastewater – State of the science*. https://www.epa.gov/research-states/pfas-treatment-drinking-water-and-wastewater-state-science

Yadava, S., Ibrar, I., Al-Juboori, R.A., Singha, L., Ganbata, N., Kazwinia, T., Karbassiyazdia, E., Samal, A.K., Subbiah, S., &, Altaee, S.A. (2022, June). Updated review on emerging technologies for PFAS contaminated water treatment. *Chemical Engineering Research and Design*, *182*, 667-700. https://doi.org/10.1016/j.cherd.2022.04.009

Xu, B., Zhou, J.L., Altaee, A., Ahmed, M.B., Johir, M.A.H., Ren, J., & Li, X. (2020). Improved photocatalysis of perfluorooctanoic acid in water and wastewater by Ga_2O_3/UV system assisted by peroxymonosulfate. *Chemosphere*, *239*, 1-9. https://doi.org/10.1016/j.chemosphere.2019.124722

7.0 Appendix

Appendix A. PFOA Standard Curve Calculations

Dilutions for Standard Curve

Making a series of dilutions of PFOA concentrations, 4.0mM, 2.0mM, 1.0mM, 0.5mM and 0.1mM.

4mM PFOA (stock solution):
PFOA molar mass: 414.07 g/mol

$$concentration(M) = \frac{n\ (mols)}{volume\ (L)}$$

Desired concentration is 0.004M, and the desired amount is 0.4 liters.

$$0.004M = \frac{n\ (mols)}{0.4\ L}$$
$$n\ (mols) = 0.0016\ mols$$
$$0.0016\ mols * \left(\frac{414.07\ g}{1\ mol}\right) = 0.662512\ g\ PFOA\ is\ required\ to\ make\ the\ 4mM$$

2mM PFOA:
Using the dilution equation, where M_1 is the initial concentration and V_1 is the amount of the initial volume, M_2 is the desired concentration, and V_2 is the total final volume. 20mL is the total final volume for all dilutions.

$$M_1V_1 = M_2V_2$$
$$(4mM) * (V_1) = (2mM) * (20mL)$$
$$V_1 = 10mL\ of\ the\ 4mM\ stock\ solution\ is\ required\ to\ make\ the\ 2mM\ dilution$$

1mM PFOA:
$$(4mM) * (V_1) = (1mM) * (20mL)$$
$$V_1 = 5mL\ of\ the\ 4mM\ stock\ solution\ is\ required\ to\ make\ the\ 1mM\ dilution$$

0.5mM PFOA:
$$(1mM) * (V_1) = (0.5mM) * (20mL)$$
$$V_1 = 10mL\ of\ the\ 1mM\ stock\ solution\ is\ required\ to\ make\ the\ 0.5mM\ dilution$$

0.1mM PFOA:

$(1mM) * (V_1) = (0.1mM) * (20mL)$

$V_1 = 2mL\ of\ the\ 1mM\ stock\ solution\ is\ required\ to\ make\ the\ 0.1mM\ dilution$

Creating Standard Curve

These dilutions are put in the NMR to create a standard curve. Looking at the peak at -80.73 ppm which will obtain the integral peak area (abs) of the -CF_3 group.

Table 20. The integral area under the -CF_3 peak for PFOA samples at the following concentrations: 4, 2, 1, 0.5, and 0.1 mM.

Concentration (mM)	**-CF_3 integral peak area (abs)**
4	6.1E+13
2	3.1E+13
1	1.4E+13
0.5	7.0E+12
0.1	1.5E+12

The graph for the standard curve can be generated. A linear fit was applied and equation which yields the equation:

$$y = (6.457 \cdot 10^{-14})(x) + 0.0338$$

Calculating Concentration from Standard Curve: Example

Using the equation generated from the line of best fit, $y = (6.457 \cdot 10^{-14})(x) + 0.0338$, y represents the concentration and x represents the peak integral area.

Peak integral area of 1:1 Ga_2O_3/PMS/UV at time 0 minutes: 1.308 E-13

$y = 6.457 \cdot 10^{-14}(1.308 * 10^{-13}) + 0.0338$

$y = 0.88$

The PFOA concentration of the sample is 0.88mM based on the standard curve.

Appendix B. Error Analysis

Standard Curve Dilution Errors

4 mM PFOA Example:

$$m_{PFOA} = 0.4140 \pm 0.0001\ g$$

$$n_{PFOA} = 0.4140\ g \cdot \frac{1\ mol}{414.07\ g} = 9.998\ x\ 10^{-4} \pm 2\ x\ 10^{-7} moles$$

$$\delta n_{PFOA} = \frac{0.0001\ g}{414.07\ g/mol} = 2\ x\ 10^{-7} moles$$

The volume of water was measured using a 100-mL graduated cylinder with an uncertainty of 0.5 mL. Therefore, the uncertainty was calculated as shown below:

$$V_{H2O} = (100 + 100 + 50)mL = 250.0 \pm 0.9\ mL$$

$$\delta V_{H2O} = \sqrt{(0.5)^2 + (0.5)^2 + (0.5)^2} = 0.9\ mL$$

$$C_{PFOA} = \frac{n_{PFOA}}{V_{H2O}} = \frac{9.998\ x\ 10^{-4}\ moles}{250.0\ mL} \cdot \frac{1000\ mL}{1\ L} \cdot \frac{1000\ mmoles}{1\ mole} = 4.00 \pm 0.01\ mM$$

$$\delta C_{PFOA} = C_{PFOA}\sqrt{\left(\frac{\delta V_{H2O}}{V_{H2O}}\right)^2 + \left(\frac{\delta n_{PFOA}}{n_{PFOA}}\right)^2} = 4.00 mM\sqrt{\left(\frac{0.9}{250}\right)^2 + \left(\frac{2\ x\ 10^{-7}}{9.998\ x\ 10^{-4}}\right)^2} = 0.01\ mM$$

2 mM PFOA Dilution Example:

(1) 4 mM & (2) 2 mM

The volumes for each dilution were measured using 5 mL graduated pipettes with uncertainties 0f 0.05mL. Therefore, the uncertainty was calculated as shown below:

$$V_1 = (5 + 5)mL = 10.0 \pm 0.1\ mL$$

$$\delta V_1 = \sqrt{(0.05)^2 + (0.05)^2} = 0.07\ mL \approx 0.1\ mL$$

$$V_2 = (5 + 5 + 5 + 5)mL = 20.0 \pm 0.1\ mL$$

$$\delta V_1 = \sqrt{(0.05)^2 + (0.05)^2 + (0.05)^2 + (0.05)^2} = 0.1 mL$$

$$C_2 = \frac{C_1V_1}{V_2} = \frac{(40.0\ mM \cdot mL)}{20.0\ mL} = 2.00\ \pm\ 0.02\ mM$$

$$C_1V_1 = (4.00mM)(10.0mL) = 40.0\ \pm\ 0.3\ mM\ \cdot\ mL$$

$$\delta C_1V_1 = C_1V_1\sqrt{(\frac{\delta C_1}{C_1})^2\ +\ (\frac{\delta V_1}{V_1})^2} = 40.0\ mM\ \cdot\ mL\sqrt{(\frac{0.01}{4.00})^2\ +\ (\frac{0.1}{10})^2} = 0.3\ mM\ \cdot\ mL$$

$$\delta C_2 = C_2\sqrt{(\frac{\delta C_1V_1}{C_1V_1})^2\ +\ (\frac{\delta V_2}{V_2})^2} = 2.0\ mM\sqrt{(\frac{0.3}{40.0})^2\ +\ (\frac{0.1}{20.0})^2} = 0.02\ mM$$

Concentration Error from Standard Curve

PFOA Standard Curve Example:

The concentration of PFOA was plotted against the peak integral area to create the standard curve. A linear fit was applied to the data to yield the following equation:

$$y = mx + b \rightarrow y = 6.457 \cdot 10^{-14}(x)\ + 0.0337$$

where "y" represents the concentration and "x" represents the peak integral area. From Excel, the slope and y-intercept errors were obtained as shown below:

$$slope\ error: \delta m = 9 \cdot 10^{-16}$$
$$y - intercept\ error: \delta b = 0.0292$$

To calculate the concentration of a given sample, the peak integral area for the -CF_3 signal was obtained from TopSpin and plugged into the equation for the standard equation. For a sample with a peak integral area of $7.213 \cdot 10^{12}$, the concentration was calculated as followed:

$$C_{PFOA} = 6.457 \cdot 10^{-14}(7.213 \cdot 10^{12})\ + 0.0337 = 0.50\ \pm\ 0.03\ mM$$

$$\delta mx = mx\sqrt{(\frac{\delta m}{m})^2\ +\ (\frac{\delta x}{x})^2} = 6.457 \cdot 10^{-14}(7.213 \cdot 10^{12})\sqrt{(\frac{9 \cdot 10^{-16}}{6.457 \cdot 10^{-14}})^2\ +\ (\frac{1 \cdot 10^{8}}{7.213 \cdot 10^{12}})^2}$$
$$\delta mx = 0.47$$

$$\delta C_{PFOA} = \sqrt{(\delta mx)^2\ +\ (\delta b)^2} = \sqrt{(0.47)^2\ +\ (0.0292)^2} = 0.03$$

Appendix C. NMR Spectrum

PFOA Standard Curve:

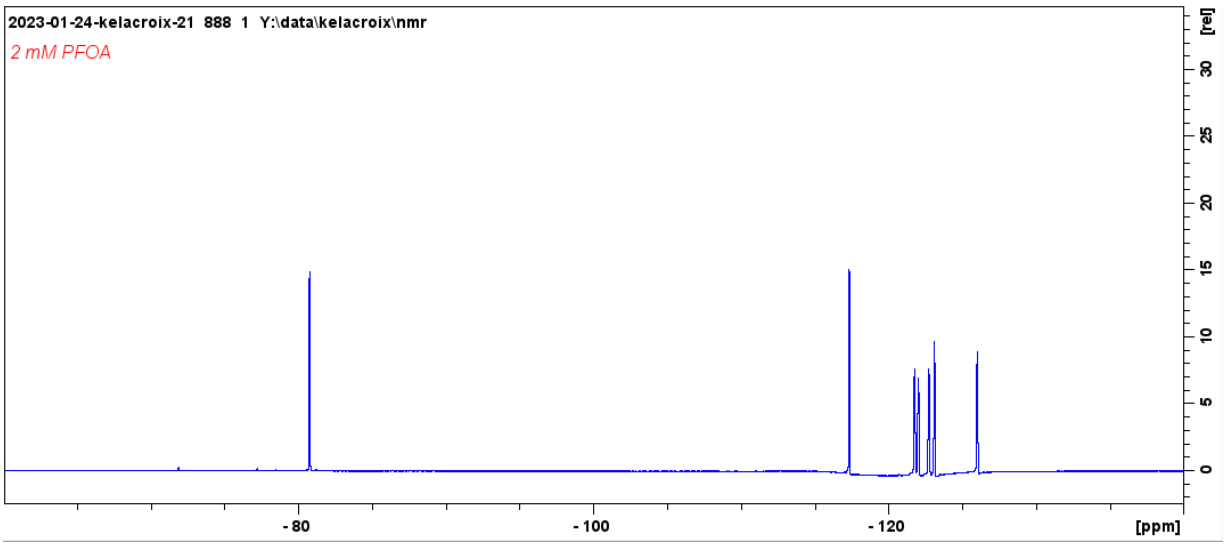

Figure 63. NMR Spectrum for 2 mM aqueous PFOA solution.

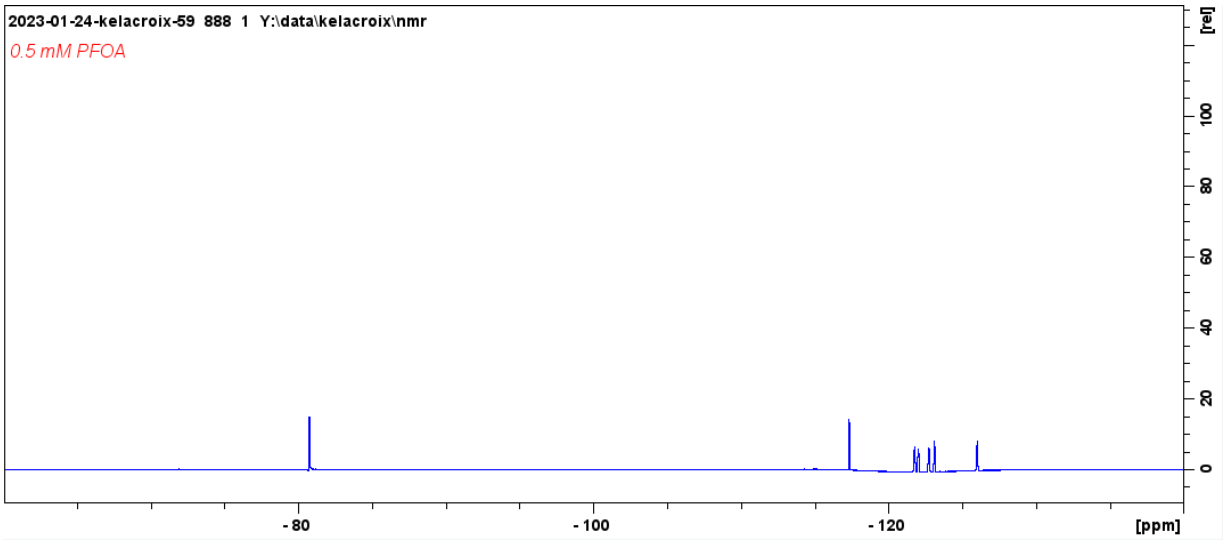

Figure 64. NMR Spectrum for 0.5 mM aqueous PFOA solution.

GenX Standard Curve:

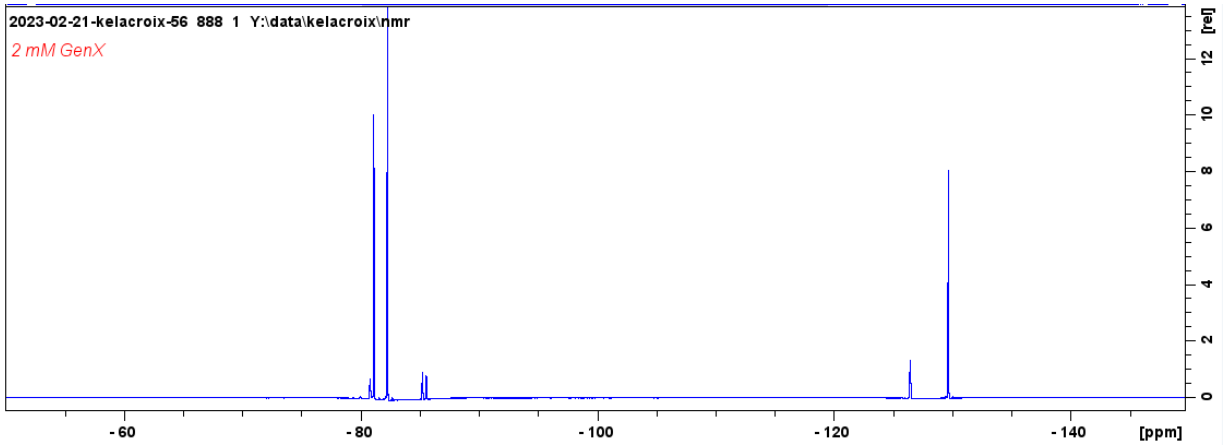

Figure 65. NMR Spectrum for 2 mM aqueous GenX solution.

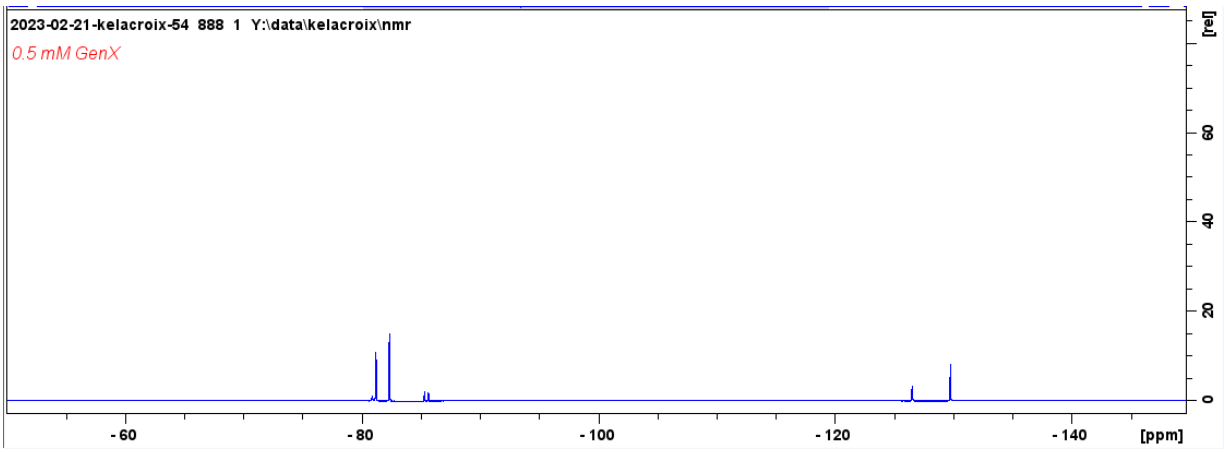

Figure 66. NMR Spectrum for 0.5 mM aqueous GenX solution.

$\underline{Ga_2O_3/PMS\ Controls:}$

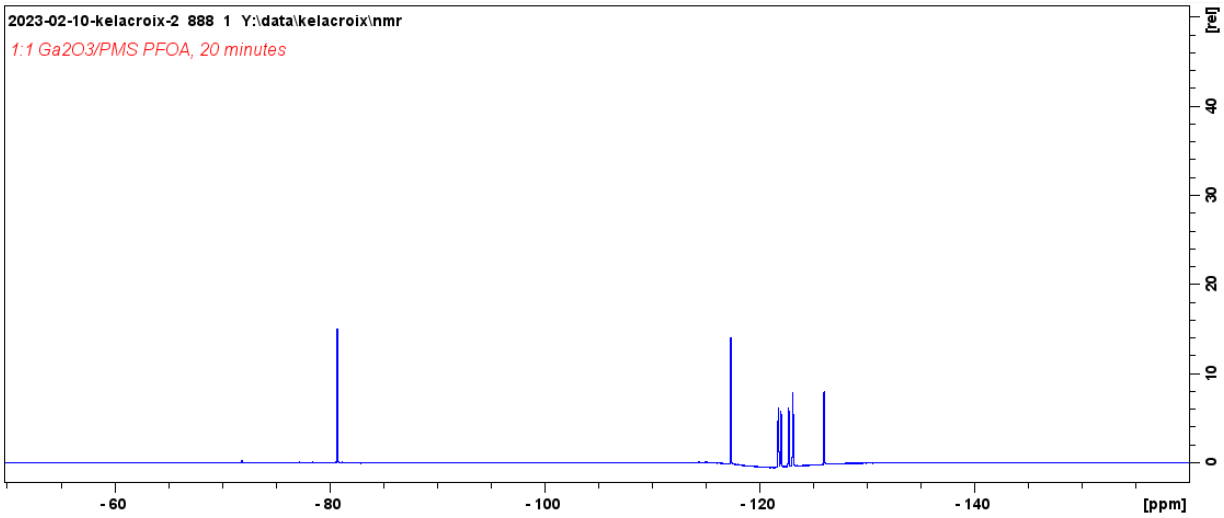

Figure 67. NMR Spectrum for the 1:1 Ga_2O_3/PMS, PFOA control at 20 minutes.

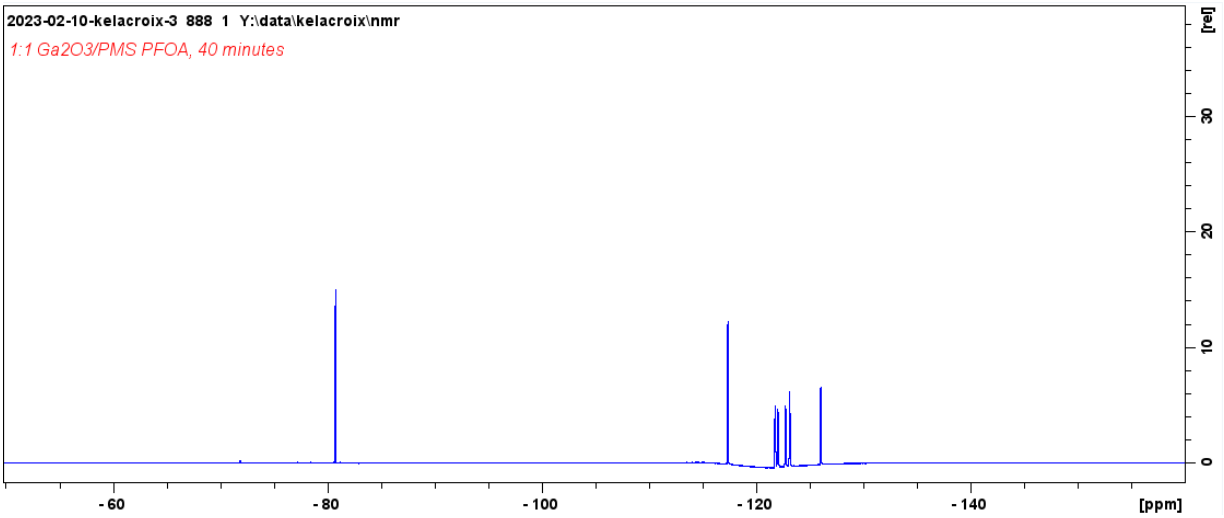

Figure 68. NMR Spectrum for the 1:1 Ga_2O_3/PMS, PFOA control at 40 minutes.

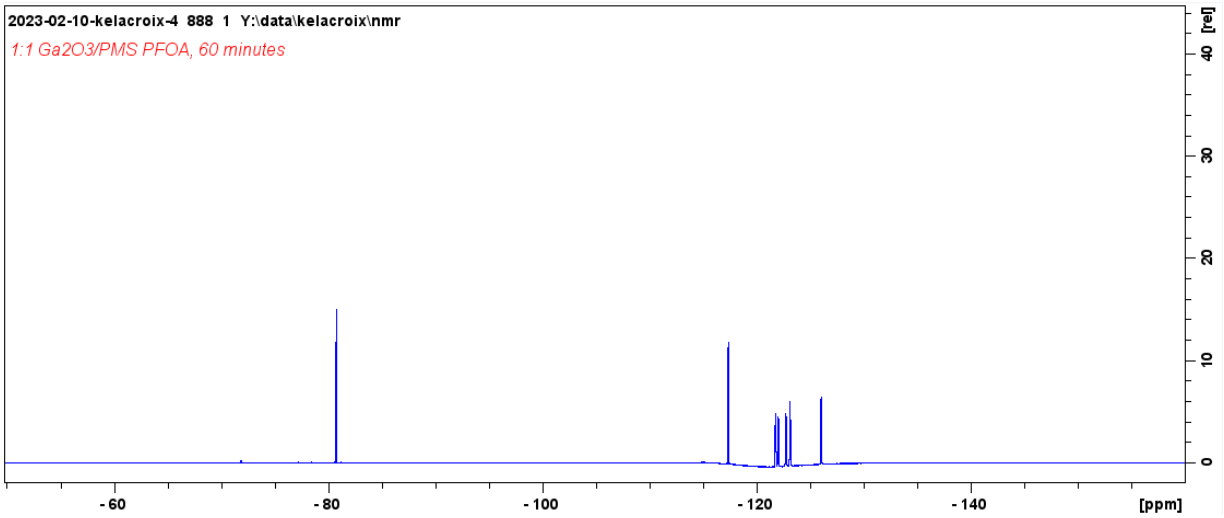

Figure 69. NMR Spectrum for the 1:1 Ga_2O_3/PMS, PFOA control at 60 minutes.

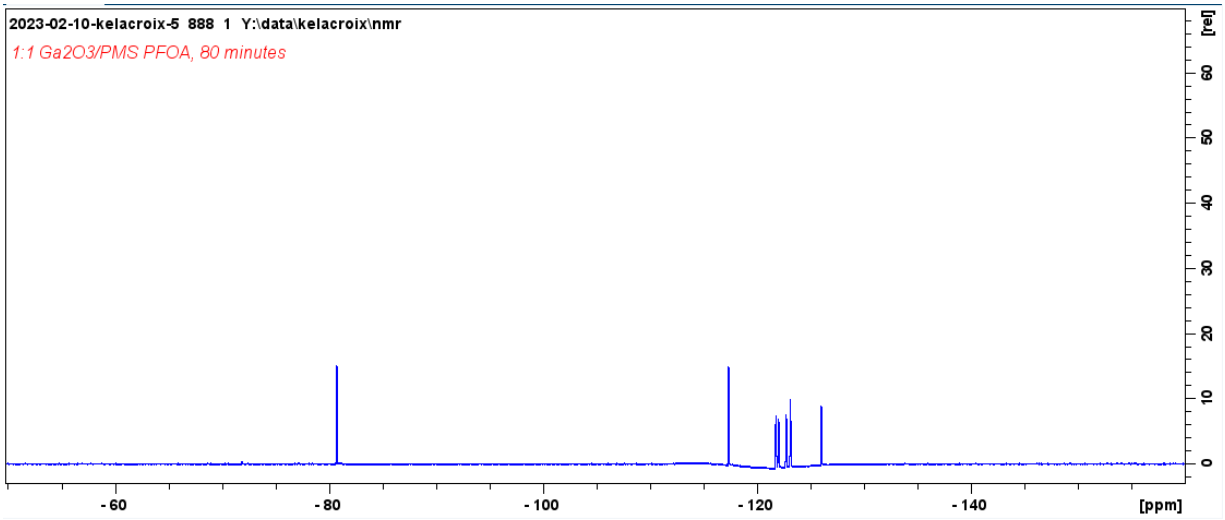

Figure 70. NMR Spectrum for the 1:1 Ga_2O_3/PMS, PFOA control at 80 minutes.

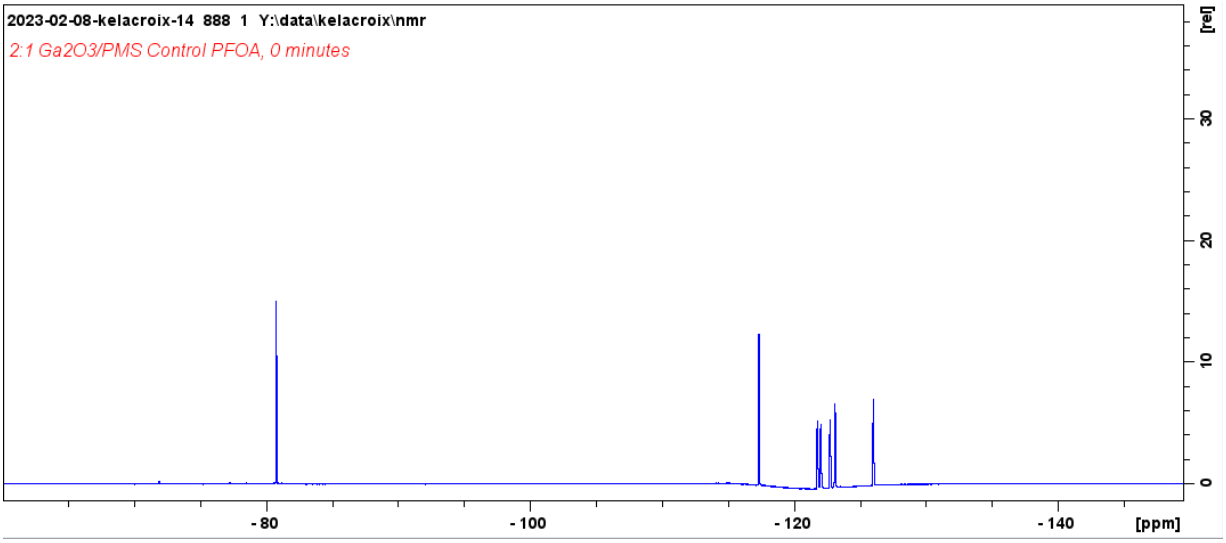

Figure 71. NMR Spectrum for the 2:1 Ga_2O_3/PMS, PFOA control at 0 minutes.

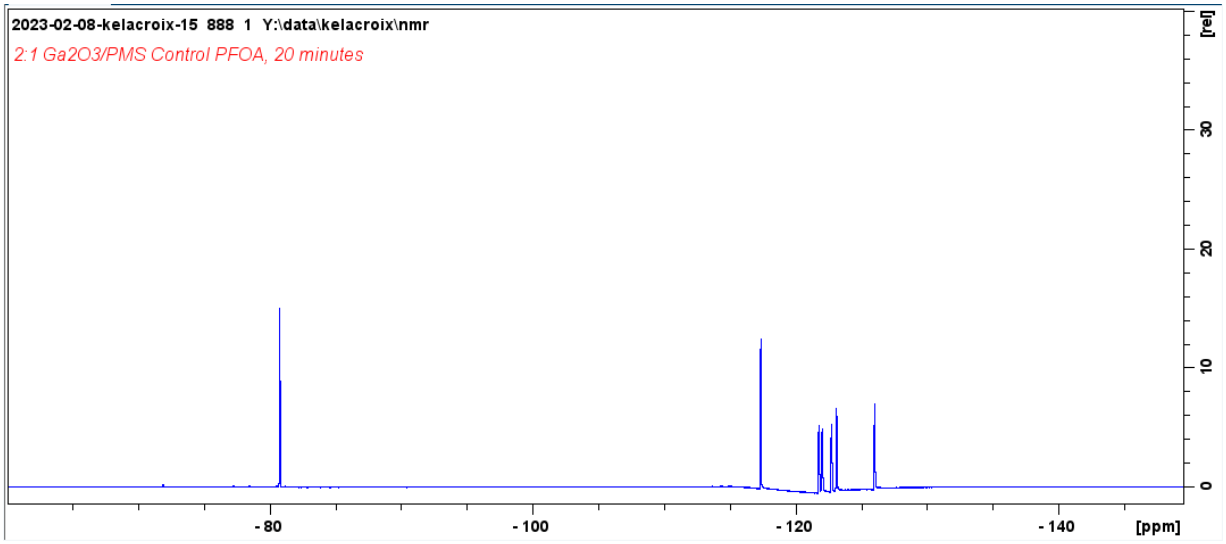

Figure 72. NMR Spectrum for the 2:1 Ga_2O_3/PMS, PFOA control at 20 minutes.

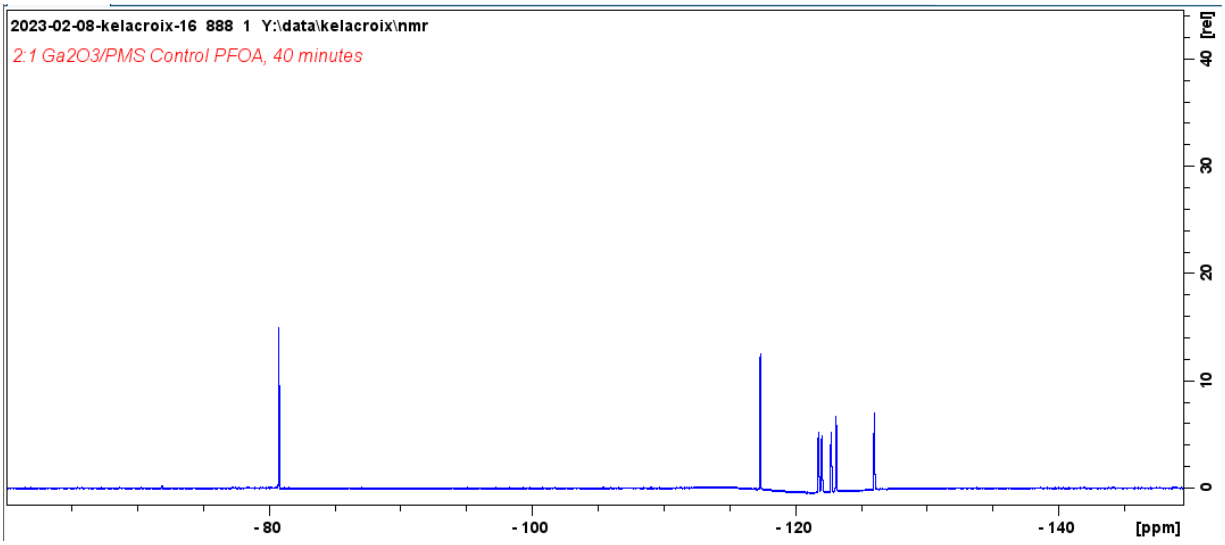

Figure 73. NMR Spectrum for the 2:1 Ga_2O_3/PMS, PFOA control at 40 minutes.

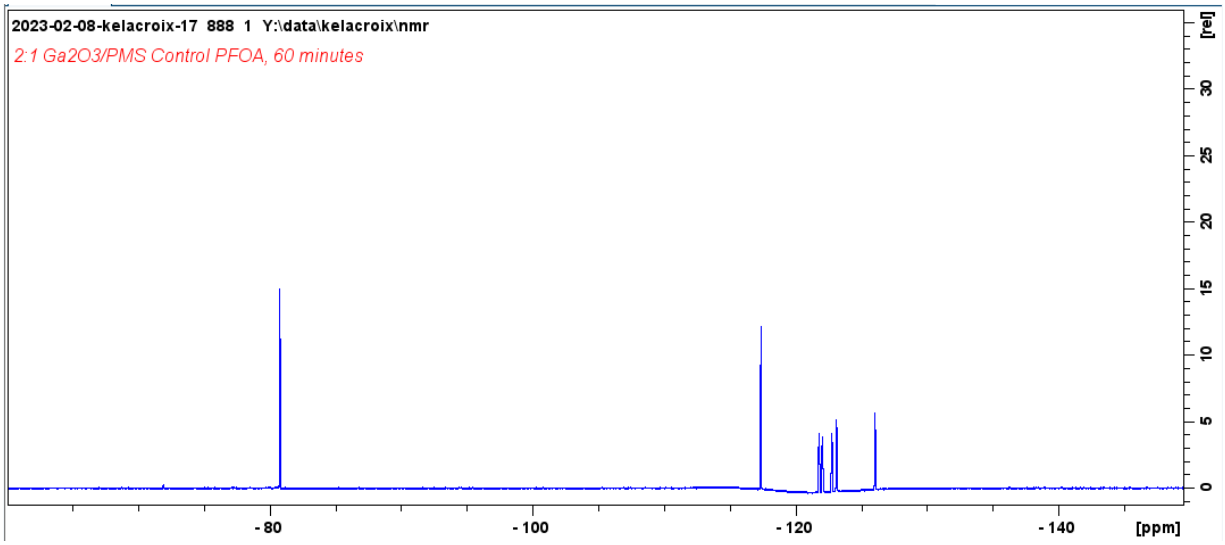

Figure 74. NMR Spectrum for the 2:1 Ga_2O_3/PMS, PFOA control at 60 minutes.

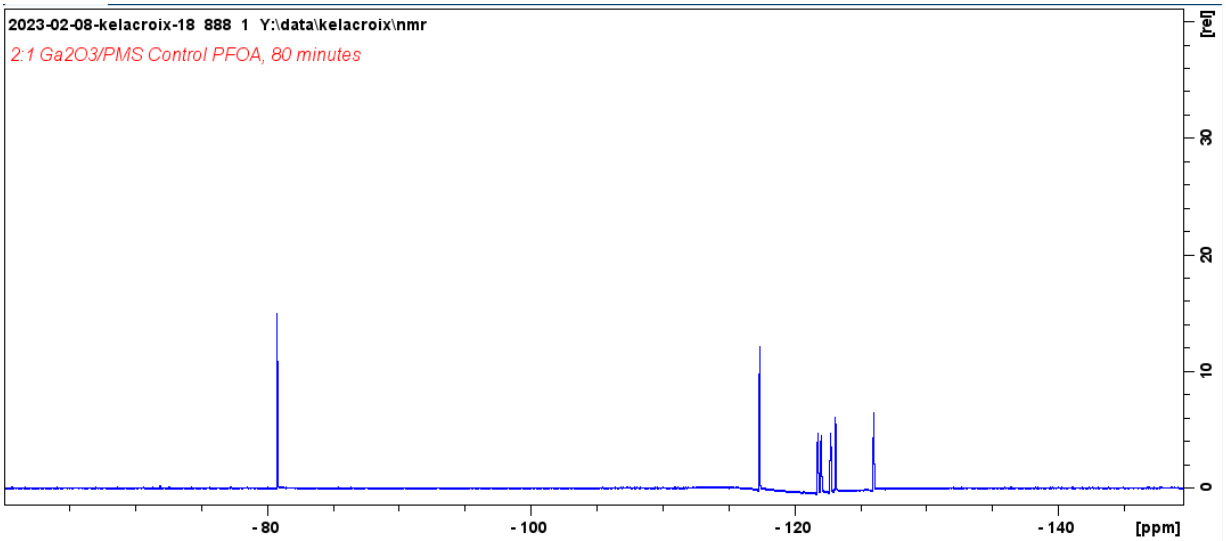

Figure 75. NMR Spectrum for the 2:1 Ga_2O_3/PMS, PFOA control at 80 minutes.

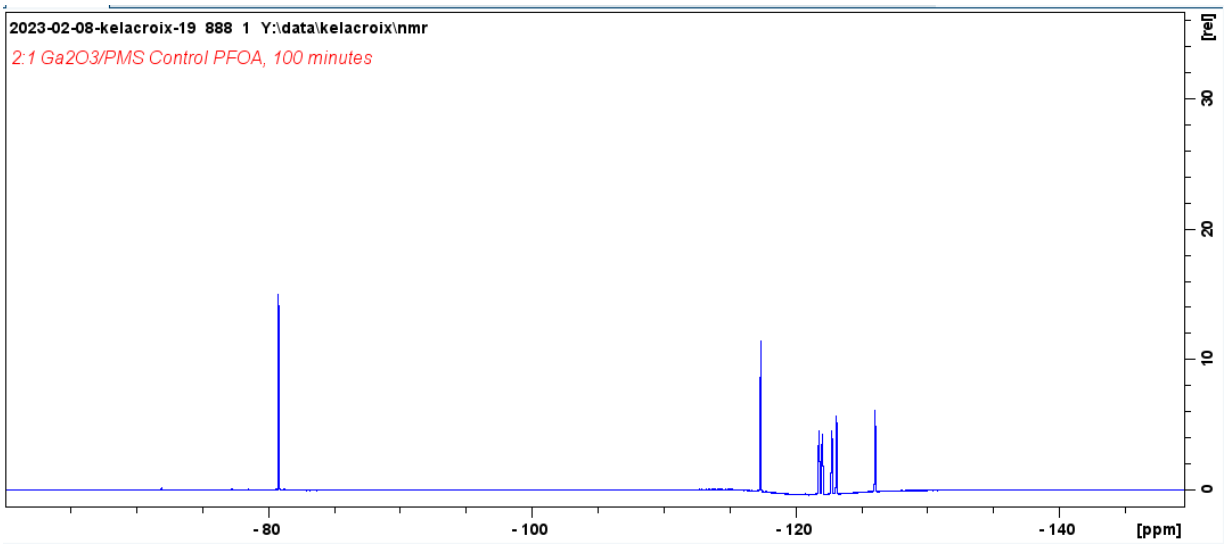

Figure 76. NMR Spectrum for the 2:1 Ga_2O_3/PMS, PFOA control at 100 minutes.

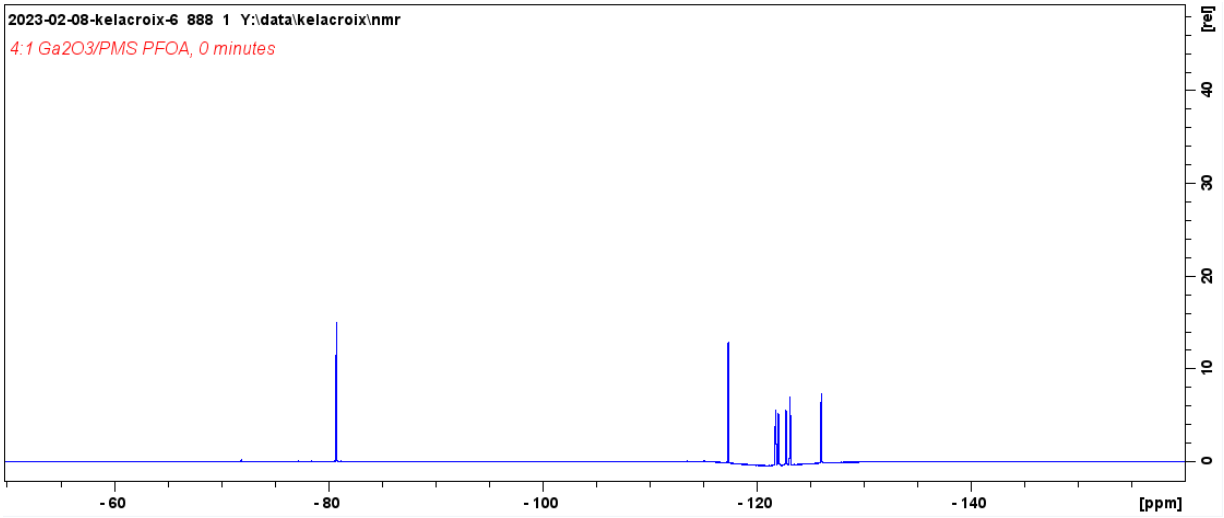

Figure 77. NMR Spectrum for the 4:1 Ga_2O_3/PMS, PFOA control at 0 minutes.

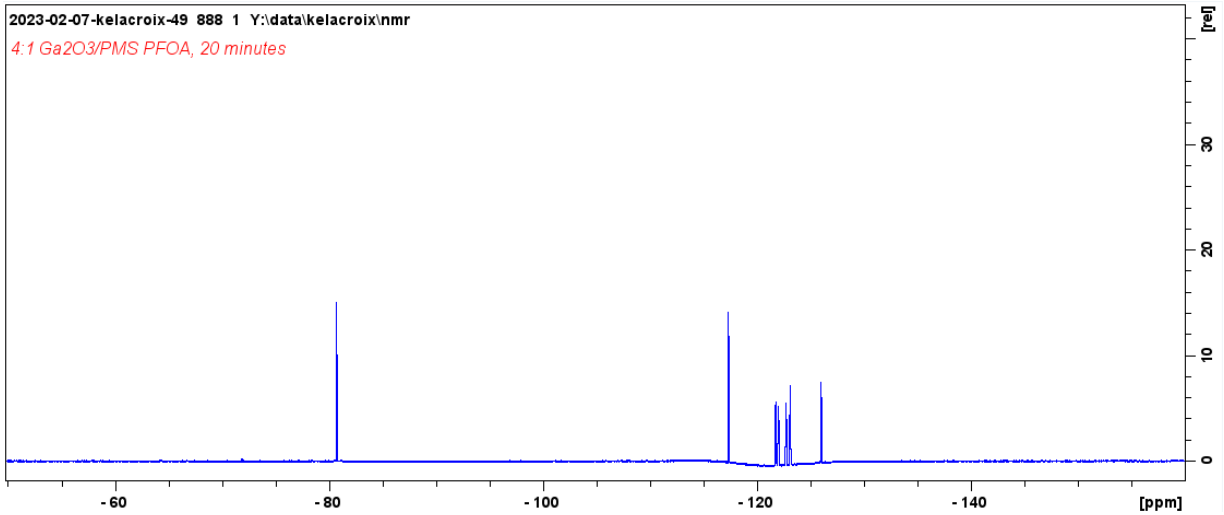

Figure 78. NMR Spectrum for the 4:1 Ga_2O_3/PMS, PFOA control at 20 minutes.

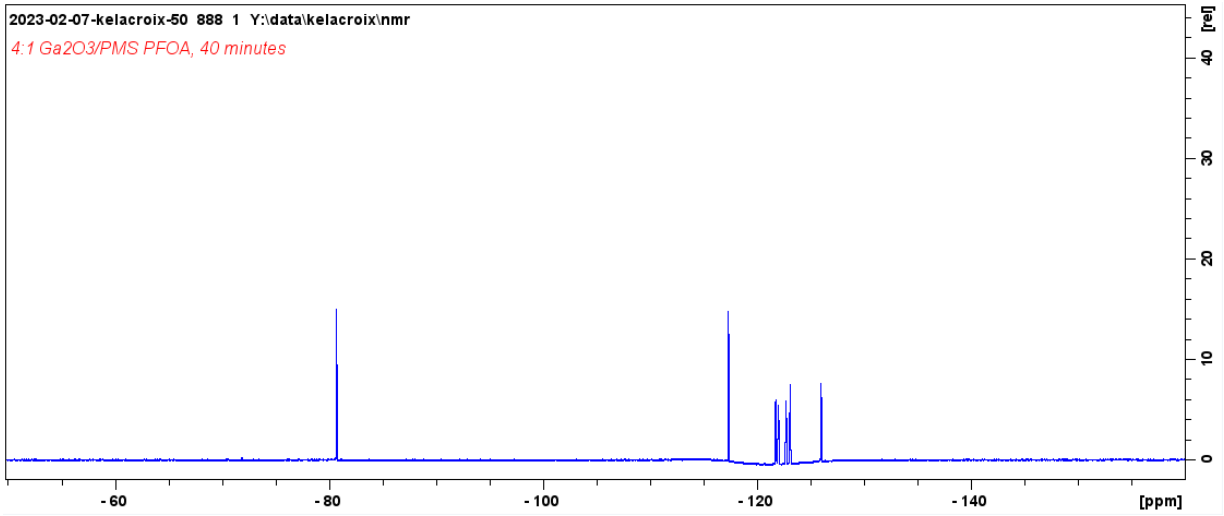

Figure 79. NMR Spectrum for the 4:1 Ga_2O_3/PMS, PFOA control at 40 minutes.

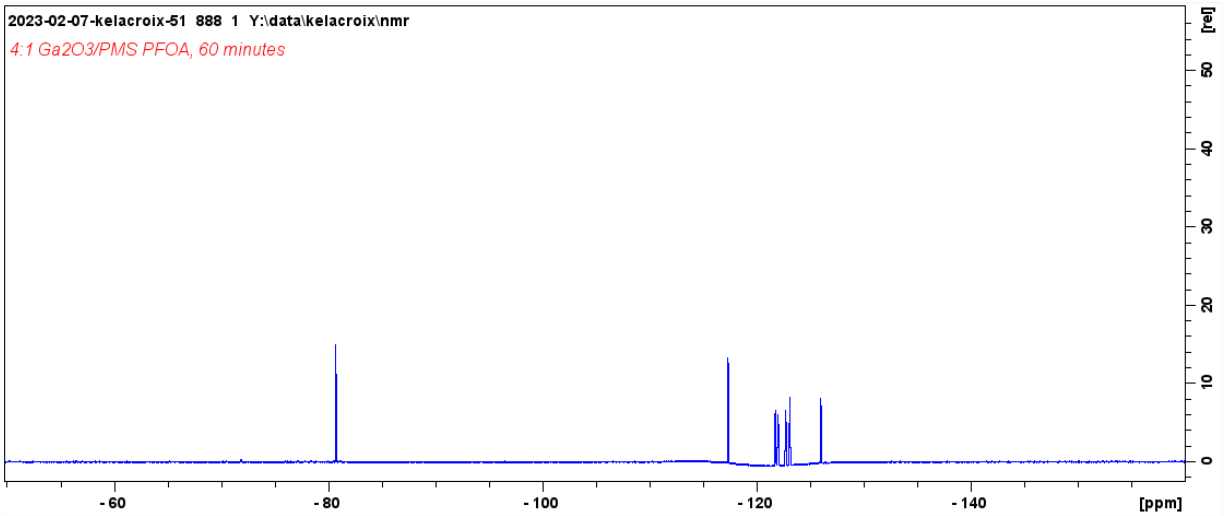

Figure 80. NMR Spectrum for the 4:1 Ga_2O_3/PMS, PFOA control at 60 minutes.

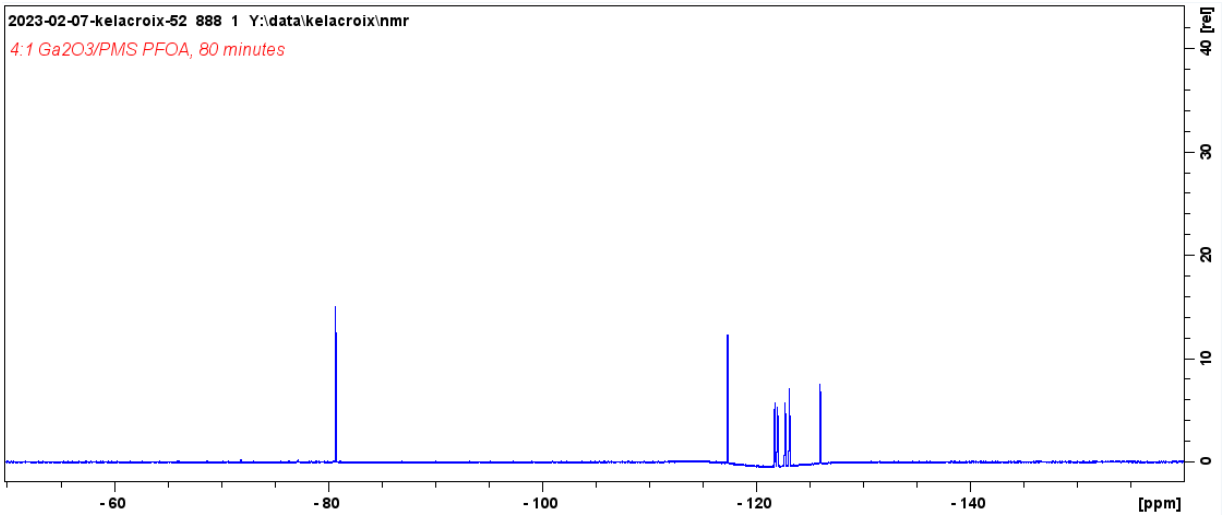

Figure 81. NMR Spectrum for the 4:1 Ga_2O_3/PMS, PFOA control at 80 minutes.

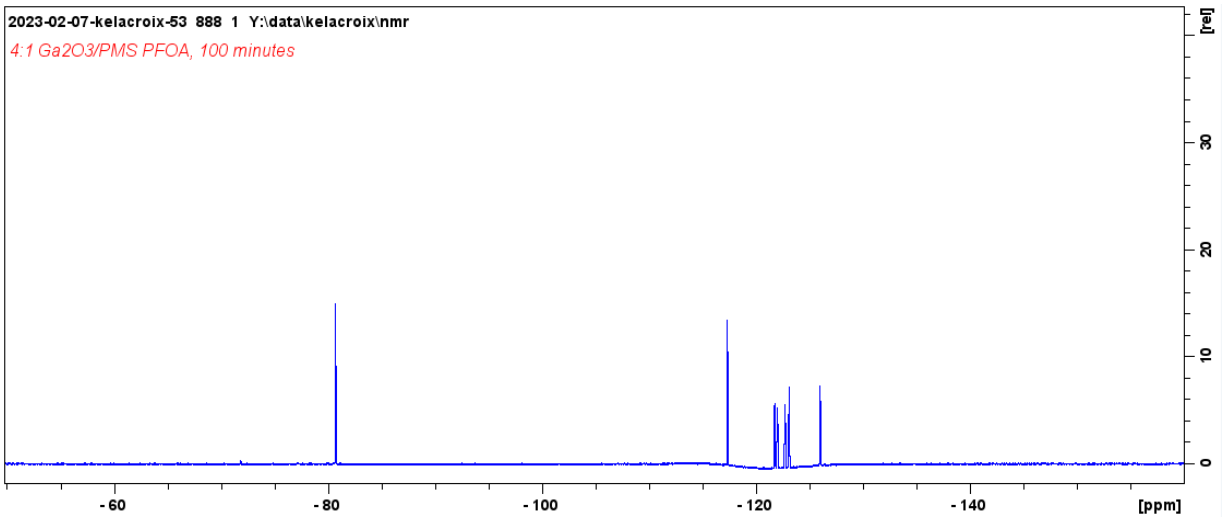

Figure 82. NMR Spectrum for the 4:1 Ga_2O_3/PMS, PFOA control at 100 minutes.

Ga_2O_3/PMS/UV Reactions:

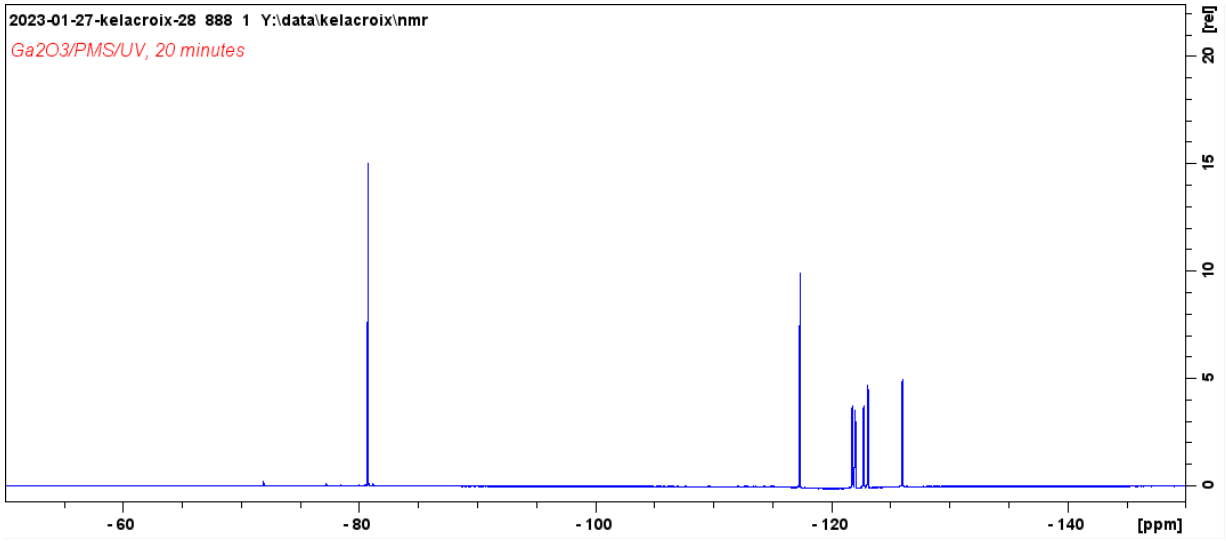

Figure 83. NMR Spectrum for the 1:1 Ga_2O_3/PMS/UV, PFOA control at 20 minutes.

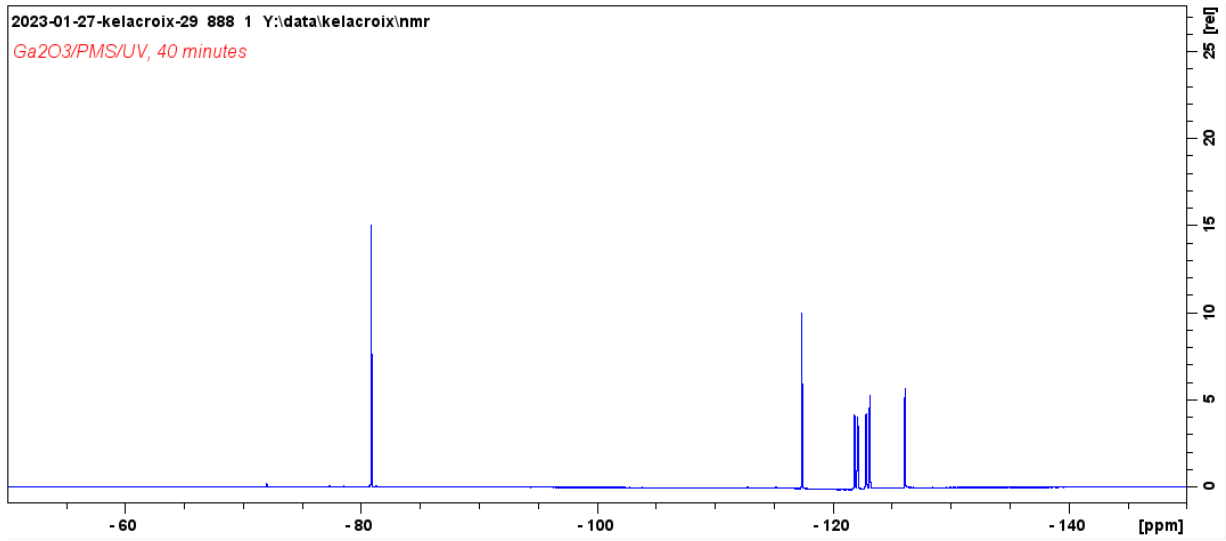

Figure 84. NMR Spectrum for the 1:1 Ga_2O_3/PMS/UV, PFOA control at 40 minutes.

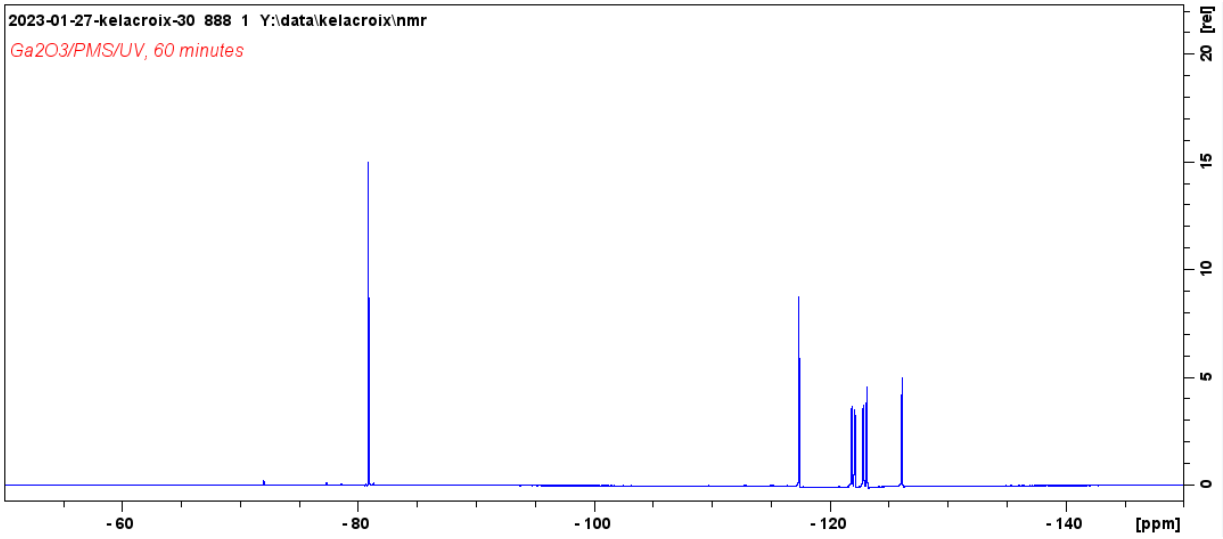

Figure 85. NMR Spectrum for the 1:1 Ga_2O_3/PMS/UV, PFOA control at 60 minutes.

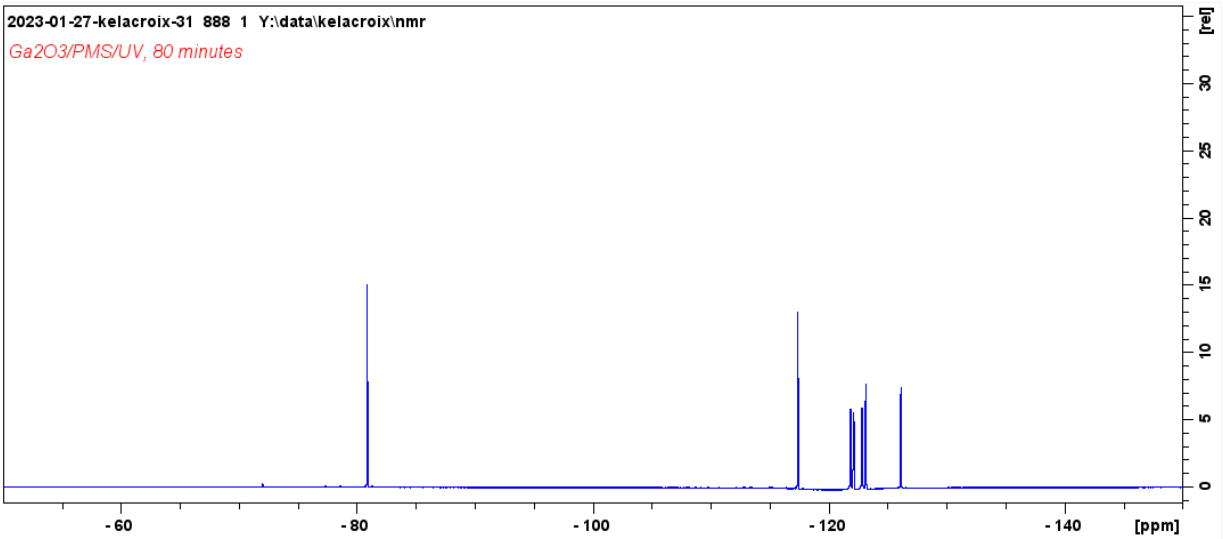

Figure 86. NMR Spectrum for the 1:1 Ga_2O_3/PMS/UV, PFOA control at 80 minutes.

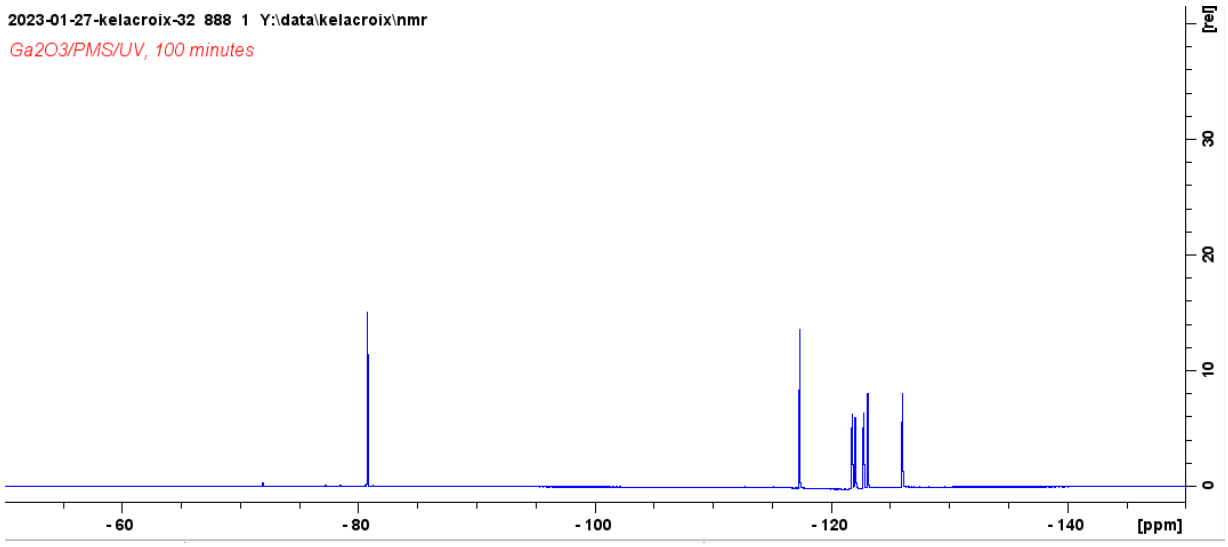

Figure 87. NMR Spectrum for the 1:1 Ga_2O_3/PMS/UV, PFOA control at 100 minutes.

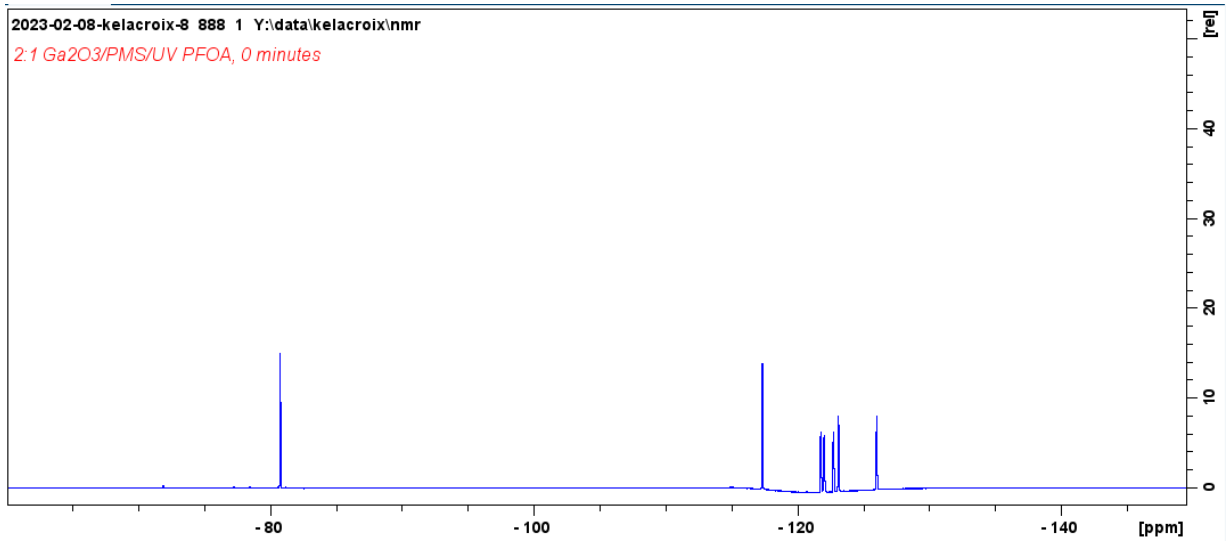

Figure 88. NMR Spectrum for the 2:1 Ga_2O_3/PMS/UV, PFOA control at 0 minutes.

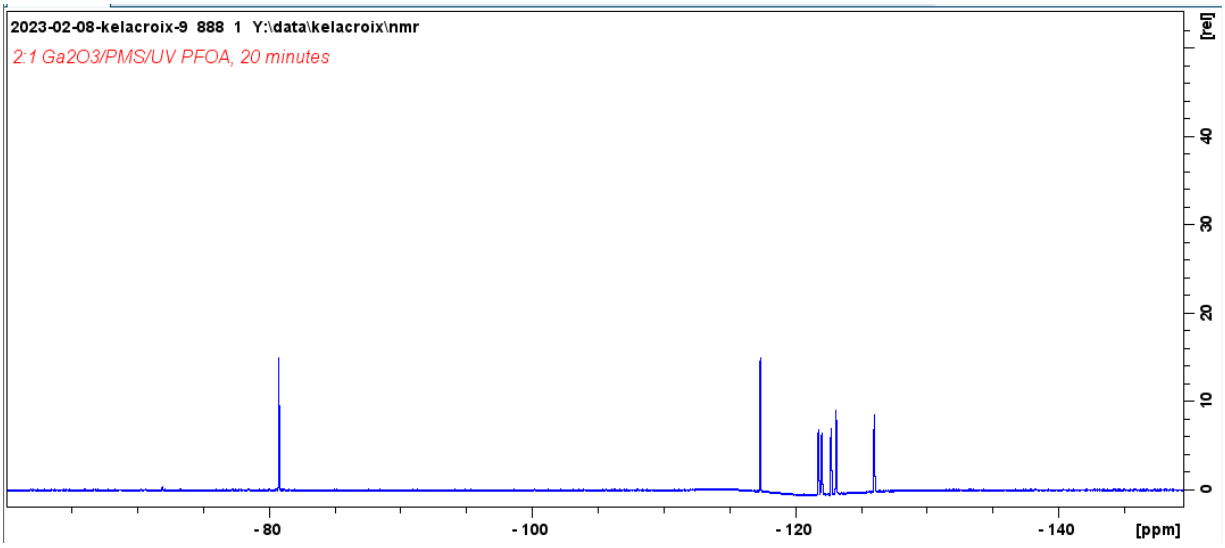

Figure 89. NMR Spectrum for the 2:1 Ga_2O_3/PMS/UV, PFOA control at 20 minutes.

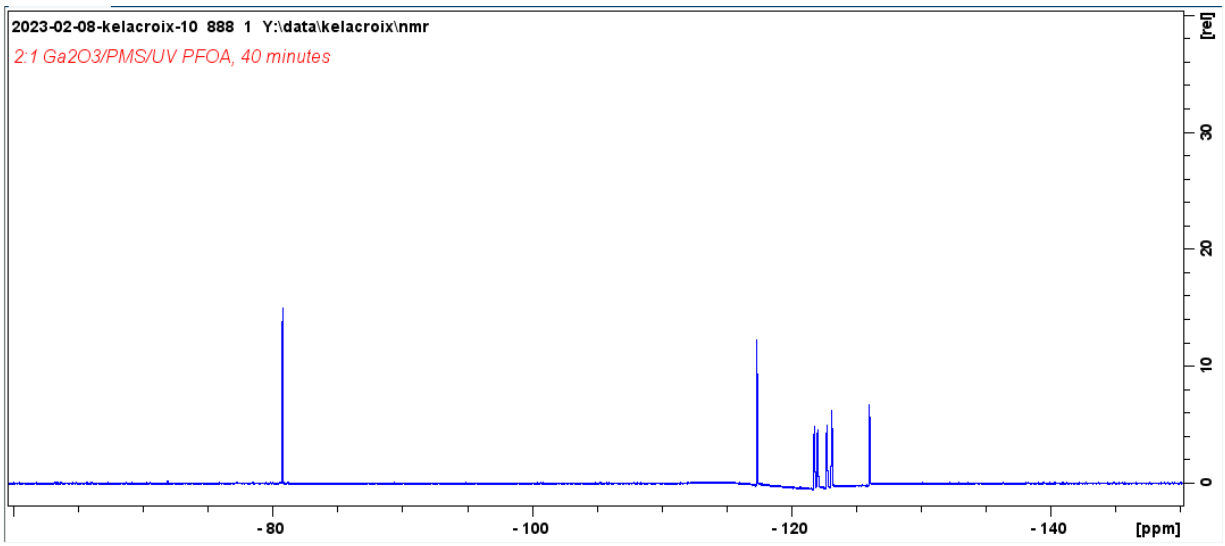

Figure 90. NMR Spectrum for the 2:1 Ga_2O_3/PMS/UV, PFOA control at 40 minutes.

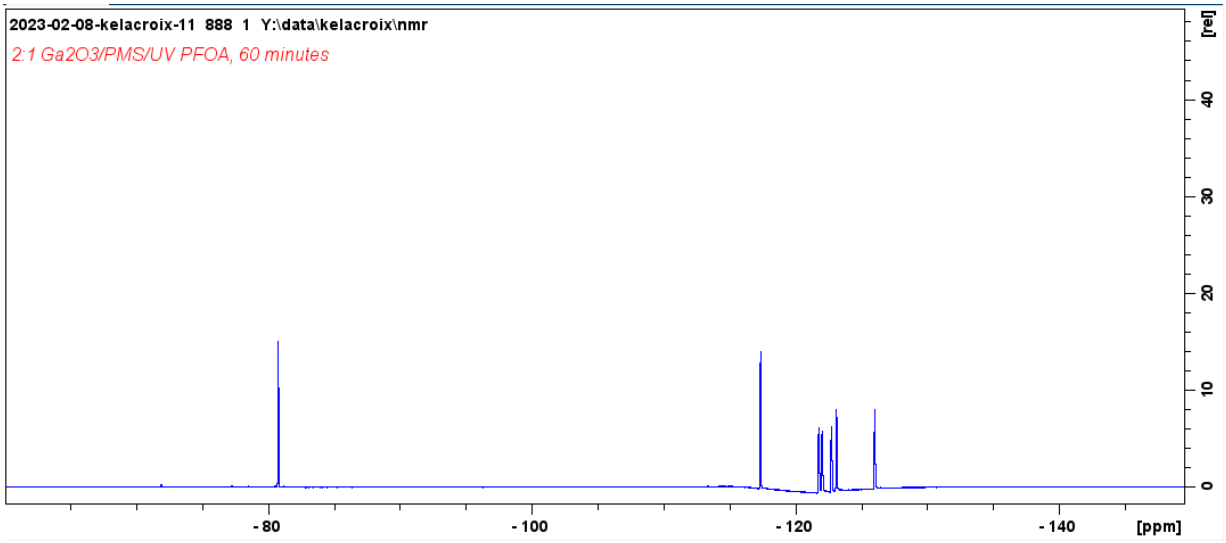

Figure 91. NMR Spectrum for the 2:1 Ga_2O_3/PMS/UV, PFOA control at 60 minutes.

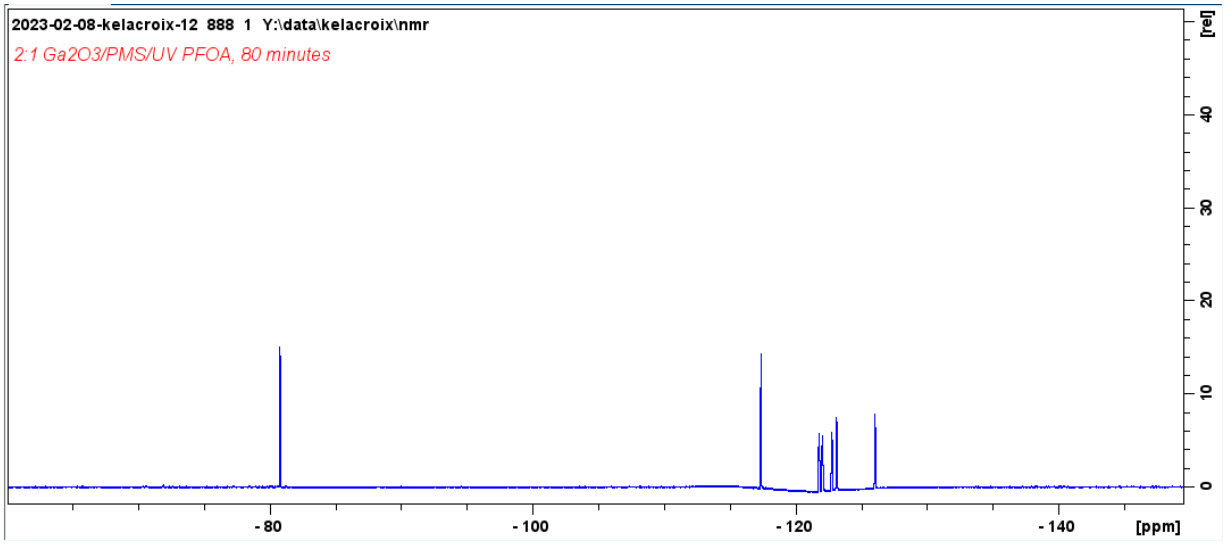

Figure 92. NMR Spectrum for the 2:1 Ga_2O_3/PMS/UV, PFOA control at 80 minutes.

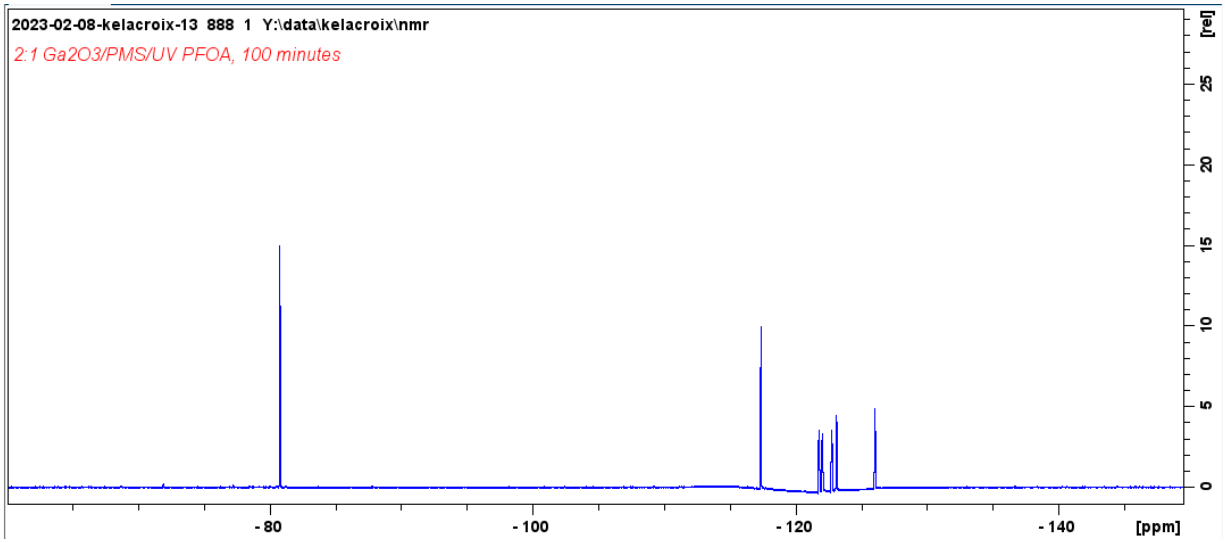

Figure 93. NMR Spectrum for the 2:1 Ga_2O_3/PMS/UV, PFOA control at 100 minutes.

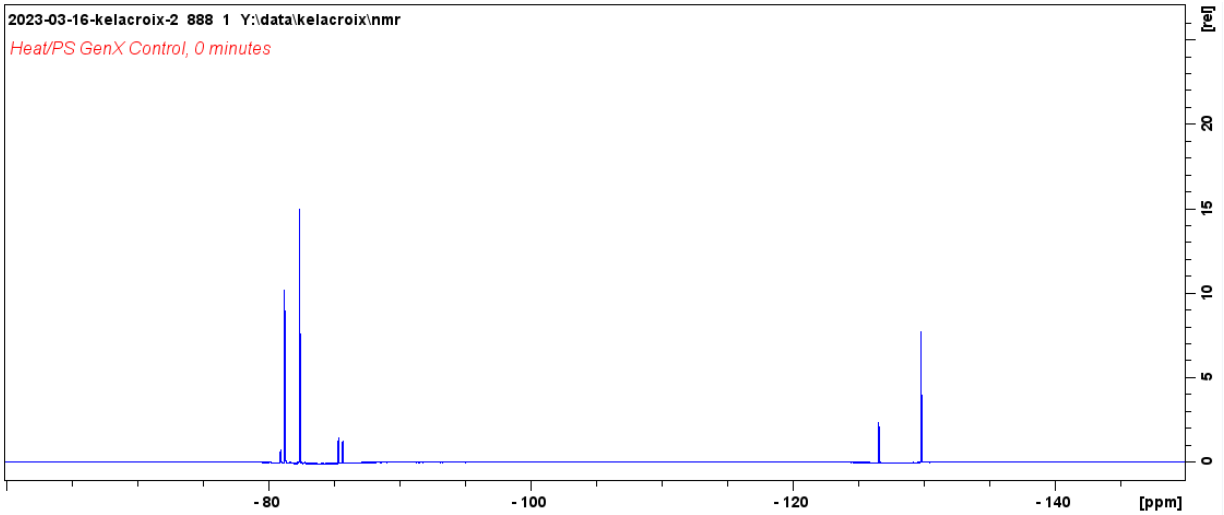

Figure 94. NMR Spectrum for the 4:1 Ga_2O_3/PMS/UV, PFOA control at 0 minutes.

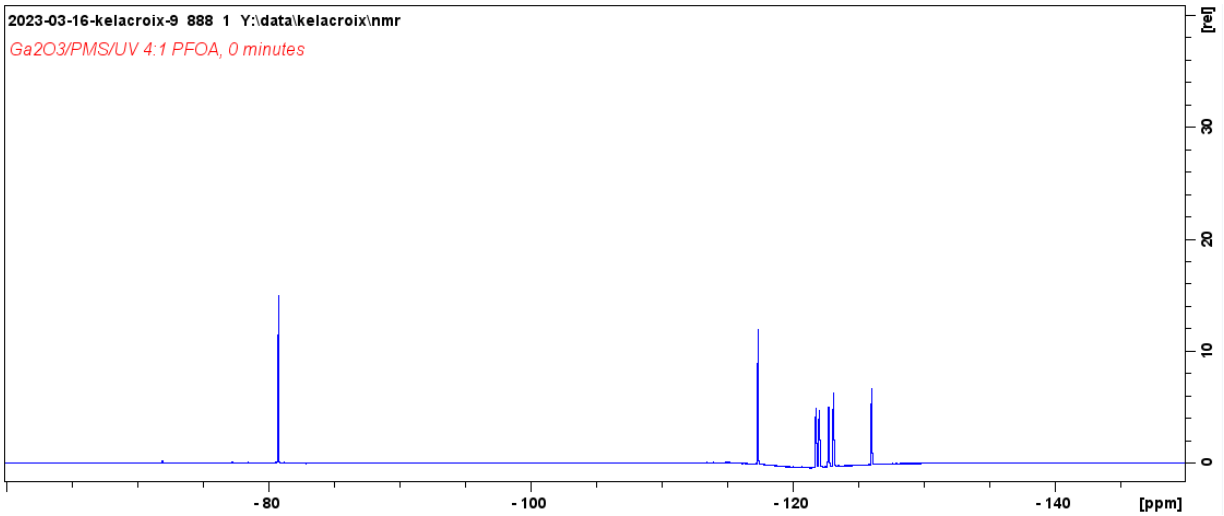

Figure 95. NMR Spectrum for the 4:1 Ga_2O_3/PMS/UV, PFOA control at 0 minutes.

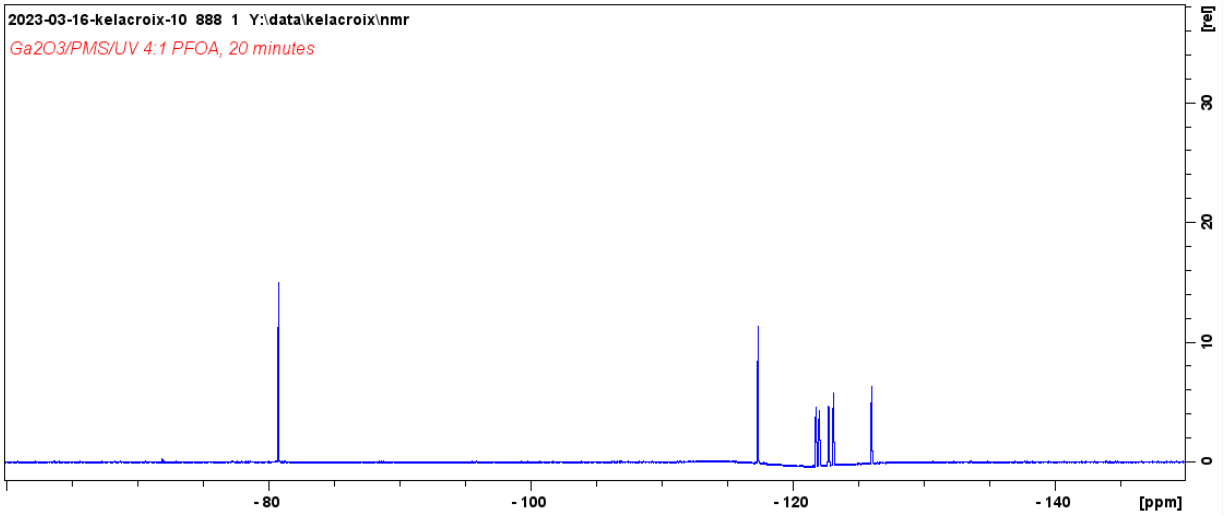

Figure 96. NMR Spectrum for the 4:1 Ga_2O_3/PMS/UV, PFOA control at 20 minutes.

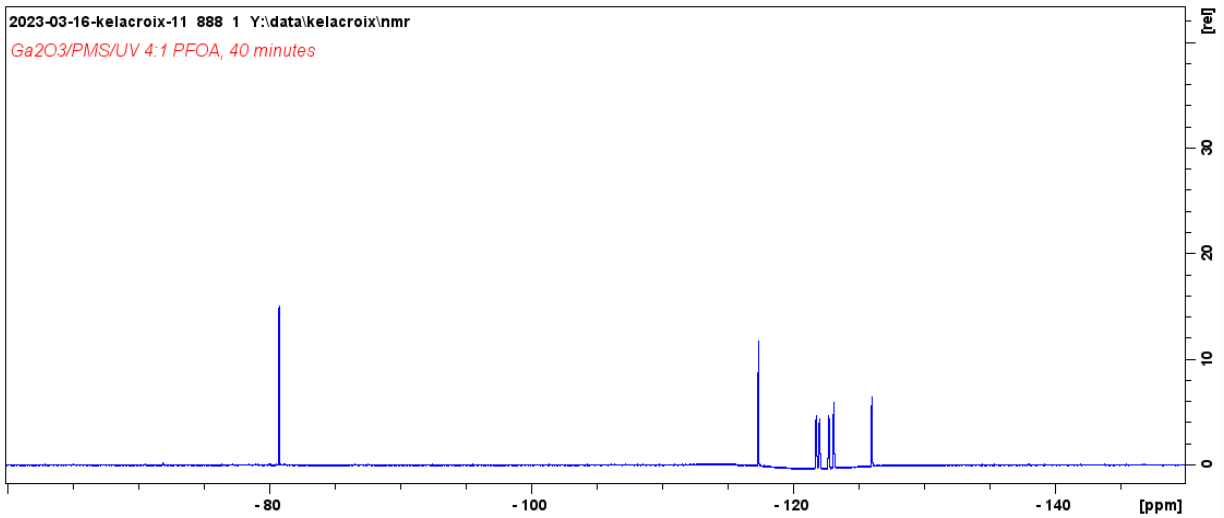

Figure 97. NMR Spectrum for the 4:1 Ga_2O_3/PMS/UV, PFOA control at 40 minutes.

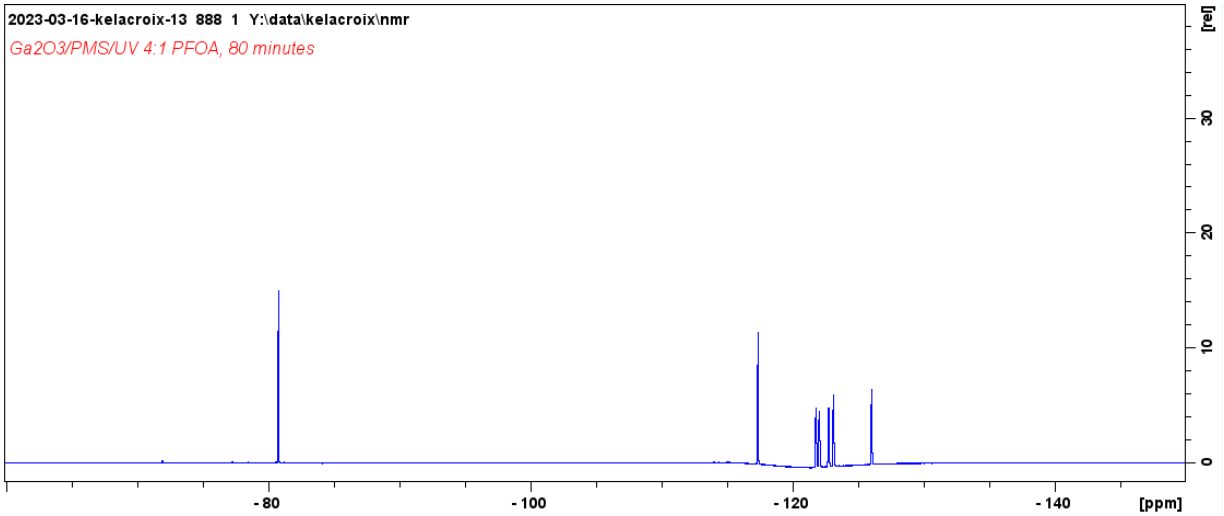

Figure 98. NMR Spectrum for the 4:1 Ga_2O_3/PMS/UV, PFOA control at 80 minutes.

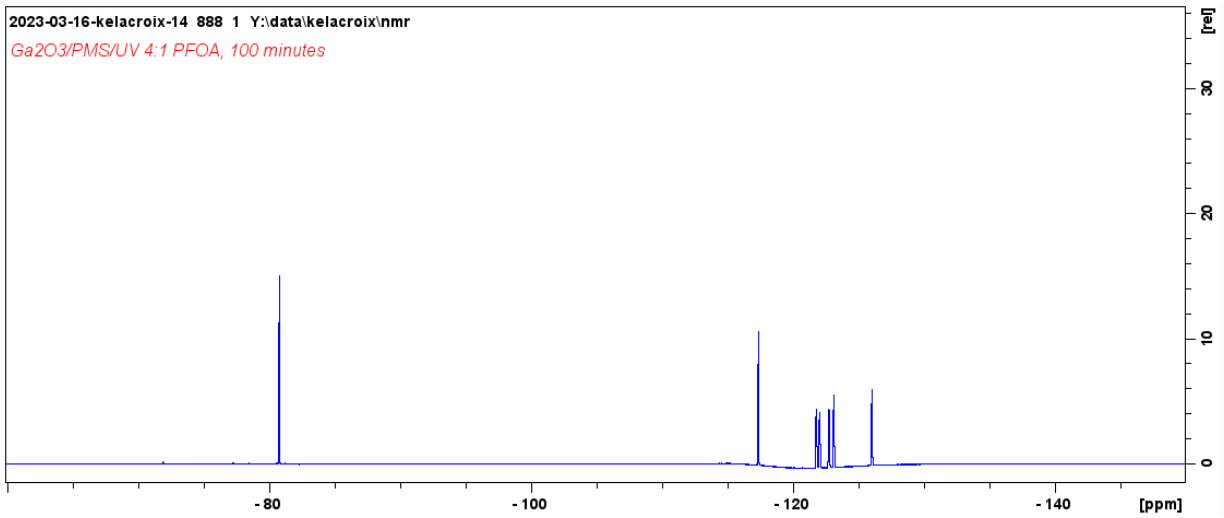

Figure 99. NMR Spectrum for the 4:1 Ga_2O_3/PMS/UV, PFOA control at 100 minutes.

<u>*TiO_2/PMS Controls:*</u>

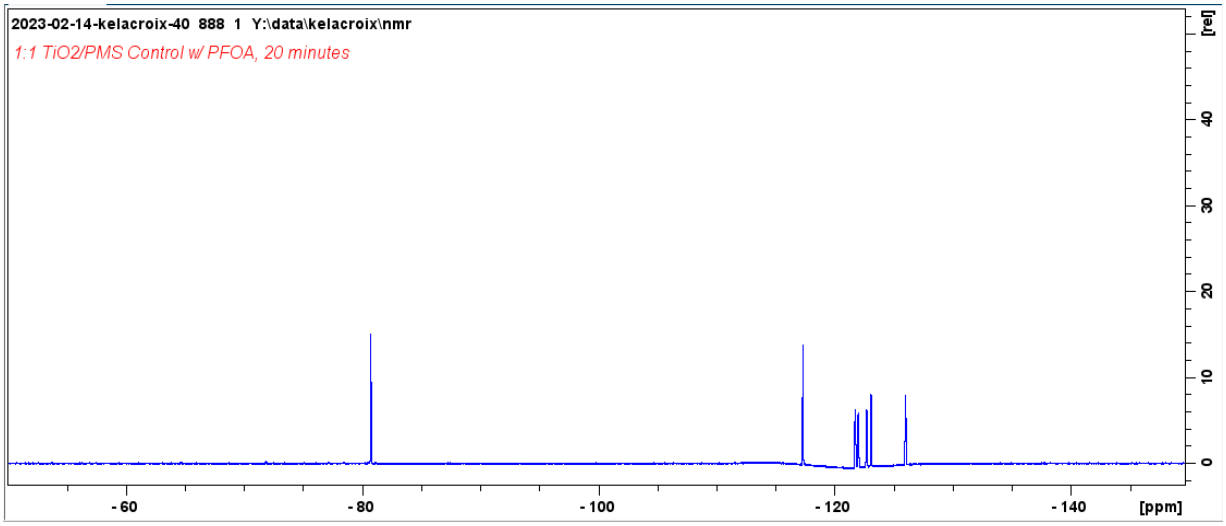

Figure 100. NMR Spectrum for the 1:1 TiO_2/PMS, PFOA control at 20 minutes.

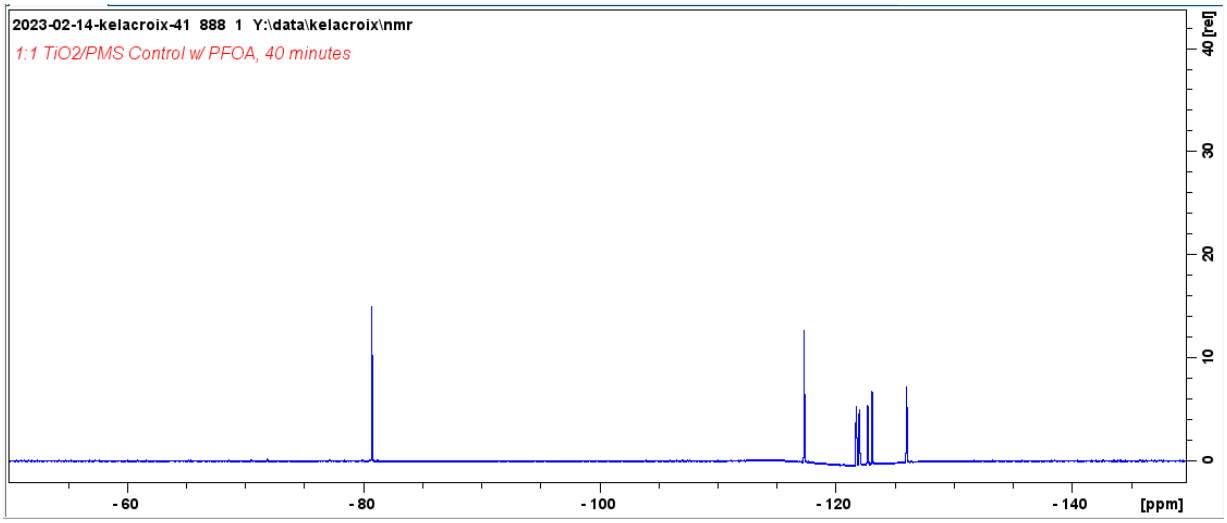

Figure 101. NMR Spectrum for the 1:1 TiO_2/PMS, PFOA control at 40 minutes.

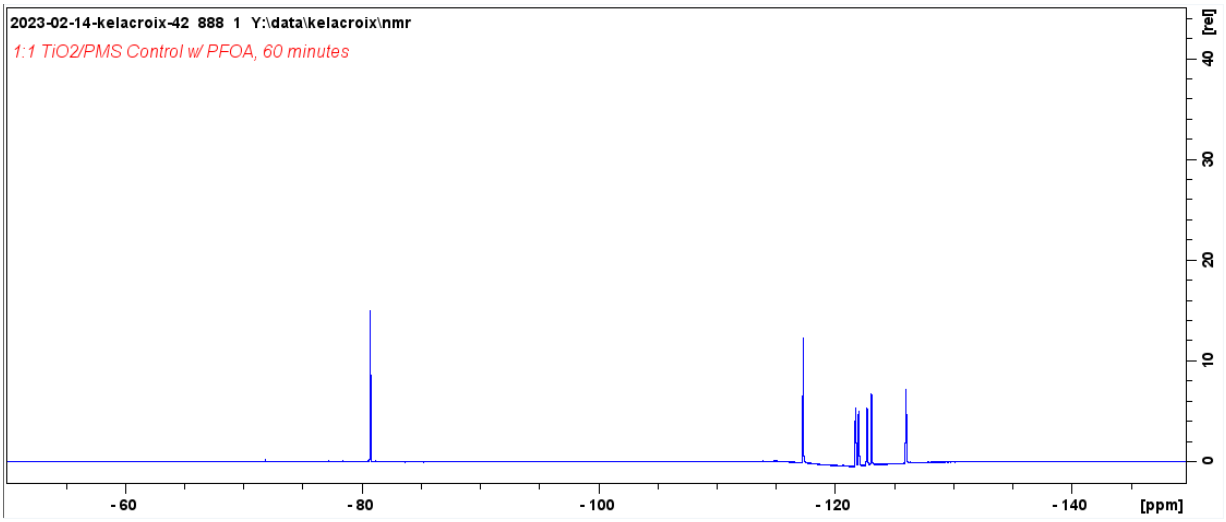

Figure 102. NMR Spectrum for the 1:1 TiO_2/PMS, PFOA control at 60 minutes.

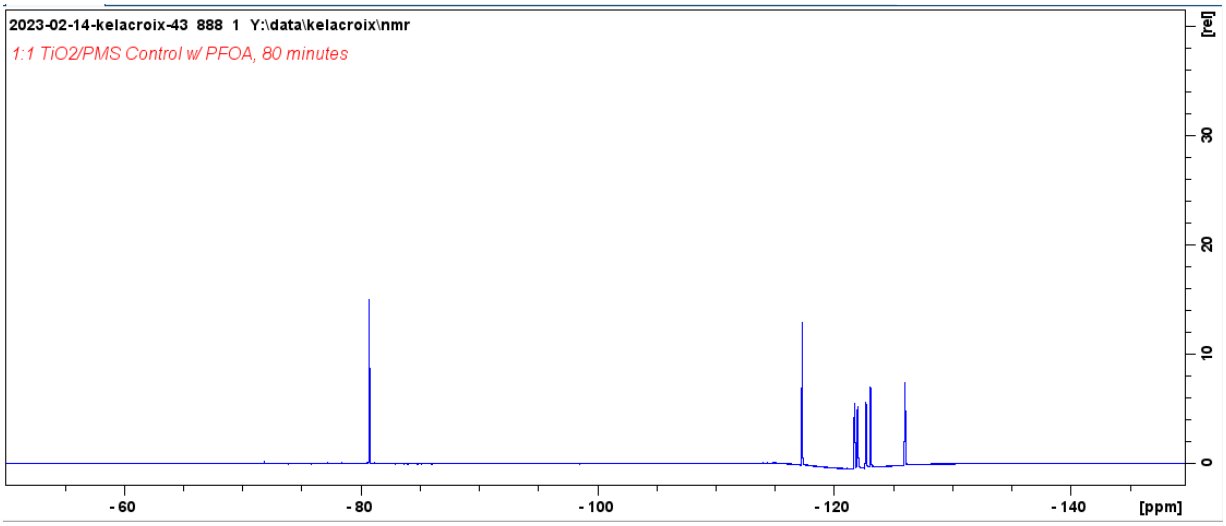

Figure 103. NMR Spectrum for the 1:1 TiO_2/PMS, PFOA control at 80 minutes.

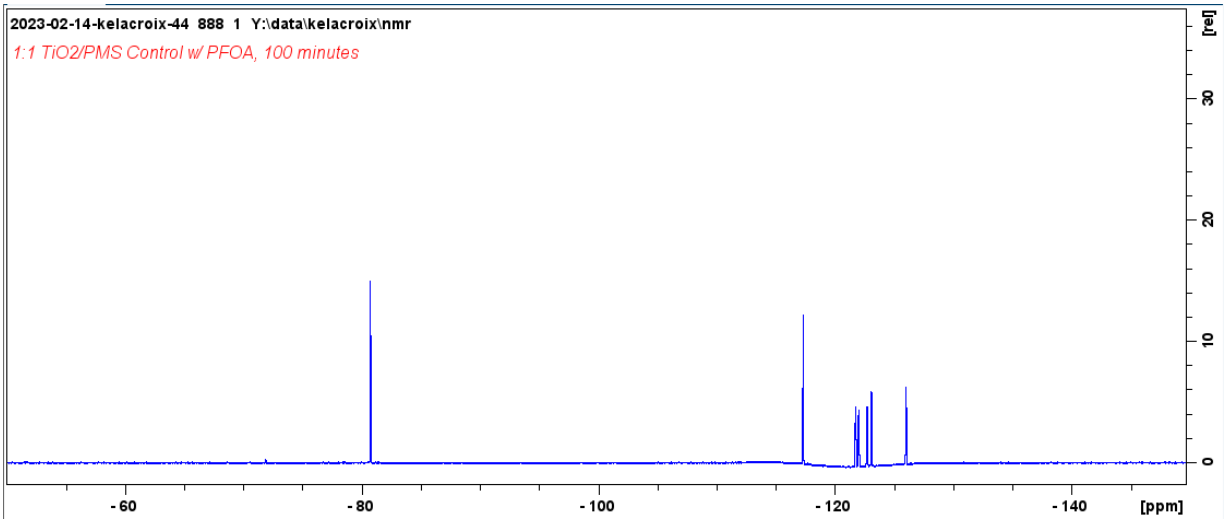

Figure 104. NMR Spectrum for the 1:1 TiO_2/PMS, PFOA control at 100 minutes.

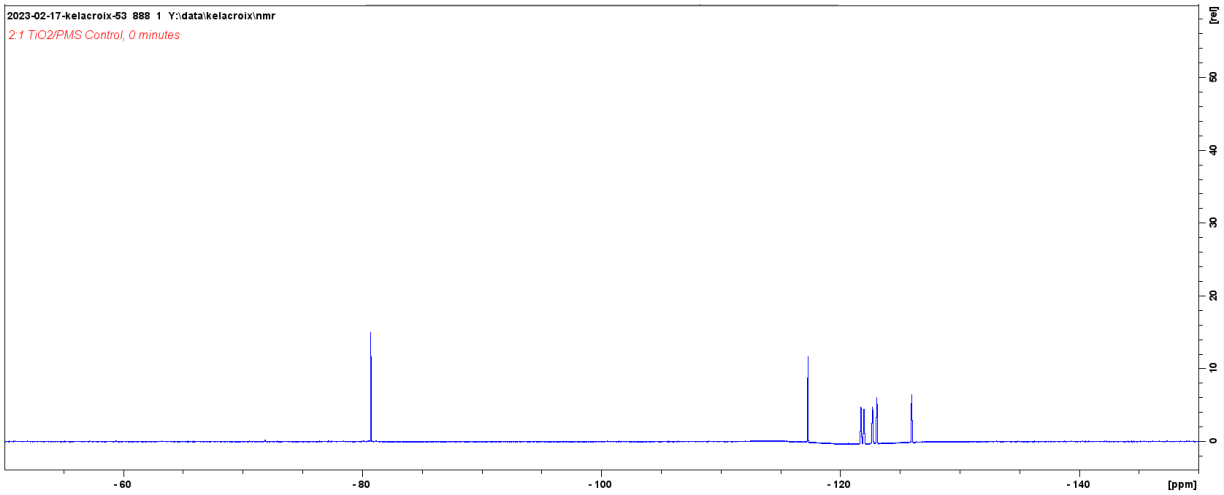

Figure 105. NMR Spectrum for the 2:1 TiO_2/PMS, PFOA control at 0 minutes.

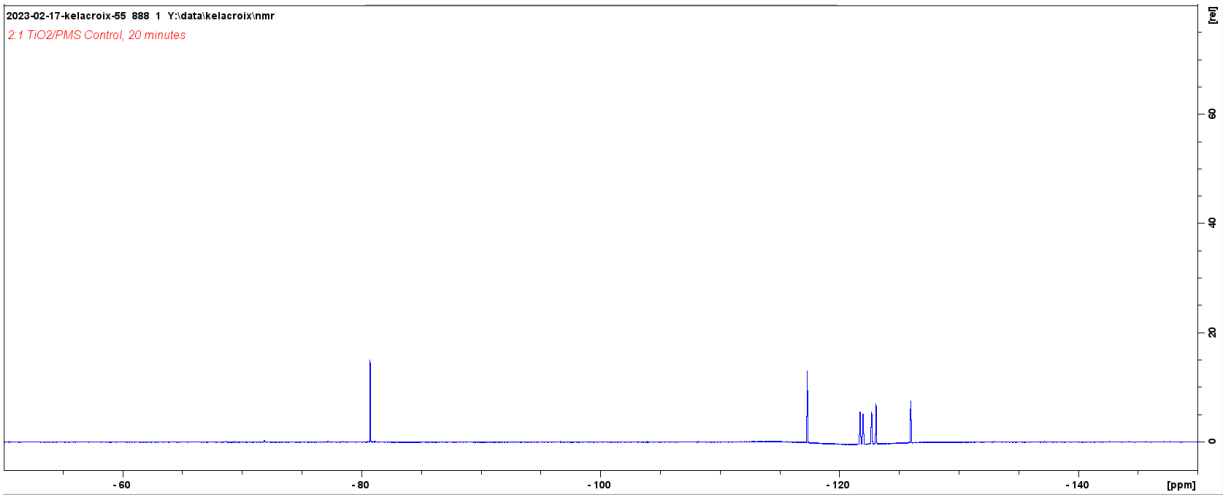

Figure 106. NMR Spectrum for the 2:1 TiO_2/PMS, PFOA control at 20 minutes.

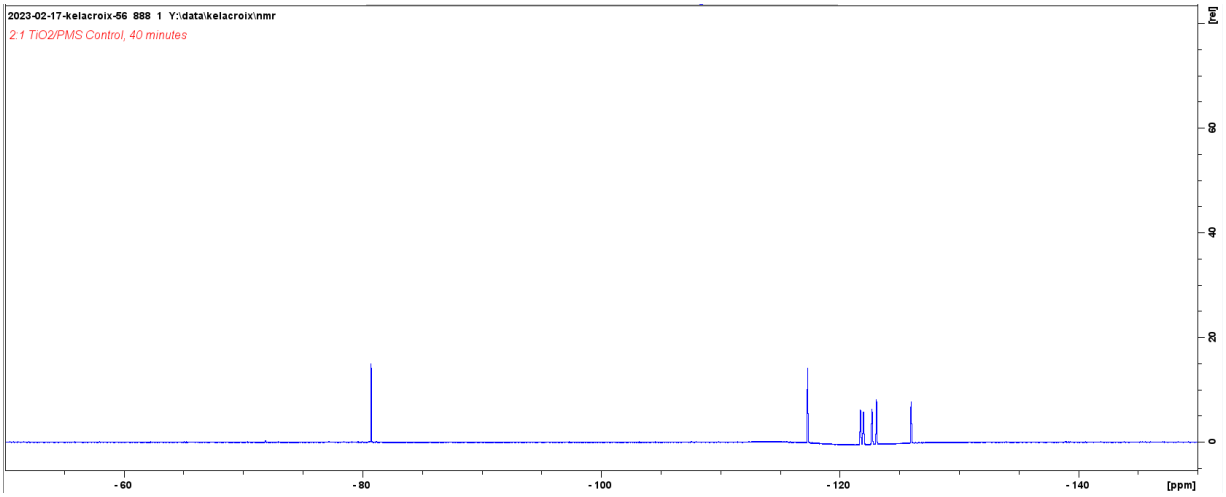

Figure 107. NMR Spectrum for the 2:1 TiO_2/PMS, PFOA control at 40 minutes.

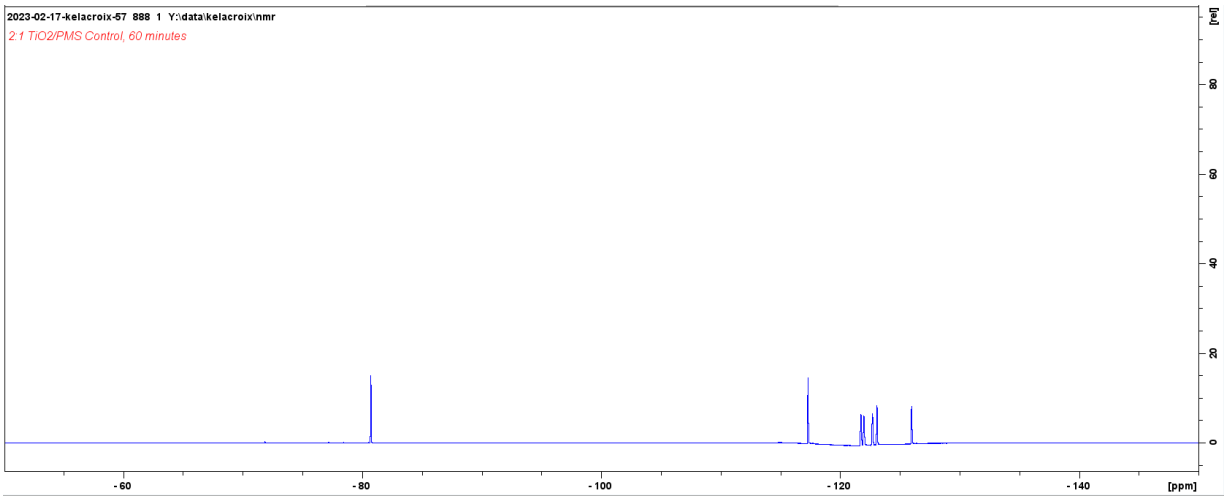

Figure 108. NMR Spectrum for the 2:1 TiO_2/PMS, PFOA control at 60 minutes.

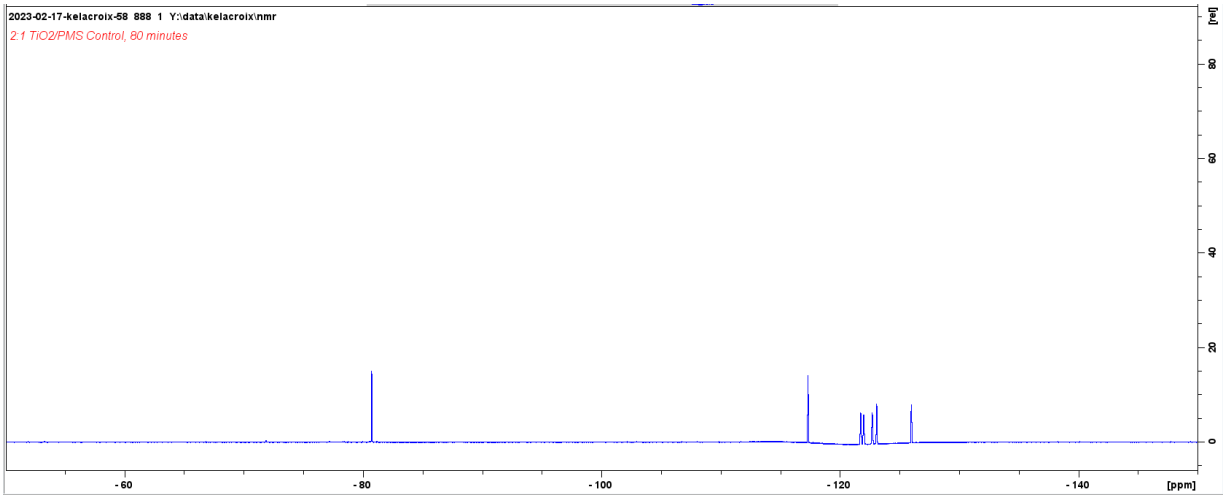

Figure 109. NMR Spectrum for the 2:1 TiO_2/PMS, PFOA control at 80 minutes.

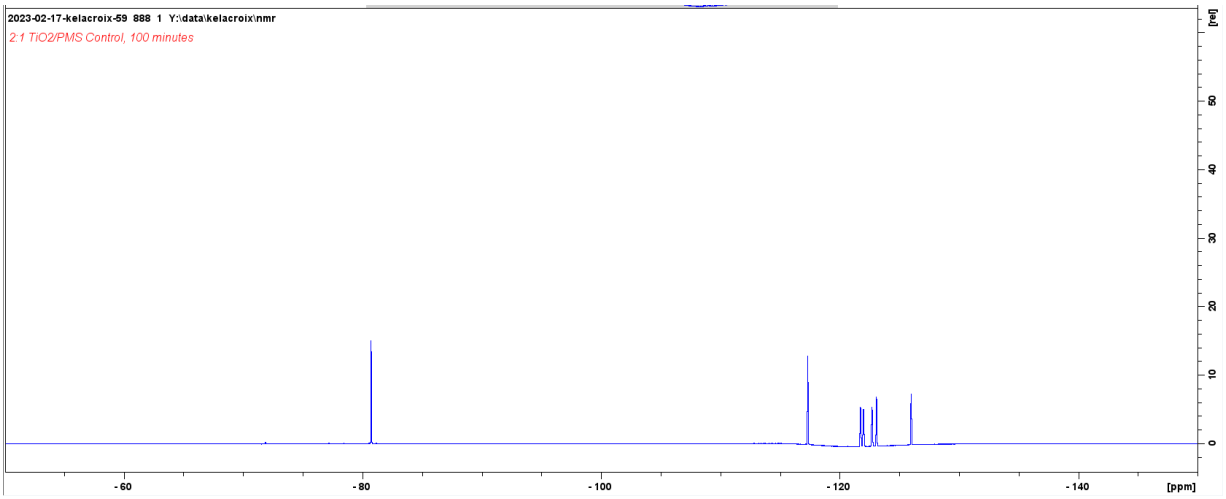

Figure 110. NMR Spectrum for the 2:1 TiO_2/PMS, PFOA control at 100 minutes.

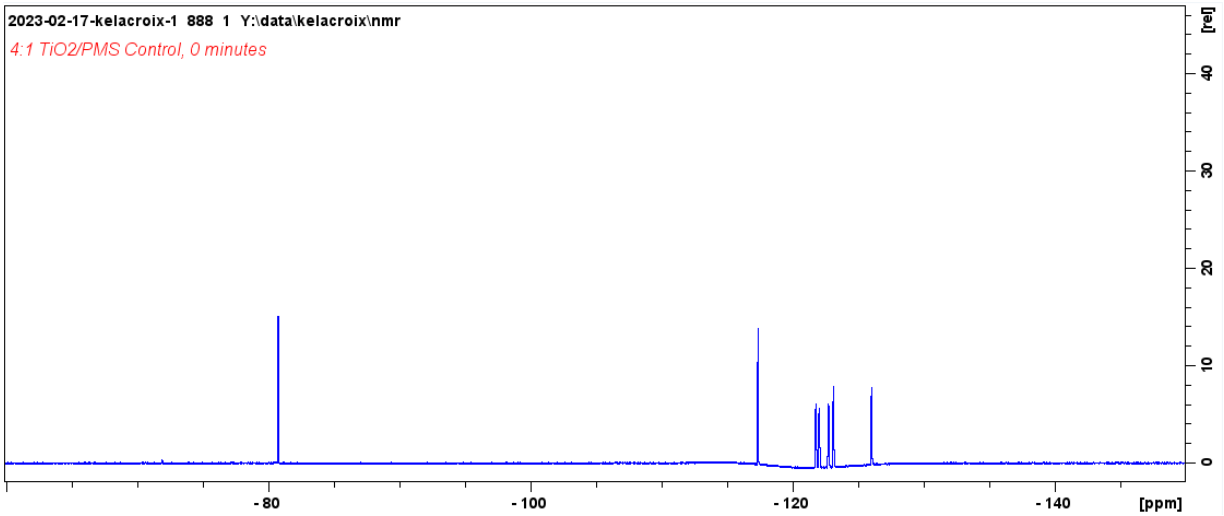

Figure 111. NMR Spectrum for the 4:1 TiO_2/PMS, PFOA control at 0 minutes.

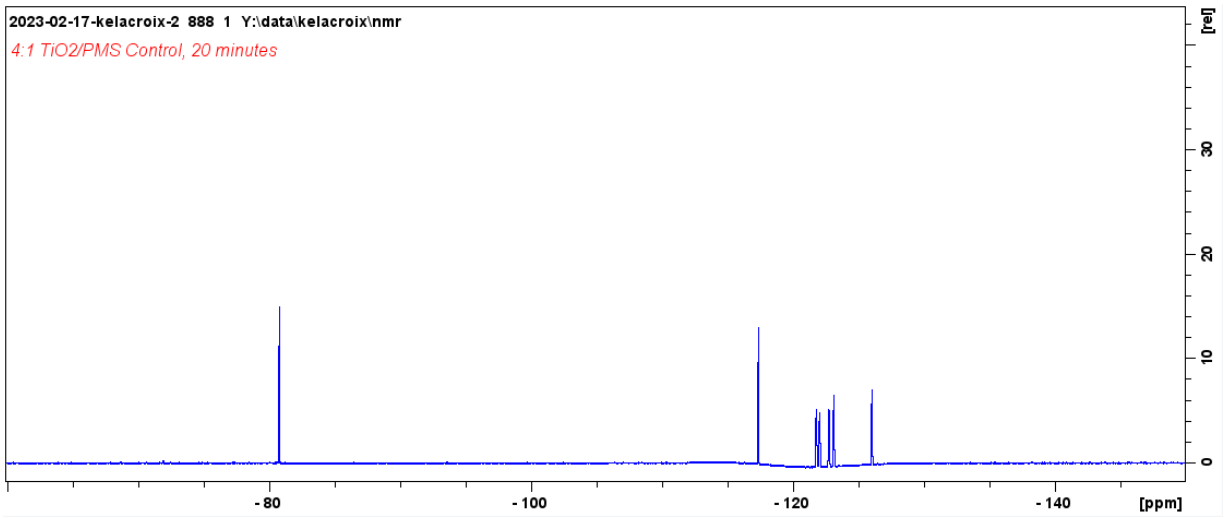

Figure 112. NMR Spectrum for the 4:1 TiO_2/PMS, PFOA control at 20 minutes.

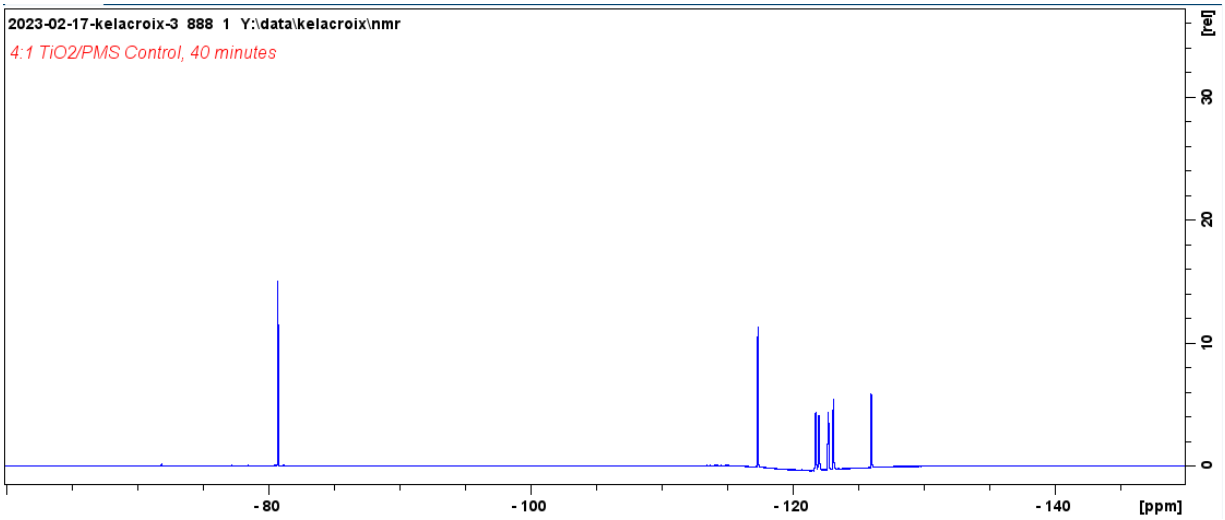

Figure 113. NMR Spectrum for the 4:1 TiO_2/PMS, PFOA control at 40 minutes.

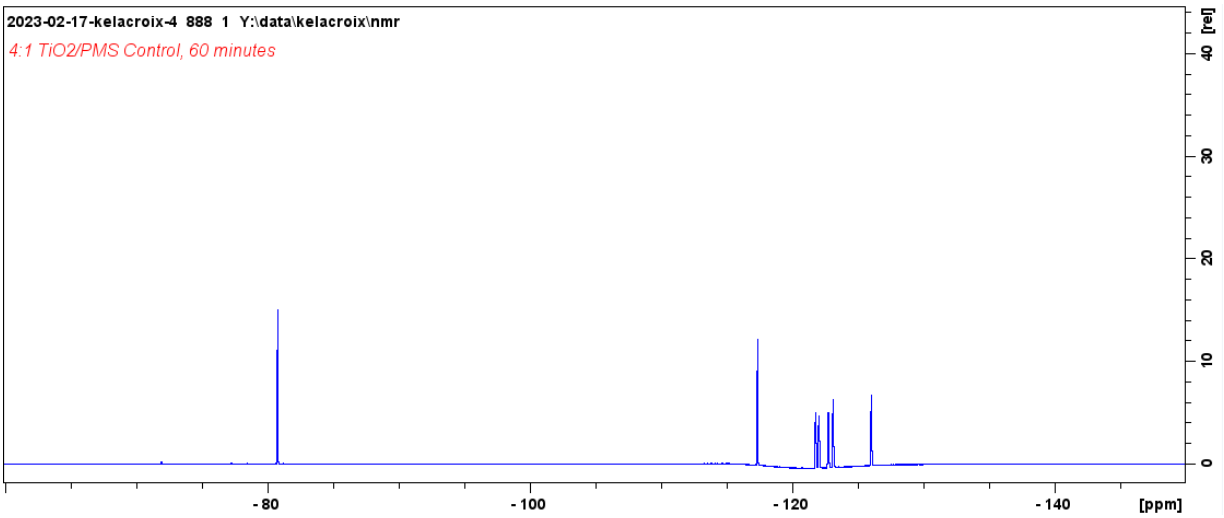

Figure 114. NMR Spectrum for the 4:1 TiO_2/PMS, PFOA control at 60 minutes.

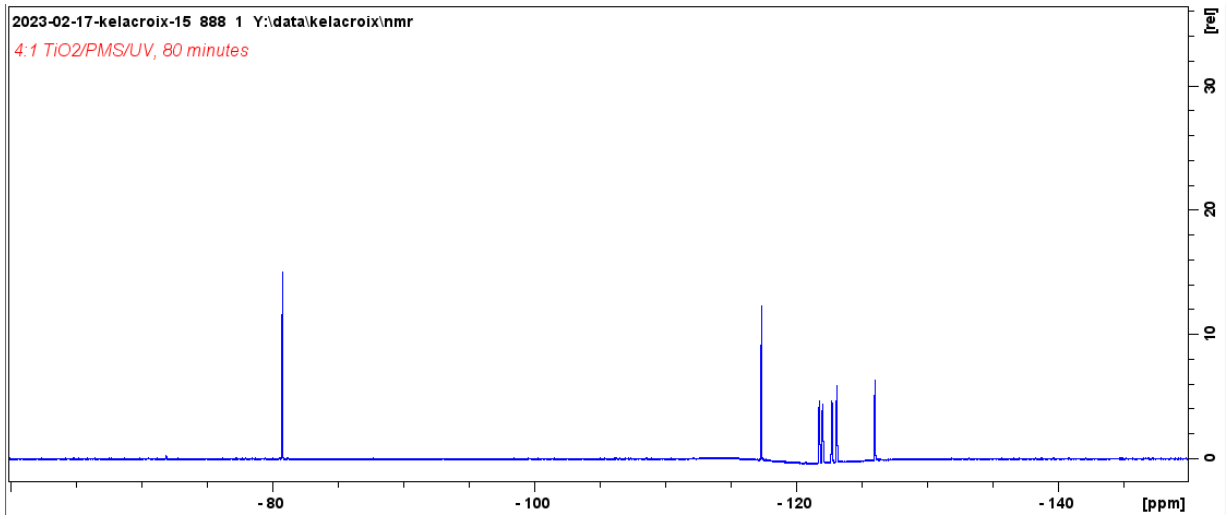

Figure 115. NMR Spectrum for the 4:1 TiO_2/PMS, PFOA control at 80 minutes.

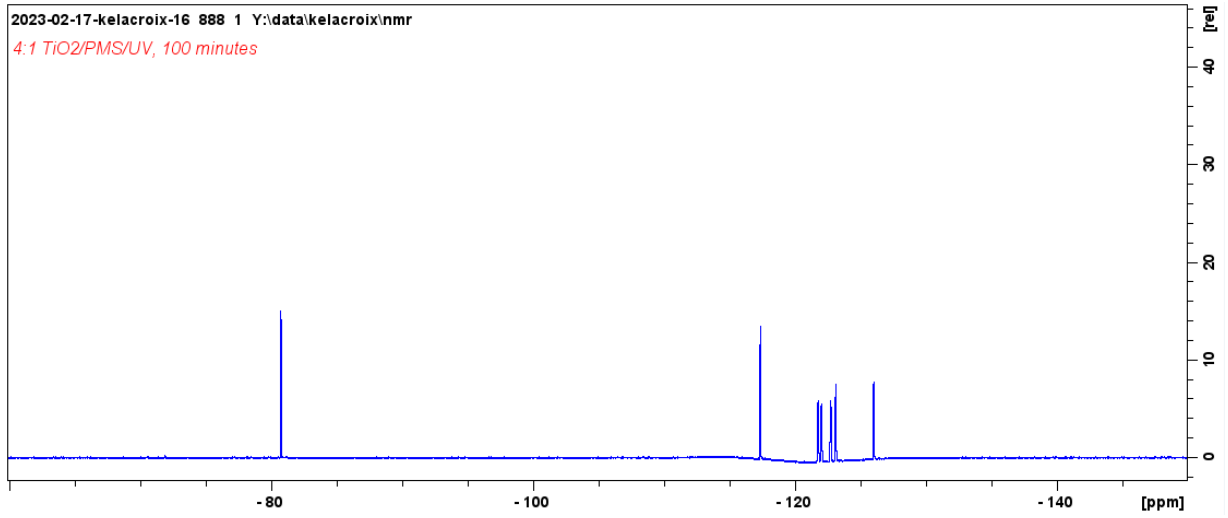

Figure 116. NMR Spectrum for the 4:1 TiO_2/PMS, PFOA control at 100 minutes.

TiO_2/PMS/UV Reactions:

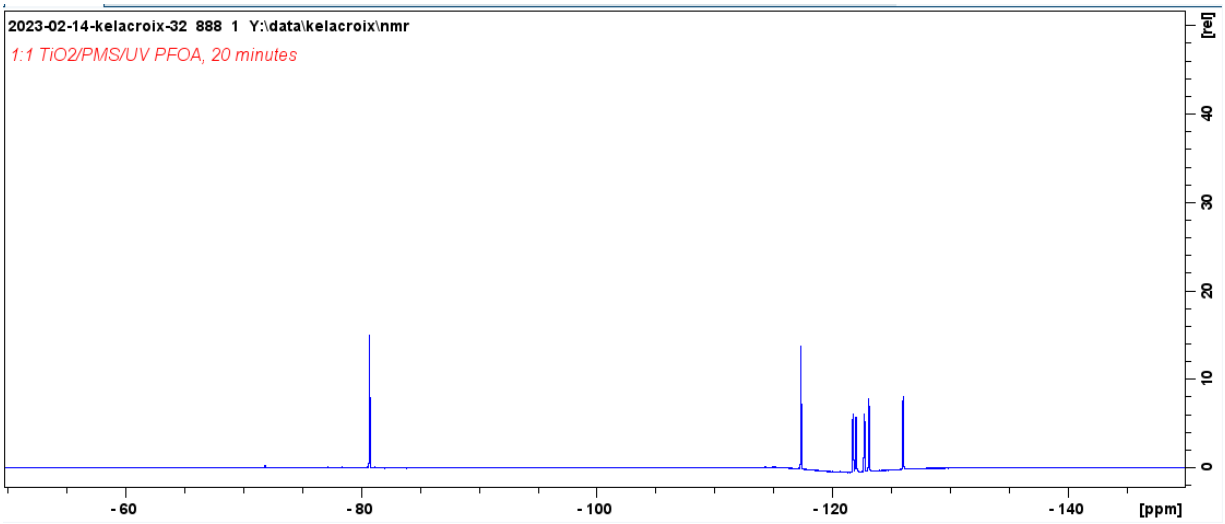

Figure 117. NMR Spectrum for the 1:1 TiO_2/PMS/UV, PFOA reaction at 20 minutes.

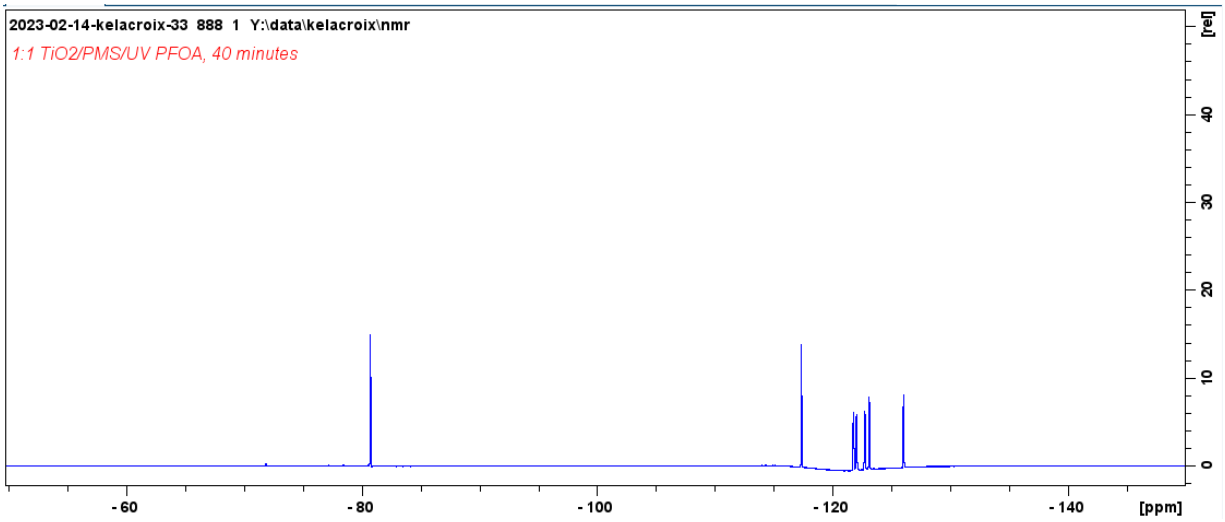

Figure 118. NMR Spectrum for the 1:1 TiO_2/PMS/UV, PFOA reaction at 40 minutes.

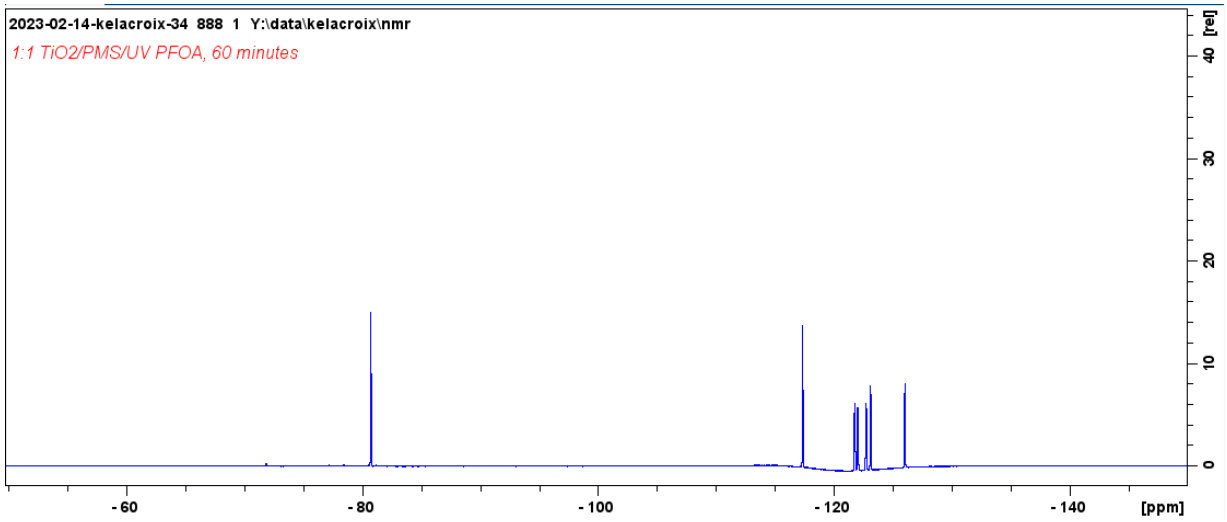

Figure 119. NMR Spectrum for the 1:1 TiO_2/PMS/UV, PFOA reaction at 60 minutes.

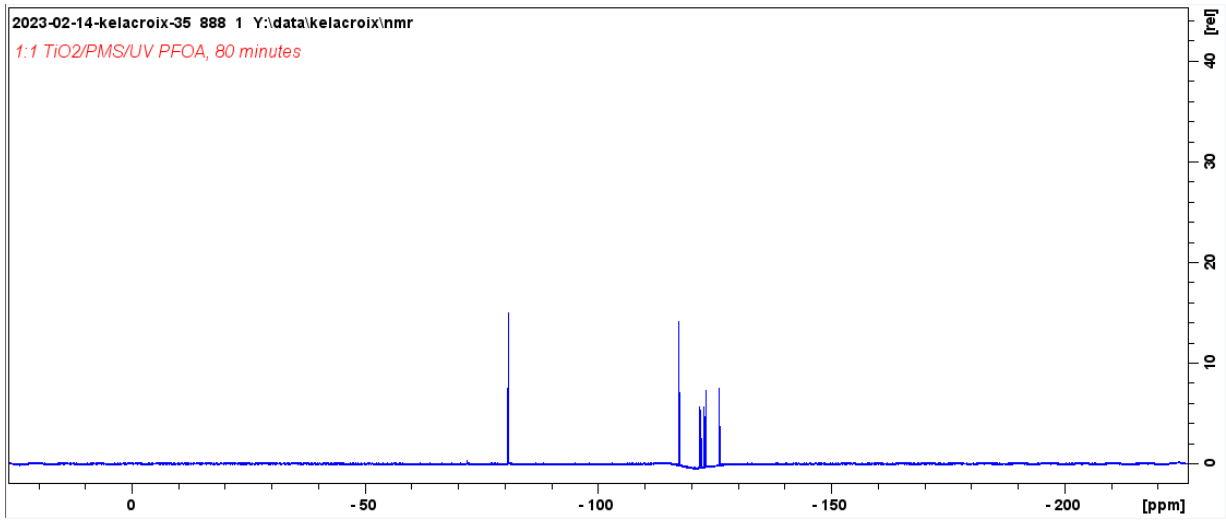

Figure 120. NMR Spectrum for the 1:1 TiO_2/PMS/UV, PFOA reaction at 80 minutes.

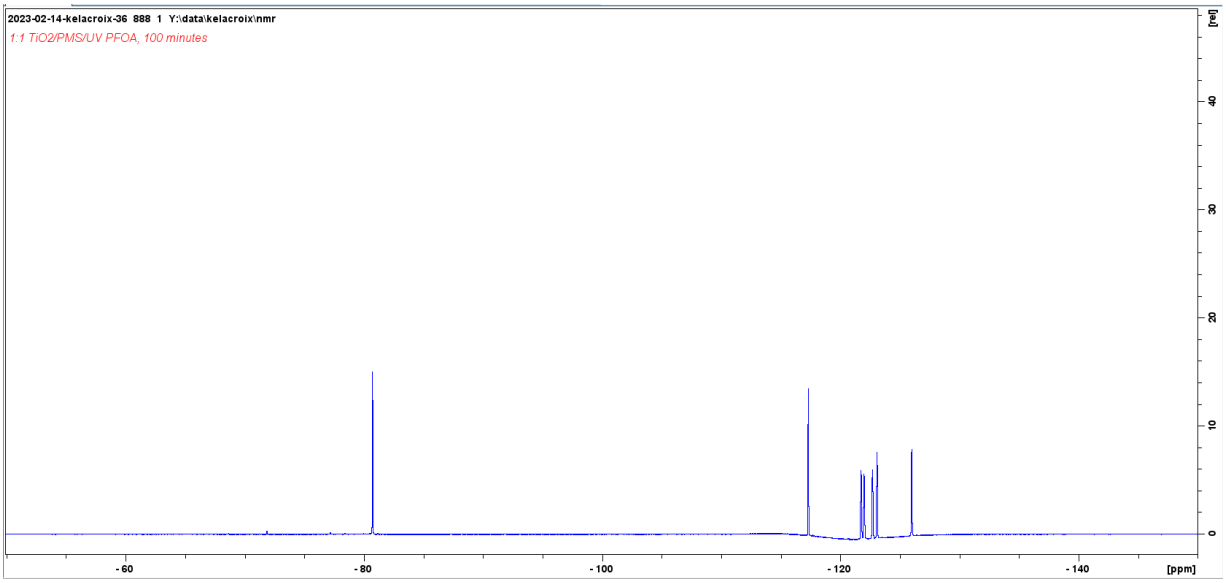

Figure 121. NMR Spectrum for the 1:1 TiO_2/PMS/UV, PFOA reaction at 100 minutes.

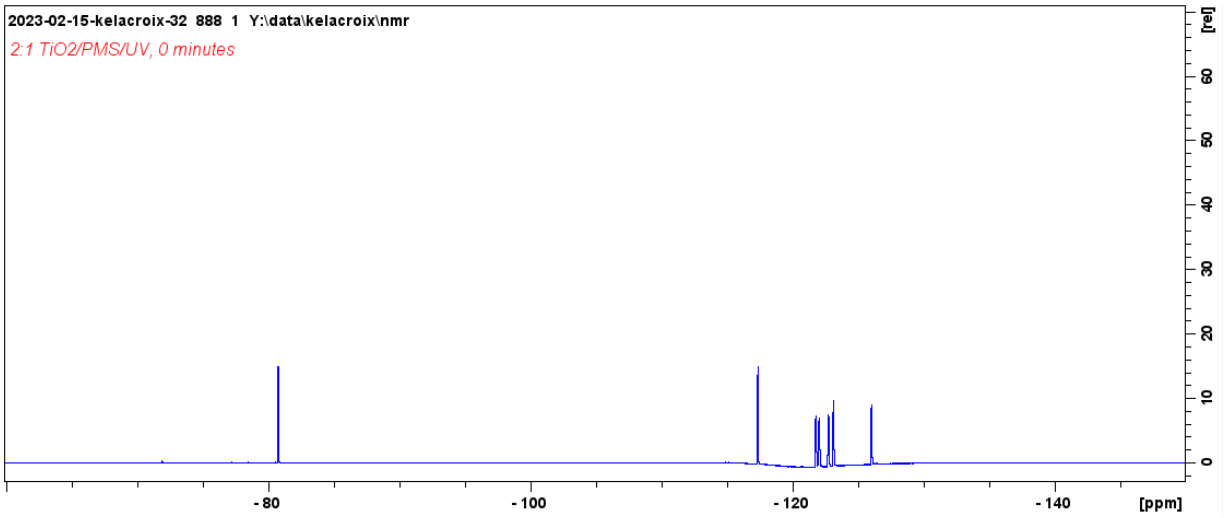

Figure 122. NMR Spectrum for the 2:1 TiO_2/PMS/UV, PFOA reaction at 0 minutes.

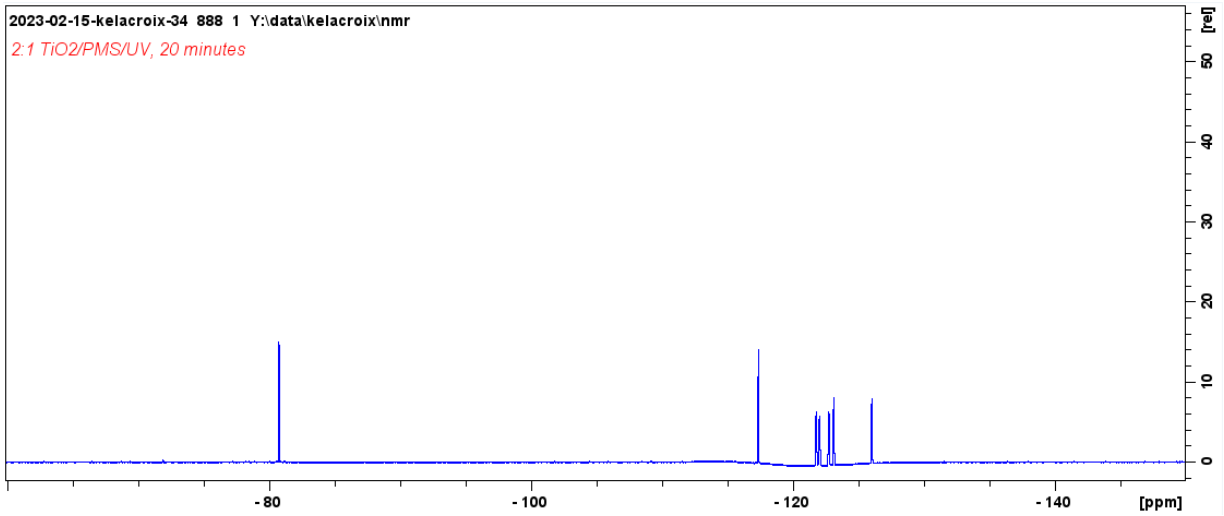

Figure 123. NMR Spectrum for the 2:1 TiO_2/PMS/UV, PFOA reaction at 20 minutes.

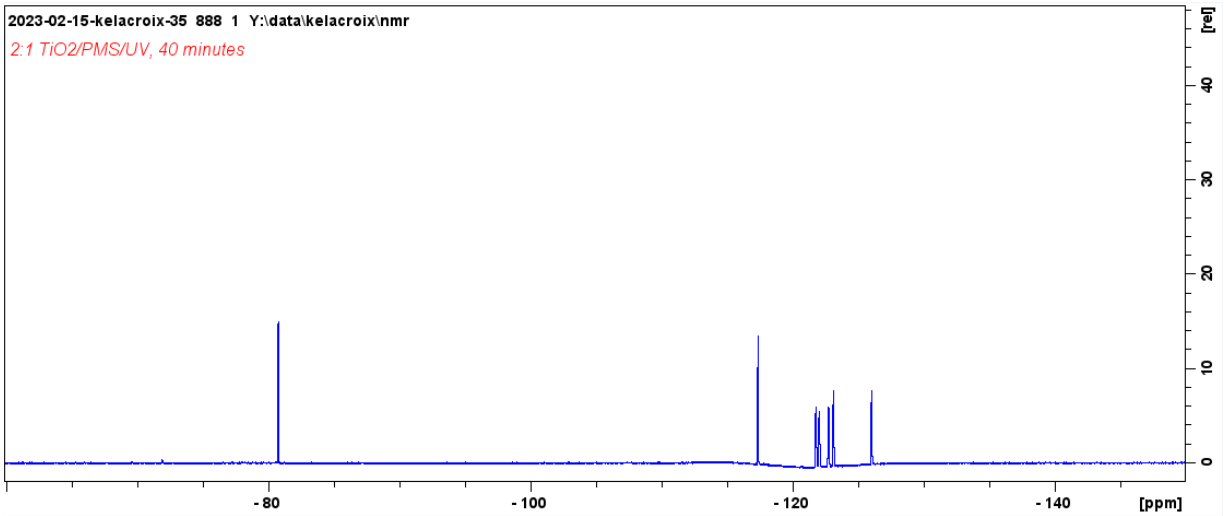

Figure 124. NMR Spectrum for the 2:1 TiO2/PMS/UV, PFOA reaction at 40 minutes.

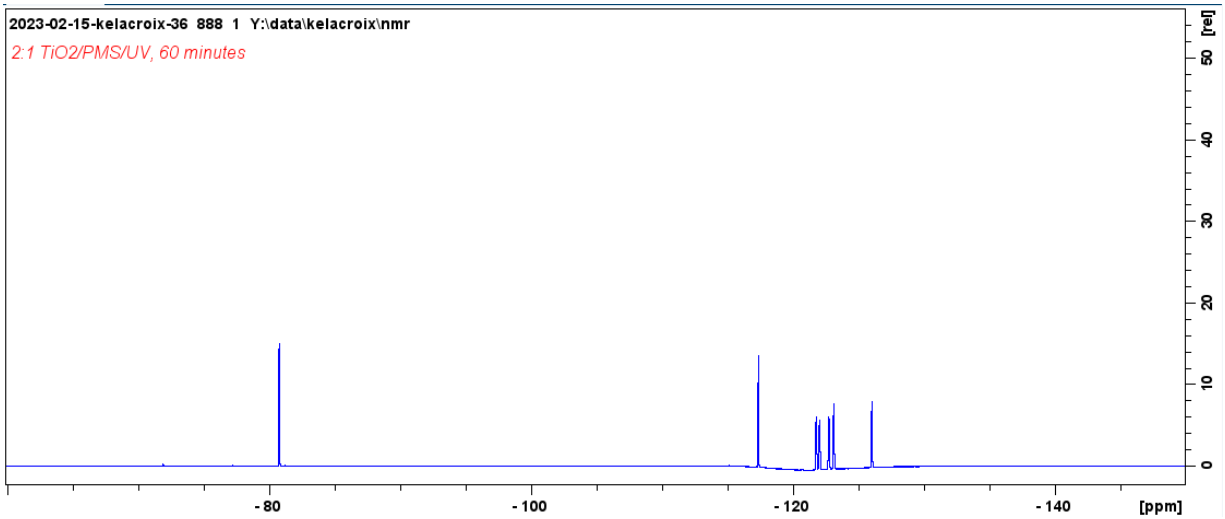

Figure 125. NMR Spectrum for the 2:1 TiO_2/PMS/UV, PFOA reaction at 60 minutes.

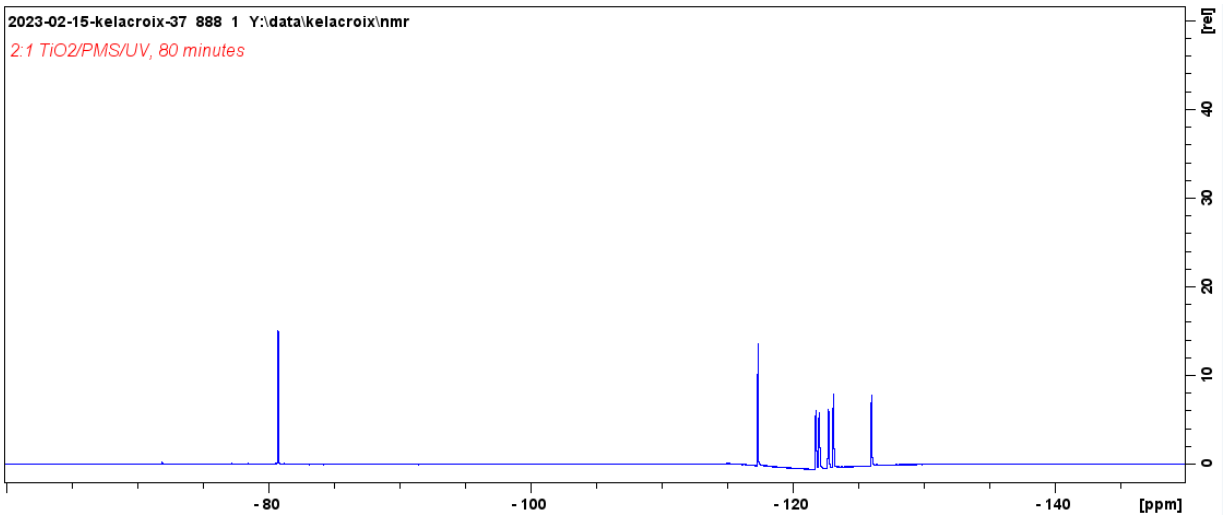

Figure 126. NMR Spectrum for the 2:1 TiO_2/PMS/UV, PFOA reaction at 80 minutes.

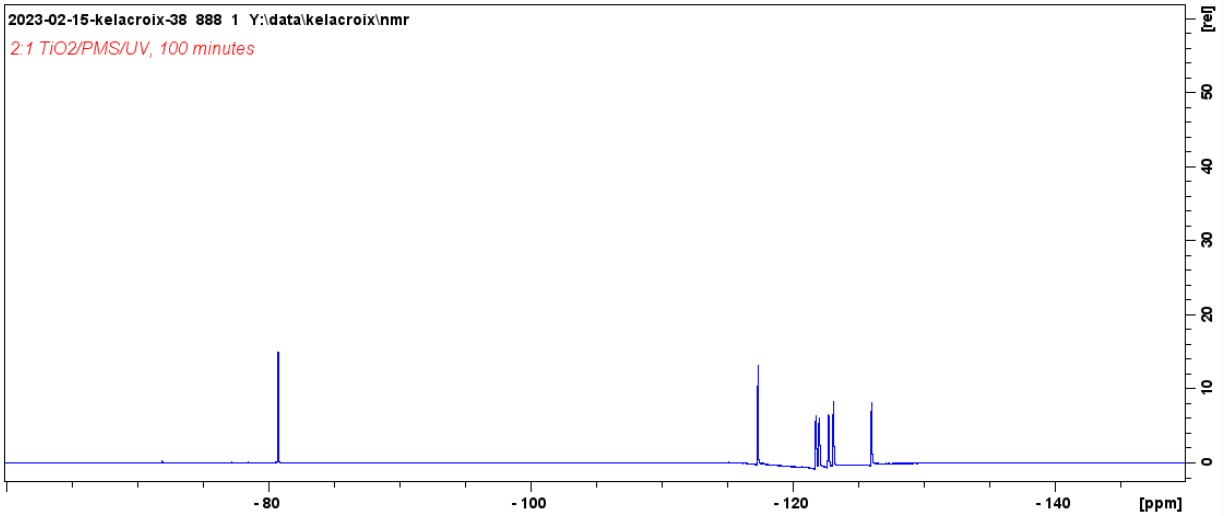

Figure 127. NMR Spectrum for the 2:1 TiO_2/PMS/UV, PFOA reaction at 100 minutes.

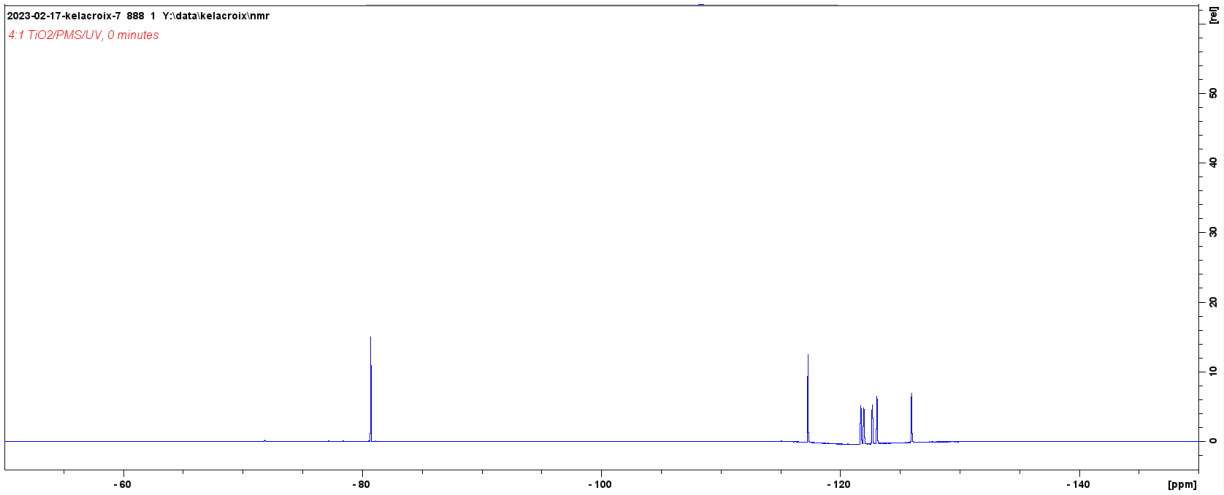

Figure 128. NMR Spectrum for the 4:1 TiO_2/PMS/UV, PFOA reaction at 0 minutes.

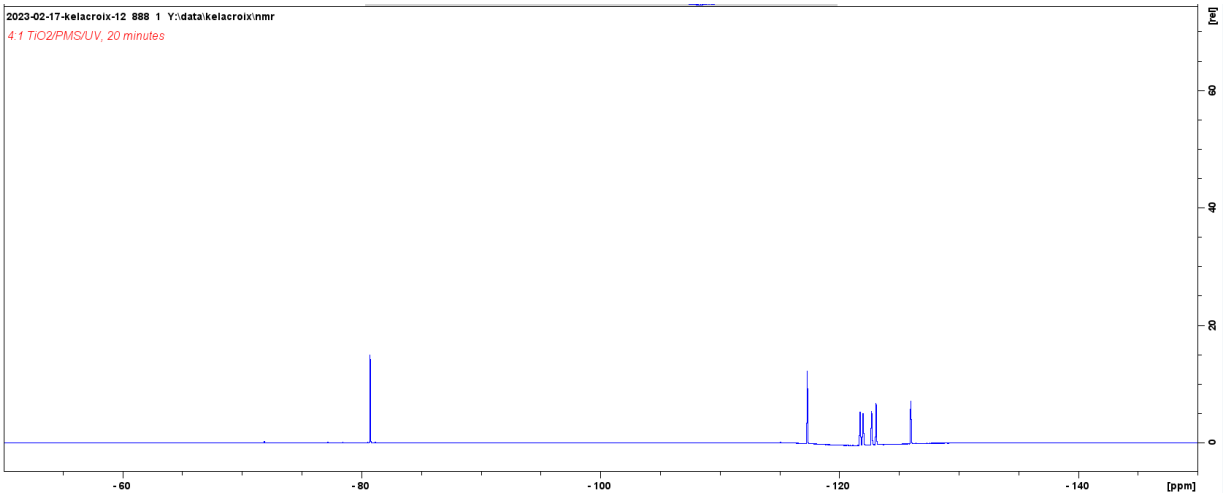

Figure 129. NMR Spectrum for the 4:1 TiO_2/PMS/UV, PFOA reaction at 20 minutes.

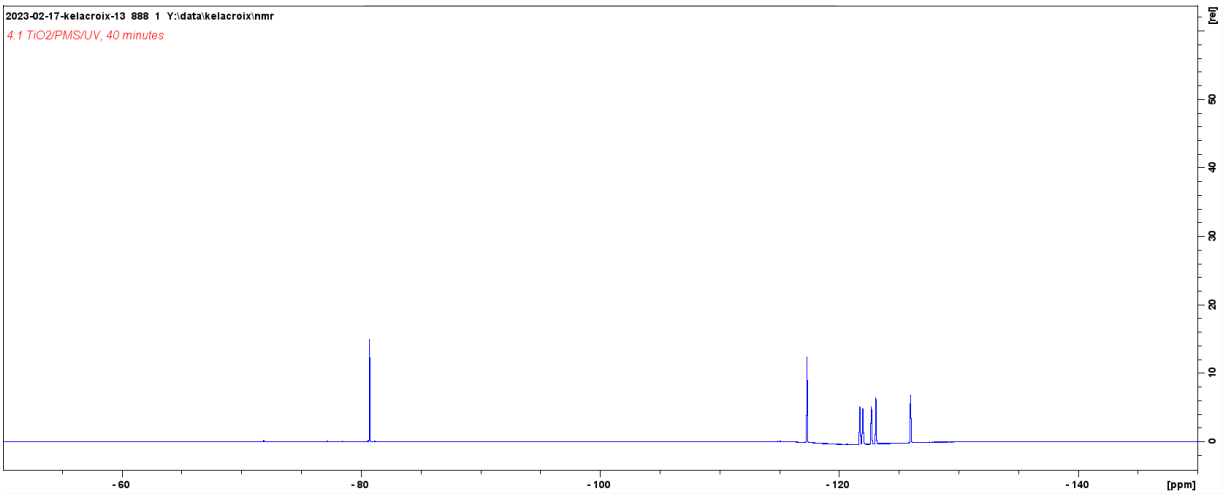

Figure 130. NMR Spectrum for the 4:1 TiO_2/PMS/UV, PFOA reaction at 40 minutes.

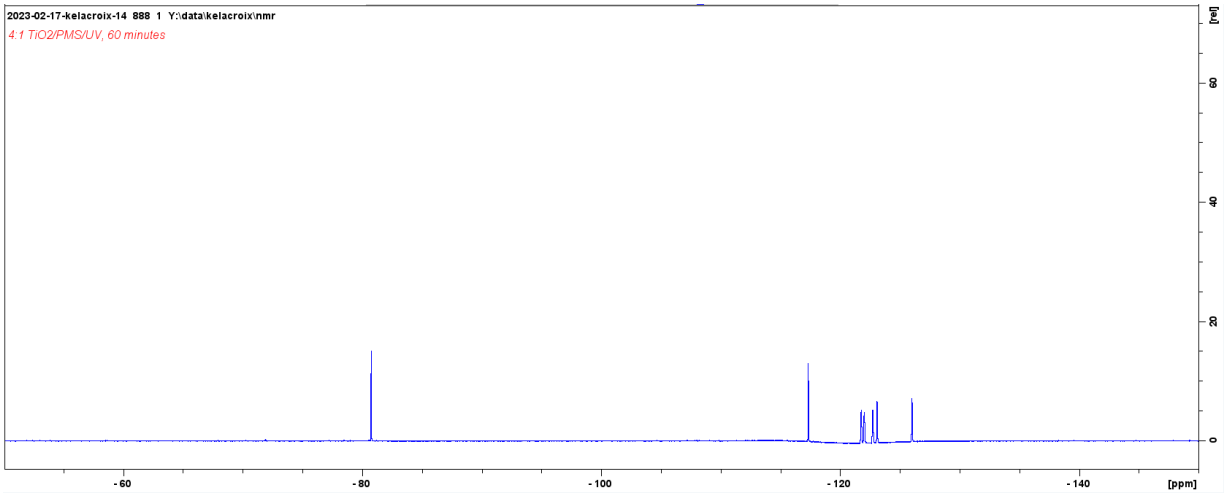

Figure 131. NMR Spectrum for the 4:1 TiO_2/PMS/UV, PFOA reaction at 60 minutes.

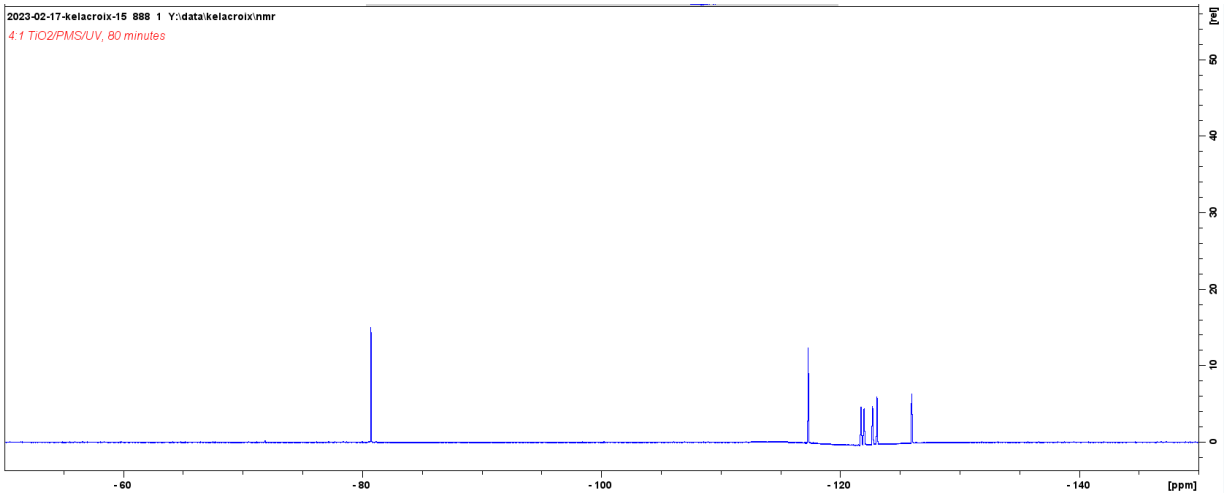

Figure 132. NMR Spectrum for the 4:1 TiO_2/PMS/UV, PFOA reaction at 80 minutes.

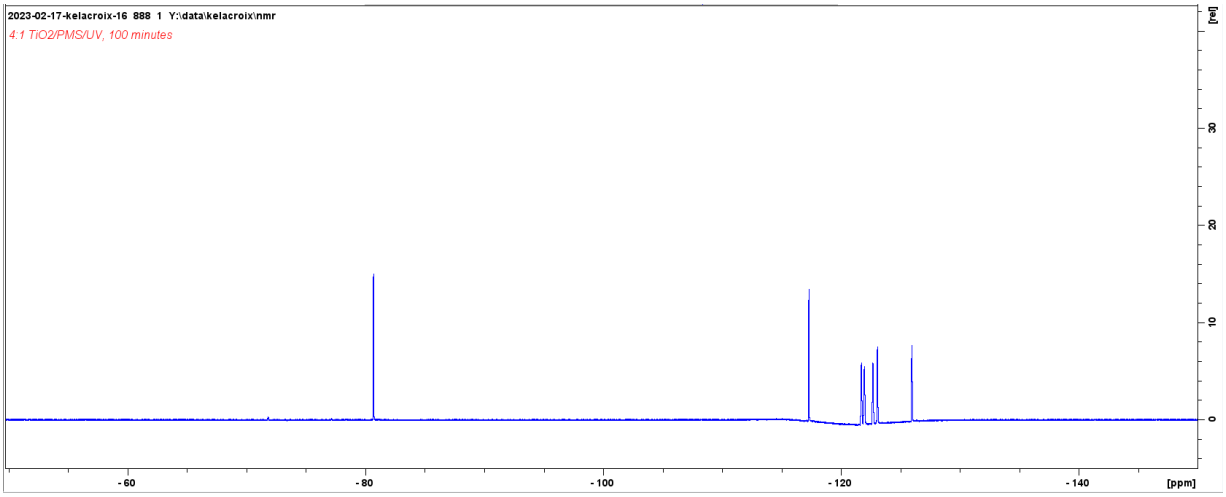

Figure 133. NMR Spectrum for the 4:1 TiO_2/PMS/UV, PFOA reaction at 100 minutes.

<u>Heat/PS, PFOA Control:</u>

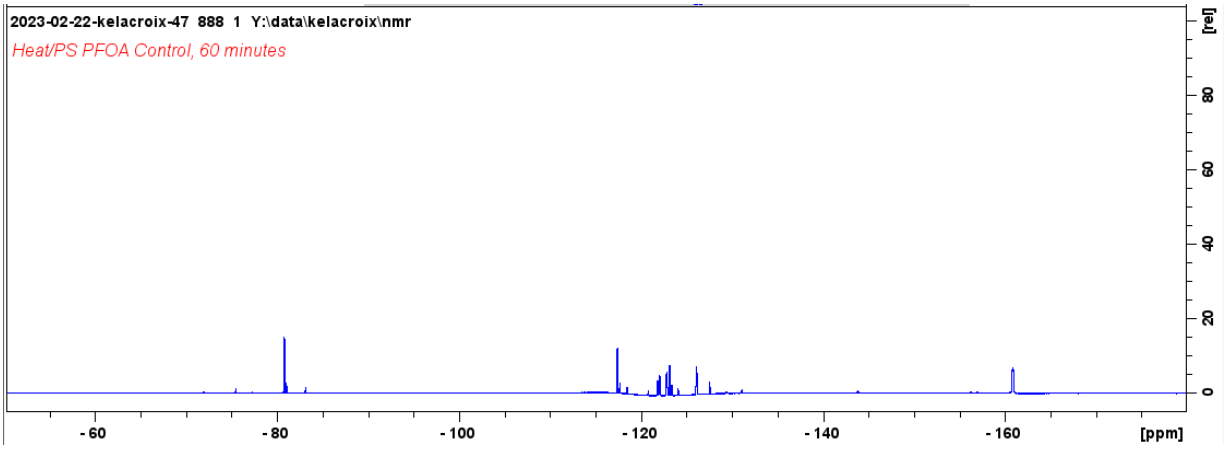

Figure 134. NMR Spectrum for the heat/PS, PFOA control at 60 minutes.

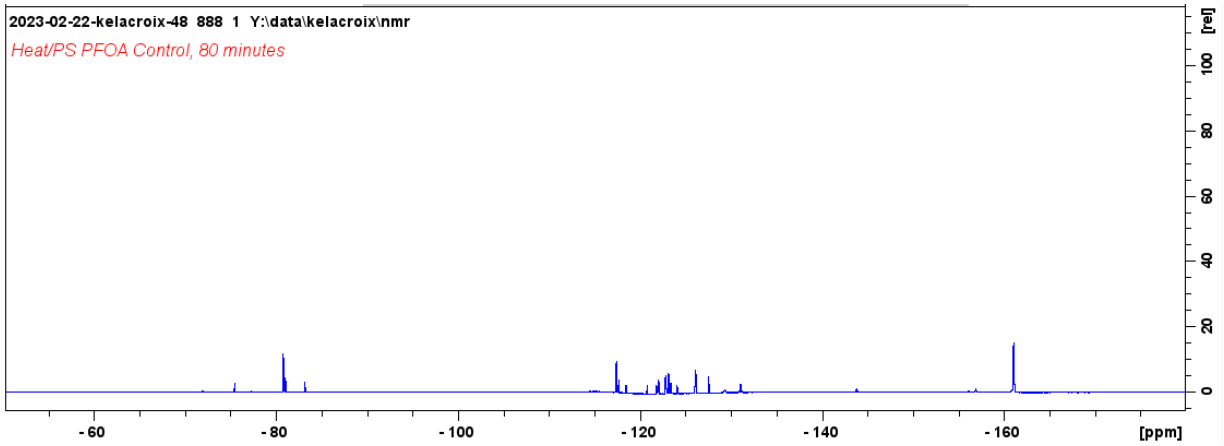

Figure 135. NMR Spectrum for the heat/PS, PFOA control at 80 minutes.

Heat/PS/Zeolite, PFOA Reactions:

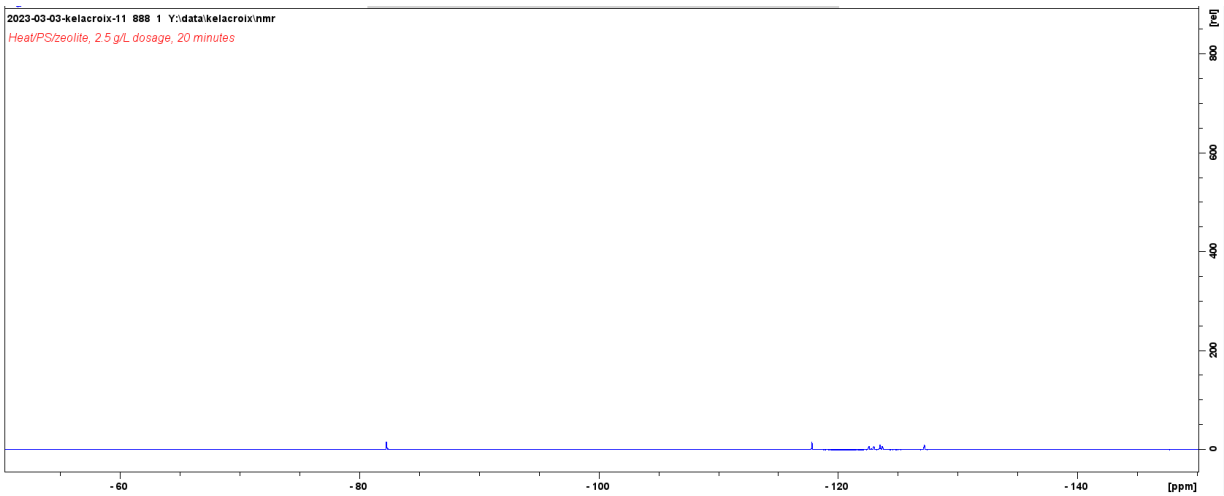

Figure 136. NMR Spectrum for the heat/PS/zeolite, PFOA reaction with 2.5 g/L dosage at 20 minutes.

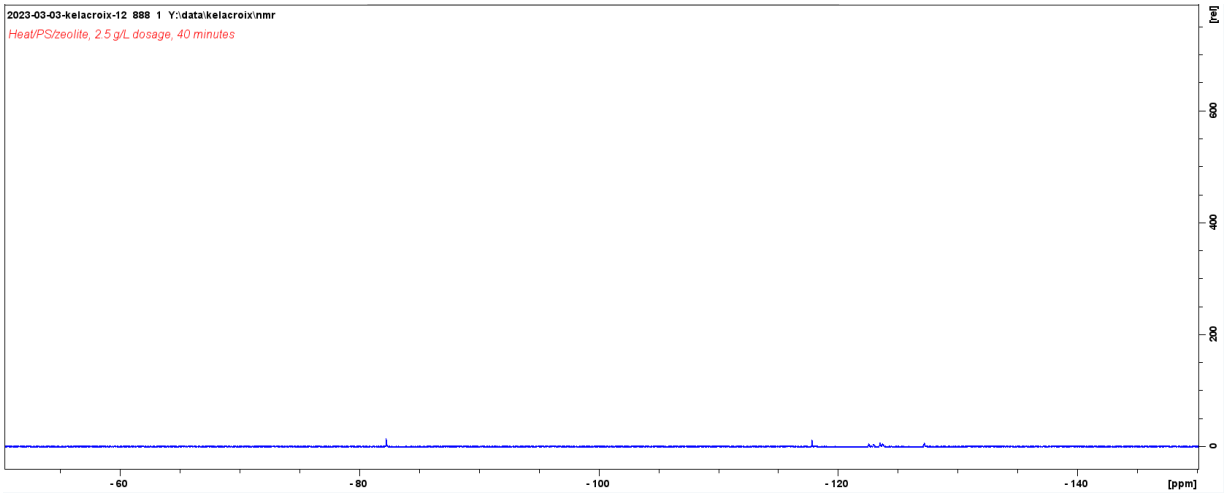

Figure 137. NMR Spectrum for the heat/PS/zeolite, PFOA reaction with 2.5 g/L dosage at 40 minutes.

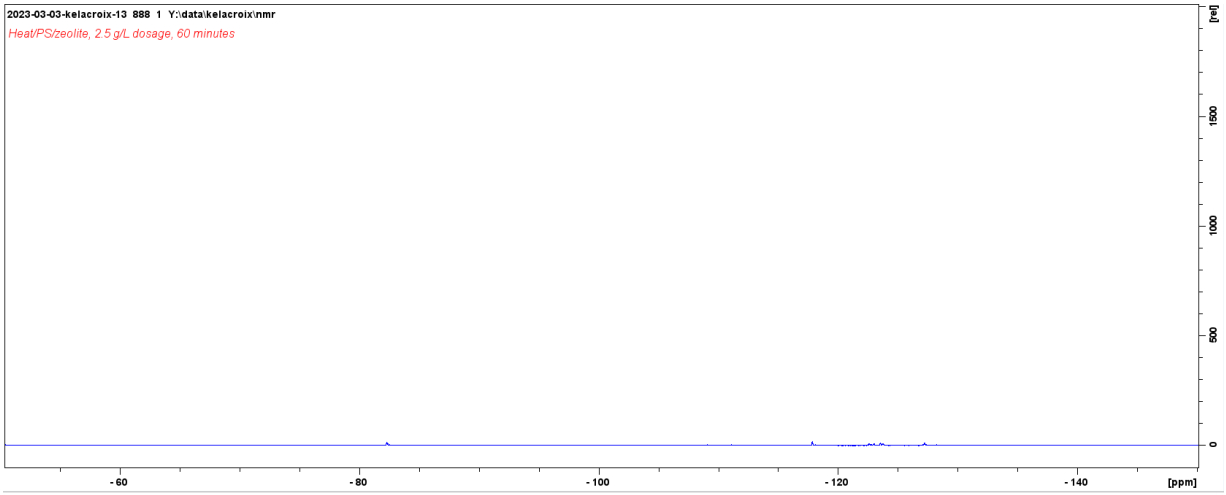

Figure 138. NMR Spectrum for the heat/PS/zeolite, PFOA reaction with 2.5 g/L dosage at 60 minutes.

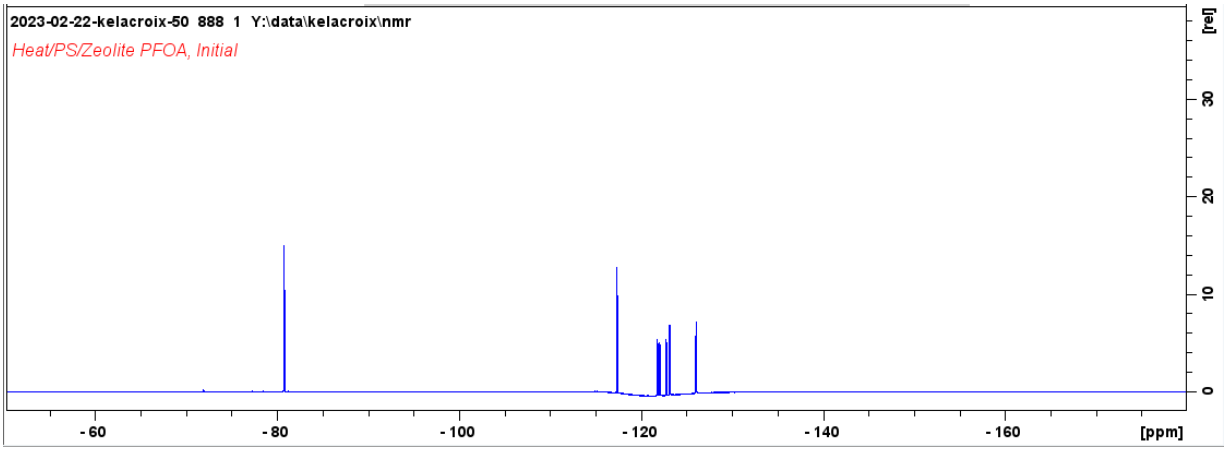

Figure 139. NMR Spectrum for the heat/PS/zeolite, PFOA reaction with 5 g/L dosage before 2 hours in laboratory shaker.

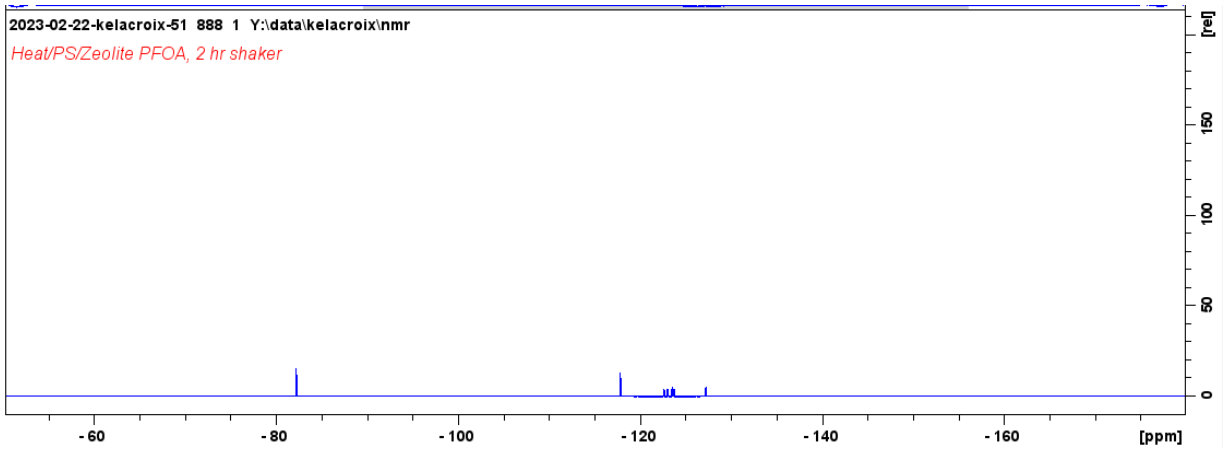

Figure 140. NMR Spectrum for the heat/PS/zeolite, PFOA reaction with 5 g/L dosage after 2 hours in laboratory shaker.

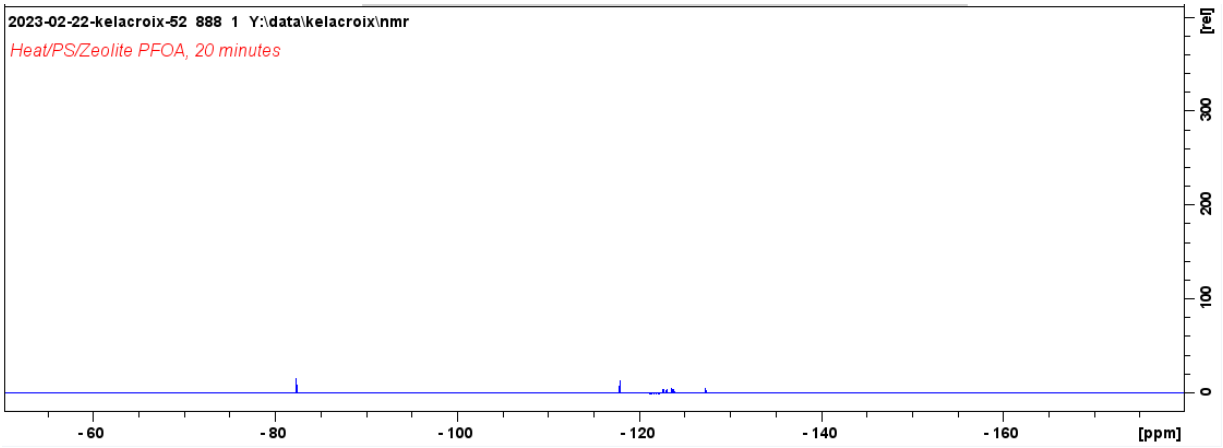

Figure 141. NMR Spectrum for the heat/PS/zeolite, PFOA reaction with 5 g/L dosage at 20 minutes.

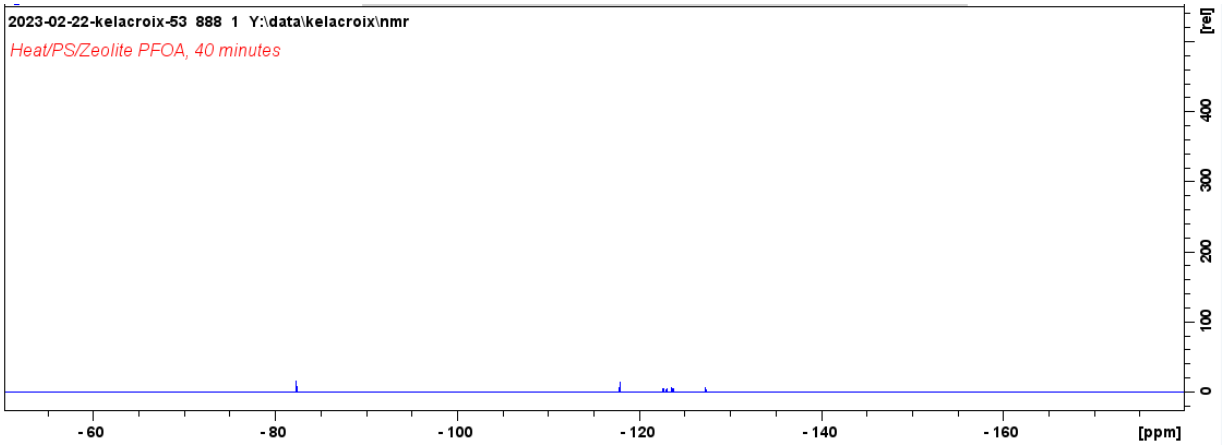

Figure 142. NMR Spectrum for the heat/PS/zeolite, PFOA reaction with 5 g/L dosage at 40 minutes.

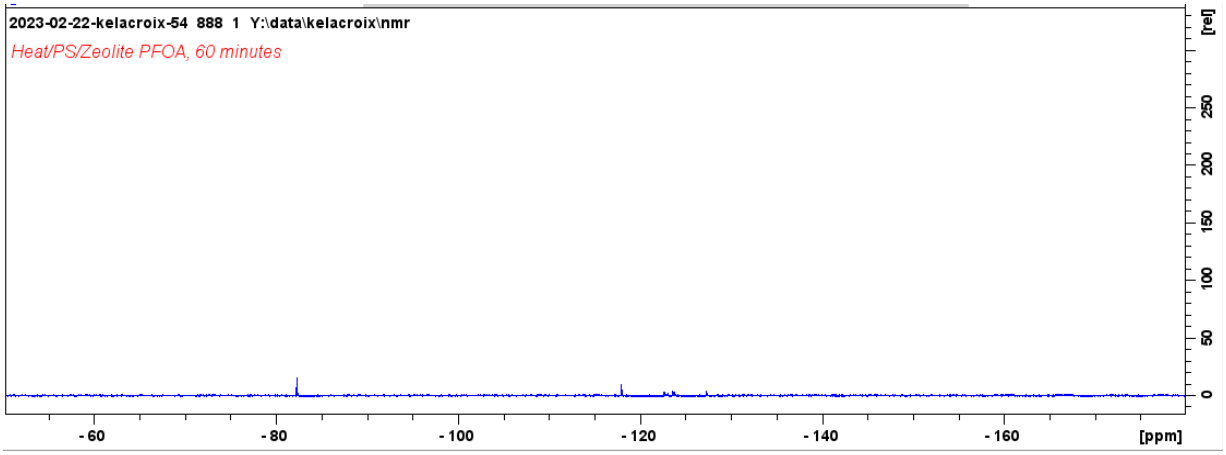

Figure 143. NMR Spectrum for the heat/PS/zeolite, PFOA reaction with 5 g/L dosage at 60 minutes.

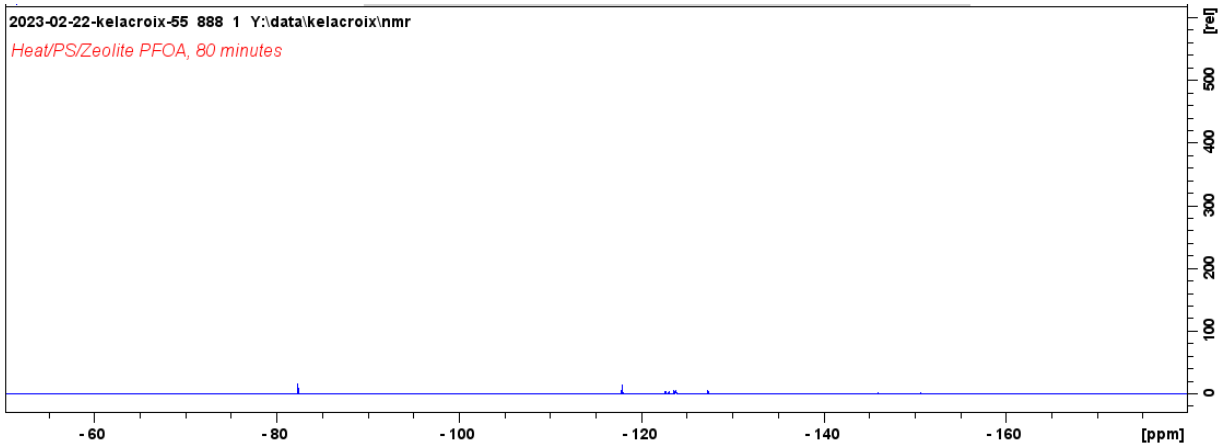

Figure 144. NMR Spectrum for the heat/PS/zeolite, PFOA reaction with 5 g/L dosage at 80 minutes.

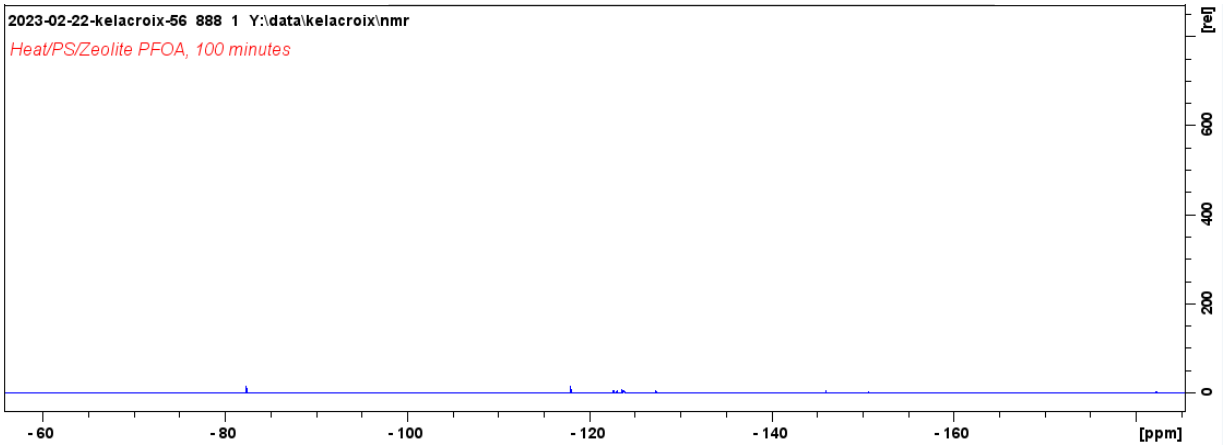

Figure 145. NMR Spectrum for the heat/PS/zeolite, PFOA reaction with 5 g/L dosage at 100 minutes.

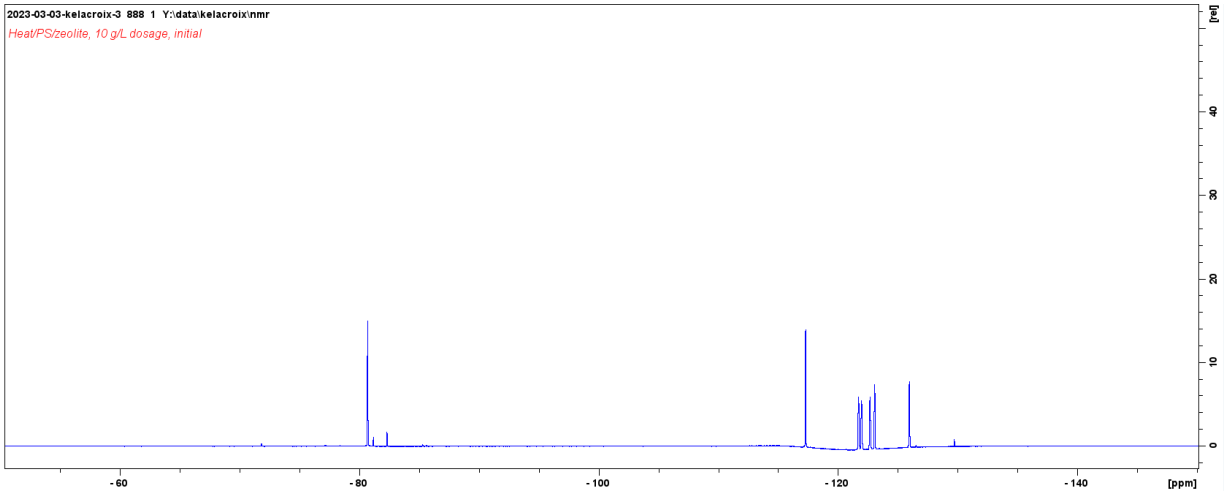

Figure 146. NMR Spectrum for the heat/PS/zeolite, PFOA reaction with 5 g/L dosage before 2 hours in laboratory shaker.

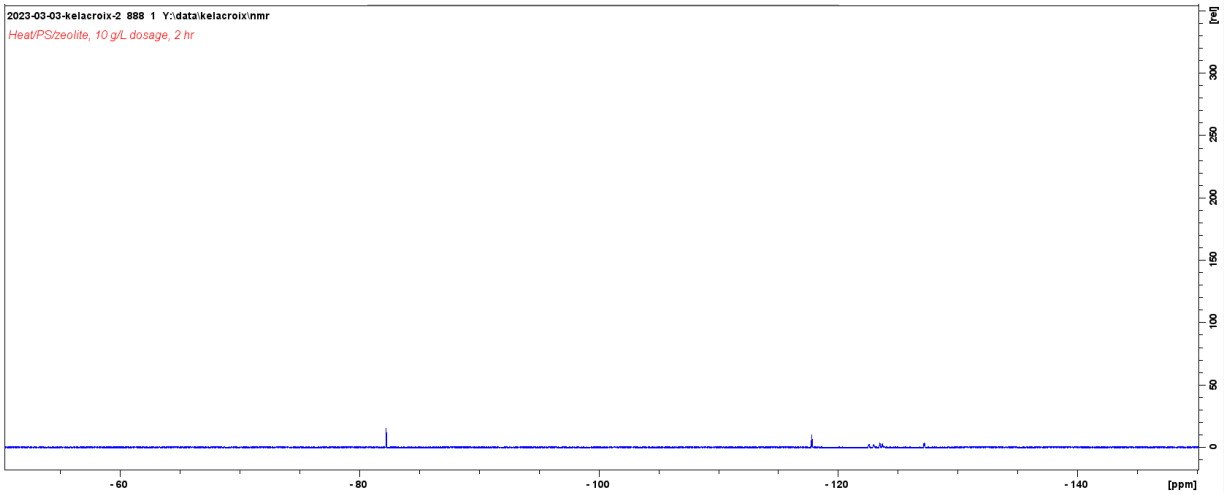

Figure 147. NMR Spectrum for the heat/PS/zeolite, PFOA reaction with 10 g/L dosage after 2 hours in laboratory shaker.

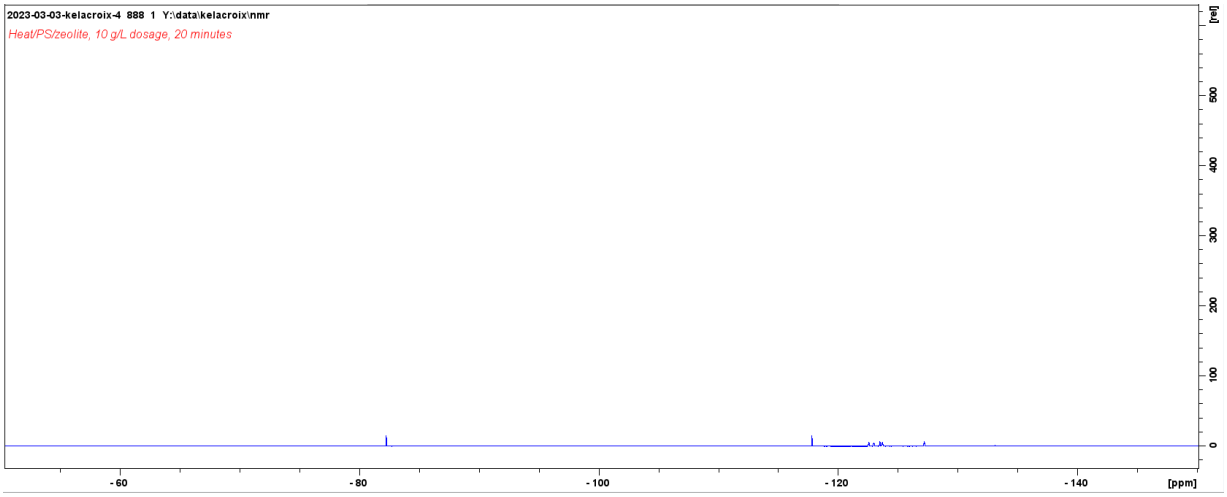

Figure 148. NMR Spectrum for the heat/PS/zeolite, PFOA reaction with 10 g/L dosage at 20 minutes.

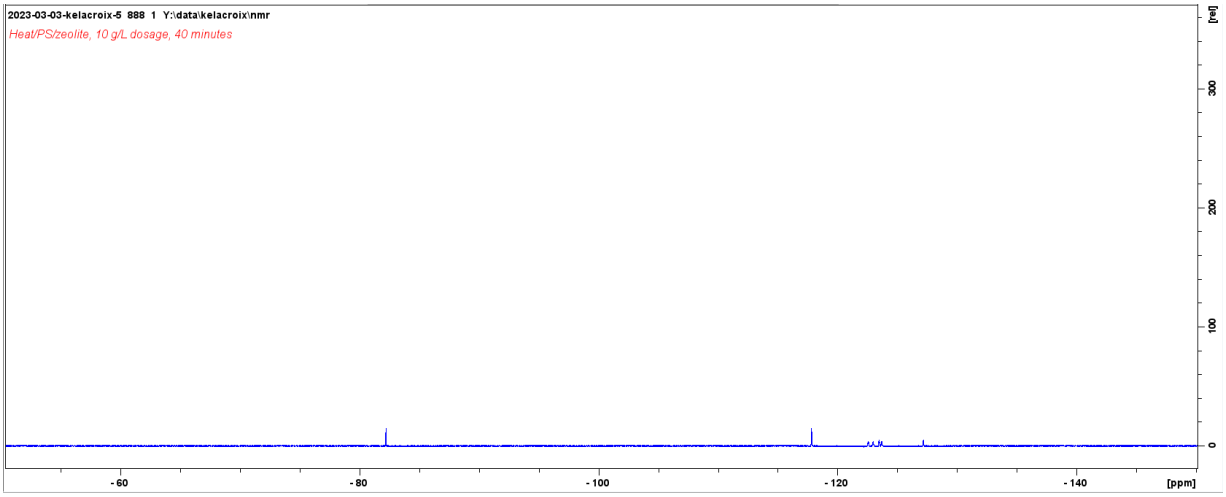

Figure 149. NMR Spectrum for the heat/PS/zeolite, PFOA reaction with 10 g/L dosage at 40 minutes.

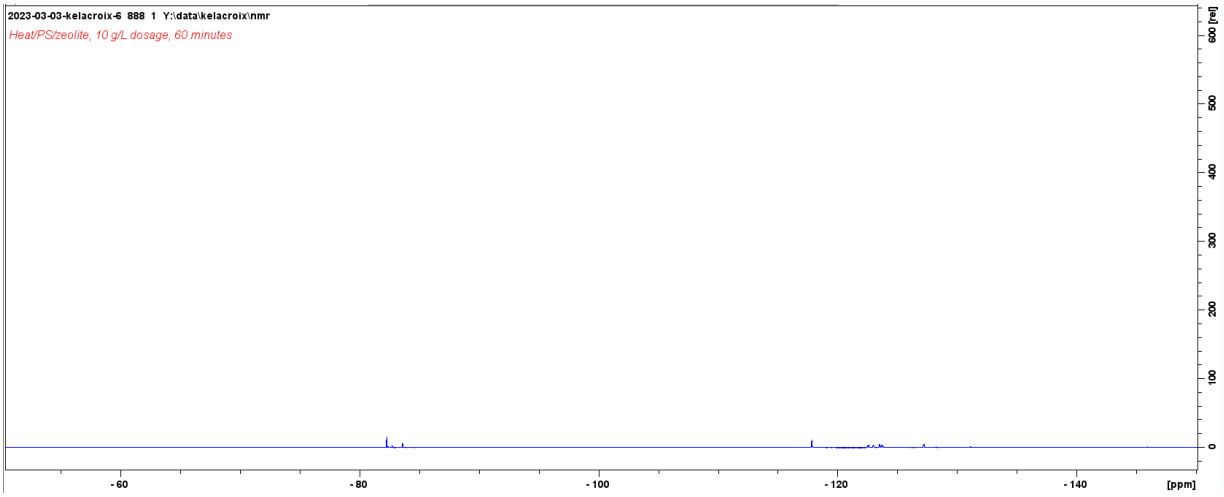

Figure 150. NMR Spectrum for the heat/PS/zeolite, PFOA reaction with 10 g/L dosage at 60 minutes.

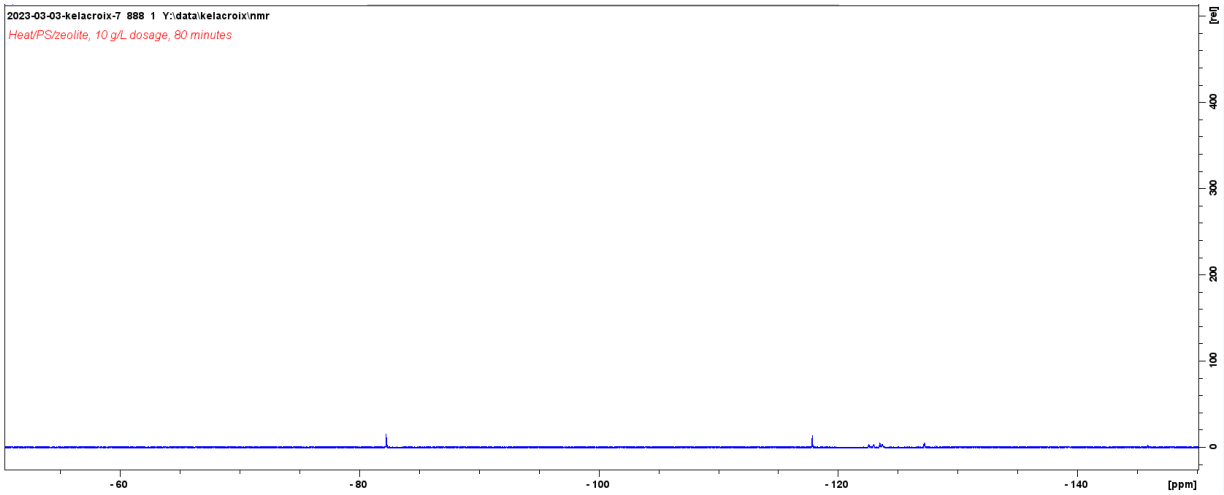

Figure 151. NMR Spectrum for the heat/PS/zeolite, PFOA reaction with 10 g/L dosage at 80 minutes.

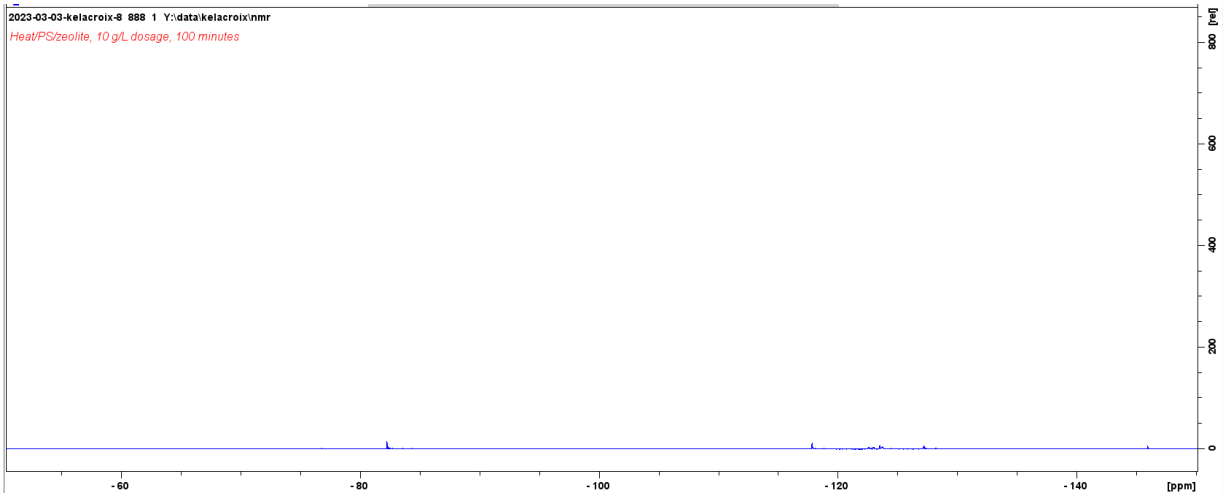

Figure 152. NMR Spectrum for the heat/PS/zeolite, PFOA reaction with 10 g/L dosage at 100 minutes.

Heat/PS, GenX Control:

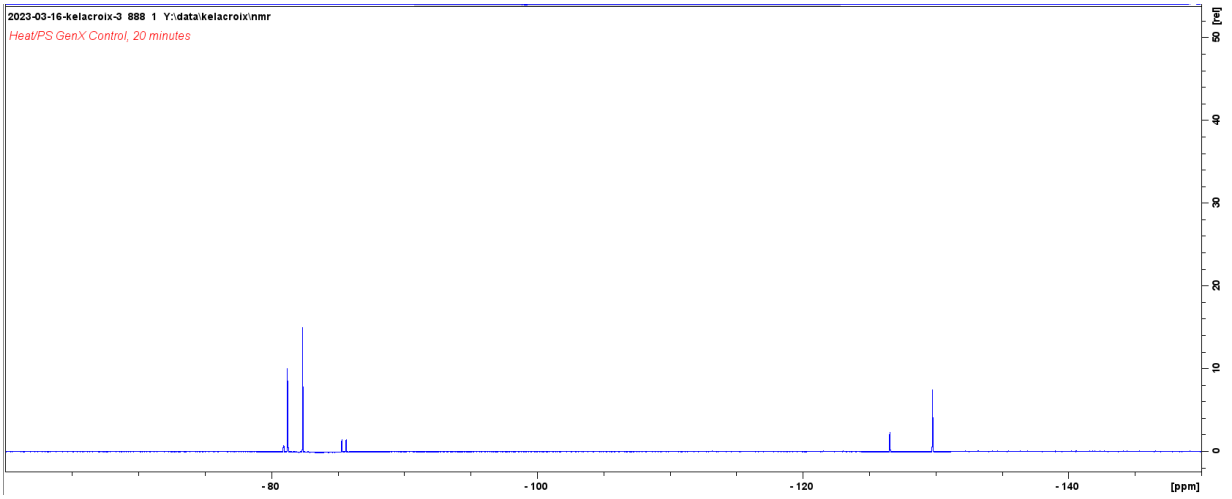

Figure 153. NMR Spectrum for the heat/PS, GenX control at 20 minutes.

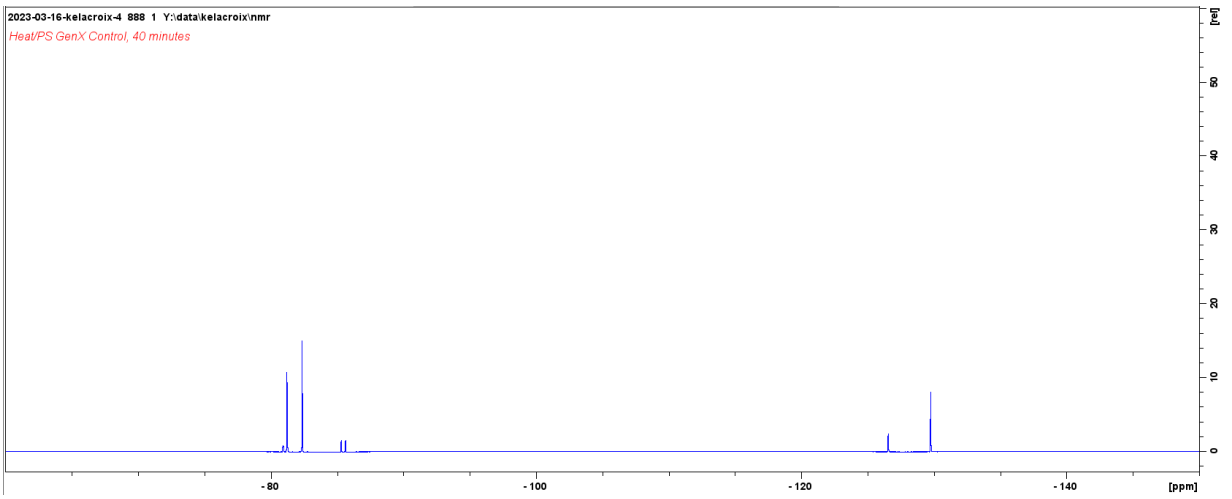

Figure 154. NMR Spectrum for the heat/PS, GenX control at 40 minutes.

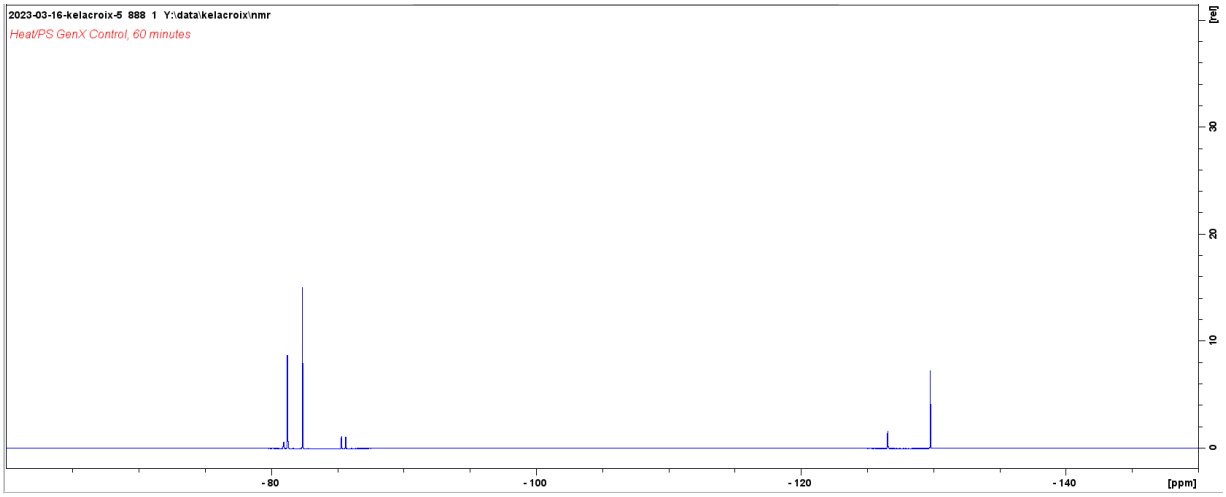

Figure 155. NMR Spectrum for the heat/PS, GenX control at 60 minutes.

<u>Heat/PS/Zeolite, GenX Reactions:</u>

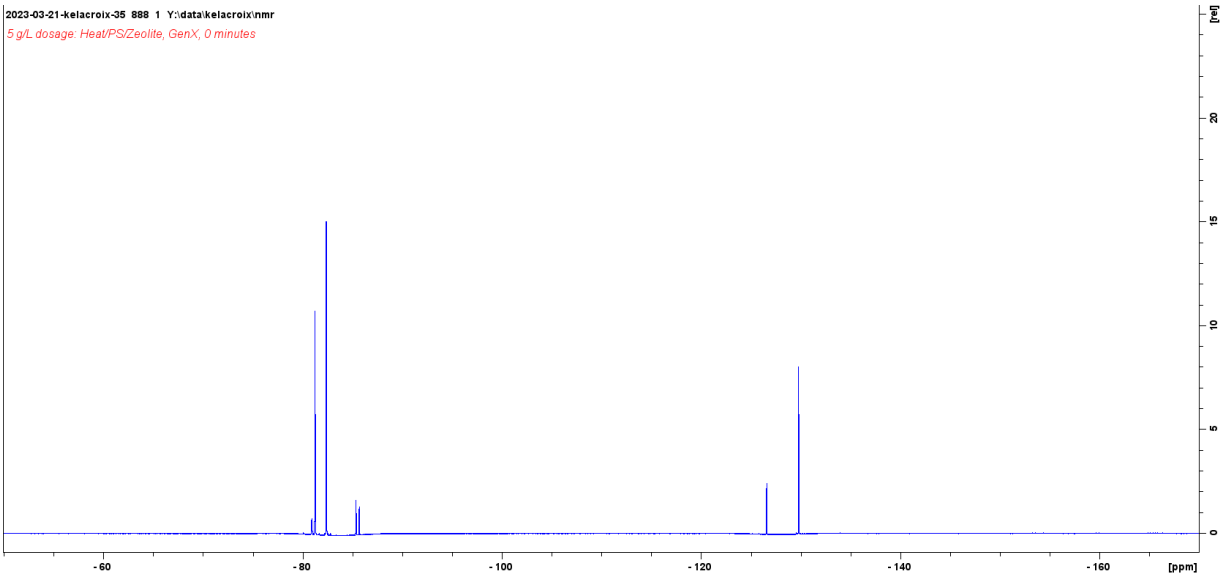

Figure 156. NMR Spectrum for the heat/PS/zeolite, GenX reaction with 5 g/L dosage before 2 hours in laboratory shaker.

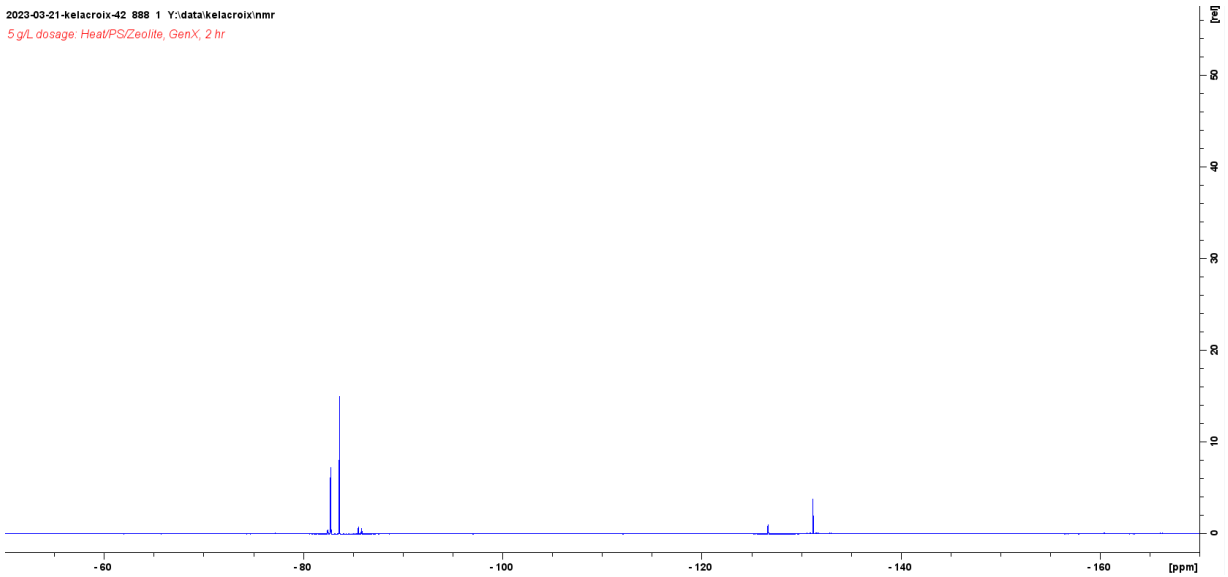

Figure 157. NMR Spectrum for the heat/PS/zeolite, PFOA reaction with 5 g/L dosage after 2 hours in laboratory shaker.

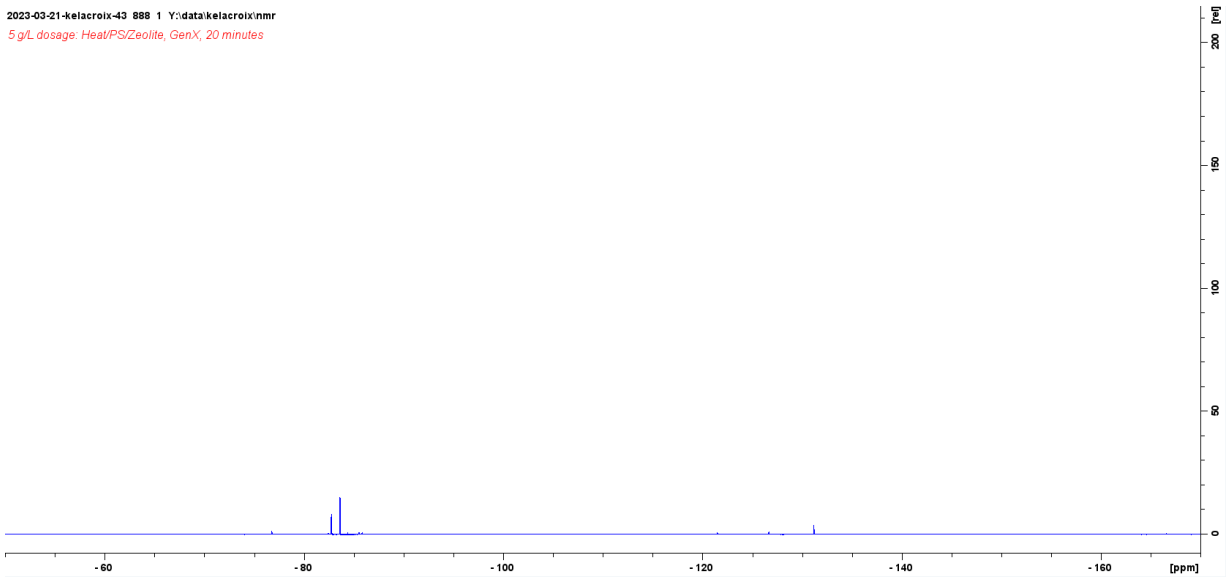

Figure 158. NMR Spectrum for the heat/PS/zeolite, PFOA reaction with 5 g/L dosage at 20 minutes.

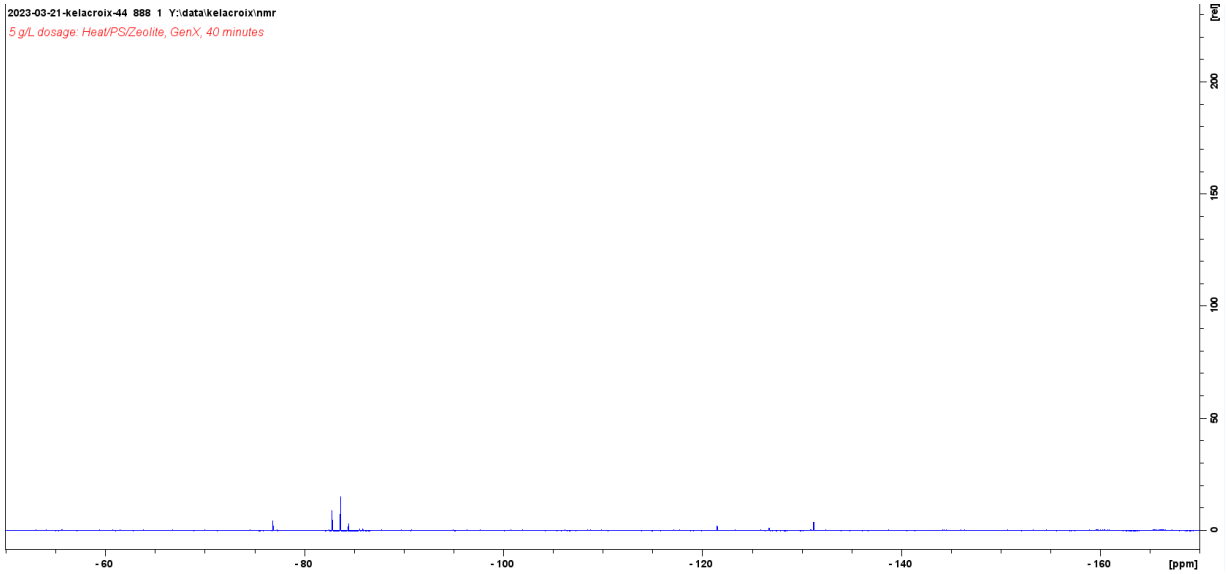

Figure 159. NMR Spectrum for the heat/PS/zeolite, PFOA reaction with 5 g/L dosage at 40 minutes.

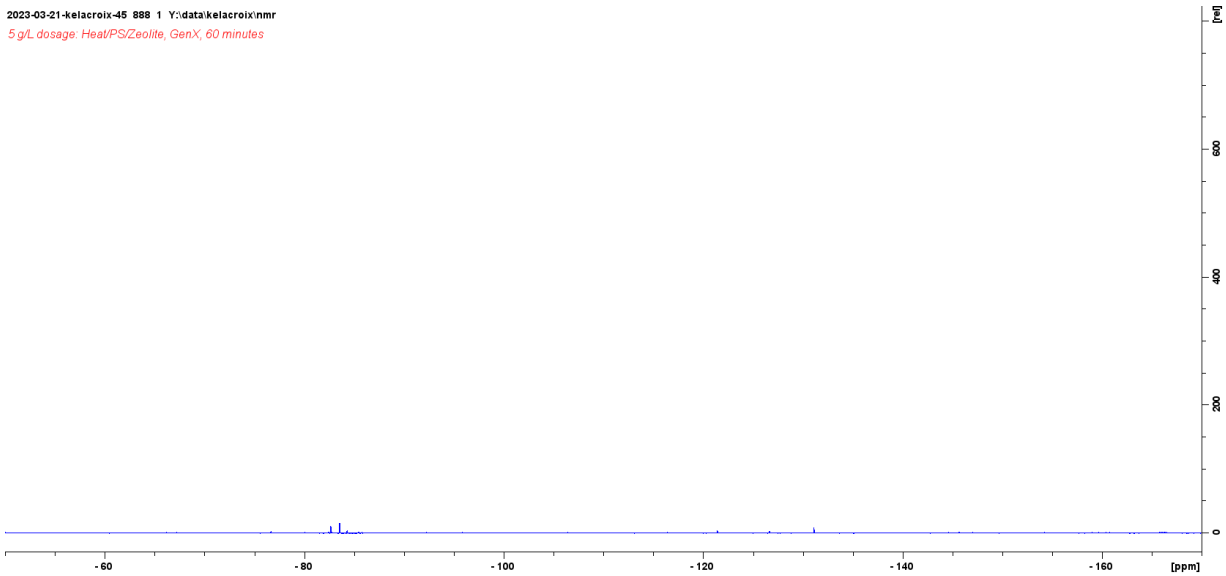

Figure 160. NMR Spectrum for the heat/PS/zeolite, PFOA reaction with 5 g/L dosage at 60 minutes.

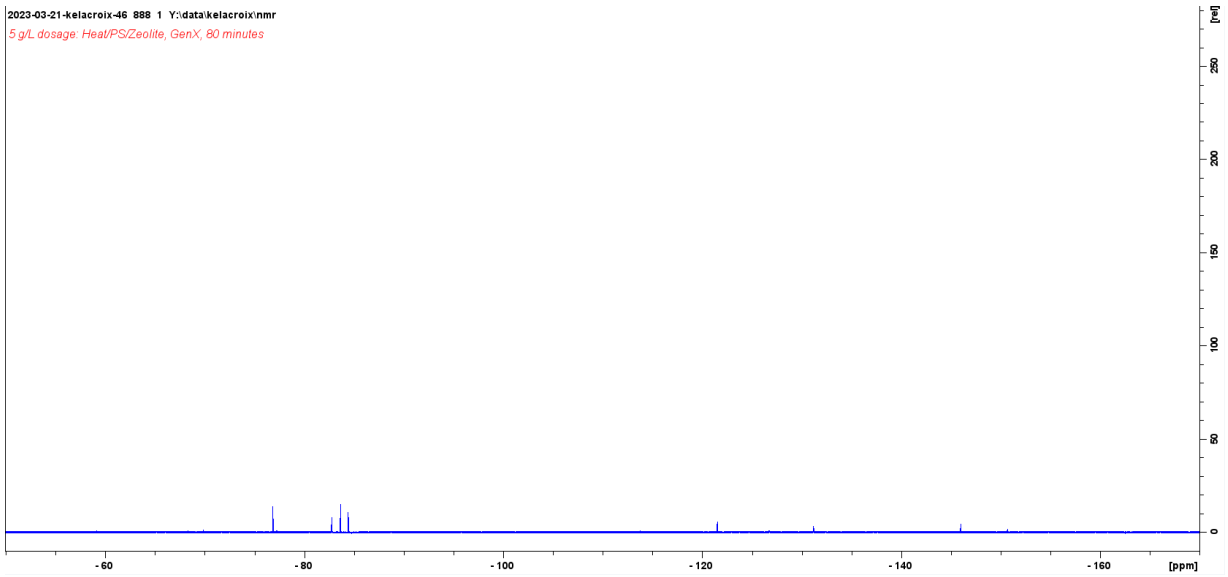

Figure 161. NMR Spectrum for the heat/PS/zeolite, PFOA reaction with 5 g/L dosage at 80 minutes

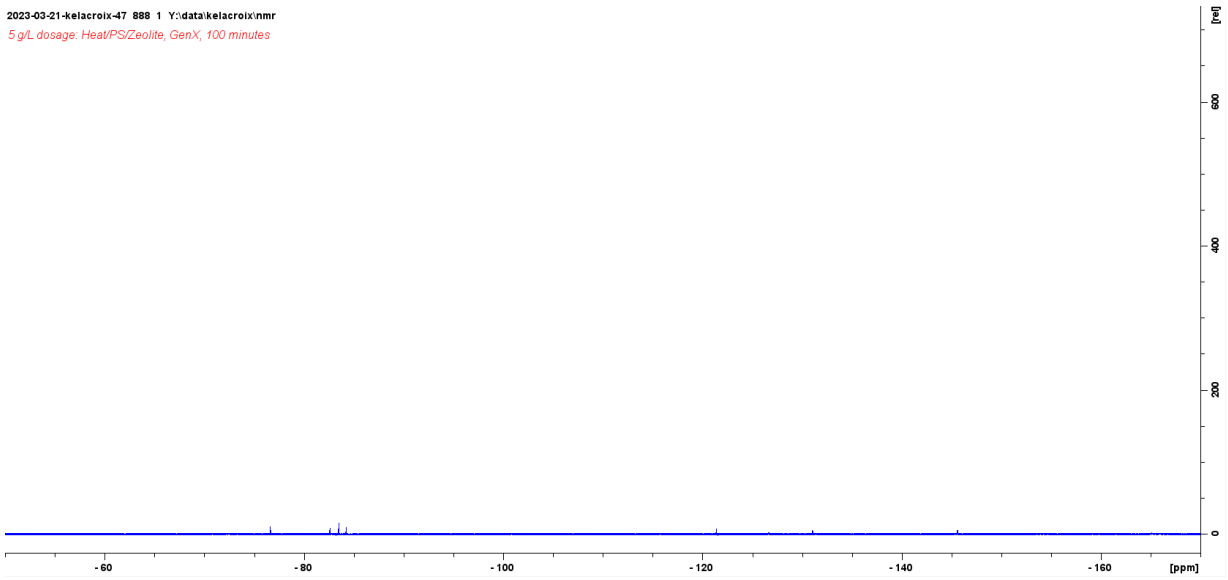

Figure 162. NMR Spectrum for the heat/PS/zeolite, PFOA reaction with 5 g/L dosage at 100 minutes

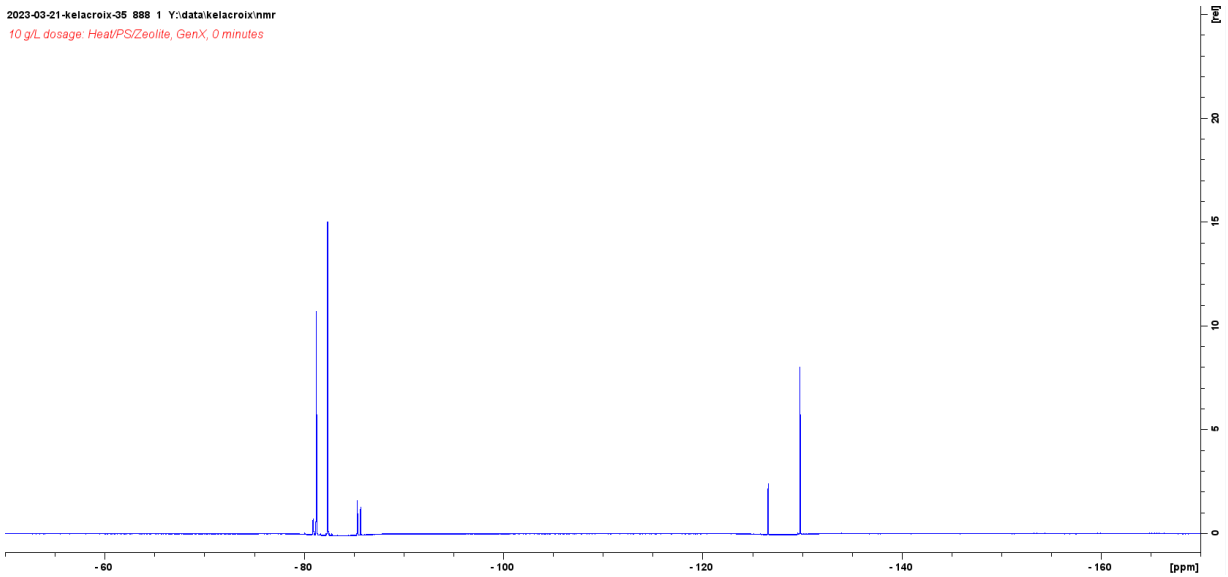

Figure 163. NMR Spectrum for the heat/PS/zeolite, GenX reaction with 10 g/L dosage before 2 hours in laboratory shaker.

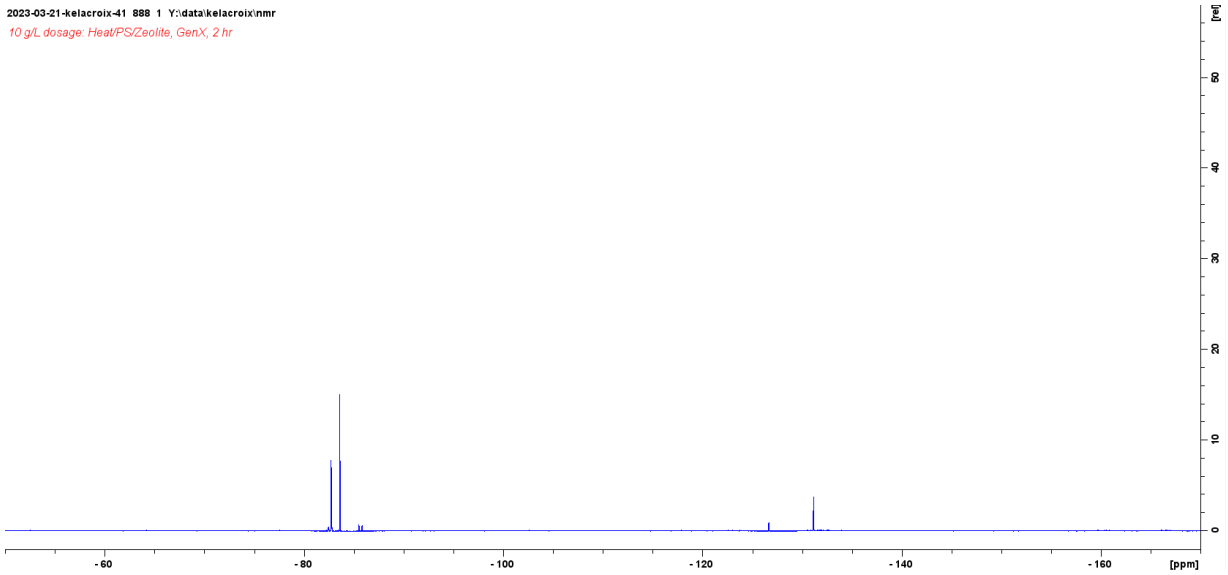

Figure 164. NMR Spectrum for the heat/PS/zeolite, PFOA reaction with 5 g/L dosage after 2 hours in laboratory shaker.

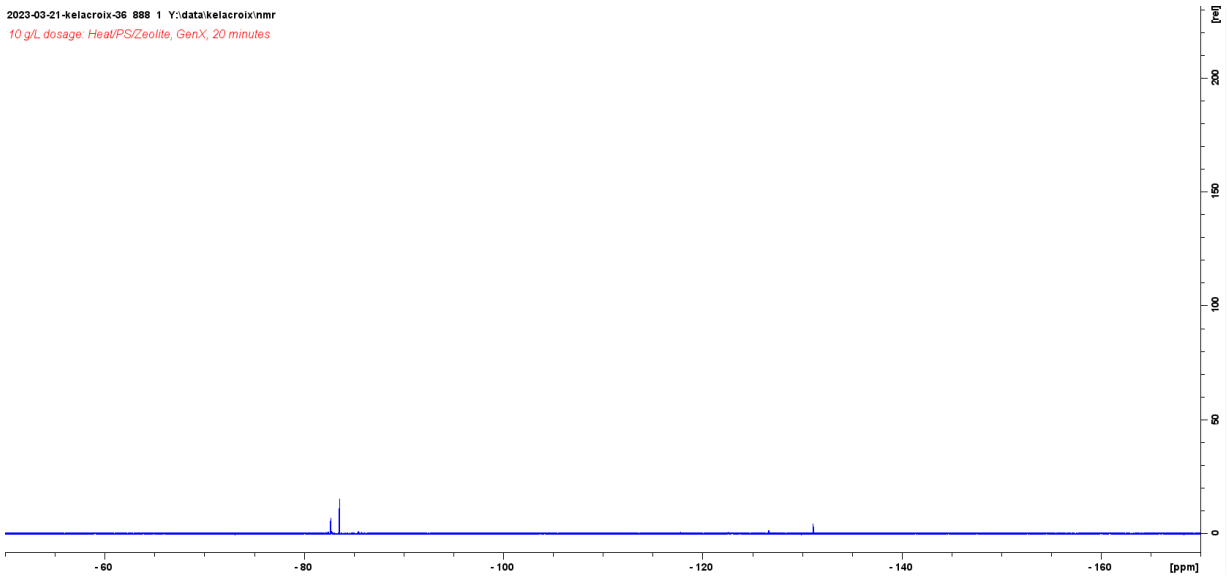

Figure 165. NMR Spectrum for the heat/PS/zeolite, PFOA reaction with 5 g/L dosage at 20 minutes.

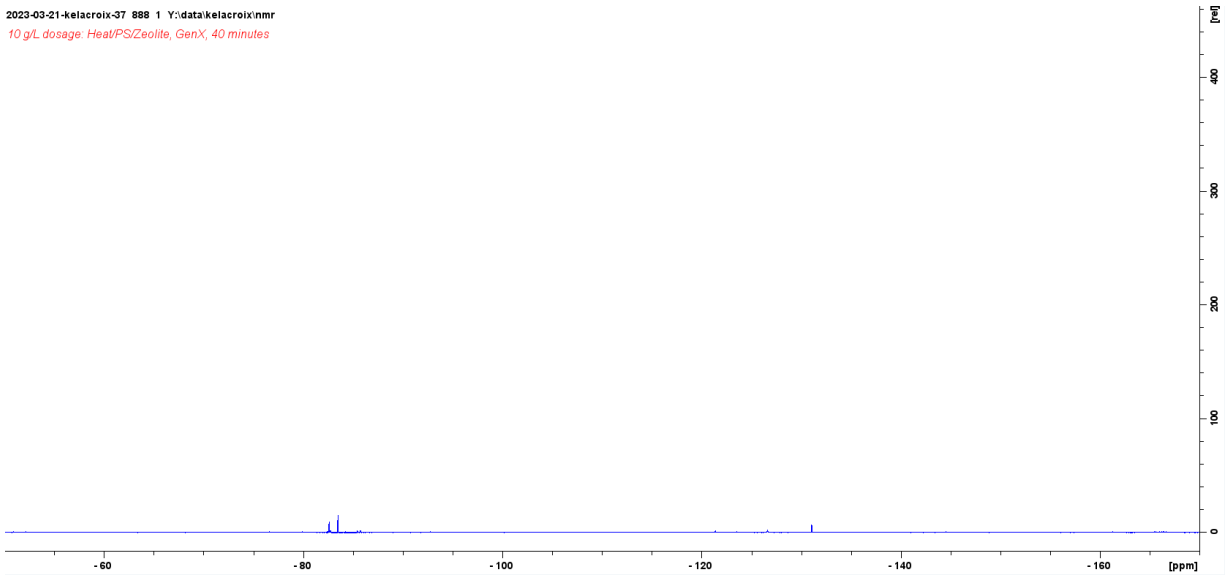

Figure 166. NMR Spectrum for the heat/PS/zeolite, PFOA reaction with 5 g/L dosage at 40 minutes.

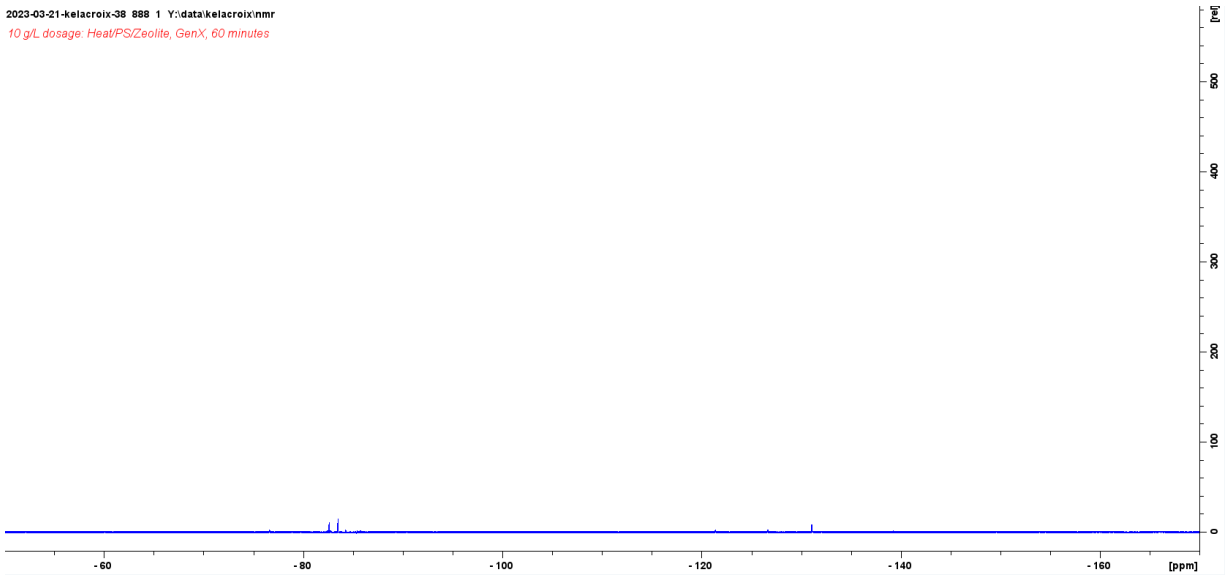

Figure 167. NMR Spectrum for the heat/PS/zeolite, PFOA reaction with 5 g/L dosage at 60 minutes.

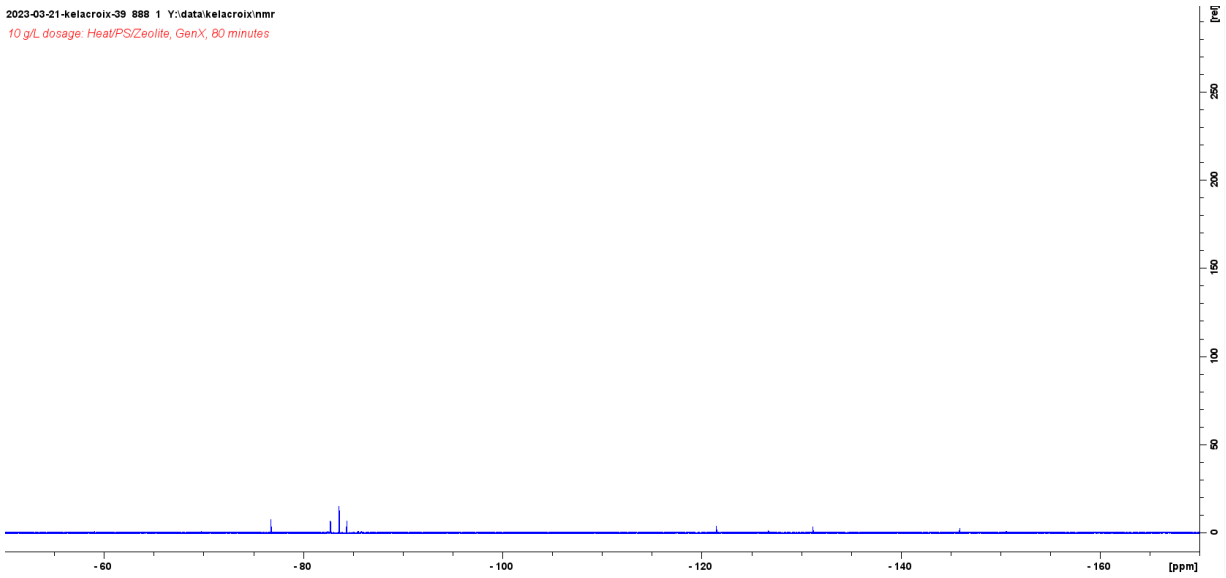

Figure 168. NMR Spectrum for the heat/PS/zeolite, PFOA reaction with 5 g/L dosage at 80 minutes

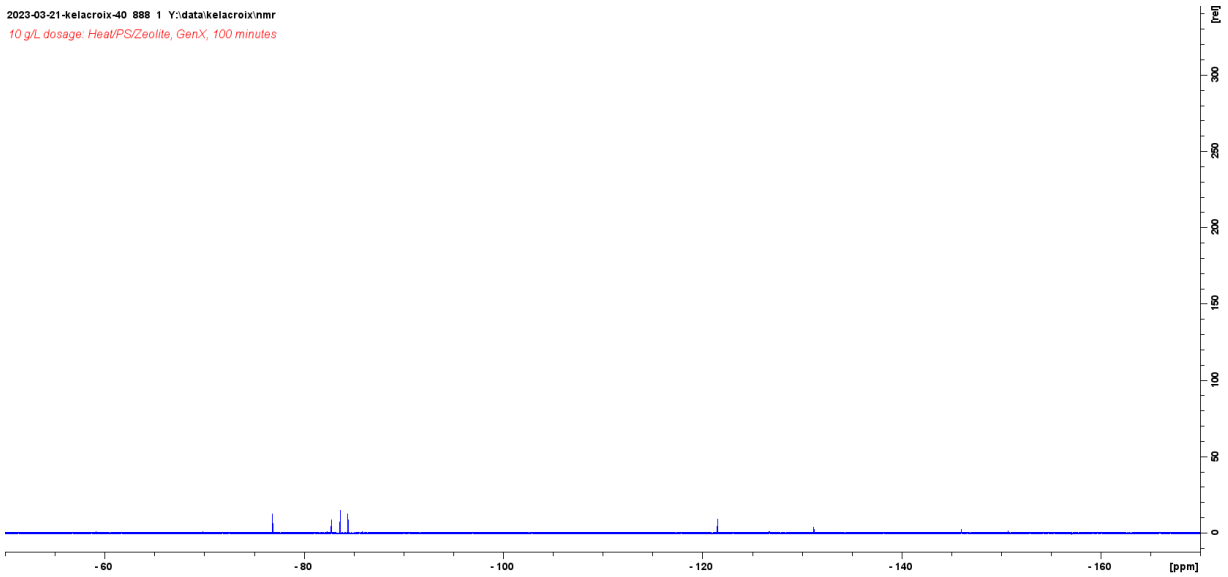

Figure 169. NMR Spectrum for the heat/PS/zeolite, PFOA reaction with 5 g/L dosage at 100 minutes